Nº. 9

Leibniz Universität Hannover

Berichte des Instituts für Massivbau

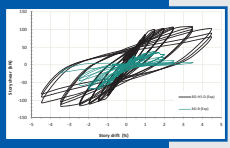

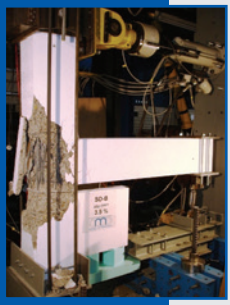

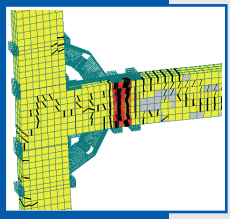

Mahdi Hayatrouhi

Strengthening of reinforced concrete beam-column joints to increase seismic resistance

Fraunhofer IRB Verlag

Berichte

des Instituts für Massivbau der Leibniz Universität Hannover
Herausgeber:
Univ.-Prof. Dr.-Ing. Steffen Marx
Leibniz Universität Hannover – Institut für Massivbau
Heft 9, Februar 2014

Fraunhofer IRB Verlag

Herausgeber
Univ.-Prof. Dr.-Ing. Steffen Marx
Leibniz Universität Hannover
Institut für Massivbau
Appelstraße 9 A
30167 Hannover

ISBN (Print): 978-3-8167-9177-5
ISBN (E-Book): 978-3-8167-9178-2

Fraunhofer IRB Verlag
Fraunhofer-Informationszentrum Raum und Bau IRB
Postfach 80 04 60, 70504 Stuttgart
Telefon 0711 970-2500
Telefax 0711 970-2508
E-Mail irb@irb.fraunhofer.de
URL http://www.baufachinformation.de

Abstract

Current research attempted to explore the behaviour of critical regions of reinforced concrete frame structures under seismic loading to investigate the deficiencies and evaluate the performance of gravity load designed (GLD) reinforced concrete (RC) beam-column joints. The categorized literature review of retrofitting and strengthening methods of RC beam-column joints clarified that non-disruptiveness; practical implementation, ductility and perseverance of lateral resistance as well as economical issues still remain the most challenging aspects of seismically retrofitting the vulnerable existing RC beam-column joints.

The seismic design principals of RC frame structures were observed in seismic retrofitting of the vulnerable frames as a strategy of retrofitting based on the capacity design concept. Accordingly, the beam sidesway mechanism was redefined for seismic retrofitting by relocating the beam plastic hinges far enough away from the joints. Afterwards, with introducing innovative energy dissipation devices such as Multi Functional Corbels (HMFC) and Harmonica Damper Plates (HHDP), the innovative Retrofitting Techniques 1 and 2 (RT1 and RT2) were proposed. The introduced devices of HMFC and HHDP as a passive energy dissipation system absorb energy through inelastic deformations. For efficiently and extensively evaluating and arranging the anticipated hierarchy of strength in beam-column joints before and after retrofitting, the Strength and Failure Sequence Diagram (SFSD) was proposed in a new coordinate. To implement the proposed RT1 and RT2 and achieve the desired hierarchy of strength, the design procedures were presented. Subsequently, to clarify the behaviour and founding the proposed innovative devices and techniques a comprehensive numerical analysis was carried out by nonlinear finite element analysis software ATENA.

The proposed RT1 and RT2 were experimentally evaluated through a series of five 3/4-scale beam-column joint specimens including two units for reference and the three others for retrofitting. A particular loading setup was designed and fabricated in structural laboratory so that the applying of horizontal cyclic and vertical static loads became simultaneously possible. An extremely severe loading history including three cycles (push and pull) at every particular drift level as a displacement-controlled series of progressively increasing displacement amplitudes in accordance with [ACI 374.1-05] was imposed to every specimen. The excellent performance of retrofitted specimens through the experimental study confirmed that the proposed RT1 and RT2 are able to retain structural integrity with the minimum strength and

stiffness degradation. As intended, the energy dissipation capacity was dramatically increased and beam sidesway mechanism was actually formed.

Finally, non-linear finite element analysis using ATENA was carried out on all reference and retrofitted specimens. The FEM models were validated with experimental outcomes. Subsequently, the validated models were utilized to develop a new simplified method for upgrading based on the advantages of RT1 and RT2. In the new proposed innovative Retrofitting Technique 3 (RT3), HHDP was replaced by Frictional-Bending Damper Plate (HFBDP) which dissipates energy based on friction and bending. The effectiveness and reliability of the proposed RT3 was investigated through a numerical analysis. The results of simulation showed that RT3 could efficiently achieve the intention of seismic retrofitting too.

At the end, as confirmed through experimental and numerical investigation, it is claimed that the all acceptance criteria of ACI Committee 374 [ACI 374.1-05] were effectively satisfied by the proposed retrofitting techniques.

Keywords: beam-column joint; retrofitting; seismic; analysis; design; energy dissipation; plastic hinge; inelastic deformation; corbel; friction

Kurzzusammenfassung

Die Arbeit enthält eine kategorisierte Übersicht von Nachrüst- und Verstärkungsmethoden bewehrter Balken-Stützen-Verbindungen aus der Literatur. Es zeigt sich, dass sowohl baulicher Eingriff, praktische Ausführung, Duktilität und Dauerhaftigkeit bezüglich seitlichen Widerstands, als auch ökonomische Randbedingungen die herausforderndsten Aspekte seismischer Verstärkungen gefährdeter Balken-Stützen-Verbindungen aus Stahlbeton sind.

Die seismischen Konstruktionsprinzipien von Stahlbetonrahmenkonstruktionen wurden entsprechend der Strategie für Nachrüstungen nach dem „capacity design concept“ untersucht. Dabei wurde der „beam sidesway mechanism“ für seismische Verstärkungen durch eine Verlagerung des plastischen Gelenks in geeigneter Entfernung zur Rahmenecke neu definiert. Danach werden durch Einführung innovativer Energiedissipationsgeräte, wie Multifunktionskonsole (HMFC) und Harmonika-Dämpfer-Platte (HHDP), innovative Verstärkungstechniken 1 und 2 (RT1 und RT2) vorgeschlagen. Die innovativen Geräte HMFC und HHDP als passives Energiedissipationssystem absorbieren Energie durch unelastische Verformung. Zur effizienten und ausgedehnten Bewertung und Anordnung erwarteter Widerstandshierarchie in Balken-Stützen-Verbindungen vor und nach der Verstärkung, wurde das Widerstands-Versagensfolge-Diagramm (SFSD) mit veränderter Ordinate vorgeschlagen. Zur Anwendung der eingeführten RT1 undRT2 und zum Erreichen der gewünschten Widerstandshierarchie wurde ein kompletter Entwurfsprozess präsentiert. Um das Verhalten und die Leistungsfähigkeit des vorgeschlagenen innovativen Geräts und Techniken zu untermauern, wurden umfassende numerische Analysen mit der nichtlinearen FE-Software ATENA durchgeführt.

Die vorgeschlagenen Verstärkungstechniken wurden experimentell mittels einer Serie von 5 Balken-Stützen-Verbindungen im ¾-Maßstab evaluiert, wobei zwei Einheiten als Referenz ohne Verstärkung und drei mit Verstärkung getestet wurden. Es wurde eine spezielle Belastungseinrichtung im Labor konstruiert und hergestellt, so dass die Prüfstücke auf dem Boden stehen und seitliche zyklische Last, mit der Maßgabe einer vertikalen statischen Last, an den Proben angreifen. An allen Proben wurde eine extrem harte Belastungsgeschichte weggesteuert eingetragen, die in Übereinstimmung mit [ACI 374.1-05] aus progressiv ansteigenden Verschiebungsamplituden besteht, wobei drei Zyklen (Druck und Zug) auf

einem bestimmten Driftniveau liegen. Durch die experimentellen Untersuchungen bestätigt sich die exzellente Leistungsfähigkeit der verstärkten Probestücke sowie die Annahme, dass RT1 und RT2 in der Lage sind das Widerstandsvermögen mit einem Minimum an Festigkeits- und Steifigkeitsverlusten beizubehalten. Wie erwartet stieg die Kapazität zur Energiedissipation drastisch an und der „beam sidesway mechanism“ bildete sich tatsächlich aus.

Letztlich wurde die nichtlineare FE-Analyse durch Benutzung von ATENA alle verstärkten und nicht verstärkten Proben angewendet. Das FE-Modell wurde durch die experimentellen Ergebnisse validiert. Anschließend wurden die validierten Modelle benutzt, um eine neue vereinfachte Methode zur Verbesserung zu entwickeln, die auf den Vorzügen von RT1 und RT2 basieren. In der neu vorgeschlagenen innovativen Verstärkungstechnik 3 (RT3) wurde das HHDP durch eine Biegereibungsdämpferplatte (HFBDP) ersetzt, welche Energie basierend auf Reibung und Biegung dissipiert. Die Effektivität und Funktionsfähigkeit der vorgeschlagenen RT3 wurde mit Hilfe numerischer Analysen untersucht. Die Ergebnisse der Simulation zeigten, dass RT3 die Intention seismischer Verstärkung ebenfalls effizient erzielen könnte.

Letztlich, wie durch experimentelle und numerische Untersuchungen bestätigt, wird behauptet, dass alle geforderten Kriterien des ACI-Komitees [ACI 374.1-05] durch die vorgeschlagenen Verstärkungstechniken befriedigt wurden.

Schlagworte: Balken-Stützen-Verbindungen; Nachrüstung; Seismisch; Analyse; Konstruktion; Energiedissipation; Plastisches Gelenke; unelastische Verformung; Konsole; Reibung

Acknowledgments

First, and foremost, praises and thanks to the God, the Almighty, for providing me the blessings to complete this research successfully.

I wish to express my deep and sincere gratitude and appreciation to my research supervisors Prof. Dr.-Ing. Steffen Marx, Prof. Dr.-Ing. Nabil A. Fouad, and Prof. Dr.-Ing. Jürgen Grünberg for giving me the opportunity to develop this research and for providing me the guidance, encouragement and supporting throughout the course of this study that made this project possible.

I would like to appreciate Dr.-Ing. Michael Hansen for his supports during experimental study.

I would like to thank the all colleagues of Institute of Concrete Construction (IFMA), Leibniz University of Hannover, particularly Mrs. Kerstin Bensch, Mrs. Simone Matern and my dear friend Dipl.-Ing. Jens Piehler for their kindly assistance.

All experiments were conducted at structural laboratory of Institute of Concrete Construction (IFMA), Leibniz University of Hannover. I would like to show gratitude to technical staffs of the laboratory Mr. Ernst Heine and Mr. Olaf Menze for their distinguished assistance during the experimental study. I wish also to show appreciation to the other institutes' staff in the structural laboratory, Mr. Lothar Beer, Mr. Karl-Heinz Hentschel, Dipl. Ing. Christian Fricke, Mr. Viktor Wall, and Mr. Gerd Hargesheimer for their advices and assistance.

Materials (FRP composites, adhesives and SAS670 bolts) donated by FIDIA, Hardwire, Sika and Stahlwerk Annahute are thankfully acknowledged.

Last but not least, I wish to express my deep thankfulness to my family for their patience to wait in loneliness for the right time. Thanks to my lovely sons Amirhossein and Amirreza for their accompanying. My sincere gratitude to my wife Sonia for her supports, encourages and patience during this study so that without her this work could not have been possible.

Table of contents

List of figures

List of tables

Notation

A_{ch} cross-sectional area of a structural member measured to the outside edges of transverse reinforcement, mm^2

A_e effective joint cross-sectional area, mm^2

A_g gross area of concrete, mm^2

A_h the area of the third cycle to the drift ratio of 3.5%

A_j effective joint cross-sectional area, mm^2, computed from joint depth (h_c) times effective joint width (the overall width of the column, except where a beam frames into a wider column, effective joint width shall not exceed the smaller of: a) beam width plus joint depth, b) twice the smaller perpendicular distance from longitudinal axis of beam to column side

A_{s1} area of the beam top reinforcement, mm^2

A_{s2} area of the beam bottom reinforcement, mm^2

A_{sh} total cross-sectional area of transverse reinforcement including crossties within spacing s and perpendicular to dimension b_c, mm^2

$A_{sv,i}$ total area of the intermediate bars placed in the relevant column faces between corners of the column including bars contributing to the longitudinal reinforcement of columns, mm^2

A_{Tjh} total area of the horizontal hoops in a beam-column joint, mm^2

b_b width of the longitudinal beam, mm

b_c width of the column, mm

b_j effective joint width, mm, should not exceed the smallest of ($\frac{b_b+b_c}{2}, b_b + \frac{\sum mh_c}{2}, b_c$), where beam-column eccentricity exceeds $b_c/8$, m=0.3, otherwise m=0.5

b_{jj} effective joint width, if $b_c > b_w$: $b_{jj} = \min\{b_c; (b_w + 0.5h_c)\}$; if $b_c < b_w$: $b_{jj} = \min\{b_w; (b_c + 0.5h_c)\}$

b_w width of beam web, mm

d_b nominal diameter of bar, mm

E_0 initial elastic modulus for concrete, MPa

E_c secant elastic modulus at the peak stress for concrete, MPa

E_1 the peak lateral resistance for the positive lateral loading direction

E_2	the peak lateral resistance for the negative lateral loading direction
f_{cd}	design value of concrete compressive strength, MPa
F_{ps}	post-tensioning force of the bottom corbel, N
$f_c^{'}$	specified compressive strength of concrete, MPa
$f_c^{'ef}$	concrete effective compressive strength, MPa
$f_t^{'ef}$	the effective tensile strength, MPa
f_{cd}	design value of concrete compressive strength, MPa
f_{ck}	strength of concrete, MPa
f_{ctd}	design value of the tensile strength of concrete, MPa
f_{ctm}	mean value of tensile strength of concrete, given as $0.3f_c^{'(0.667)}$
f_y	specified yield strength of reinforcement, MPa
f_{yd}	design value of yield strength, MPa
f_{yt}	specified yield strength of transverse reinforcement, MPa
f_{ywd}	design value of the yield strength of the transverse reinforcement, MPa
h_c	overall cross-sectional depth of column, mm
h_{jc}	distance between extreme layers of column reinforcement, mm
h_{jw}	distance between the top and the bottom reinforcement of the beam, mm
h_v	vertical distance of horizontal LVDTs at the end of beam or HMFC, mm
h_h	horizontal distance of vertical LVDTs at the end of column, mm
h_x	Max. center-to-center spacing of crosstie legs on all faces of the column, mm
J_2	second invariant of stress deviator tensor
k	shape parameter the relation of Stress-strain for concrete
l_c	story height, length of column, measured center-to-center of the top and bottom beams, mm
l_{cn}	clear length of the column, mm
l_b	span length of beam, measured center-to-center of the column, mm
l_d	development length in tension of deformed bar based on the building codes, mm
l_{dh}	development length in tension of deformed bar with a standard hook, measured from critical section to outside end of hook, mm
l_{nb}	clear length of beam from face of columns, mm

M_{bc}	Joint moment at the beam joint interface, N.m
$\bar{M}_{bc}$	joint moment capacity of the exterior beam-column joint at the beam joint interface, N.m
M_{nbc}	beam bending moment capacity or beam yielding at joint interface, N.m
M_{ncb}	column bending moment capacity or column yielding at joint interface, N.m
N	column axial load, N
N_{Ed}	design axial force from the analysis for the seismic design (the minimum value from load combination), is assumed positive when compressive, N
s	center-to-center spacing of transverse reinforcement within the joint, mm
r_{ec}	reduction factor of the compressive strength
r_{et}	reduction factor of the tensile strength
V_b	shear force across the beam, N
V_c	shear force in the column above the joint, from the analysis in the seismic design situation, N
V_{col}	shear force in the column above the joint, N
$\bar{V}_{col}$	story shear capacity of the as-built exterior beam-column jointcorresponding to the certain strength, N
$\bar{\bar{V}}_{col}$	story shear capacity of the retrofitted exterior beam-column jointcorresponding to the certain strength, N
v_d	normalized design axial force of column
V_{jhd}	horizontal shear force acting on the concrete core of the exterior joint, N
V_{jh}	horizontal shear force acting on the concrete core of the exterior joint, N
V_{nb}	beam shear strength, N
V_{nc}	column shear strength, N
w	the crack opening, mm
w_c	crack opening at the complete release of stress, mm
x	normalized strain
z_b	internal moment arm in the beam, mm
z_{ps}	proper moment arm of the bottom corbel post-tensioning, mm
α	stress multiplier for beam longitudinal bars
β	relative energy dissipation ratio
γ	joint shear strain
γ_{Rd}	model uncertainty factor for the design value of resistance for beam

	longitudinal bars, given as 1.2
γ_{xz}	shear strain
ε	normal strain
ε_c	strain at the peak stress $f_c'^{ef}$
ε_x	normal strain of joint panel in the x direction
ε_z	normal strain of joint panel in the z direction
ε_φ	strain in joint panel in an arbitrary direction (diagonal) with an angle of φ measured counter clockwise from the x axis
Θ'_1	drift ratio in positive direction
Θ'_2	drift ratio in negative direction
σ_c^{ef}	concrete compressive stress for the relation of Stress-strain for concrete, MPa
η	reduction factor on concrete compressive strength due to tensile strain in transverse direction
$\sum M_{nc}$	sum of nominal flexural strength of columns framing into the joint, N.mm
$\sum M_{nb}$	sum of nominal flexural strength of beams framing into the joint, N.mm

ACI	American Concrete Institute
ASCE	American Society of Civil Engineers
BD	Bond Deficiency
CFRP	Carbon Fiber-Reinforced Polymer
CORDIS	Community Research and Development Information Service
CSA	Canadian Concrete Design Code
DIN	Deutsches Institut für Normung
DTAM	Digital World Tectonic Activity Map
FRP	Fiber-Reinforced Polymer
EN	Europäisiche Norm
HFBDP	Hayatrouhi Frictional-Bending Damper Plate
HHDP	Hayatrouhi Harmonica Damper Plate
HMFC	Hayatrouhi Multi Functional Corbel

HPFRC	High-Performance Fiber-Reinforced Concrete
GFRP	Glass Fiber-Reinforced Polymer
GLD	Gravity Load Designed
GSHAP	Global Seismic Hazard Assessment Program
LVDT	Linear Variable Distance Transducer
NASA	National Aeronautics and Space Administration
NPO	Non Profit Organisationen
NSM	Near-Surface-Mounted
RC	Reinforced Concrete
RT1	Retrofitting Technique 1
RT2	Retrofitting Technique 2
RT3	Retrofitting Technique 3
SD	Shear Deficiency
SRP	Steel Fiber-Reinforced Polymer
SFSD	Strength and Failure Sequence Diagram
UNIDO	United Nations Industrial Development Organization
USGS	Unite States Geological Survey

Chapter 1

Introduction

1.1 Introduction

Every month the earth is shaken by approximately 80,000 earthquakes; at a rate of 2 earthquakes a minute, [CORDIS-12]. Earthquakes can be a devastating and catastrophic phenomenon when they hit density populated areas. Taking a short look at the seismic hazard map of the world, Fig. 1.1, earthquake epicentres, Fig. 1.2 and compare them with the world population density, Fig. 1.3, shows that nearly most of the populated areas are located in the earthquake hazard zones. Fig. 1.4 displays also seismic hazard map for D-A-CH countries (Germany, Austria, and Switzerland). The geological researches show that even in Germany, earthquake risks may be greater than it has been thought before. Discovering the unique geological traces of strong damaging earthquakes with a magnitude exceeding 6.5 on the Richter scale in Germany demonstrates that existing regulations for earthquake resistant construction must be reviewed and supplemented if necessary [NPO, Geologischer Dienst NRW-07].

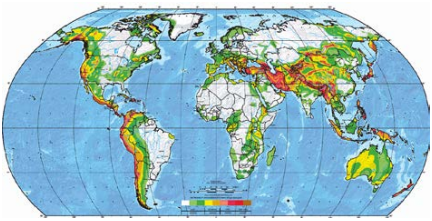

Fig. 1.1: Global seismic hazard map produced by the Global Seismic Hazard Assessment Program(GSHAP 1999)

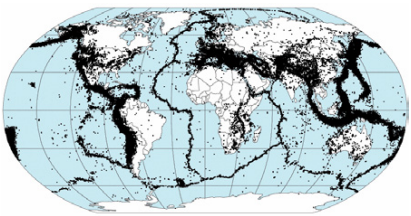

Fig. 1.2: Preliminary determination of Earthquake epicenters, 1963-1998(NASA, DTAM project team)

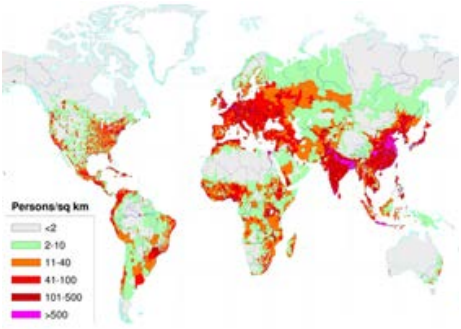

Fig. 1.3: Population density (people per km2) map of the world in 1994 (Wikipedia)

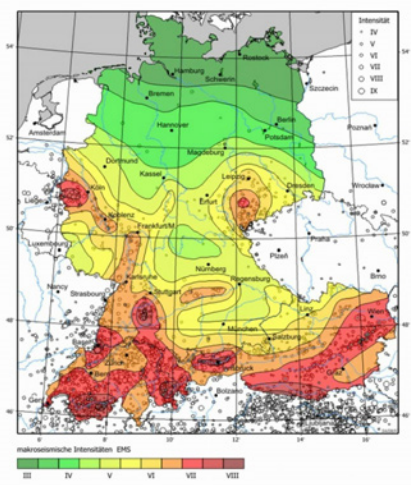

Fig. 1.4: Probabilistic Seicmic hazard map for Germany, Austria, and Switzerland with map of epicenters, (Grüntal u.a. 1998)

The majority of existing reinforced concrete (RC) structures in different parts of the world even seismic hazard zones have been designed only to carry gravity loads, gravity load designed (GLD). In earthquake hazard zones, these structures are mostly vulnerable to any moderate or severe ground motions. The typical characteristic of these structures include non-ductile detailing of members, strong beam-weak column behaviour, and vulnerable joints. During recent years, the vulnerability of existing structures to moderate and major earthquakes have been documented. The findings from recent major earthquakes, such as the 1995 Kobe (Japan) and the 1999 Kocaeli (Turkey), emphasise the consequences of poor performances of beam-column joints and show that their failure destabilizes the integrity of the whole structure, even if the beams and columns in a RC frame remain undamaged, [Muguruma et al.-95], [Anderson et al.-96], [Saatcioglu et al.-01]. Distress in beam-column joints such as excessive shear deformation in the non-ductile frames and high bond stresses of longitudinal bars of beams into the joints as well as slippage of beam bottom positive bars and inadequate joint confinement contribute to the collapse of structures, [Moehle-91], Fig 1.5 to Fig. 1.7.

Fig. 1.5: Collapsed RC frame structure due to failure of beam-column joints, 1999, 7.2 Richter earthquake, Duzce, Turkey

Fig. 1.6: RC frame structure was collapsed via failure of beam-column joints, 1999, 7.4 Richter earthquake, Kocaeli, Turkey

(a) (b)

Fig. 1.7: Joins failure leaded to completely collapse of RC frame structure: a): 1994, Northridge earthquake, USA, 6.7 Richter (reprinted from [Moehle]); b) 20.04.2013, China's Sichuan province, 6.9 Richter, (Trend News)

After determination of equivalent lateral earthquake loads and concept of ductile-design method for structural members as well as understanding the post-elastic behaviour of structures, design of earthquake resistant structures have been significantly developed since 1970s around the world. However, as building standards are updated, some existing RC structures may not satisfy the current codes even though they may have been properly designed and constructed according to earlier building codes. Consequently, many existing RC structures will be found that may have inadequate structural performance during earthquakes and accordingly must be efficiently retrofitted.

Seismic retrofitting and rehabilitation of existing structures is one of the most effective methods of reducing seismic risks and providing safety to building occupants and protecting their investments [Alcocer et al.-93]. However, the seismic performance of the structure may not be improved by retrofitting or rehabilitation unless the designer selects an appropriate and feasible strengthening approach based on seismic evaluation of the structure.

1.2 Motivation of the research

The behaviour of beam-column joints is extremely important in global performance of RC frame structures so that their failure during an earthquake can lead to substantial drifts and increase the possibility of structural collapse. Consequently, their retrofitting and strengthening is as important as their overall performance in the structures so that their upgrading improves not only the joint behaviour, but also the global structural response. Because of the large extent of the problem, it is necessary to develop effective, non-disruptive, practical and economical rehabilitation techniques for the upgrading of the joint resistance capacity in existing structures. By now several retrofit methods have been proposed and experimentally validated but considering the important of the subject it is needed to extend the literature to find new approaches. Simultaneously taking into account the different structural performance factors such as stability, strength, stiffness, ductility, and energy dissipation in addition to constructional parameters, for instance, non-disruption, ease to installation, and practicability as well as economical issues can lead to the effective retrofitting and strengthening techniques.

The current research wants to response to the “areas needing research” represented by joint ACI-ASCE committee 352, “recommendations for design of beam-column connections in monolithic reinforced concrete structures” [ACI 352R-02], to establish the adequacy of the joints in existing structures, develop innovative joint designs, and extend evaluation guidelines for building rehabilitation through improving the performance of older joints.

1.3 Objectives

The study is mainly focused on exterior beam-column joints, since it is recognized that in RC frame structures designed and constructed with outdated codes, prior to 1970, they are the most vulnerable [Calvi et al.-02], due to their lack of a reliable joint shear transfer mechanism. The purposes of the present research are framed as:

1. Understanding the deficiency and evaluation of performance of beam-column joint subassembly of existing RC frame structures designed to carry only gravity loads and establish seismic adequacy of pre-1970 exterior joints.
2. Development an effective, non-disruptive, ductile, and practical retrofitting technique (Retrofitting Technique 1, RT1) for existing deficient non-ductile beam-column joints through transmitting beam end flexural plastic hinges to the points far enough away from the joints by innovative Multi Functional Corbels (HMFC) to have extra energy dissipation and provide the principals of strong-column and weak-beam concept.
3. Trying to increase the lateral carrying capacity as well as preserving the strength and ductility through introducing other innovative retrofitting techniques RT2 and RT3 using HMFCs with innovative Harmonica Damper Plates (HHDP) or Frictional-Bending Damper Plates (HFBDP).
4. Development of numerical analysis to simulate the behaviour of existing deficient joints and upgraded ones.

1.4 Organization of the research

The research is organized in six chapters and a few appendixes including previous researches, introducing new devices and techniques, explanation of experimental programs, numerical analysis, and finally conclusions. The outcomes of the research are presented in the following chapters as below.

Chapter 2 presents the performance criteria and features of beam-column joint behaviours and establishes the seismic adequacy of pre-1970 joints. Furthermore, a summary of findings in strengthening and retrofitting of joints as a literature review along with a discussion regarding their principals and requirements of codes of practices are illustrated in this chapter.

Chapter 3 describes the basic principles of upgrading technique through transferring flexural plastic hinges inside the beams and introduces innovative devices to develop these methods with extra energy dissipation. Moreover, a new composite fabric as SRP, steel reinforced polymers, is also introduced which is used to locally upgrade of specimens.

Chapter 4 presents the experimental study of the research with illustration of production process and details of test specimens including beam-column joint specimens with different deficiencies, bond deficiency BD-B and shear deficiency SD-B, innovative devices, Multi

Functional Corbels (HMFC) and Harmonica Damper Plates (HHDP), locally retrofitting with SRP to satisfy shear resistance, and final retrofitted specimens, BD-H1, SD-H2-D, and BD-H3-D through Retrofitting Techniques 1 and 2 (RT1 And RT2). Furthermore, details and production process of loading setup as a main part of the experimental activities are presented in this chapter. Description of instrumentation to record displacements and strains as well as estimation of deformation and their components in beam-column joint specimens assemblies are the other parts of chapter 4. Finally, test results along with their interpretations, decompositions, and comparisons are ended this chapter.

Chapter 5 depicts the simulation of tested specimens including non-retrofitted specimens, BD-B and SD-B, and retrofitted specimens, BD-H1, SD-H2-D, and BD-H3-D by non-linear finite element method using software ATENA. First, the used constitutive models for different materials and behaviours are illustrated and then the numerical models developed for specimens are presented. The chapter is ended by proposing another innovative upgrading method (Retrofitting Technique 3, RT3) based on the test results of retrofitted specimens to improve their performance and behaviour.

Chapter 6 summarizes the outcomes of the research and compares the study results. Then the discussion is followed by conclusions and recommendations and ended with remarks for the future studies.

Appendix A pictorial reviews the laboratory activities to give more information about the experimental study.

Appendix B depicts details of loading setup subassemblies and the process of its design and construction.
Appendix C represents some supplementary pictorial explanations regarding the installation of specimens into the loading setup.

Appendix D illustrates decomposition approach of specimen deformation.

Appendix E describes the concept of relative energy dissipation ratio.

Chapter 2

Background and State of the Art

2.1 Introduction

Connections are one of the most important components of structures affecting the global behavior of them. In a RC frame structure, beam-column joints are critical zones for effectively transfer of loads among the connection components, beams and columns. Joints are generally assumed as rigid in traditional analysis of RC moment resistant frames. When the frame is not subjected to seismic loads, it may be acceptable to design beam-column joints without more specific requirements only to satisfy anchorage of beam longitudinal reinforcements, but in seismic provisions it needs extra criteria. In other words, prior to the developing of new codes of seismic resistant structures in 1970s, beam-column joints were classically not engineered, but vulnerability of structures and their catastrophic collapse during the past earthquakes, which have been attributed to poorly detailed joints, have depicted that as the crucial zones they must be codified.

In an earthquake, seismic bending moments with opposite signs are circumferentially developed in beam-column joints through beams and columns. Therefore, the joint regions are subjected to horizontal and vertical shear forces whose magnitude are usually more times higher than in the adjacent members, beams and columns. If the joints were not designed for, joint shear failure can result. On the other hand, the reversal in bending moments across the joint means that for instance in interior joints the beam reinforcement is at tensile yield on one side of the joint and simultaneously at compression on the other side. Consequently, there is a high force gradient across the joint that leads to the high bond stresses and may cause bond failure and subsequently degradation of moment capacity accompanied with excessive drift. A brittle joint shear failure or bond slip failure greatly reduces also the ductility of the structure.

After 1970s extensive experimental and analytical researches have been performed on seismic behaviour of RC beam-column joints and their retrofitting. Furthermore, simultaneously variety of criterions in the form of codes of practice and recommendations has been periodically issued to integrate the outcomes of the researches. This chapter deals with the background on the seismic performance of RC beam-column joints and briefly looks at the retrofitting and strengthening techniques as a chronological literature review.

2.2 Seismic behaviour of substandard RC beam-column Joints

The majority of the substandard RC building frames are gravity load designed (GLD) structures which are generally dominated by weak column-strong beam behaviour and performances due to joint insufficiencies such as joint shear and bond-slip deficiencies as well as joint bond deteriorations which may be outcome of discontinuity of positive bottom beam flexural reinforcement in joints. Under strong ground motion weak columns-strong beams and also discontinuities of positive bottom beam longitudinal reinforcements in joints, joint bond deteriorations, lead to an undesirable column side-sway/soft-story collapse mechanism [Bracci et al.-95-1], [Aycardi et al.-94], [Moehle-91]. On the other hand, joint deficiencies during a major earthquake provide hybrid local and global failure mechanisms [Calvi et al.-02]. A hybrid failure mechanism is a combination of plastic hinges in beam and column elements and shear hinges in joint regions which are related to joint shear damage so that the hinge is resulted by shear behaviour without post-elastic performance. The global failure mechanisms comprise beam-sway, column-sway, joint-shear hinge or combination of them. Through a capacity assessment of strength in subassemblies of a system (beams, columns, and joints) the expected sequence of strength, hierarchy of strength, can be obtained and consequently, useful information on the local and global failure mechanisms is provided.

Calvi et al. (2002) by a simplified analytical model for joint behaviour analysed three multi story GLD frame systems under different ground motions with some simplicities to show the relevance of beam-column joint damage and collapse of these frames [Calvi et al.-02]. Furthermore, they have carried out an experimental test on a three story GLD frame, according to Italian construction practice between the 1950's and the 1970's, to evaluate seismic response of the frame and joints under quasi-static cyclic loading [Calvi et al.-Sep. 02]. It was reported that the process of damage in the joints can start at early stages and terminate to strange hybrid mechanisms at both local and global level. Extreme vulnerability

of exterior joints has been detected which can reach collapse well before any significant damage takes place in column and beams. It was found out that shear hinge mechanisms after joint damaging with their higher local deformations can protect or delay soft-story mechanism through spreading the inter storey drift demand between damaged joint top and bottom stories which leads to reducing the rotational demand in the adjacent column elements. However, the withstanding of the joint to suffer high local deformation demands as a strong limit of the benefit given by the development of the shear hinge is a subject in which there is no definitive experimental information available. Experimental results show that in these frames because of joint deficiencies brittle behaviour and rapid strength degradation of the joint panels can occur and lead to the loss of vertical load-bearing capacity of the entire system.

The growth in research on the seismic performance of RC frame joints has led to a number of publications that present detailed studies on the behaviour of deficient joints to improve the performance of these joints through new design concepts and codification of new practical regulations. Here as a literature review some of these studies are briefly presented.

Megget (1974) provided research on two exterior RC beam-column joints subjected to cyclic loading to study the effect of low column axial load and transverse beams on the joint behaviour. The significant results were:

- The presence of transverse beams improves the confinement of the joint core concrete significantly and helps to form plastic hinge in the beam rather than in the joint, joint hinge. However, this benefit in actual cases under non-unidirectional loading should be studied since transverse beams are cracked.

- The nominal horizontal joint shear stress was between $0.15f'_c$ and $0.17f'_c$ [Megget-74].

Townsend and Hanson (1977) to study the function of column axial forces on the performance of the joint provided research on 22 RC beam-column exterior joints which were tested under column different axial forces such as no column load, $0.15f'_cA_g$ compression load, and $0.25f'_cA_g$ tension load. The important findings were:

- Increasing in column tension load leads to decrease moment capacity more rapidly. That means the specimens with tension column loads present a faster rate of concrete deterioration in joint panel zone than the others with compressive loads or without loads [Townsend-77]

Uzumeri (1977) performed research on eight specimens subjected to slow lateral cyclic loads and different column axial compression loads. The specimens had variable amount, size, and mechanical characteristic of joint reinforcements with and without transverse beams. The considerable conclusions were:

- The loading history does not affect the strength but seriously affects the stiffness of beam-column subassemblies.

- The truss analogy of 45 degree does not predict the performance of joints with transverse reinforcements.

- The mechanical characteristic of joint reinforcements and anchorage of beam longitudinal reinforcements provided at joints have significant effect on joint confinement and energy dissipation capacity of beams respectively.

- In three exterior joints subjected to constant high axial column load, $0.45f'_cA_g$, although the high axial compression helped to system at the early stages of lateral loading had destructive effect at the latter stages.

- Tests of corner and exterior joint specimens which were not joint reinforced depicted that cyclic loads after bond loss led to large deformations in the concrete and then splitting along column bars and anchorage failure of the beam longitudinal reinforcements. The beam remained undamaged while the joint rapidly deteriorated through increasing imposed displacements. The joints were able to provide 92% to 98% of the nominal moment strength of beams and were unable to sustain the anchorage of the beam bars in cycles subsequent to this load level [Uzumeri -77].

Ehsani and Wight (1985) to study the function of slabs and transverse beams as well as joint transverse reinforcement on joint behaviour performed research on six RC bream-column exterior joint specimens with transverse beams and slab which were subjected to inelastic cyclic loading. The major consequences were:

- The formation of flexural hinges outside of the joint leads to a more stable behaviour than those formed in the joint. Obviously, column hinges may cause structural instability.

- Contribution of slab reinforcements reduces the flexural strength ratio M_R of the joint considerably and they must be considered effective over a region at least equal to the

width of the beam on each side of it and to insure formation of flexural hinge in beams it is recommended that M_R should be no less than 1.4.

- Transverse beams help eliminate beam bar pullout and improve significantly improve the joint performance.

- The joint shear stress, v_{jh} , not more than $1.0\sqrt{f'_c}$ MPa can reduce excessive joint damage, column bars slippage, and beam bars pullout. However, the specimens with minor slippage and bar pullout in the later cycles of loading depict a very good overall performance therefore it is not needed to eliminate these problems completely.

- Transverse reinforcement of joint, when combines with the conditions mentioned above regarding M_R and v_{jh} , $1.4 < M_R$ and $v_{jh} \leq 1.0\sqrt{f'_c}$, does enhance the joint behaviour [Ehsani-85-1], [Ehsani-85-2].

Durrani and Zerbe (1987) performed research on six exterior beam-column joints subjected to simulated earthquake loads. The specimens comprised four cases with slab and transverse beams, one case with transverse beams but no slab, and one case without slab and transverse beams. The considerable findings were:

- Specimens with slab and transverse beams show 70% increasing in the negative flexural capacity of beams.

- The transverse beams are effective in confining the joint until they are cracked by torsion. Therefore, they may not be relied upon for confining the joint when the cracking of transverse beams is expected [Durrani-87].

Pantazopoulou and Bonacci (1992) provided investigate on the mechanics of beam-column joints in laterally loaded frame structures and presented the formulation to establish compatibility of strains and stress equilibrium. The significant results were:

- Shear strength of a joint depends on the usable compressive strength of concrete, which decreases with increasing principal tensile strain.

- Joint shear strength could decrease with increasing column axial force.

- Joint capacity could be limited by bond failure, crushing along the principal diagonal (either before or after joint reinforcement yield), and yielding of vertical reinforcement after joint reinforcement yield [Pantazopoulou-92].

Clyde et al. (2000) provided research on four exterior beam-column joints, built based on provisions in 1964 with the same dimensions and detailing and without joint transverse reinforcement, subjected to quasi-static cyclic loading. The specimens were tested under two column axial compressive forces of $0.1f'_cA_g$ and $0.25f'_cA_g$. The main conclusions were:

- Maximum lateral load: The maximum lateral load in all specimens had a very slight variation thus the column axial load had not appreciably affect the strength under cyclic loading.

- Ductility: A distinct differences in ductility has been observed so that the ductility of specimens with the low column axial compression loads ($0.1f'_cA_g$) was about 1.5 times greater than the ones with the high axial loads ($0.25f'_cA_g$).

- Joint shear strength: The joint shear strength capacity of specimens subjected to low column axial compression ($0.1f'_cA_g$) were less than the ones with the high axial loads ($0.25f'_cA_g$). The maximum nominal joint shear stress of specimens under low and high loaded columns was obtained equal to $1.5\sqrt{f'_c}$ MPa and $2.24\sqrt{f'_c}$ MPa , respectively.

- Column axial compressive load: For all four specimens the column axial compressive load was reduced due to stiffness degradation and concrete cracking in the joint and column. The reduction rate was between 10 to 24 percent.

- Energy dissipation: Energy dissipation of specimens subjected to low column axial loads ($0.1f'_cA_g$) were about 20% more than the specimens with high loads ($0.25f'_cA_g$).

- Yielding of the beam longitudinal reinforcement: The initial yielding in the longitudinal reinforcement of beams in the specimens under low and high column axial compressions ($0.1f'_cA_g$ and $0.25f'_cA_g$) have been observed at drift of 0.5% to 0.6% and drift of 0.7% to 1.0%, respectively.

- Maximum joint shear strain: The specimens subjected to low and high column axial compressive loads ($0.1f'_cA_g$ and $0.25f'_cA_g$) demonstrated the maximum joint shear strain of 0.0035-0.0045 and 0.0030-0.0035 respectively [Clyde et al.-00].

Pantelides et al. (2002) carried out study on six test unit full-scale model of exterior beam-column joints, build based on the provisions in the United States before 1970 with inadequate embedment of beam longitudinal bottom bars and unreinforced joints, subjected to cyclic loads. The significant results were:

- There were two preliminary failure modes: (a) a bond slip failure mode, and (b) a joint shear failure mode. Units with the joint shear failure mode failed at the end of the test due to loss of the column axial compression capacity and the specimens with bond-slip failure mode failed at the end due to loss of lateral load capacity.

- Average joint shear strain at the peak lateral load in bond slip and joint shear failure modes are 0.0035 and 0.0033 respectively.

- The units with $0.1f'_cA_g$ column axial load that failed by joint shear mode had a 24% higher hysteretic energy dissipation compared to the unit that failed by a bond-slip mechanism. While in units with $0.25f'_cA_g$ column axial load this amount is the same for the specimens with joint shear and bond-slip failure modes.

- For specimens with bond slip failure mode and $0.1f'_cA_g$ column axial load:
  - ✓ Joint strength coefficient, ($\gamma = V_n / \sqrt{f'_c}\,.\,A_j$), was 0.43 MPa,
  - ✓ Principal joint tensile stress was 0.86 $\sqrt{f'_c}$ MPa,
- For specimens with bond slip failure mode and $0.25f'_cA_g$ column axial load:
  - ✓ Joint strength coefficient, ($\gamma = V_n / \sqrt{f'_c}\,.\,A_j$), was 0.58 MPa,
  - ✓ Principal joint tensile stress was 1.87 $\sqrt{f'_c}$ MPa,
- For specimens with joint shear failure mode and $0.1f'_cA_g$ column axial load:
  - ✓ Joint strength coefficient, ($\gamma = V_n / \sqrt{f'_c}\,.\,A_j$), were 0.84 MPa and 0.80 MPa
  - ✓ Principal joint tensile stress was 1.19 $\sqrt{f'_c}$ MPa,
- For specimens with joint shear failure mode and $0.25f'_cA_g$ column axial load:
  - ✓ Joint strength coefficient, ($\gamma = V_n / \sqrt{f'_c}\,.\,A_j$), were 0.97 MPa and 0.91 MPa
  - ✓ Principal joint tensile stress was 2.02 $\sqrt{f'_c}$ MPa, [Pantelides et al.-02].

Hegger et al. (2003) performed monotonic tests on exterior and interior beam-column joints with different details of beam reinforcement in reinforced and unreinforced joints and developed a model to predict the failure load and failure mode for exterior and interior joints. The considerable consequences were:

- The failures of the joint can be either in the beam (bending failure) or inside the joint (shear and bond failures).

- The behaviour of exterior joints is different from that of interior connections. The factors influencing the shear strength of exterior joints are the concrete compressive strength, the column reinforcement ratio, the efficiency of the beam reinforcement anchorage, the joint slenderness (ratio of beam height to column width), and amount as well as the efficiency of the joint shear reinforcement. For interior joints, the main parameters are only the concrete compressive strength and the development length of the beam reinforcement.

- Increasing joint slenderness decreases the shear strength of an exterior joint.

- The shear resistance of an exterior joint depends on the joint shear reinforcement.

- A minimum development length for the beam reinforcement passing through an interior joint is necessary to ensure that a the nominal bending moment of the beam can be reached in case of joints subjected to unbalanced moments [Hegger et al.-03].

2.2.1 Summary of results

The considerable results of the studies on the seismic behavior of substandard RC beam-column joints can be summarized as the follows:

Relevance of beam-column joint damage and collapse of frames:

- Discontinuities of positive bottom beam longitudinal reinforcements in joints lead to column side-sway/soft-story collapse mechanism.

- Joint deficiencies provide hybrid local and global failure mechanisms.

- Extreme vulnerability of exterior joints can reach collapse well before any significant damage takes place in column and beams.

- Joint shear hinge mechanisms after joint damaging with their higher local deformations can protect or delay soft-story mechanism.

Failure modes:

- Bond slip failure mode: Sliding bond failure of the beam bars in the joints from localized crushing of the concrete due to repeated inelastic cyclic deformations which failed at the end due to loss of lateral load capacity.

- Joint shear failure mode: failure at the end due to loss of the column axial compression capacity.

- Pull-out of the discontinuous beam bars in the beam-column joints: This failure results in an overall structural stiffness degradation that leads to large deformations in earthquakes.

- Spalling of the concrete cover in the exterior beam-column joints: This failure mode can lead to a column failure due to reducing axial load capacity.

Energy dissipation:

- Energy dissipation of specimens subjected to low column axial loads is more than the ones with high loads.

- The specimen with low column axial load that failed by joint shear mode has a higher hysteretic energy dissipation compared to the one that failed by a bond-slip mechanism. While in units with high column axial load this amount is the same for the specimens with joint shear and bond-slip failure modes.

- The anchorage of beam longitudinal reinforcements provided at joints has significant effect on energy dissipation capacity of beams.

The function of transverse beams:

- Transverse beams help eliminate beam bar pullout.

- The transverse beams are effective in confining the joint until they are cracked by torsion. Therefore, they may not be relied upon for confining the joint when the cracking of transverse beams is expected

The function of slab reinforcements:

- Contribution of slab reinforcements reduces the flexural strength ratio M_R of the joint considerably and they must be considered effective over a region at least equal to the width of the beam on each side of it and to insure formation of flexural hinge in beams it is recommended that M_R should be no less than 1.4.

The function of column axial forces:

- Increasing in column tension load leads to decrease moment capacity more rapidly.
- The high axial compression helps to system at the early stages of lateral loading but has destructive effect at the latter stages.
- The column axial load has not appreciably affect on the strength under cyclic loading.
- The ductility of specimen with the low column axial compression load is greater than the one with the high axial load.
- The joint shear strength capacity and principal joint tensile stress of specimen subjected to low column axial compression are less than the one with the high axial load.
- The column axial capacity is reduced due to stiffness degradation and concrete cracking in the joint and column.

The function of transverse reinforcements:

- The truss analogy of 45 degree does not predict the performance of joints with transverse reinforcements.
- Transverse reinforcement of joint, when combines with the conditions regarding M_R and ν_{jh}, $1.4 < M_R$ and $\nu_{jh} \leq 1.0\sqrt{f'_c}$, does enhance the joint behaviour
- The mechanical characteristic of joint reinforcements has significant effect on joint confinement.

The function of higher strength of reinforcements:

- Higher strength (higher yield and strain hardening) of the reinforcement than the nominal design values may result in over strength in the beam flexural capacity which may cause excessive shear stresses in the joint and lead to a brittle joint shear failure.

2.3 Retrofitting and strengthening techniques of beam-column joints

The growth in application and development of different rehabilitation methods of RC beam-column joints has led to a number of publications that present detailed studies on the principals of repair, strengthening, and retrofitting. In the following it will be chronologically represented a brief of whatever has been achieved in this field as a literature review.

2.3.1 Epoxy repair procedures

2.3.1.1 Vacuum impregnation procedure

French et al. (1990) performed research on two test series of interior RC beam-column joints which were damaged under a series of cyclic lateral loads to simulate moderate earthquake and then repaired with one of two epoxy repair techniques: pressure injection (RPI) or vacuum impregnation (RVI). Finally, repaired specimens were again subjected to the same load history. For pressure injection technique following the preparation of the damaged specimen including brushing around the cracks, forcing compressed air into the cracks, and placing small strips of tapes along each crack at approximately three locations on the sides of the beam, an about 50 mm strip quick-setting viscose epoxy was applied to the surface of all the cracks. Then the tape strips were removed and the injection began at the lowest port along each crack and continued until emerged from the highest port. The process was continued upward at each crack along the beam. For vacuum impregnation technique following the covering of the damaged specimen with a plastic mesh and a 0.3 mm polyethylene sheet to provide a path over for epoxy flow and seal the system to achieve a vacuum respectively, epoxy inlet ports were located at the bottom of each beam and base of the column repair region. Then a vacuum source was connected from the top of the repair region through a hose and three served hoses as interceptors to prevent air entering were also attached at the boundaries of the sealed region, Fig. 2.1. Finally, inlet ports were sealed and a vacuum was drawn on the system until the specimen was completely submerged. The significant results were:

- Both repair techniques worked well and proved to be an effective method to repair moderate earthquake damage.
- The repaired specimens achieved over 85% of the initial stiffness of the originally undamaged units.
- The strength and energy dissipation capacities were restored.
- The bond was restored but its deterioration was observed one half-load cycle earlier [French et al.-90].

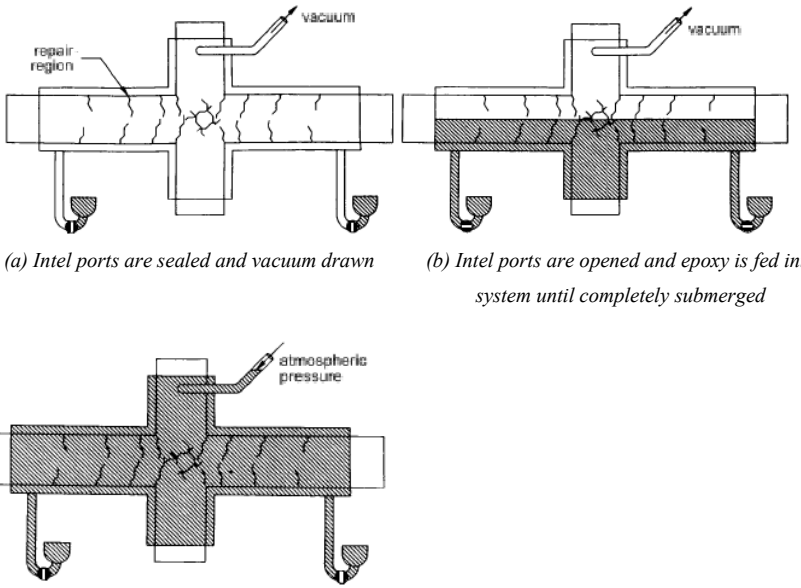

(a) Intel ports are sealed and vacuum drawn

(b) Intel ports are opened and epoxy is fed into system until completely submerged

(c) Inlet ports are closed and vacuum is released

Fig. 2.1: Vacuum impregnation procedure [French et al.-90]

2.3.1.2 Vacuum injection technique

Beres et al. (1992) provided study on lightly reinforced concrete structures. Among 34 full-scale interior and exterior beam-column specimens one of the already tested and damaged interior units was repaired by vacuum resin injection method and retested without removing the initially applied gravity load. The selected specimen was deficiently detailed so that the joint was unreinforced and discontinuous beam bottom bars had a short embedment length in the joint. Moreover, lapped splices of column reinforcements were just above the floor level and column ties were spaced widely that provided little confinement to concrete. The considerable findings were:

- Failure mode of both original and repaired specimen was pull-out the discontinuous embedded beam bars in the joint with extensive diagonal cracks.
- The repaired specimen achieved only 75% of the initial stiffness of the originally undamaged unit.
- The energy dissipation capacity was restored due to reduced rate of strength deterioration.

- The repaired specimen attained 72% of the initial shear capacity of the originally undamaged unit [Beres et al.-92].

2.3.1.3 Pressure injection technique

Lee (1976) carried out research on three half-scale exterior beam-column joint units to investigate two repairing techniques, the epoxy injection and the removal and replacement techniques. The specimens experienced two different cyclic quasi-static loadings to simulate moderate and severe earthquake loadings. The epoxy injection technique was used for the specimen subjected to the moderate earthquake and sustained only cracking. The applied technique was mainly based on the use of thin epoxy resin injected under pressure into the propagated crack system of the damaged unit. The findings of the removal and replacement technique will be explained in the next article and following are described only the important results of the epoxy injection method.

- Epoxy injected cracks in the beam remained closed and unrepaired ones opened, and new cracks formed both within and adjacent to the repaired rejoin. During retest, no additional cracking in the joint was observed and column was not cracked.
- Epoxy injection technique can effectively restore the stiffness, strength and energy dissipation capacity to a RC beam when it damaged by flexural behaviour [Lee-76].

Filiatrault and Leburn (1996) performed study on two full-scale one-way exterior beam-column joint specimens, one as a existing 1950s and 1960s joint without seismic detailing and another as a new joint with the full seismic recommendations according to the current building code related to the spacing of transverse reinforcement in the beam, column, and joint. The specimens were damaged under a series of reverse cyclic pseudo-static displacements to simulate earthquake and then repaired with an epoxy pressure injection technique. Finally, repaired specimens were again subjected to the same displacement history. The considerable results indicated that:

- The epoxy pressure injection technique effectively restored the strength, stiffness, and energy dissipation capacity of the specimens.
- For the nonseismic designed specimen, repaired unit was displayed increase in strength and energy dissipation.
- For the seismic designed specimen, repaired unit was shown pinched hysteretic loops [Filiatrault-96].

Karayannis et al. (1998) provided research on 17 exterior beam-column joint specimens covering all commonly used joint reinforcement practices to investigate the effects of joint reinforcement arrangement on the efficiency of the epoxy repair technique. Eleven of the specimens were repaired by epoxy injection and the rest, 6 units, by removal and replacement technique (explained in the next article). Specimens were initially damaged by increasing full cyclic deformation until the cycle maximum load decreased to 40% of the yield load level measured in the first cycle. The specimens exhibited the following main results under retesting in the same way:

- All repaired joints displayed equal or higher reaction load values and loading stiffness compared to the origin ones so that the increases in maximum reaction load and energy dissipation amount were 8 to 40% and 53 to 139% respectively.
- Although the failures were eventually related to the beam flexural hinge, cracking was propagated at the beam end and joint region during the first cycle.
- After repairing, the specimens with two joint crossties or intermediate column bars crossed within the joint displayed only beam flexural failure with considerable pinched hysteretic loops.
- The units with one joint crosstie showed the same failure made before and after repairing [Karayannis et al.-98].

2.3.1.4 Removal and replacement technique

Lee (1976), as described in last article, conducted also research on two exterior beam-column joint specimens subjected to the severe earthquake loading and sustained extensive damage. The specimens were repaired using the removal and replacement technique. This method includes supporting temporarily damaged system to ensure stability during repairing, removing the loose concrete, checking the reinforcement for fracture, adding reinforcement (if it is needed), forcing compressed air into the cracks and voids to cleaning, and finally filling the resulting voids with high early strength replacement material with considering achievement a good bond between the old and new concrete. In the research different replacement materials were used, epoxy-sand mortar, Duracel cement concrete, high strength quick setting concrete, and high early strength (cement type III). Then the repaired units were retested in the way as same as the original ones. The significant results can be described as:

- Removal and replacement technique can effectively restore the stiffness, strength and energy dissipation capacity to a RC beam when it damaged by flexural behaviour.

- As a replacement material high early strength (cement type III) concrete leads to a reasonable results and can be used in this technique.
- Attribution of strain-hardening step in beam bar reinforcement and higher strength repair material results to stronger repaired beams in comparison with the originals. Consequently, the joint stresses to higher level that leads to the possibility of damage moving from the beam to the unrepaired joint and column and causing loss of strength [Lee-76].

Karayannis et al. (1998), as described in last article, provided also study on repairing 6 exterior beam-column joint units sustained extensive deterioration in the joint region. The specimens with unreinforced joints and low flexural strength ratio (M_R = 0.67), exhibited this failure mode. The damaged regions were removed and then replaced by high-strength low-shrinkage cement paste. Finally, the repairing technique was completed by epoxy injection into the propagated crack system of the damaged unit. The findings showed that:

- Repairing of unreinforced joint specimens could not change their failure mode in comparison with the originals, even though the developments of strength, stiffness, and energy dissipation were observed.
- Repairing of specimens with two joint crosstie hoops displayed not only more rate of increase in strength, stiffness, and energy dissipation but also another failure mode with flexural beam hinge [Karayannis et al.-98].

2.3.1.5 Thin steel plate and pressure-injection technique

Adin et al. (1993) provided study on four full-scale joint reinforced exterior beam-column joint specimens to investigate the efficiency of a new epoxy repair technique using steel plates. The units were primarily subjected to low-level, gradually increasing cyclic loading to cause controlled damage at the joint and then thin steel plate attached, sealed, and low-pressure epoxy injected. Finally, the repaired specimens were retested as the first stage before repairing. The considerable findings were:

- The technique was effective to improve the overall performance of the specimens such as stiffness, ultimate resistance, and energy dissipation.
- The technique not only repaired the deteriorated regions but also forced plastic hinges away from the joints [Adin et al.-93].

2.3.2 Jacketing and other mechanical retrofitting techniques

2.3.2.1 Masonry block jacketing technique

Bracci et al. (1995) introduced and analysed a new method to retrofit GLD buildings through masonry units, but did not test it .Interior columns in masonry block technique are surrounded by masonry units with additional longitudinal bars within the corner cores extending continuously through the slabs and later post-tensioned, as well as wire meshes providing in the mortar joint beds to increase shear capacity. Any void space between the masonry jackets and columns is then grouted, Fig 2.2. Moreover, the shear strength, joint confinement, and development length for the bottom longitudinal beam reinforcement are increased by reinforced concrete fillets (see Detail A, Fig. 2.2). The dimensions of the filets are obtained based on the required development length of the discontinuous beam bottom bars and the desired beam hinges locations. To build a filet, at four sides of the column rectangular segments are removed to place the filet and vertical reinforcement, moreover to place horizontal reinforcement going through surrounded beams all of them are drilled. The nonlinear analysis led to the following results:

- The overall structural response and damage formation can be adequately controlled.
- Although in comparison with existing structures the natural period and base shear of the structure decreased and increased respectively the drifts and flexural strength ratios (M_R) considerably improved so that the catastrophic soft-story collapse were enforced to a more ductile beam side-sway mechanism [Bracci et al.-95-2].

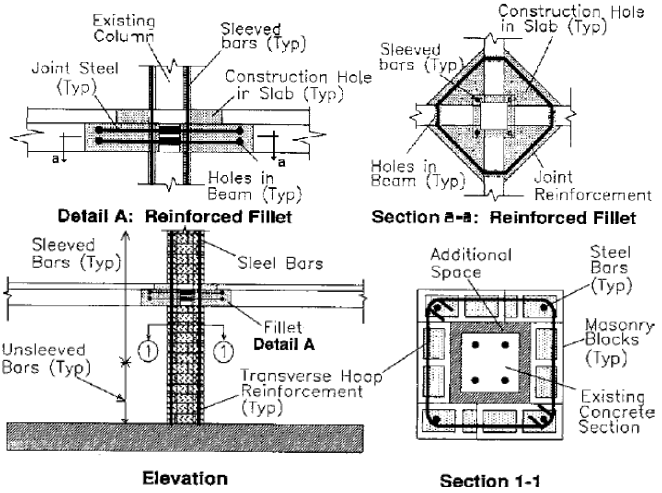

Fig. 2.2: Masonry block jacketing technique [Bracci et al.-95-2]

2.3.2.2 Partial masonry infill technique

Bracci et al. (1995) theoretically initiated and analysed also another method to upgrade GLD buildings by masonry blocks. In partial masonry infill technique, partial walls are constructed on each side of columns and reinforced by post-tensioned vertical bars extending continuously through the slabs as shown in Fig. 2.3. Furthermore, transverse hoop reinforcement as well as cross ties are performed in the mortar joint beds. The extension of partial masonry infill on each column sides is governed by the required development length of the discontinuous bottom beam bars. To protect the system from joint failure, additional transverse reinforcement is anticipated that wrap the joints through drilled holes in beams.

The final results of analysis showed that:

- The overall analysis outcomes were the same results of the masonry block jacketing method, however, the structural responses were not the same so that for instance by this method drift amounts became smaller and flexural strength ratios dramatically increased [Bracci et al.-95-2].

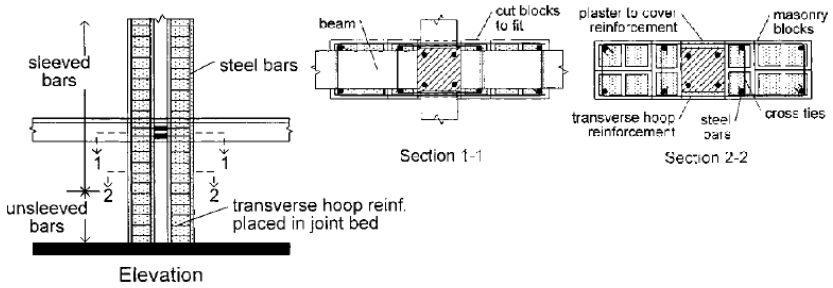

Fig. 2.3: Partial masonry infill technique [Bracci et al.-95-2]

2.3.2.3 Prestressed concrete jacketing technique

Bracci et al. (1995) evaluated analytically and experimentally the application of a retrofitting method that was first studied by Choudhuri et al. (1992) on a interior beam-column joint with slab previously experimented by Aycardi et al. (1992) without retrofitting. The method, Fig. 2.4, consists of strengthening existing columns through high-strength concrete jacketing with

additional transverse and post-tensioned reinforcement, and enhancing unreinforced beam-column joint regions by performing a reinforced concrete filets (as described in masonry block jacketing technique) to enforcing beam side-sway mechanism. To avoiding the transmission of considerably forces into the weak foundation and don't altering the desired strength at that level, the added column longitudinal reinforcement is not anchored into the foundation. Added transverse reinforcement provides additional rotational ductility and enhances shear capacity. The presented retrofitting technique was experimentally studied on one-third scale threes story model RC frame building by shaking table. It was obtained that:

- The seismic vulnerability of GLD frames (soft-story mechanism) may be effectively enhanced and changed into the failure mode of beam-sidesway mechanism with acceptable story deformation levels by this retrofitting technique.
- In GLD frame systems, moderate to severe earthquakes leads to significant sidesway deformations but minor quakes can be sustained without considerable damage. Their seismic response can be predicted by reasonable awareness of the component behavior [Bracci et al.-95-2], [Choudhuri et al.-92], [Aycardi et al.-92].

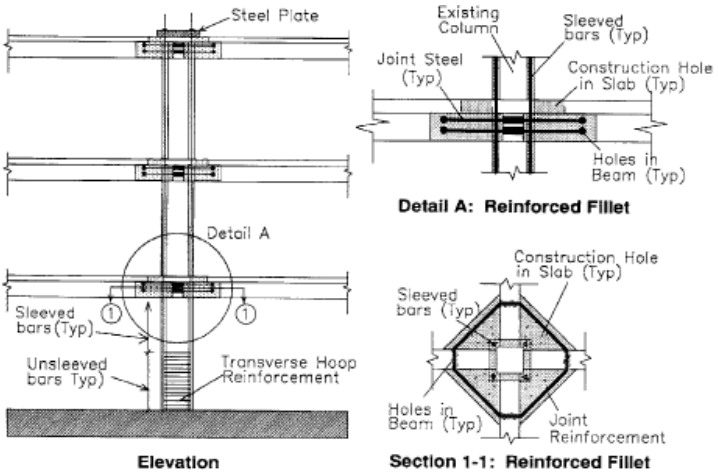

Fig. 2.4: Prestressed concrete jacketing technique [Bracci et al.-95-2]

2.3.2.4 Concrete jacketing

Corazao and Durrani (1989), for evaluation and improvement techniques of repairing and strengthening beam-column joints damaged by earthquakes, performed an experimental study on single beam-column joints and multiple joints (two-bay) subassemblies, each consisting of two exterior and one interior joint with some including a floor slab were subjected to cyclic displacements. The specimens were repaired through replacement of damaged concrete and enlargement of section. Finally, the repaired specimens were again subjected to the same displacement history as that used in the original test. The findings showed that:

- Single beam-column joint specimens retrofitted by concrete jacketing exhibited increased strength, stiffness, and energy dissipation and moreover desirable failure mechanism, except for the plane exterior joint that absorbed less energy after strengthening.
- The retrofitting of multiple joint specimens was not effective to improve their behaviour.
- Load transmitting between beams and columns is as important as column jacketing in repair and retrofit of RC frames [Corazao -89].

Alcocer and Jirsa (1993) carried out research on four large-scale interior beam-column joint specimens designed according to the design practice of the 1950s and subjected to severe bidirectional cyclic loads. The units were retrofitted by jacketing the columns only, or both the columns and beams. The method comprised encasing the existing column and joint region in new concrete with additional transverse and longitudinal reinforcement overpassing continuously through joint due to opening the slab at the column corners, Fig 2.5. The joint confinement was provided by welding a structural steel cage around the joint. The first unit was tested to cause severe column damage (original specimen) and then repaired by jacketing the column with bundled longitudinal reinforcement and retested. The second specimen was undamaged prior to jacketing like the first one with bundled bars, the third one was jacketed using distributed bars around the column, and finally the forth unit was strengthened by column jacketing with distributed longitudinal reinforcement and jacketed beams. The main conclusions were:

- The confinement cage satisfactorily prevented spalling of the concrete core.
- ACI 352 recommendations can be used in design of rehabilitated joints using this technique.

- While flexural strength ratios (M_R) in both of bundled and distributed longitudinal reinforcement cases were greater than 2.3, the specimens were displayed good bond behavior. With lower ratios, the results may be not as favorable.
- Ideally, column and beam bars in the existing subassemblies and jackets should satisfy the ACI 352 criterion for bar development.
- For the specimens retrofitted with column jackets only the critical section was within the jacket, while in units strengthened through column and beam jacketing the failure region moved outside the cage [Alcocer -93].

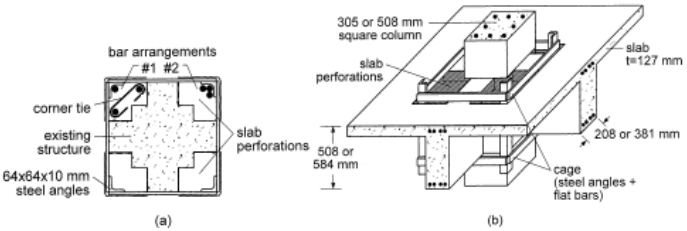

Fig. 2.4: Concrete jacketing technique [Alcocer -93] (reprinted from [Engindeniz et al.-05])

Shih et al. (2001) performed an experimental study on 11 beam-column joint specimens with stubs as transverse beams in two perpendicular directions, interior joint, or one stub in one perpendicular direction, perimeter joint, to investigate the strengthening efficiency of concrete jacketing and proposed improving details. Totally 17 tests were performed in three categories: original, repaired, and retrofitted, with the eleven constructed specimens. Each group comprised two series with different designed failure modes, flexural failure in column hinge, shear failure in joint region, and having strong beam-weak column even after repairing or retrofitting. Repair procedure included of: 1. Removing loosen concrete, 2. Hols drilling in beams for joint ties, 3. Injecting epoxy into the cracks, 4. Rebar planting or additional reinforcement, if need, and 5. Forming and concrete pouring. The considerable results were:

- RC frames with deficient column and joint details can be repaired or retrofitted by concrete jacket with a performance of both the lateral strength and stiffness and strong column-weak beam behaviour due to the enlargement of column cross-section, if sufficient joint shear ties for shear are provided.
- The column jacketing can extensively reduce the yield displacement.

- The amount of previous damage in original unit has a little influence in lateral stiffness and ultimate strength, but affects the post-peak behaviour so that the sooner deterioration is occurred [Shih et al.-01].

Wang and HSU (2009) prepared experimentally research on 7 one-way nonductile interior beam-column joint specimens subjected to quasistatic cyclic loading to investigate the strengthening of beam-column joints only by RC jackets encasing as-built columns without new joint shear hoops and dowel anchors between old and new concrete. The main results were:

- The RC jacketing is able to efficiently rehabilitate nonductile frames with very poor joint details.
- The joint shear strength of the retrofitted units with joint shear failure modes were less likely to be affected by joint shear slippage than by the axial column loads so that the generating of joint shear degradation depended on the axial loading of the columns not the concrete interfacial slippage in the joint region.
- The strengthened specimens designing to a ductile behaviour with the failure mode of strong column and weak beam were showed the main flexural cracks were formed at beams adjacent to the jacketed column faces at the end of test [Wang-09].

2.3.2.5 Concrete jacketing using HPFRC

Shannag and Alhassan (2005) performed study on ten 1/3-scale interior GLD beam-column joint specimens subjected to reverse cyclic loading without column axial load or with low levels of axial loads to investigate the efficiency of the retrofitting method through jacket of high-performance fiber-reinforced concrete (HPFRC). The HFRC matrix provided an average strength in tension and compression of 9 and 75 MPa, respectively, and contained 2% by volume of short brass-coated and hooked steel fibers. The jackets were 25 mm in thickness all around the joint-column region and extended 100 mm from the original joint face along the beam from both sides. The considerable results of the test were:

- Strengthened specimens attained higher load levels, larger energy dissipation, and slower stiffness degradation.
- Whereas the excessive damage of joint regions of the original units led to failure, the upgraded ones failed as result of plastic hinges in the beams.
- Hooked fibers provided a better confinement and more ductility to the joint region compared with the brass-coated ones and the jackets containing brass-coated fibers

completely transferred the brittle failure mode to a ductile one only at a higher level of column axial loads.

- Below 25% of the column capacity (low column axial load), the performance of the joints improved as the level of column axial load increased [Shannag-05].

2.3.2.6 Concrete jacketing using UNIDO strengthening technique

Tsonos (1999) conducted his experimentally research on two exterior beam-column joint specimens designing as typical seismically designed structures in Greece from the late 1960's to the early 1980's to exam the effectiveness of the United Nations Industrial Development Organization (UNIDO) manual guidelines for repair and strengthening of beam-column joints damaged by severe earthquakes. The specimens were damaged by cyclic loads simulating severe earthquake, then repaired and strengthened by jacketing according to UNIDO manual guidelines, and finally, retested by the same loading history that used in the original test. Strengthening involved encasing the joint and critical regions of the columns with a nonshrink, rhinoplastic, flowable, and nonsegregating high strength cement grout jacket reinforced with collar inclined stirrup bars bent diagonally across the joint core, additional longitudinal reinforcement placed at each corner of the jacket and welded to the existing column bars, and closely spaced transverse ties around the jacket additional longitudinal bars, Fig. 2.5. To develop adequate bond of beam bars, new stubs at the beam line opposite the beam sides were constructed to anchor beam end reinforcement extended by welding new additional reinforcement to the existing anchored beam bars. The significant conclusions were:

- Strengthened specimens displayed higher strength, greater stiffness, and better energy dissipation capacity than the original units.
- The retrofitted specimens failed in flexure and depicted high strength, without any appreciable deterioration in post-peak loads [Tsonos-99].

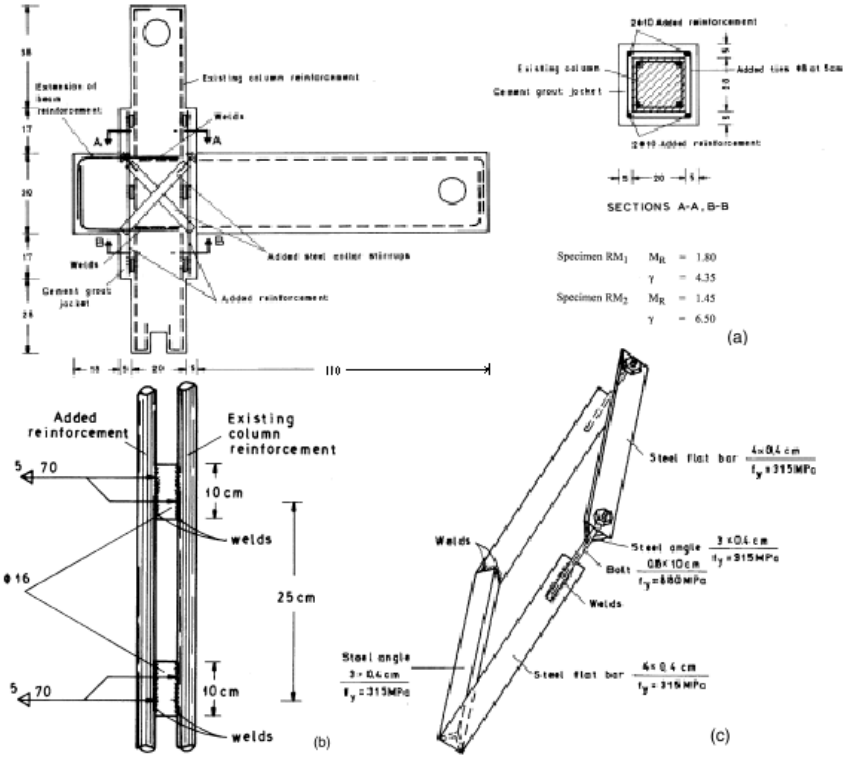

Fig. 2.5: a) Concrete jacketing using UNIDO strengthening technique; b) welding of new reinforcement to existing column reinforcement; c) details of steel collar stirrup. [Tsonos-99]

2.3.2.7 Steel jacketing

Corazao and Durrani (1989) carried out research on strengthened one exterior and one interior beam-column joint specimen including floor slab subjected to cyclic displacements. Retrofitting comprised bolting and epoxy-bonding external 6 mm-thick steel plates on each column face, welding steel angles to the plates, and enlarging the joint region with a reinforced concrete filet, Fig. 2.6. For reinforcing concrete filets, #3 bended bars were planted into the beam sides as dowels and overlapped to provide joint hoops. The test of strengthened specimens showed that:

- Due to slippage between concrete and steel plates, interior beam-column joint specimen had more improvement in energy dissipation compared to the other one.

- Improvement of strength, initial stiffness, and energy dissipation in interior specimen was more than exterior one.
- In both strengthened specimens, beam failure at the end of RC filet was observed [Corazao -89].

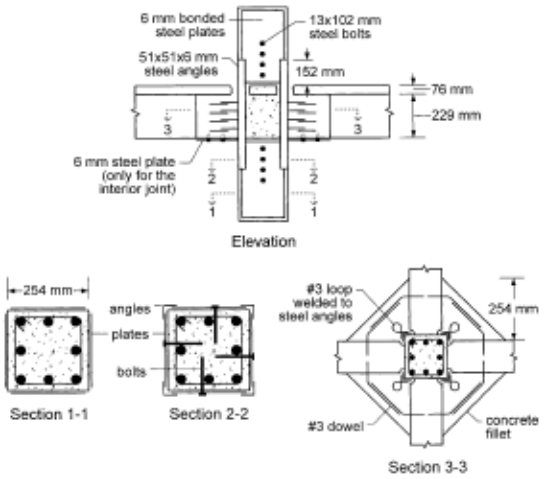

Fig. 2.4: Steel jacketing technique [Corazao -89]
(reprinted from [Engindeniz et al.-05])

Beres et al. (1992) conducted experimental study on strengthening of one interior and one exterior full-scale one-way beam-column joint specimens with discontinuous beam bottom reinforcement through external steel plate and steel section arrangements. For testing the specimens, cyclic loading were imposed. The retrofit of interior joint was intended for preventing pull-out of the beam bottom reinforcement. Whereas the rehabilitate of exterior joint was planned to preventing splice failure in the column, spalling of the concrete cover of the joint, and pull-out of the beam bottom bars. To prevent pull-out of the beam bottom reinforcement in the interior joint, two steel channel sections were bolted to the underside of the beams and connected to each other by two steel tie-bars running alongside the column, Fig. 2.5(a). The exterior joint was strengthened by external steel plates placing along the opposite faces of the upper and lower columns. The opposite faces plates were connected to each other by threaded rods, Fig 2.5(b). The test results showed that:

- This retrofitting method was proposed for zones of moderate seismicity.

- In interior retrofitted joint, the resulting damage was transferred from the embedment zone to elsewhere in the joint panel. The increasing of strength and stiffness were 10 to 20% and no considerable change in energy absorption was observed.
- In exterior strengthened joint, the resulting plastic hinge formed in the joint panel zone near the top of the beam and followed by the pullout of the beam bottom reinforcement. However, the extending of cracks into the column bar splice region was prevented. The increasing of strength and stiffness were 33% and 12%, respectively, and considerable increase in energy absorption was observed in the final stages of loading [Beres et al.-92].

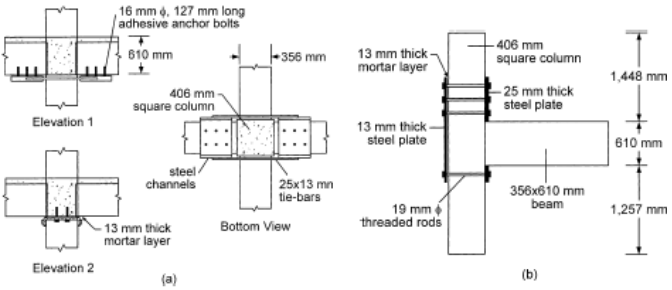

Fig. 2.5: Steel jacketing technique [Beres et al.-92]
(reprinted from [Engindeniz et al.-05])

Biddah et al. (1997) performed research on six 1/3-scale exterior beam-column joint specimens subjected to severe cyclic loading to study the efficiency of upgrading by a corrugated steel jacket. The investigated test parameters included the amount of joint and column transverse reinforcement, sufficient or insufficient embedment length of beam bottom bars in joints, corrugated steel sheet thickness (2.8 mm or 3.5 mm), and jacketing of column only or of both column and beam. Four of specimens with different deficiencies were retrofitted by variety of corrugated steel jacket arrangements and the rest, 2 units, were tested as reference units without any retrofitting, one represented a nonductile exterior joint of an existing frame and another characterized a ductile designed joint (based on Canadian concrete design code, CSA A23.3-94). To confine the critical regions of the specimens, corrugated steel casing was welded around the subassemblies and then the gap between concrete face and steel sheet was grouted, Fig. 2.6. The research led to the following conclusions:

- The corrugated steel jacketing method was found to be an effective system of upgrading as it increased the joint shear strength and energy dissipation capacity.

- The code-designed specimen sustained a higher applied displacement as compared to the existing joint with brittle joint shear failure.
- Beam jacketing prevented the shear failure in the beam and instead flexural failure occurred. However, beam shear capacity must be sufficient to develop beam flexural hinge. In using beam jacketing, a gap (in this test 20 mm) should be provided at the critical section of the column face to minimize flexural strength enhancement for beams [Biddah et al.-97].

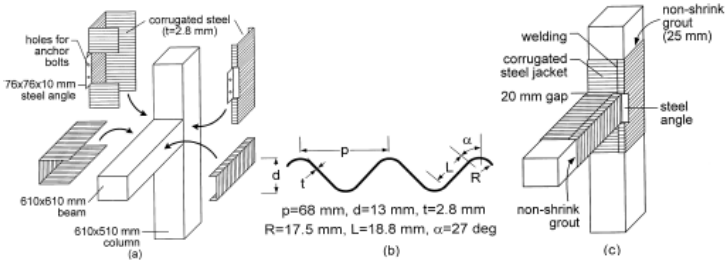

Fig. 2.6: Corrugated Steel jacketing technique [Biddah et al.-97]

2.3.2.8 Diagonal steel bracing methods

Pampanin et al. (2006) provided study on four 2/3-scale pre-1970 designed exterior beam-column joint specimens in a 2D configuration subjected to quasi-static cyclic lateral loading along with variable imposed column axial loading to evaluate the efficiency of proposed retrofitting system by diagonal metallic haunch. Plain round bars with end hook anchorage of beam longitudinal bars and one single stirrup in the joint were used. Three of specimens were retrofitted by proposed system and the rest, one unit, was tested as a reference unit without retrofitting. The design of the haunch retrofit system was carried out to protecting the joint region from excessive damage and forcing a plastic hinge in the beam. The haunch system consisted of elastic or yielding steel bar elements were diagonally connected to the concrete members (column and beam) through either a hinged base or a welded base. The considerable findings of the test were:

- The retrofitted specimens exhibited an enhanced response when compared to the non-retrofitted unit so that damage to the joint was eliminated and a flexural plastic hinge formed in the beam. The lateral strength was increased and a stable hysteretic behavior and enhanced energy dissipation capacity was observed.

- The yielding of the haunch element did not considerably enhance the performance of the proposed upgrading method but protecting the joint panel and forming a flexural hinge in the beam were obtained [Pampanin et al.-06].

Said and Nehdi (2006) carried out a test on two full-scale one-way exterior beam-column joint specimens subjected to reverse cyclic load to assess the efficiency of recommended upgrading method by local steel bracing. Two specimens representing a standard designed joint to satisfy both CSA A23.3-94 (1994) and ACI 352R-02 (2002), and a deficient designed joint according to the pre-1970s codes which had been constructed for retrofitting were tested and compared to a deficient specimen tested in the literature [El-Amoury-02]. The local bracing elements consisted of steel H sections were diagonally connected to the columns and beam by U formed steel plates and threaded rods overpassing through the drilled holes in the concrete members. The test results showed that:

- The retrofitted specimen exhibited improved performance compared to that of a baseline non-rehabilitated specimen and achieved adequate ductility requirements.
- Brittle joint shear failure and beam bottom bars slippage as well as shear failure of the subassemblages were delayed.
- The beam plastic hinge was moved away from the column's face.
- The brace members did not act as energy dissipation elements and remained elastic [Said-08].

2.3.2.9 Planar joint expansion

Chaimahawan and Pimanmas (2009) conducted research on three half-scale sub-standard interior beam-column joint specimens subjected to reverse cyclic loads to investigate efficiency of retrofitting through planar joint expansion. To simulate gravity load on column, the axial load of 12.5% column axial capacity was applied by vertical prestressing. Two of specimens were retrofitted by triangular and square joint expansion and another one was tested as a reference unit without upgrading. In retrofitted specimen with square expansion, reinforcing and concrete casting of expanded parts were carried out together with beam and column. On the other hand, in specimen retrofitted by triangular expansion, the prototype unit was prepared first, and then the joint expansion was fabricated afterward. The construction stages of triangular expansion included drilling column and beam, inserting dowel bars and injection epoxy into the drilled hols, completing reinforcement of expanded joint, molding and concrete casting, and finally, filling the gap between bottom face of the beam and upper

face of the bottom expansion joint by non-shrinkage grout, Fig 2.7. The significant conclusions of the test were:

- Retrofitting non-standard joints by this method is effective to increase stiffness, ultimate strength, energy dissipation and ductility.
- The plastic hinge transferred to the edge of joint expansion and specimens failed with mixed beam bending and shear failure mode.
- Nearly the same results of triangular and rectangular joint expansion were observed. However, triangular expansion was more effective to delay spalling of concrete and buckling of bars at compression zone in beam.
- The post-fabricated joint expansion specimen performed equally well compared with the pre-fabricated one [Chaimahawan-09].

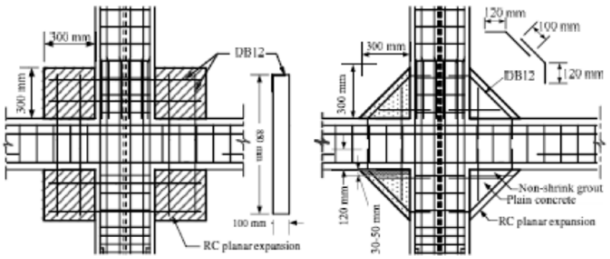

(a) *(b)*

Fig. 2.7: Planar joint expansion: a) Rectangular expansion, b) Triangular expansion [Chaimahawan-09]

2.3.3 Utilization of fiber-reinforced polymer composites, FRP

The upgrading of existing RC structures using fiber-reinforced polymer (FRP) composites is a subject which has grown very popular, due to the need to retrofitting and well-known advantages of FRP composites, such as high strength-weight ratios and good corrosion resistance, in recent years. The composites in the different forms, epoxy-bonded flexible sheets, shop manufactured strips, or near-surface-mounted (NSM) rods, and different fabric materials, such as carbon (CFRP), glass (GFRP), Kevlar, and steel (SRP), are used. Composite laminates are externally bonded to a concrete element to provide concrete confinement for ductility enhancing and raise flexural and shear strength [Alkhrdhaji et al.-99], and near-surface mounted (NSM) rods are applied to increase

flexural and shear strength of structural concrete elements [De Lorenzis et al.-00]. Since 1998, research attempts on retrofitting of beam-column joints have been focused on the use of these composites. To retrofitting a beam-column joint, composite sheets are wrapped in different directions and layers around the joints, columns, and beams close to the joint region. At present, except for a few researches, nearly the all literature in this field is based on simplified two-dimensional tests. In the following, summery of existing researches on FRP strengthening of RC beam-column joints will be presented.

2.3.3.1 Utilization of carbon-fiber-reinforced polymer, CFRP

Geng et al. (1998) prepared research on 19 one-way beam-column joint specimens of full-scale and ¼- scale subjected to cyclic loading for ductility retrofitting and monotonic loading for developing upgrading of joints containing insufficient development length. CFRP tow sheets were wrapped around the column near the joint for ductility retrofitting, and longitudinally bonded to and/or wrapped around the column close to the joint with a set of steel angles and rods for development upgrading, Fig. 2.8. The considerable conclusions were:

- Externally bonded CFRP sheets could effectively improve both the ductility and strength of the joints containing insufficient bar development.
- Ductility upgrading and development retrofitting exhibited 24-35% and 154-172% increase in strength, respectively [Geng et al.-98].

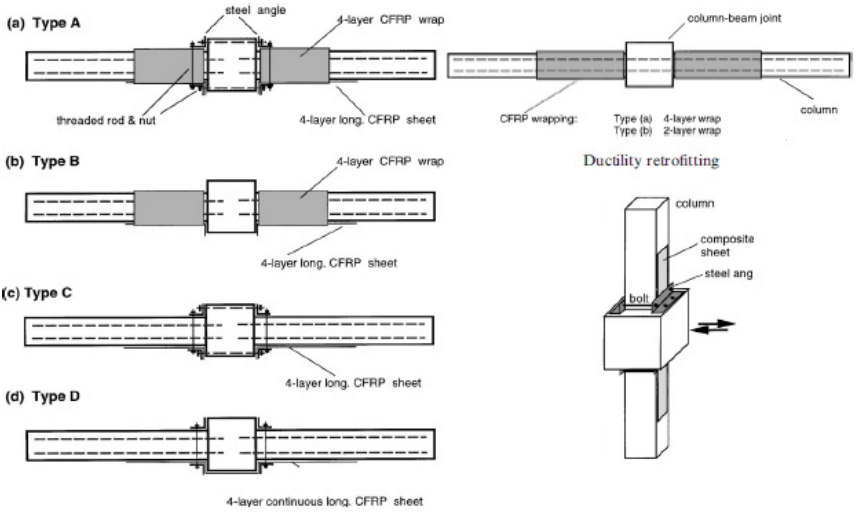

Fig. 2.8: CFRP ductility and development retrofitting of beam-column join [Gen et al.-98]

Mosallam (2000) prepared study on six half-scale one-way sub-standard interior beam-column joint specimens subjected to cyclic loading to evaluate the repair and retrofit of joints by epoxy injection as well as carbon-epoxy and E-glass-epoxy quasi-isotropic laminates. Two specimens were tested as reference units, two repairable damaged specimens were retested after repairing with epoxy injection as well as carbon or E-glass quasi-isotropic composites, and finally two other undamaged specimens were retrofitted with both of the composites. The test results indicated that:

- A considerable increase in stiffness, strength, and ductility was observed.
- The ductility and strength of repaired specimens with E-glass-epoxy quasi-isotropic composites were increased up to 42 and 53%, respectively, as compared to the reference unit.
- Retrofitting of undamaged specimens by E-glass-epoxy laminates displayed an increase of about 20% in stiffness.
- Inherent lower stiffness of E-glass-epoxy composites led to enhance the ductility of both repaired and retrofitted units.
- If the ductility is the major criterion, E-glass composites and whenever strength is important parameter, Carbon composites are recommended.
- In all tests, composite-concrete bonded interface failure mechanism was observed [Mosallam-00].

Antonopoulos and Triantafillou (2003) performed study on 18 poorly detailed 2/3-scale exterior beam-column joint specimens subjected to cyclic loading to investigate the role of various parameters on the effectiveness of CFRP or GFRP strengthening of joints. Sixteen of the specimens were not joint- reinforced, and the other two units had only one stirrup in the joint. Three of the 16 non joint-reinforced specimens had a transverse beam only in one side to evaluate the efficiency of transverse beams on the joint confinement. All specimens which were designed to have a joint shear deficiency were strengthened with carbon and glass fiber composite sheets in different strengthening alternative forms, Fig. 2.9. The main conclusions are summarized as:

- Debonding dominated the behavior of external FRP upgrading.
- Flexible sheets were more effective than strips.
- Both the strength and the dissipated energy increased significantly with the number of FRP layers but due to debonding that was not proportionally.
- The effectiveness of FRP area fraction in column was rather limited compared to the beam.
- Mechanical anchorage or transverse wrapping of longitudinal FRP sheets increased effectiveness of FRP upgrading.
- High axial column load had a quiet positive effect on the shear capacity of the FRP strengthened joint.
- In damaged FRP strengthened joint, FRP sheets were less effective in term of energy dissipation as opposed to strength increase.
- With the same axial rigidity, glass fiber sheets proved marginally more effective than carbon fiber sheets. In terms of strength, glass fibers proved only slightly more effective than carbon but in terms of energy dissipation displayed more effective performance (30% in carbon versus 40% in glass).
- The effectiveness of FRP strengthening increased as the joint transverse reinforcement decreased.
- The effectiveness of FRP sheets in specimens with a transverse beam was reduced compared to the planar joints, but not so much for the energy dissipation as for the strength [Antonopoulos -03].

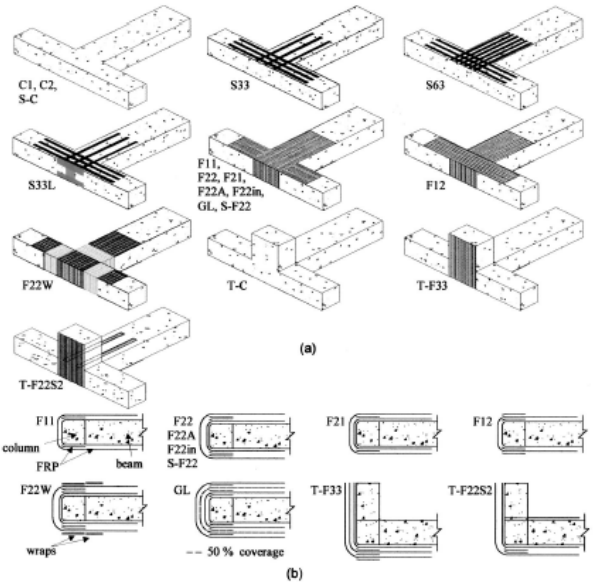

Fig. 2.9: a) Description of specimens and strengthening alternatives; b) layout of FRP layers [Antonopoulos -03]

D'Ayala et al. (2003) performed study on one-way GLD interior beam-column joint specimens with two different geometry configurations and various strengthening arrangements by externally bonded CFRP fabrics. The specimens were reinforced by smooth bars. Two geometry configurations, one governed by beam failure (weak beam: WB) and another dominated by column failure (strong beam: SB) were considered. One of the strengthening configurations was designed for WB consisted of L form corner FRP strips at the beam-column junction with beam and column wraps to increase the moment capacity of the beam. The other two strengthening configurations, first consisted of thin rectangular strips were wrapped diagonally around the joint core with narrow L form strips positioned at the beam-column junction to improve the shear capacity of the joint and the bending capacity of the beam, and second comprised similarly diagonal strips without L form strips at the beam-column junction and instead wide vertical strips was glued to the column sides before applying the diagonal stripping were designed for SB specimens. The test carried out under reversed cyclic loading with constant vertical load for column. The results showed that:

- The maximum bending moments of the column and beam for control specimens, due to efficiency of smooth bars on bond degradation and the premature failure of the joint

core in the SB case were approximately 20% and 35% less than the section analysis predicted for SB and WB units, respectively.

- CFRP strengthening was more effective as a means of retrofitting than as a means of repair of the damaged specimens. However, for repairing the damaged units FRP wrapping was adequate than removal of only loose concrete and replacement with grout.
- For CFRP strengthening of strong-beam weak-column (SB) arrangements brittle failure of the joint core could shift towards flexural hinging at the beam-column interface.
- CFRP diagonal wrapping of the joint was more successful compared to the orthogonal wrapping.
- For weak-beam (WB) configurations the application of strengthening did not alter the initial failure mode and the final failure mode was in bending of the beam with partial failure of the FRP in tension [D'Ayala et al.-03].

Biddah and Ghobarah (2004) conducted research on nine one-way medium scale exterior beam-column joint specimens subjected simultaneously to a static load at the beam tip and constant column axial load of $0.2f'_cA_g$ to obtain an upgrading method using prefabricated CFRP L-shaped plates to retrofit the inadequate anchorage of beam bottom bars at joints. The prefabricated L-shaped CFRP plates were passed through the drilled holes in the column and glued in the column hole and to the top beam soffit by epoxy. The results of three retrofitted deficient specimens with reference ones, three sub-standards and three standard specimens, were compared and following conclusions were obtained:

- The feasibility of using proposed method to increase the load carrying capacity and the corresponding stiffness with limited ductility was indicated.
- The CFRP plates have not reached their full capacity due to debonding.
- The joint shear strength should be checked before strengthening the beams to prevent increase the shear demand on the joint [Biddah-04].

Prota et al. (2004) carried out an experimental study on eleven one-way GLD interior beam-column joint specimens subjected to cyclic loads to investigate the efficiency of column axial load level, the type of FRP reinforcement (laminate or bars), and the amount of FRP reinforcement applied on joint upgrading. For retrofitting specimens, combination of externally bonded CFRP laminates and carbon near-surface-mounted (NSM) bars were used.

Three different axial loads equal to $0.1f'_cA_g$, $0.2f'_cA_g$, and $0.3f'_cA_g$ were selected for the columns. The experimental pointed out the following considerable results:

- Strengthening the column could improve the behavior of the subassemblage, but, due to the brittle failure of the joint, it did not provide much in terms of ductility.
- The retrofitting of the joint zone increased its deformability and also provided a significant contribution to the ductility of the system.
- In the direction perpendicular to the beam axis, the termination of the laminate at the column joint interface to account for the presence of the floor system could conclude a shear failure at the column joint interface.
- For different axial load levels, shear failure of the joint occurred at very similar values of the column shear. Therefore column axial load level has an effective influence on the global behavior of the system [Prota et al.-04].

Mukherjee and Joshi (2005) conducted research on two different types of small-scale one-way interior beam-column joint specimens subjected simultaneously to beam cyclic and column monotonic loading to study the efficiency of adequate and deficient bond of reinforcements at the joints and their repairing and upgrading by different arrangements of CFRP and GFRP composites. The damaged control specimens were repaired, retrofitted and again retested. Epoxy and sand mortar, and wrapped CFRP plates were used for repairing and retrofitting, respectively, Fig. 2-10). Considerable results were:

- Due to the higher stiffness of carbon than of glass, the glass reinforced specimens had much higher displacement at yield than the carbon reinforced.
- The energy dissipation of the upgraded specimens followed closely that of the control specimens. The carbon specimens exhibited higher energy absorption than the glass specimens. Energy dissipation capacity could be increased with the use of small amount of composites.
- CFRP strengthened specimens displayed stiffer behavior than GFRP upgraded ones.
- The strengthening of repaired specimens showed that FRP restored the original strength and enhanced significantly the yield load, initial stiffness and energy dissipation capacity [Mukherjee-05].

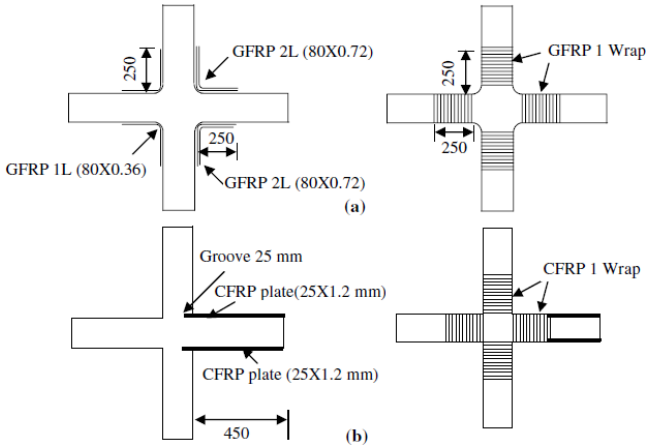

Fig. 2.10: a) CFRP or GFRP strengthening; b) Strengthening of repaired specimens [Mukherjee-05]

Ghobarah and El-Amoury (2005) performed study on six substandard one-way exterior beam-column joint subjected to cyclic loading and column axial load of $0.2f'_cA_g$ to develop effective rehabilitation system to upgrade the resistance to bond –slip of the beam bottom bars and to upgrade the shear strength of joints. The first three specimens had joint reinforcement with joint anchorage-deficiency; therefore two of them were retrofitted by using CFRP sheets attached to the beam bottom face (T-B10, T-B11, and T-B12). The second three units had joint shear/anchorage-deficiency with no joint reinforcement; therefore two of them were strengthened by GFRP jackets of the joint core and steel roads or plates (T-SB3, T-SB7, and T-SB8). Several retrofitting schemes using composite materials and steel elements were proposed to improve the seismic performance of the specimens, Fig. 2.11. The experiment pointed out the following significant results:

- Joint shear reinforcement is needed not only to avoid joint shear failure but also to restore concrete integrity in the anchorage zone, so that the capacity of the beam reinforcement can be fully developed.
- A GFRP jacket of joint core can effectively provide confinement and shear strength to the joints with shear deficiency.
- Brittle shear failure was prevented, and instead ductile beam flexural hinging was developed.
- CFRP sheets glued to the beam bottom face with adequate anchorage systems were effective in replacing the anchorage-deficiency of beam reinforcement.

- The simple method of external steel tie-rods welded to the existing deficient beam bars effectively improved the anchorage conditions and fully developed the tensile strength of these bars.
- The proposed rehabilitation methods significantly increased the joint energy dissipation and reduced the joint stiffness degradation [Ghobarah-05].

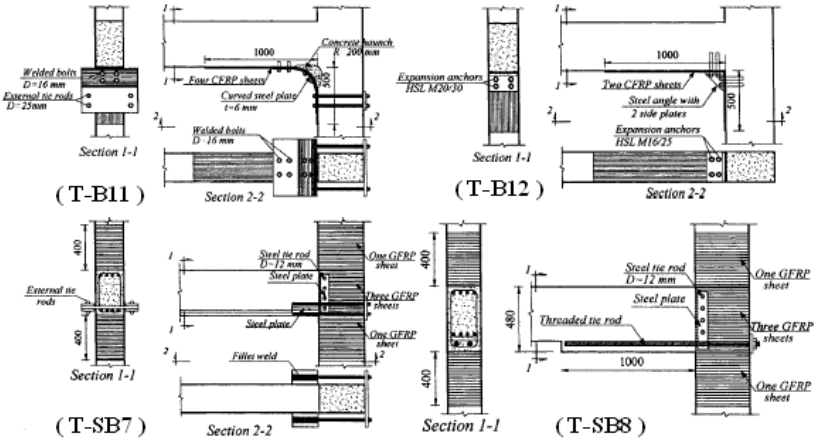

Fig. 2.11: Rehabilitation schemes [Ghobarah-05]

Mahini and Ronagh (2007) carried out research on five one-way 1/2.2-scale ordinary moment resisting exterior beam-column joint specimens subjected to monotonic/cyclic loading and column axial load to evaluate the ability of CFRP sheets in preventing the plastic hinge formation at the face of the column. The prototype was designed according to AS3600 (Australian Concrete Code) with details similar to non-ductile RC frames designed to ACI318. The specimens were retrofitted with one or a few ply uni-directional CFRP sheets in the beam longitudinal direction at a distance from the column face and extended over the joint core area to the back of the column and the beams were not fully wrapped. The considerable results were:

- We-bonded CFRP retrofitting could relocate the beam plastic hinging zone away from column face.
- Energy was dissipated in the hysteretic behavior to occur in a ductile manner.
- At least 1.3 times of the beam height is recommended for retrofitting length to fully relocate the plastic hinge away from the column face [Mahini-07].

Almusallam et al. (2009) conducted study on a full-scale sub-standard one-way corner beam-column joint specimen subjected to only reversed cyclic loading to investigate repairing of severe damaged unit using the suggested scheme. The prototype was poorly detailed with inadequate joint shear strength and no joint transverse reinforcement. The specimen was subjected to a cyclic loading history to provide severe earthquake damage effects and then repaired through injection epoxy and externally bonding with CFRP sheets. To prevent debonding, the sheets were mechanically anchored by bolted steel plates, Fig. 2.12. The repaired unit was then subjected to the similar cyclic load history. The results showed that:

- The CFRP repairing method improved the load carrying capacity by 88% and ductility by 97%.
- The repaired unit exhibited slower stiffness degradation that is a desirable property during a major earthquake to prevent sudden loss of stiffness of structural joints [Almusallam et al.-09].
-

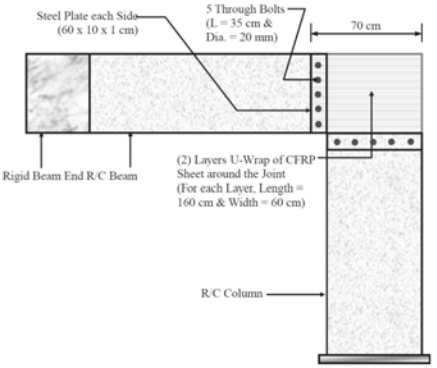

Fig. 2.12: Schematic representation of FRP repaired joint [Almusallam et al.-09]

Ilki et al. (2011) performed two series of tests on eight full-scale sub-standard exterior beam-column joint specimens subjected to cyclic reversed loading history and axial loading on column ($0.125f'_cA_g$) to investigate FRP-retrofitted unreinforced joints built with plain bars and low-strength concrete (f'_c=8.3 MPa for the testing day). The two specimens were one-way and the rest was included of transverse beam and slab only on one side of the joint (corner joint). In the first test series, the strength of the specimens were limited by shear strength of the joint and slippage of the beam longitudinal bars due to sufficient and insufficient anchorage of beam longitudinal bars into the joint, respectively. In the second test series, significantly better strength and ductility was obtained that the slip of the beam bars

was prevented. The retrofitted specimens were targeted to achieve ductile behavior through flexural failure of the beam. Different arrangements of FRP sheets and strengthening methods were used to retrofit the specimens, for instance, the square bi-directional FRP sheets to cover the joint core as well as unidirectional FRP sheets in two diagonal directions of the joint to eliminate brittle joint shear failure, and welding of hooks in the joint by removing a layer of concrete behind the column to preventing slip of the beam longitudinal bars, Fig. 2.13. The experiment pointed out the following considerable results:

- The reference (non-strengthened) and FRP-retrofitted specimens without welding of hooks of beam longitudinal bars into the joint, could not achieve the flexural capacity of the framing beam and columns.
- When the specimen was upgraded only by welding of hooks at the joint, the strength was governed by the beam flexural capacity and specimen could keep the strength until the drift ratio of 4%, but after 4% drift, the shear damage of the joint caused a sharp decrease in the strength of the specimen.
- The FRP strains in all FRP-retrofitted units varied between 0.1% and 0.4% at peak load levels and after peak increased with increasing drift ratios so that in diagonal directions reached to 1.5%. Consequently, the effective FRP strain can be considered as 0.4% (approximately 25 to 30% of the FRP ultimate strain) in the force-based design to obtain ductile behaviour [Ilki et al.-11].

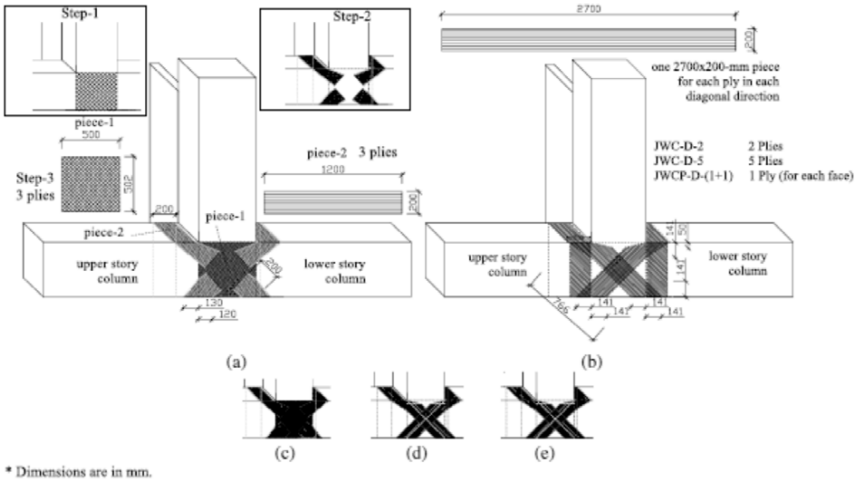

Fig. 2.13:a) FRP application details of specimens [Ilki et al.-11]

Li and Kai (2011) carried out an experimental research on four full-scale nonseismically detailed one-way interior beam-wide column joint specimens to study their repairing through epoxy injection and externally bonding of CFRP or GFRP sheets after severe earthquake damaging. The major deficiencies of the prototypes which were designed and constructed according to BS 8110 code were: a) utilizing of hoop stirrups with 90 ° hooks as transverse reinforcements, b) unreinforced joints, and c) no additional transverse reinforcements within the beam potential plastic hinge zones. The specimens were divided into two categories C1 and C2 with the column-to-beam width ratios of approximately 3.56 and 7, respectively. Moreover, the ratio of the column widths of C1 and C2 to the effective joint width was 2.2 and 4.2, respectively. The specimens were tested under two levels of axial column load $0.1f'_cA_g$ and $0.35f'_cA_g$ and a reversed cyclic loading, repaired through epoxy and different arrangements of FRP sheets, and retested in the way as same as the original ones. The design principle of the repair systems was to restore the specimen to its original strength and drift capacity. Therefore, in rehabilitation of every specimen its failure mode was considered. Fig. 2.14 displays typical rehabilitation schemes 1 and 2. The repair scheme 2 is similar to the scheme 1; only the retrofitting assemblies No.1 and No.3 with GFRP were replaced by CFRP. The test pointed out the following significant results:

- The strength and energy dissipation capacity of reference specimens were not considerably affected by the column axial loading.
- Although debonding of L formed FRP sheets was observed in all rehabilitated units, transverse fiber wraps as anchor could effectively prevent premature delamination of FRP sheets.
- Scheme 1 could effectively improve the strength, stiffness and energy dissipation capacity of specimen C1.
- Scheme 1 could only improve the strength and energy dissipation of specimen C2.
- Scheme 2 could effectively improve the overall (strength, stiffness, and energy dissipation) behavior of specimen C1 and C2 [Li-11].

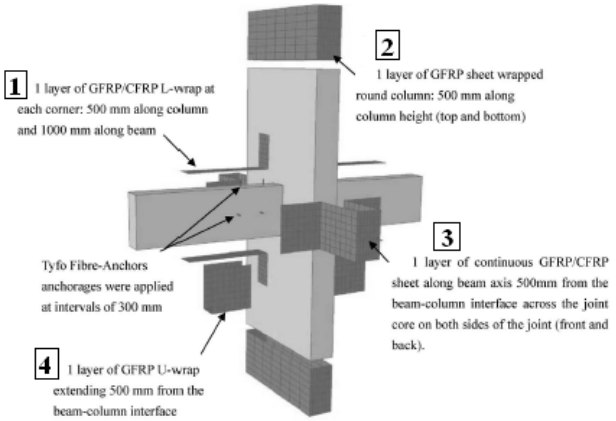

Fig. 2.14: Typical rehabilitation schemes 1 and 2 [Li-11]

2.3.3.2 Utilization of glass-fiber-reinforced polymer, GFRP

Mosallam (2000) performed an experimental study on repairing and strengthening of interior beam-column joint specimens through epoxy injection and carbon-epoxy or E-glass-epoxy quasi-isotropic laminates that was mentioned in the last article [Mosallam-00].

Ghobarah and Said (2001) conducted an experimental study on a full-scale non-ductile one-way exterior beam-column joint specimen subjected to increased cyclic loading and constant column axial load of $0.2f'_cA_g$ to investigate utilizing the suggested repair procedure on the rehabilitation of damaged joint. To do the research, the prototype as a control specimen was tested and severely damaged and then was repaired through fresh concrete and externally bonded bi-directional GFRP sheets on the joint core. The FRP laminates covered the joint core and wrapped around the column and did not extend onto the beam and the fibers were in the 45º direction with the vertical. Moreover, the ends of the laminates close to the beam joint interface were anchored by bolted steel plates at the joint core. Based on the test results the following conclusions were obtained:

- The GFRP jacket enhanced the performance of the joint from the brittle shear and high rate of strength degradation in control specimen to the dramatically increased shear strength and ductility in the rehabilitated one.
- The bolted steel plates kept the jacket in place despite the delamination and prevented the premature failure of the joint. Finally, due to the intentional under-design of the

GFRP jacket the fiber material completely separated into two pieces revealing the failure of the concrete underneath [Ghobarah-01].

El-Amoury and Ghobarah (2002) prepared an experimental study on three substandard full-scale one-way exterior beam-column joint specimens subjected to reversed cyclic loading and constant column axial load of $0.2f'_cA_g$ to upgrade the shear strength and reduce the bond-slip potential of beam bottom bars in retrofitted units through externally bonded GFRP laminates. Bi-directional GFRP composites in ±45º directions were used in the joint retrofitting and unidirectional sheets were applied for upgrading the beam bars bond-slip. Furthermore, bolted flat and U-shaped steel plates and an angle were used to effectively anchor the GFRP sheets, Fig. 2-15. The experimental results showed the following considerable conclusions:

- GFRP jacketing restored the concrete integrity by confinement and considerably improved the ductility and the load –carrying capacity of the upgraded specimen.
- The proposed approach eliminated the brittle joint shear failure, improved the bond conditions of the beam top bars, delayed the slippage of the beam bottom bars, increased the energy dissipation, and reduced the stiffness degradation of the unit.
- In specimen TR1, the fiber debonded when the strain of 0.004 was achieved.
- In specimen TR2, due to U-shaped steel plates the GFRP laminates reached the strain of 0.005. Moreover, 52% higher load-carrying capacity and six times more energy dissipation compared to control specimen was observed [El-Amoury-02].

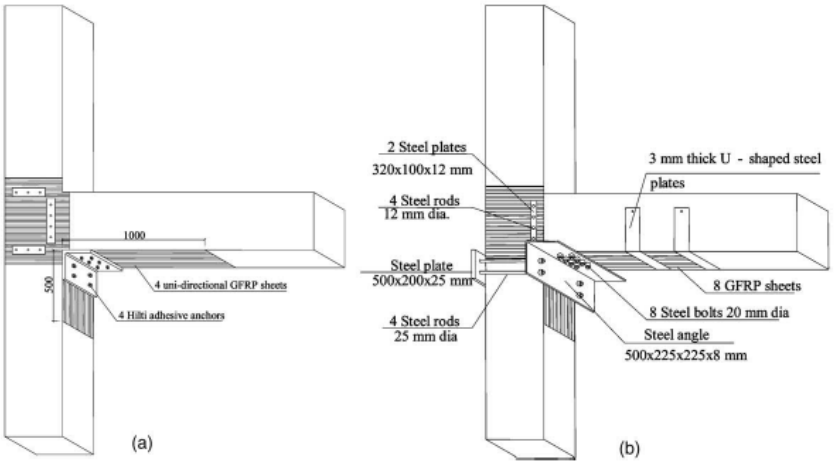

Fig. 2.15: Typical rehabilitation schemes: a) TR1; b) TR2 [El-Amoury-02]

Antonopoulos and Triantafillou (2003) performed a comprehensive experimental study on upgrading of exterior beam-column joints through CFRP and GFRP composites that shortly explained in the last article [Antonopoulos -03].

Ghobarah and Said (2002) carried out research on four full-scale substandard exterior beam-column joint subjected to cyclic loading and column axial load of $0.1f'_cA_g$ and $0.2f'_cA_g$ to develop rehabilitation techniques for the repair and upgrade of the joint shear-resistance capacity in existing structures with non-ductile detailing. Two control specimens, T1 and T2 were tested under $0.2f'_cA_g$ and $0.1f'_cA_g$ column axial loads, respectively, and then with GFRP jacketing repaired and again retested, but the other two specimens were only retrofitted. Damaged specimen T1 was repaired by one bi-directional U-shaped GFRP sheet, same height as the joint with bolted plats for anchoring the sheet (T1R). Damaged specimen T2 was rehabilitated by two bi-directional U-shaped GFRP layers extending above and below the joint with bolted cover steel plates for anchoring the sheets (T2R). T4 specimen was retrofitted as the same as T1R but without anchor plates, and T9 specimen was rehabilitated by three diagonal unidirectional GFRP layers at the joint using steel angles to accommodate the GFRP wraps, Fig. 2.16. The test led to the following considerable results:

- The GFRP jacket was increased the shear resistance of the deficient joint and enhanced the ductile performance of the connection.
- The proposed techniques changed successfully the brittle joint shear failure mode of the specimens into the ductile beam flexural failure mode.
- The rehabilitated specimens, (T1R, T2R, andT9), displayed higher energy dissipation amount compared to the original ones.
- In using FRP sheets for strengthening joint cores, it is needed to anchor the edges of the sheets effectively because the joint area is too small to develop the strength of the fibers.
- In FRP retrofitting of the joints the bulging of the FRP wrap must be considered, because it leads to form and widen the cracks under the fibers due to the limited confinement of the rectangular column sections.
- The maximum strain in the fiber was measured at 0.0055 [Ghobarah-02].

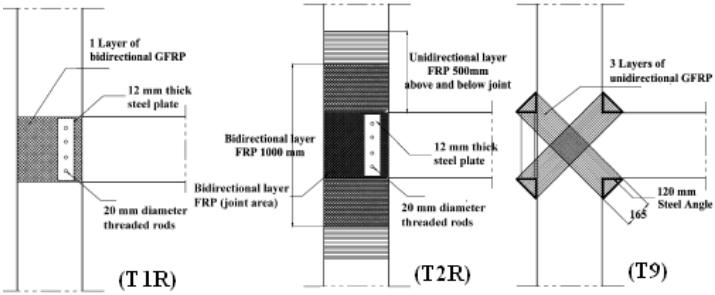

Fig. 2.16: Typical rehabilitation schemes: a) T1R; b) T2R; c) T9 [Ghobarah-02] (reprinted from[Said-04])

Said and Nehdi (2004) made a full-scale code-confirmed exterior beam-column joint specimen, tested it under cyclic loading, and compare the outcomes with the results of the last research on the four rehabilitated sub-standard specimens ([Ghobarah-02]). They concluded that:

- Target of rehabilitation techniques should be the current code standard. Consequently, the common approach of comparing the performance of retrofitted ones with the substandard units may be inadequate.
- A successful rehabilitation scheme should achieve a shift from a brittle mode of failure (joint or column hinging) to a ductile beam flexural hinging mechanism of failure.
- The rehabilitated specimens displayed considerable behavior enhancements compared to that of control substandard units, but did not achieve current standard level performance [Said-04].

Ghobarah and El-Amoury (2005) tried to develop several rehabilitation schemes using combination of CFRP and GFRP composites, and steel elements which was explained in the last article [Ghobarah-05].

Mukherjee and Joshi (2005) tested different arrangements of CFRP and GFRP composites in rehabilitation of joints which was mentioned in the last article [Mukherjee-05].

Pampanin et al. (2007) prepared an experimental study on two 3D (without floor system) substandard 2/3-scale exterior (corner) beam-column joint specimens subjected to reversed bi-directional cyclic loading and variable column axial load (as a function of the lateral force) to evaluate the feasibility and efficiency of the proposed retrofit scheme using GFRP sheets through controlling the hierarchy of strength within the joint to protect the panel zone and

relocating the plastic hinge in the beam. One specimen was tested as a reference unit and another one was retrofitted and then tested. The specimens were reinforced by plain round bars and beam longitudinal reinforcements were anchored into joints through 180º hooks. Moreover, only one single stirrup in the middle of each joint was used. Retrofitting scheme by unidirectional GFRP sheets comprised one vertical FRP layer on each of the two external faces of the column, one L-shaped horizontal laminate wrapped around the exterior face of the specimen at the joint level, and additional smaller strips to provide better anchorage to the main FRP laminates, Fig. 2.17. The experimental results showed the following considerable conclusions:

- Overall, the targeted minimum performance level, consisting of joint protection from excessive damage and concentrating inelastic deformation in the beam element, was achieved.
- Retrofitted unit exhibited a considerable increase in the lateral load-carrying capacity.
- Until 2% of drift, stable hysteresis behaviour was observed and subsequently following cycling to 2.5% strength degradation occurred [Pampanin et al.-07].

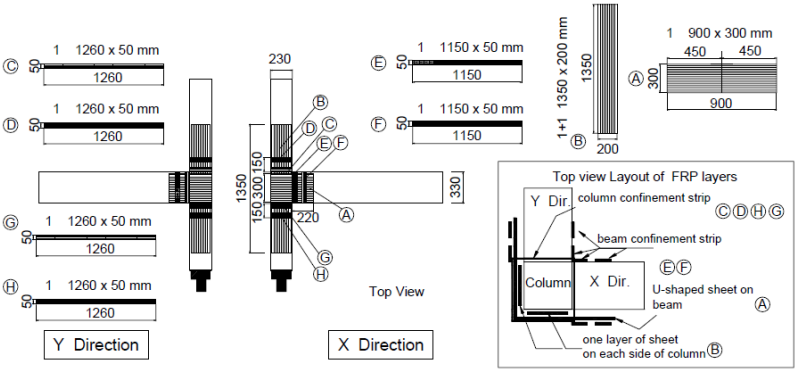

Fig. 2.17: GFRP retrofit configuration for the 3D corner joint specimen [Pampanin et al.-07]

Li and Kai (2011) studied the strengthening of interior beam-wide column joints by CFRP and GFRP composites through an experimental research which was explained before in the last article [Li-11].

2.3.4 The summary of the results and discussion

The significant conclusions of the retrofitting and strengthening techniques of the substandard RC beam-column joints can be summarized as the follows:

- Epoxy repair method have shown limited success in repairing the bond of reinforcement, filling the cracks, and restoring shear strength in one way beam column joints, although it would be difficult to inject epoxy into the actually joints surrounded by floor members. Furthermore, this technique is indeed a restoring method for repairing moderately damaged joints and cannot be accounted as a retrofitting technique for beam-column joints. Because of difficulty in filling all the internal cracks, the epoxy repaired specimens could not restore the stiffness and energy dissipation capacity. Epoxy injection and replacement concrete method restored the strength of specimens.

- The joint strengthening method with reinforced masonry units through an analytical study can lead to desirable ductile beam failures and reduction of inter-story drifts; however there is no experimental data and nearly it has also the same disadvantages of concrete jacketing technique.

- Although concrete jacketing of columns and encasing the joint region in a reinforced fillet is an effective method to create weak beam-strong column mechanisms, it is the most labour-intensive strengthening method. Meanwhile it suffers from considerable loss of floor space, disruption to building occupancy, and additional masses. For these reasons, the application of concrete jacketing for joints remains limited.
- In steel jacketing methods:

  - Retrofitting method by externally bonded steel plates with steel angles and RC filet is effective to move the cracks to the enlarged joint region after retrofitting and preventing local failures. The relative increasing of strength, initial stiffness, and energy dissipation of the interior joint in comparison with exterior one is more. However, disruption to building occupancy is undeniable.

  - Externally retrofitted method through steel plates attached on the upper and lower faces of column prevents the cracks to extend into the column bar splices region but beam bottom bars are pullout due to flexural hinge formed in the joint panel close to the beam.

- The proposed systems to upgrade the bond slip resistance of beam bottom steel bars by bolting two steel channel sections to the underside of the beams, did not completely improve the joint response, because the damage is transferred from the joint embedment zone to other parts of the joint.

- Corrugated grouted steel jackets method can change the joint shear failure mode to a ductile flexural mode in the beam if both the column and beam are jacketed. The improvement of the method in preventing of beam bottom bar pullout is not observed. It cannot be practically applied in cases where floor members are present. It should be considered that such techniques can result in excessive capacity increase and create unexpected failure modes.

- In diagonal steel bracing methods the retrofitted specimens in comparison with non-retrofitted ones show a substantially enhanced response so that damage to the joint is eliminated and a flexural plastic hinge formed in the beam at the location of haunch connection. Furthermore, this method leads to an increase in strength and enhancing in energy dissipation. It seems that prevention of diagonal element to buckling under high compression forces may limit the application of this method.

- Experimental results of planar joint expansion technique show that in retrofitted specimens brittle joint shear is eliminated and beam flexural failure is observed. Meanwhile, the strength, stiffness, energy dissipation and ductility of retrofitted specimens are improved. However, it seems that disruption to building occupancy and additional masses is undeniable.

- In retrofitting methods through FRP composites, the relatively higher initial cost of these materials is outweighed by their several attractive features such as high strength-weight ratios (minimizing additional masses, and no significant increase in member size), have a relatively high-energy dissipation capability, resistant to corrosion, fast and ease of application even in limited locations, nearly non-disruptive to occupants, low labour costs, tailor-ability, no require skilful workmanship, and increasing the site safety.

  At present, the most literature on FRP- strengthened joints mainly consist of simplified two-dimensional tests and a few analytical studies. Therefore practical use

of findings through 2D tests in 3D issues is an essential problem. However, higher material costs specially CFRP composites, concerns related to performance under high temperature, and the resulting fire rating issues have limited their use. In addition, their low off axis-strength has made it very difficult to develop adequate systems to anchor them. To account for their low off-axis properties, corners of the concrete member receiving FRP must be rounded to prevent FRP failure due to stress concentration.

Factors on the shear capacity of the joints in using of FRP strengthening are: a) effectiveness of strips versus sheets; b) number of strips or number of sheet layers; c) mechanical anchorages; d) type of fibers (Carbon, versus Glass); e) level of axial loads in column; f) damage in the joint prior to strengthening; and g) effect of transverse beam.

Most studies have been shown that the behaviour of externally bonded FRP composites is dominated by debonding of the composites from the concrete surface, for that reason, ductile beam failures were observed in only a few specimens. Subsequently, it is necessary to indicate the need for a thorough surface preparation as well as for reliable mechanical anchorage methods that would lead to effective joint confinement and full development of fiber strength. Several rehabilitation schemes using composite materials and steel elements show that CFRP sheets attached to the beam bottom face were found effective in replacing the anchorage-deficient beam bars, when an adequate anchorage system of these sheets is provided. External steel tie-rods welded to the existing deficient beam reinforcement are found to be a simple and effective technique to improve the anchorage conditions of these bars. A GFRP jacket of the joint zone is found to be an effective system to provide confinement and shear strength to shear-deficient joints. Brittle joint shear failure is avoided and ductile beam flexural hinging instead developed. The rehabilitation systems are effective in significantly increasing the joint energy dissipation and in reducing the joint stiffness degradation.

2.4 Design approaches by codes of practice

The main criterion of beam-column joint design is that the joint should be stronger than the beam and column. To achieve the target, the codes of practice for design and construction of beam-column joints as a part of the seismic-force-resisting system comprise the set of recommendations and minimum requirements on the basis of energy dissipation in the nonlinear range of response without critical deterioration in strength, such as portion of members, ratio of column-to-beam flexural strength at the joint, confinement of the column core in the joint region, control of joint shear stress, details of columns and beams framing into the joint, and development of reinforcements. The design process of beam-column joints can be summarized in the following steps:

- Controlling the member depths to satisfy development or anchorage length of the longitudinal bars
- Controlling the flexural strength ratio of the joint members (columns to beams) to reduce the likelihood of yielding in the columns
- Calculating the joint shear force by considering the flexural over strength of the adjoining beams
- Comparing the joint shear force and nominal shear strength of the joint by considering only the compressive strength of the concrete and the effective joint area (Joint shear strength is not sensitive to joint shear reinforcement, [ACI-ASCE Committee 326].)
- Providing joint transverse reinforcement to confining the joint core concrete in resisting shear, [Uma and Jain].

In the following, some of the most important subjects of three international codes of practice to compare with each other are shortly reviewed.

2.4.1 The bond and shear requirements within the beam-column joints

Important factors controlling the seismic design of beam-column joints are identified through considering three international codes of practices: American Concrete Institute (ACI 318M-11), (ACI 352R-02), and Eurocode 8 (EN 1998-1: 2004). Table 2.1 presents review of recommendations of the codes regarding design of exterior joints of special moment resisting RC frames, [ACI 318M-11], [ACI 352R-02], [EN 1998-1:2004], [Fardis-09].

Table 2.1: Comparison of the codes of practice in design of exterior beam-column joints

	ACI 318M-11	ACI 352R-02	Eurocode 8 EN 1998-1:2004
Development length of hooked bars in exterior joints	$l_{dh} = \frac{f_y d_b}{\left(5.4\sqrt{f_c'}\right)}$ $\geq (8d_b, 150\ mm)$	$l_{dh} = \frac{\alpha f_y d_b}{\left(6.2\sqrt{f_c'}\right)}(0.8)$ Where: $\alpha \geq 1.25$ *	$h_c \geq \frac{\gamma_{Rd} f_{yd}}{7.5 f_{ctm}} \frac{d_b}{1 + 0.8 v_d}$ Where: $\gamma_{Rd} = 1.2$ and $v_d = N_{Ed} / (f_{cd} A_g)$
Min. flexural strength ratio of columns to beams $(\sum M_{nc} / \sum M_{nb})$	1.2	-----	1.3
Nominal shear strength of the joint	For joints confined by beams - on all four faces: $1.7\sqrt{f_c'} A_j$ - on three faces or on two opposite faces: $1.2\sqrt{f_c'} A_j$ - for other cases: $1.0\sqrt{f_c'} A_j$	For joints confined vertically on - all four faces: $1.66\sqrt{f_c'} b_j h_c$ - on three faces or on two opposite faces: $1.25\sqrt{f_c'} b_j h_c$ - for other cases: $1.0\sqrt{f_c'} b_j h_c$	$0.8\,\eta f_{cd}\sqrt{1 - \frac{v_d}{\eta}}\, b_{jj} h_{jc}$ Where: $\eta = 0.6(1 - \frac{f_{ck}}{250})$
Joint horizontal reinforcement	$A_{sh} \geq$ $\{0.3\frac{s b_c f_c'}{f_{yt}}[(\frac{A_g}{A_{ch}})\text{-}1]$ and $0.09\frac{s b_c f_c'}{f_{yt}}\}$	$A_{sh} \geq$ $\{0.3\frac{s b_c f_c'}{f_{yt}}[(\frac{A_g}{A_{ch}})\text{-}1]$ and $0.09\frac{s b_c f_c'}{f_{yt}}\}$	$A_{Tjh} \geq$ $\{\frac{b_{jj} h_{jw}}{f_{ywd}}\left(\frac{\left(\frac{V_{jhd}}{b_{jj} h_{jc}}\right)^2}{f_{ctd} + v_d f_{cd}} - f_{ctd}\right)$ and $\gamma_{Rd} A_{s2} f_{yd}(1 - 0.8 v_d) / f_{ywd}\}$ Where: $V_{jhd} = \gamma_{Rd} . A_{s1} . f_{yd} - V_c$
Joint vertical reinforcement	-----	------	$A_{sv,i} \geq \left(\frac{2}{3}\right) . A_{Tjh} . (\frac{h_{jc}}{h_{jw}})$

* The critical section for development of beam bars into the joint should be taken at the outside edge of the column core.

A_{ch} cross-sectional area of a structural member measured to the outside edges of transverse reinforcement, mm^2

A_g gross area of concrete, mm^2

A_j effective joint cross-sectional area, mm^2, computed from joint depth (h_c) times effective joint width (the overall width of the column, except where a beam frames into a wider column, effective joint width shall not exceed the smaller of: a) beam width plus joint depth, b) twice the smaller perpendicular distance from longitudinal axis of beam to column side.

A_{s1} area of the beam top reinforcement, mm^2

A_{s2}	area of the beam bottom reinforcement, mm^2
A_{sh}	total cross-sectional area of transverse reinforcement including crossties within spacing s and perpendicular to dimension b_c, mm^2
$A_{sv,i}$	total area of the intermediate bars placed in the relevant column faces between corners of the column including bars contributing to the longitudinal reinforcement of columns, mm^2
A_{Tjh}	total area of the horizontal hoops in a beam-column joint, mm^2
b_b	width of the longitudinal beam, mm
b_c	width of the column, mm
b_j	effective joint width, mm, should not exceed the smallest of $(\frac{b_b+b_c}{2}, b_b+\frac{\sum mh_c}{2}, b_c)$, where beam-column eccentricity exceeds $b_c/8$, m=0.3, otherwise m=0.5
b_{jj}	effective joint width, if $b_c>b_w$: b_{jj}= min$\{b_c; (b_w+0.5h_c)\}$; if $b_c<b_w$: b_{jj}= min$\{b_w; (b_c+0.5h_c)\}$
b_w	width of beam web, mm
d_b	nominal diameter of bar, mm
f_{cd}	design value of concrete compressive strength, MPa
$f_c^{'}$	specified compressive strength of concrete, MPa
f_{cd}	design value of concrete compressive strength, MPa
f_{ck}	strength of concrete, MPa
f_{ctd}	design value of the tensile strength of concrete, MPa
f_{ctm}	mean value of tensile strength of concrete, given as $0.3f_c^{'(0.667)}$
f_y	specified yield strength of reinforcement, MPa
f_{yd}	design value of yield strength, MPa
f_{yt}	specified yield strength of transverse reinforcement, MPa
f_{ywd}	design value of the yield strength of the transverse reinforcement, MPa
h_c	overall cross-sectional depth of column, mm
h_{jc}	distance between extreme layers of column reinforcement, mm
h_{jw}	distance between the top and the bottom reinforcement of the beam, mm
N_{Ed}	design axial force from the analysis for the seismic design (the minimum value from load combination), is assumed positive when compressive, N
l_{dh}	development length in tension of deformed bar with a standard hook, measured from critical section to outside end of hook, mm
s	center-to-center spacing of transverse reinforcement within the joint, mm
V_c	shear force in the column above the joint, from the analysis in the seismic design situation, N
v_d	normalized design axial force of column
V_{jhd}	horizontal shear force acting on the concrete core of the exterior joint, N
α	stress multiplier for beam longitudinal bars

γ_{Rd} model uncertainty factor for the design value of resistance for beam longitudinal bars, given as 1.2

η reduction factor on concrete compressive strength due to tensile strain in transverse direction

$\sum M_{nc}$ sum of nominal flexural strength of columns framing into the joint, N.mm

$\sum M_{nb}$ sum of nominal flexural strength of beams framing into the joint, N.mm

2.4.2 Summary and conclusions of the codes comparison

The considerable results of the comparison reviews are summarized below:

Development length of beam bars or column depth:

Development length in ACI 318M-11 and ACI 352R-02 depends only on the bars nominal diameter and strength of the concrete and steel bars but in EN 1998-1: 2004 the effect of the column axial load is also considered so that any increasing in column compressive axial load leads to a decrease in required minimum column depth. ACI 352R-02, ACI 318M-11, and EN 1998-1: 2004 require the smallest to largest column depths, respectively. EN 1998-1: 2004 is more sensitive to concrete higher strength than the other two codes in reducing the column depth.

Minimum flexural strength ratio of columns to beams:

To avoid the soft story mechanism, EN 1998-1: 2004 requires conservatively minimum flexural strength ratio of columns to beams adjoining in the joint.

Joint shear strength and joint reinforcement:

Strut shear mechanism is the base of evaluating the nominal shear strength in all of three codes. Nominal joint shear strength in ACI 318M-11 and ACI 352R-02 depends only on the effective joint area, joint lateral confinement, and strength of the concrete while in EN 1998-1: 2004 the effect of the column axial load is also entered so that any increasing in column compressive axial load leads to a decrease in nominal joint shear strength. In exterior joints, EN 1998-1: 2004 at higher amounts of concrete strength (more than 40 MPa) and ACI 318-11 at lower amounts of concrete strength increase the nominal joint shear strength.

ACI 318M-11 and ACI 352R-02 require joint transverse reinforcement regardless of the magnitude of the calculated shear force. EN 1998-1: 2004 requires both horizontal and vertical joint reinforcement for adequate confinement to limit the maximum diagonal tensile stress of concrete. Moreover, integrity of the joint after diagonal cracking is considered in joint transverse reinforcement design by EN 1998-1: 2004.

Chapter 3

Seismic Retrofitting by Developing the Beam Sidesway Mechanism

3.1 Introduction

It can be inferred from Section 2.4 that in the seismic design of structures, the design target of the codes of practice is to ensure the dissipation of the energy induced by an earthquake without critical deterioration in strength and stability. If the more energy is dissipated by the structure, the less strength is required to design. Consequently, this approach leads to not only safer structures but also more economic ones, [Costa-03].

Looking at the probable critical mechanisms of the structures and understanding the reasons of their creating and also considering the target of seismic design, the principles of seismic design of structures can be found. Observance of the seismic design principles not only results to the safe and economic new structures but also develops the efficient strengthening and retrofitting techniques for the existing vulnerable structures. Since the joints are connected the main components of the structures, beams and columns, in their retrofitting it is necessary to particularly pay attention to these members. Through a capacity assessment of strength in subassemblies of a joint the expected sequence of strength, hierarchy of strength, can be obtained and therefore, helpful information on the local and global failure mechanisms is provided to strengthening the joints. Moreover, considering that the failure mechanisms of the joints (shear and bond slip or bond deterioration) are brittle, to dissipating energy through the retrofitted joints considering the adjacent elements and retrofitting technique is necessary. Providing a desired subsequence of strength in subassemblies parallel with transferring the duty of dissipating the imposed energy to the capable adjacent elements (beams), according to the desired overall mechanisms (such as beam sidesway mechanism), a ductile strengthening

and retrofitting technique of RC frame structures through beam-column joints is achieved, [Pampanin et al.-06], [Said-08], [Chaimahawan-09] . If it was also possible to absorb energy by strengtheners during the earthquake, extra energy dissipation would be achieved too. Obviously, a retrofitting system should consider adequate control of inter-story drifts to limit the amount of non-structural damage. Finally, a relatively inexpensive seismic upgrading system with the minor residential and structural disturbance should be considered.

In this chapter, the critical mechanisms of frame structures are shortly discussed and subsequently the basic principles of seismic design are inferred. Then, the concept of hierarchy strength design as well as developing the plastic hinges in the beams to providing the desired failure mechanisms in retrofitted frames are presented. In the following, two innovative retrofitting devices developed to strengthening of beam-column joints with their application in the proposed retrofitting techniques as well as new composite fabric, SRP, using in the strengthening RC beams of specimens in the experimental study are introduced.

3.2 Seismic design principals of structures and joints

A strong earthquake develops the post-elastic deformations throughout the structures. In the RC frame structures, due to the different strength ratios of the subassemblages, the deformations may form different critical failure mechanisms: a) column sidesway mechanism, b) joint shear sidesway mechanism, c) beam sidesway mechanism, or d) combinational mechanism, Fig. 3.1. If in a number of joints the sum of flexural strength of the joint columns is less than the similar strength for the joint beams, weak column-strong beam, a catastrophic failure mechanism will be formed naming column sidesway or soft-story mechanism, Fig. 3.1-b and Fig. 3.2. Of course, this kind of collapse has been also attributed to the discontinuity of beam bottom longitudinal bars into the joints, joint bond deteriorations, [Aycardi et al.-94]. Weakness of joints to shear strength in a frame lead to a brittle failure and rapid strength degradation of the joint panels and form joint shear sidesway mechanism which can loss the vertical load-bearing capacity of the entire structural system and provide a catastrophic collapse, Fig. 3.1-c and Fig. 1.5-1.7. The codes of practice for seismic design of RC moment-resisting frames use the concept of strong column-weak beam behaviour resulting to the beam sidesway mechanism (Fig. 3.1-d). The desired beam sidesway mechanism could lead to a appropriate energy absorbing performance without collapse while sustain the severe imposed post-elastic deformations.

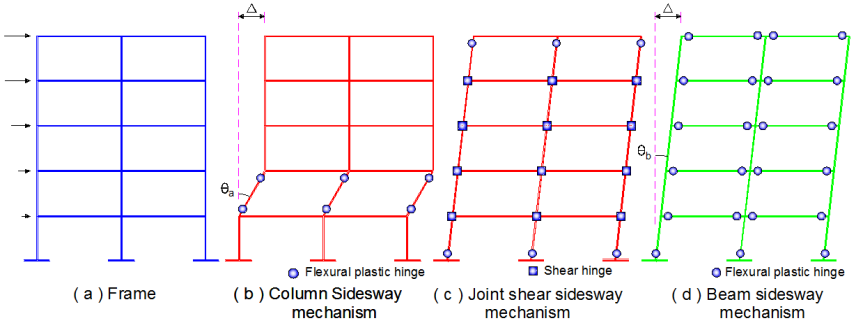

Fig. 3.1: Global failure mechanisms of frame structures during a major earthquake

Fig. 3.2: Column sidesway mechanism led to 3rd floor soft story collapse of reinforced concrete building in Nishinomiya, Kobe earthquake, Japan, 1995, Magnitude: 6.69
(Figure from USGS achieves)

The corresponding seismic design forces of structures are generally too high to be resisted within the elastic range of material response, [Paulay and Priestley-92]. For that reason, depending on the level of ductility permitted of the structure, they are usually designed for strengths which are a fraction of that corresponding to elastic response (perhaps as low as 15 to 25%). Consequently, it is expected that they experience an earthquake by large inelastic deformations and energy dissipation. Most ordinary buildings are seismically designed to response full ductile or restricted ductile and the rest elastic. Buildings of great importance are designed to remain essentially elastic during earthquakes with only insignificant inelastic deformations. Therefore, they are designed to resist seismic loads which are larger than those that would be developed in the ductile responding structures, with maximum displacements

very close to the ideal elastic structures or the real structures at the onset of yielding. Depending on the force level of strength design, the level of ductility required may vary from insignificant, requiring no special detailing, to considerable, requiring most careful consideration of detailing. In full ductile structures, inelastic regions should be carefully identified and detailed to achieve the maximum potential of ductility. Structures with restricted ductility, due to the presence of the strong lateral resisting system such as large areas of shear walls, have inherently significant strength with respect to lateral loads. Therefore, in these structures it may be difficult to develop large ductilities, which would allow the use of low-intensity seismic design forces.

In capacity design of structures for seismic resistance, the critical regions of the structural members that are selected to form flexural plastic hinges are carefully designed and detailed to have the inelastic deformation capability without shear failure. The plastic hinge regions are chosen based on a kinematically admissible failure mechanism. The selection of the most effective mechanisms is based on the overall displacement ductility that can be developed with the smallest inelastic rotation demands in the plastic hinges, and forming as possible as a significant number of plastic hinges before collapse, [Paulay and Priestley-92]. A comparison of two example mechanisms in Figs. 3.1-b and 3.1-d displays that for the same maximum displacement Δ at roof level, plastic hinge rotation $\theta\Theta_b$ in case (d) is much smaller than that in case (b), $\theta\Theta_a$ and the number of plastic hinges in case (d) is considerably more than that in case (b). Therefore, the mechanism in Fig. 3.1-d has more advantageous. The other parts of the structure that are intended to remain elastic are designed with respect to the maximum feasible actions corresponding to over strength in the plastic hinges regarding to the probability of strain-hardening effects. The nature and quality of detailing for potentially plastic regions and those which are to remain in the elastic domain should be clearly distinct.

In ductile seismic resistant frame structures the criteria for the desirable performance of RC beam-column joints may be regulated as: a) the joint strength should not be less than the maximum demand corresponding to development of the structural plastic hinge mechanism, b) the joint should be considered as an integral part of the column so that the column bearing capacity should not be threatened by any possibility of joint strength degradation, c) the joint should be mainly respond within the elastic range during mild earthquake, d) the joint deformation should not considerably increase story drift, and e) the joint reinforcement should not cause unnecessary constructional problems, [Paulay and Priestley-92].

3.3 Performance-based retrofitting through developing the beam plastic hinges

3.3.1 Strategy of seismic retrofitting through the capacity design concept

The seismic design principles of structures can be also observed in seismic retrofitting of the existing vulnerable frames. Considering the different deficiencies of RC frame structures leading to the different global collapses (Fig. 3.1), through transmitting the failure points from the joints and columns into the beams considerably away from the critical regions (joints), it is possible to redefine the capacity design concepts in upgrading the vulnerable RC frame structures. This approach can lead to the desirable failure modes such as the beam sidesway mechanism. Therefore, the beam plastic hinges can dissipate energy by means of flexural yielding rather than exploring inelastic shear and bond-slip deformations in joints. It is worth pointing out that to absorb energy by relatively stable hysteretic behaviour; these regions should be carefully checked and probably strengthened to shear forces to have a sufficient capability for post-elastic deformations under seismic excitations. Fig. 3.3 shows schematically the strategy of seismic retrofitting through the capacity design concept leading to an appropriate ductile upgrading technique based on the beam sidesway mechanism and strong column-weak beam performance. To ensure that the sequence of strengths in the subassemblies provides the required conditions to form the desired failure mechanism, a logical assessment of strength hierarchy with reliable margin of safety should be performed.

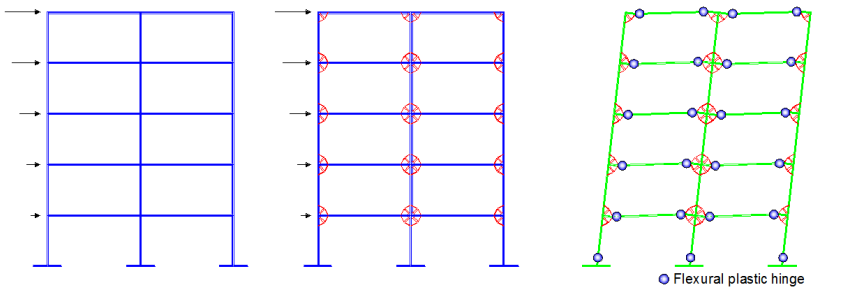

Fig. 3.3: Retrofitting of the vulnerable existing frames by developing the beam plastic hinges

3.3.2 Forces acting on an exterior beam-column joint

The forces acting on an exterior joint extending between points of contraflexure, at approximately half-story column heights and beam spans, may be shown as a free body

diagram, as displayed in Fig. 3.4-a and b. Assuming the approximation that the internal tension and compression forces of the beam are equal (T=C), equilibrium of the free body diagram shows that:

$$V_{jh} = T - V_{col} \tag{3.1}$$

then:

$$V_{jh} = V_{col}\left(\frac{l_c}{z_b} - 1\right) - V_b\left(\frac{h_c}{2z_b}\right) \tag{3.2}$$

or

$$V_{jh} = V_{col}\left(\frac{l_c l_{nb}}{l_b z_b} - 1\right) \tag{3.3}$$

then:

$$V_{col} = V_{jh}/\left(\frac{l_c l_{nb}}{l_b z_b} - 1\right) \tag{3.4}$$

where:

h_c overall depth of column, mm
l_c story height, length of column, measured center-to-center of the top and bottom beams, mm
l_b span length of beam, measured center-to-center of the column, mm
l_{nb} clear length of beam from face of columns, mm
T Tension force of longitudinal top or bottom bars of beam, N
V_{col} shear force in the column above the joint, N
V_{jh} horizontal shear force acting on the concrete core of the exterior joint, N
V_b shear force across the beam, N
z_b internal moment arm in the beam, mm

The above equations indicate that the larger column and beam depths reduce the shear force in the joint. On the contrary, the higher story and larger clear beam length increase the joint shear force.

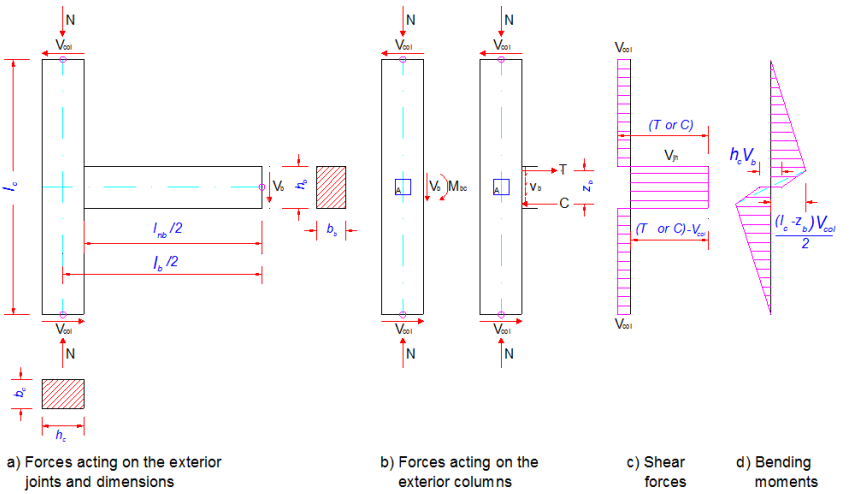

Fig. 3.4: Forces acting on an exterior beam-column joint

To predict the joint response under story shear forces and column axial loads, surveying the principal stresses at the joint region is the more reliable criterion than the joint shear stresses. This criterion is considered the combination of stresses due to the effects of the horizontal shear forces (V_{jh}) and vertical column axial loads (N) at the joint core. The horizontal shear stresses (v_{jh}) and vertical column axial stresses (f_a) are obtained by (3.5) and (3.6) equations, respectively.

$$v_{jh} = V_{jh}/A_e \tag{3.5}$$

$$f_a = N/A_g \tag{3.6}$$

where:

A_e effective joint cross-sectional area, mm^2, which is calculated based on the code of practice, according to Table (2.1) is equal to A_j , $b_j h_c$, or $b_{jj} h_{jc}$ based on ACI 318-11, ACI 352-02, or EN 1998-1: 2004, respectively

A_g gross area of column, mm^2

N column axial load, N, that for compression loads will be negative

If an element such as element A in Fig. 3.4(b) is considered in the beam-column joint core, the corresponding stresses of the horizontal shear force and column axial load are developed around it like the figure 3.5(a). According to the Mohr's circle stress, Fig. 3.5(c), the principle tensile stress of f_{tj} will be resulted on the surface of angle Θ, Fig. 3.5(b), equal to:

$$f_{tj} = \frac{f_a}{2} + \sqrt{\left[\frac{f_a}{2}\right]^2 + {v_{jh}}^2} \tag{3.7}$$

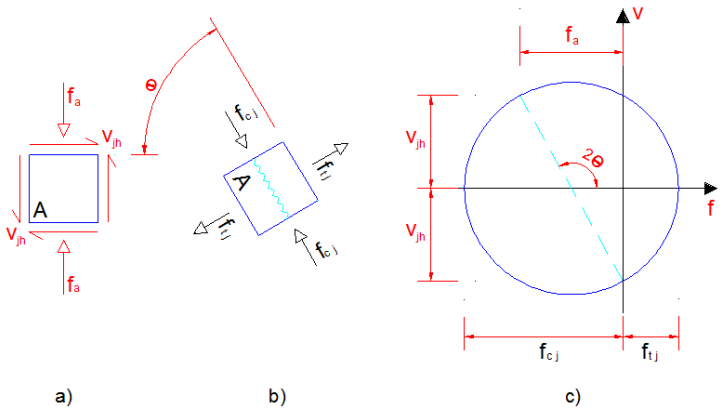

Fig. 3.5: Beam-column joint core stresses and the Mohr's circle

Therefore, the horizontal shear stress in the joint could be obtained as:

$$v_{jh} = \sqrt{{f_{tj}}^2 - f_{tj} f_a} \tag{3.8}$$

The corresponding forces will be:

$$V_{jh} = A_e \sqrt{{f_{tj}}^2 - f_{tj} N / A_g} \tag{3.9}$$

With substitution V_{jh} from Eq. (3.9) into Eq. (3.4), the story shear capacity of the as-built exterior joint, $\bar{V}_{col}$, corresponding to the joint shear will be found as follow:

$$\bar{V}_{col-joint\ shear} = \left[A_e \sqrt{{f_{tj}}^2 - f_{tj} N / A_g}\right] \Big/ \left[\frac{l_c l_{nb}}{l_b z_b} - 1\right] \tag{3.10}$$

As can be seen, the critical inter story shear force of the exterior joint can be evaluated by Eq. (3.10) with substitution the principal tensile stress f_{tj} corresponding to the defined limit state (first diagonal shear cracking or extensive damage of joint) or failure mode (bond slip failure mode or joint shear failure mode). Furthermore, the joint moment, M_{bc} can be found as:

$$M_{bc} = V_{col}\, l_c l_{nb}/l_b \tag{3.11}$$

By substituting V_{col} from Eq. (3.10) into Eq. (3.11), the joint moment capacity of the exterior beam-column joint, $\bar{M}_{bc}$ can be expressed as:

$$\bar{M}_{bc} = [l_c l_{nb} A_e \sqrt{{f_{tj}}^2 - f_{tj} N/A_g}] \Big/ [\frac{l_c l_{nb}}{z_b} - l_b] \tag{3.12}$$

3.3.3 Strength and Failure Sequence Diagram (SFSD)

The efficiency of a strengthening strategy depends on an accurate assessment of the internal strengths of prototype members to expect the sequence of strengths before and after of retrofitting. In a performance-based beam-column joint retrofitting, the strength capacity assessment of subassemblies should lead to the sequence of failures which must be organized to occur in a desired order to assure simultaneously the global strong column-weak beam performance and local ductile behaviour with sufficient margin of safety.

Pampanin et al. have proposed a simple procedure to evaluate of the expected sequence of strengths which can be carried out through comparison of capacity and demand curves within a M-N (moment-axial load) performance-domain, [Pampanin et al.-04]. Fig. 3.6 shows the sequence of strengths in a beam-column joint, with the same positive and negative beam bending moment capacity, based on the proposed domain. As can be seen, in the assumed beam-column joint, according to the imposed column axial load the minimum and maximum expected strengths are the joint shear strength and column bending moment capacity and beam bending moment strength is in the second rank between them. According to the diagram, this domain is not capable to evaluate the other strengths of subassemblies such as beam and column shear strengths and also doesn't present tactile vision of the story shear.

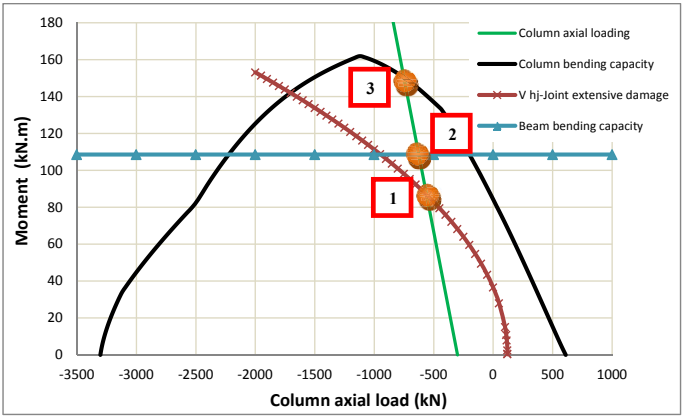

Fig. 3.6: Evaluation of hierarchy of strengths and sequence of events in M-N performance domain proposed by [Pampanin et al.-04]

To have an extensive simultaneously evaluate on the strengths of a joint assemblies as well as having a tangible concept on story shear and column lateral and vertical loadings, it is introduced a new strength and failure sequence diagram (SFSD) with the domain of performance in V_{col}- N coordinates. According to the Fig. 3.7, this domain is able to show the variation of V_{col} to N corresponding to the bending moment capacity of the column, M_{nc}, and joint shear capacity due to the substituted defined limit state for the principal tensile stress (corresponding to the first diagonal shear cracking or extensive damage of the joint), f_{tj}, and also can capture the capacity amounts of bending moments of the beam, M_{nb}, and shear strengths of the beam and the column. As can be seen, all of the five strength sequences (if the beam has the same positive and negative flexural strength) have been marked from 1 to 5 on the column axial loading line. It displays that in the assumed beam-column joint, with the same positive and negative beam bending moment capacity, corresponding to the column variable axial load the sequence of strengths from minimum to maximum are 1: joint shear strength, 2: beam bending capacity, 3: beam shear strength, 4: column shear strength, and 5: column bending capacity, respectively. It is also simply realizable that every failure event at which step of the story shear or in the other words column lateral load is expected to occur. This diagram is basically drawn by rewriting the strength of joint subassembly according to V_{col}. In an exterior beam-column joint Fig. 3.4, Eq. (3.10) presents $\bar{V}_{col}$ based on the column axial load and desired limit state of the principle tensile stress of f_{tj}. The story shear capacity

of the as-built exterior joint, $\bar{V}_{col}$, corresponding to the other strengths of the joint subassembly can be found as follow:

$$\bar{V}_{col-column\ hinge} = 2M_{ncb}/(l_c - h_b) \tag{3.13}$$

$$\bar{V}_{col-beam\ hinge} = M_{nbc}.l_b/(l_c.l_{nb}) \tag{3.14}$$

$$\bar{V}_{col-column\ shear} = V_{nc} \tag{3.15}$$

$$\bar{V}_{col-beam\ shear} = V_{nb}.l_b/2l_c \tag{3.16}$$

where:

M_{nbc} beam bending moment capacity or beam yielding at joint interface, N.m

M_{ncb} column bending moment capacity or column yielding at joint interface, N.m

V_{nb} beam shear strength, N

V_{nc} column shear strength, N

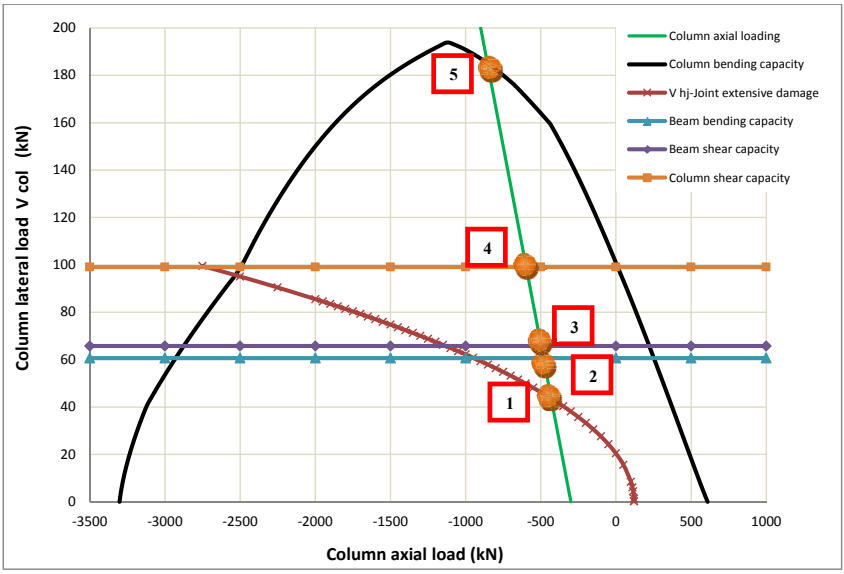

Fig. 3.7: Proposed Strength and Failure Sequence Diagram (SFSD) in a beam-column joint in V_{col}- N performance domain

By drawing SFSD for a vulnerable existing beam-column joint before retrofitting, it is possible to distinguish different weaknesses and deficiencies of subassemblies and their sequences. Then, it is conceivable to decide for a logical upgrading approach to resolving the deficiencies and providing required ductility. A logical ductile retrofitting procedure needs to arrange the failure events in retrofitted joint from ductile to brittle mechanism by redrawing SFSD, so that the shear failure mechanisms should be avoided in joint, beam, and column when the beam bending yield failure (beam flexural hinge) occurs before column bending failure. In a vulnerable beam-column joint region, performance-based retrofitting through capacity design concept requires the forcing of beam flexural plastic hinge to be formed away from the joint region through arranging and inverting the failure mechanisms in SFSD.

3.4 Innovative Multi Functional Corbels (HMFC)

3.4.1 General description

An innovative Multi Functional Corbel (HMFC) is installed between subassemblies of a joint and transmits forces and absorbs energy. It is installed in the joint through two plates parallel with the surfaces of the joint members by threaded rods or anchor bolts. The corbel can be placed in one side or two sides of the joint. It consists of a few plates and an energy dissipation device such as metallic pipe, square and rectangular profiles and pipe or profiles filled with metallic foams or elastomeric materials. Fig. 3.8 shows a sample of the innovative corbel comprises two pipe form profiles as the main energy dissipation elements. The plates transmit forces to the damper and also contribute the energy dissipation. Different materials with several geometric shapes provide to these corbels variety of desired mechanical properties and dynamical characteristics to transmit forces and dissipate energy.

The corbel provides energy dissipation through the inelastic deformation of subassemblies of the corbel in a joint via relative deformation of joint members or/and transmitting the forces. Consequently it can be categorized into hysteretic devices as a metallic yielding damper because its energy dissipation through yielding depends primarily on relative displacements within the device.

The corbel shows elastic behavior until the extended stresses to the corbel assemblies are under elastic limit. In this case it functions as an ordinary corbel or seat to transmit imposed loads or deformations. A simultaneous increasing in passed loads or deformations and

enhancement of developed strains out of the elastic limit appears inelastic behaviors so that every increase in imposed factors leads to enhancement of the inelastic deformations of corbel assemblies. Eventually removing the imposed factors leads to the plastic deformations and energy dissipation. Increasingly cyclic or seismic loadings repeat this step in positive and negative directions and consequently enhance the energy dissipation dramatically. A significant portion of the dissipative energy is converted into heat. The experimental and numerical study of this device shows that it has a stable hysteretic behavior.

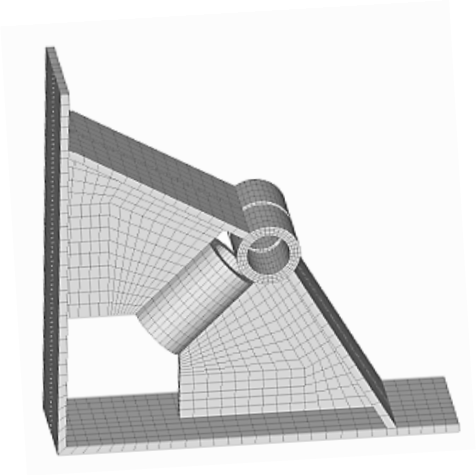

Fig. 3.8: A sample of innovative Multi Functional Corbel (HMFC) with two pipes as energy dissipation element

The Multi Functional Corbel (HMFC) provides the transferring of flexural plastic hinges to the desired points to form the desired beam sidesway mechanism. In a traditional framed structure a strong earthquake would be expected to develop plastic hinges at the end of beams and threatens the beam to column joints. To solve this problem the innovative corbel with enough stiffness as well as its damping effect can be used to simply transfer the plastic hinge inside the beam. Subsequently, the hinge by its plastic performance absorbs more energy than joint to column side and creates a controlled hinge with extra ductility. When frame collapses, plastic hinges have already appeared on every beam, which reflects that principal of “strong column and weak beam” could basically achieved in these frames.

In architectural design since the innovative corbel is assembled into framing system and integrated in connection, therefore the span between columns will be open. This device can be

also hidden behind walls and partitions, thus the architectural design will have the minimum restriction. However the innovative corbel may be considered as an architectural element because of its especially geometrical form.

Since in most cases this device is made up of traditional materials like steel, thus it is expected that environmental effects such as temperature, humidity, creep, corrosion, and dust may not become important. It is worth to be mentioned that in steel yielding devices long-term reliability, performance characteristics, and maintenance costs are well established.

3.4.2 Hysteretic behaviour

To ensure a stable hysteretic behaviour, an energy dissipation device must have a ductile form. Therefore, as far as possible it should be tried to avoid the stiffness degradation of the device by choosing the ductile forms. On the other hand, in welded devices, by forcing yielding to occur in the pre-selected area the sensitivity of welding is relaxed and energy dissipation becomes much more reliable, [Chen et al.-96]. The proposed corbels have a special form that exhibits stable hysteretic behaviour under large story displacements in compare to the common solid cross-section corbels. The ordinary solid cross-section seats because of inductile form and closed geometry cannot demonstrate a stable hysteretic behavior particularly in the case of cyclic loading with large displacement intervals that leads to the stiffness and strength degradation.

To clarifying the behavior of the innovative corbels, it is presented the results of some numerical analysis in a few types of these models. Six specimens with the same material, boundary conditions, and overall dimensions but in different types and geometrical forms, as shown in Fig. 3.9, were numerically analyzed in the case of lateral displacement control. The variations of hysteretic diagram, relative lateral resistance and stiffness of the models, and relative absorbed energy are displayed in Fig. 3.10 to 3.12. In nomination of specimens, the first number is related to the corbel angle at the toe which is 45° or 60°. The normal steel pipes with the length of 50 or 100 mm in the front flange (fp) of web (wp) were used to dissipate energy. Two reference units of semi-solid cross-section corbel (Fig. 3.9-a) and a corbel with a diagonal plate (Fig. 3.9-b) are represented to compare with the others. Evidently, the hysteretic performance of specimen 45°-full-web owe to the open part of the web and free length of the vertical flange to provide an unrestrained deformation otherwise it

has not a ductile form. As can be seen, 45°-Diag. model lose suddenly the bearing capacity under compression after the initial cycles but the other specimens can preserve their hysteretic behavior to the end. The maximum lateral resistance belongs to 60°-wp100-fp100 and the minimum is related to 45°-full-web and 45°-Diag.

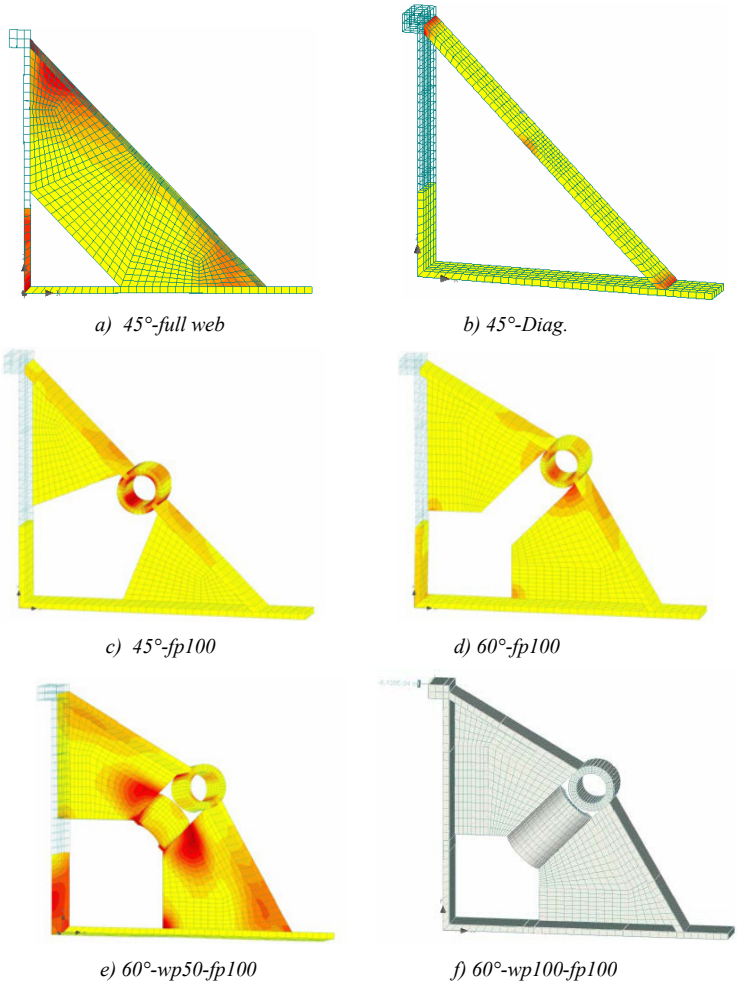

a) 45°-full web *b) 45°-Diag.*

c) 45°-fp100 *d) 60°-fp100*

e) 60°-wp50-fp100 *f) 60°-wp100-fp100*

Fig. 3.9: Different forms of Multi Functional Corbel (HMFC) and their FEM mesh patterns

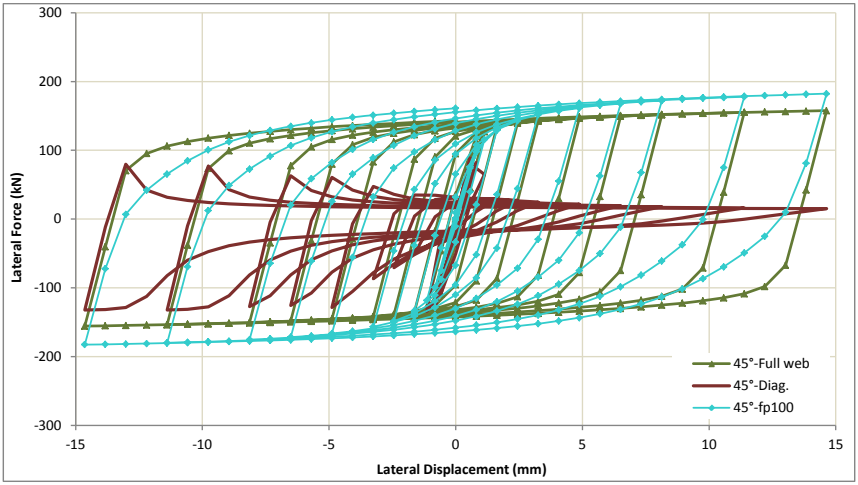

(a)

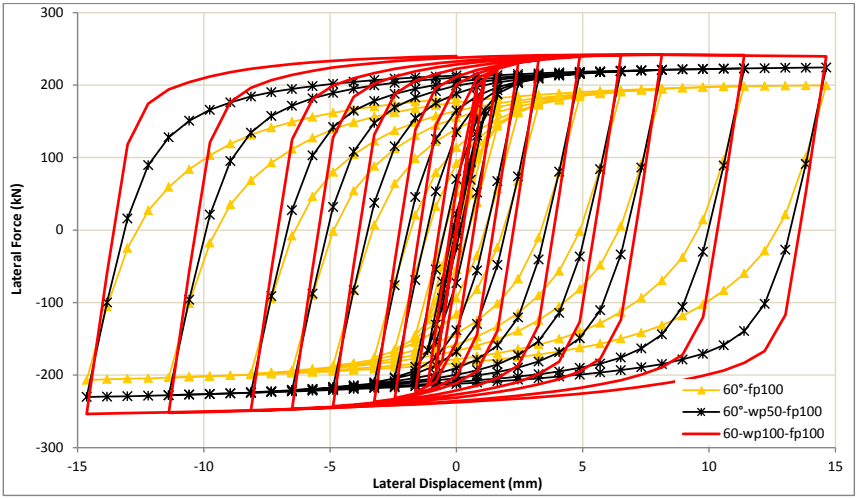

(b)

Fig. 3.10: Variations of hysteretic diagrams in six different variants of Multi Functional Corbels (HMFC)

According to Fig. 3.11 and Fig. 3.12, the Multi Functional Corbels (HMFC) not only may increase the resistance, but also enhance the energy dissipation a lot, so that for instance in 60°-wp100-fp100, increasing of 53% resistance is obtainable with 70% more energy dissipation. The changing in initial stiffness of the units in this study is also interesting (Fig.

3.11-b) so that for instance increasing of 43 and 46% in resistance and energy dissipation for 60°-wp50-fp100 is provided by enhancing 15% in initial stiffness.

Obviously, increasing the length or thickness of pipes in this investigation can lead to the higher amounts, too and in general, considering different geometries for corbel and location of damper devices as well as damper forms and materials can provide variety of properties that are required in practice.

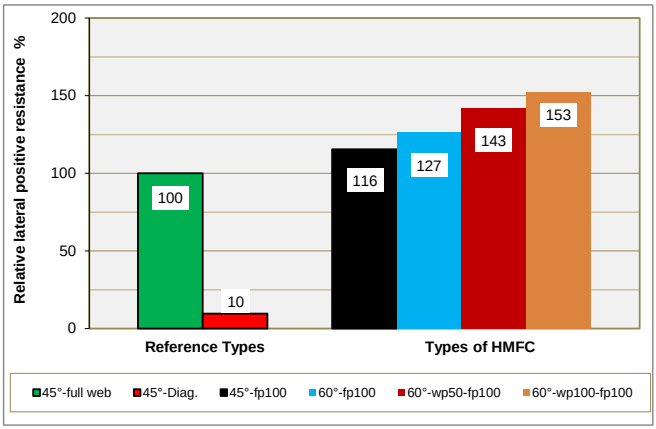

(a)

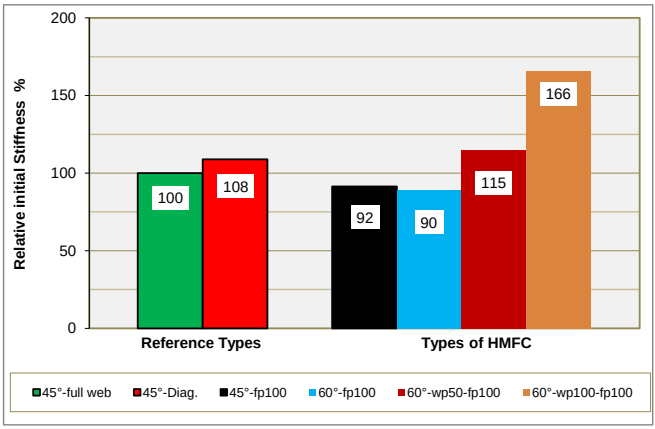

(b)

Fig. 3.11: Relative lateral resistance and initial stiffness of different variants of Multi Functional Corbels (HMFC)

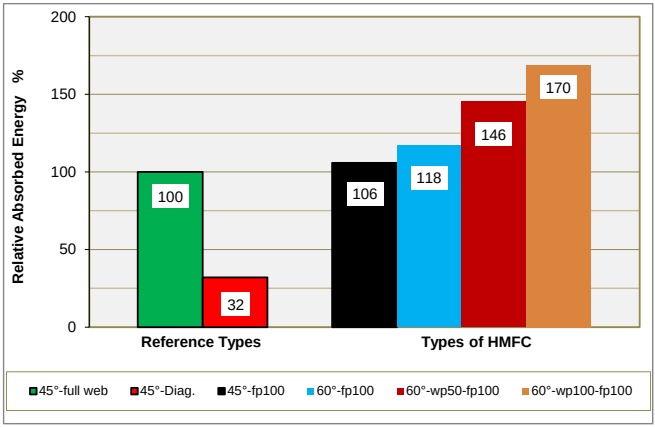

Fig. 3.12: Relative absorbed energy by different variants of Multi Functional Corbels (HMFC)

Considering the available possibilities for researcher to calibrate the simulations, it has been conducted a few compression and tension tests on different pipe specimens which one of them is presented in Fig. 3.13. As can be seen, the numerical simulation is well matched with the experimental result.

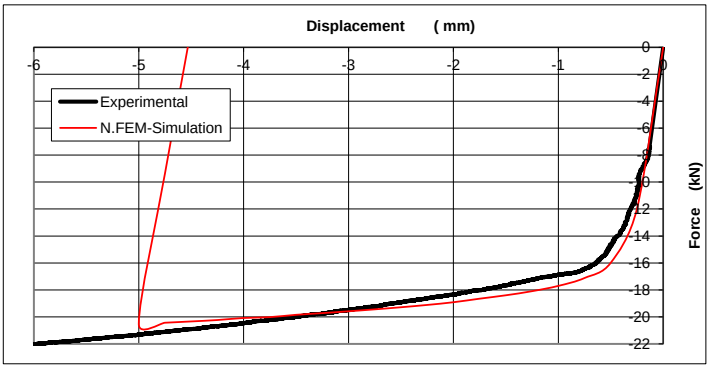

Fig. 3.13: Comparison of a compression test and numerical analysis results on a pipe specimen of 10 mm length and internal diameter and thickness of 42 and 9.15 mm, respectively

3.5 Innovative Harmonica Damper Plates (HHDP)

3.5.1 General description

An innovative Harmonica Damper Plate (HHDP) is installed between the Multi Functional Corbel (HMFC) and the cross plate which is attached on the top or bottom side of the beam away from the corbel to contribute in dissipation energy and increase the lateral strength of the beam-column joint. It is installed in a pod through screws and nuts and then the set is connected to the innovative corbel and the cross plate by screws and threaded rods. The Harmonica Damper Plate (HHDP) includes of narrow arms among the lines which is made up of a steel plate cutting in the form of a harmonica by water-jet cutting or laser cutting. Fig. 3.14 shows a sample of the innovative plate and Fig. 3.15 displays it into a pod. Different dimensions and geometrical forms of the grooves and holes provide to these plates variety of desired mechanical properties to transmit forces and dissipate energy.

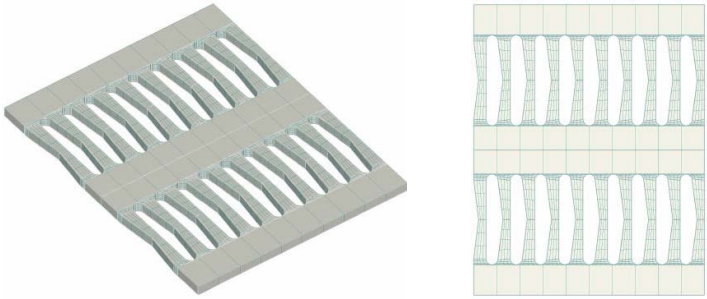

Fig. 3.14: A sample of innovative Harmonica Damper Plate

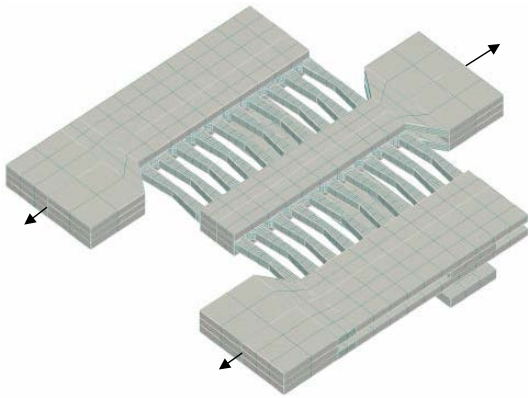

Fig. 3.15:Instalation of innovative Harmonica Damper Plate (HHDP) into a pod

The Harmonica Damper Plate (HHDP) provides energy dissipation through the inelastic deformations of its arms due to the relative displacements between middle and lateral lines. Consequently it can be categorized into hysteretic devices as a metallic yielding damper because its energy dissipation through yielding depends primarily on relative displacements within the device.

The innovative plate shows elastic behavior until the extended stresses to the plate arms are under elastic limit. In this case it functions as an ordinary force transmitter to transmit the imposed loads or displacements. A simultaneous increasing in passed loads or displacements and enhancement of developed strains out of the elastic limits appears inelastic behaviors so that every increase in imposed factors leads to enhancement of the inelastic deformations of the arms. Eventually removing the imposed factors leads to the plastic deformations and energy dissipation. Increasingly cyclic or seismic loadings repeat this step in positive and negative directions and consequently enhance the energy dissipation dramatically. The experimental and numerical study of this device shows that it has a stable hysteretic behavior and a significant portion of the dissipative energy is converted into heat.

The harmonica damper plates not only enhance the absorbed energy performance of the beam hinge but also increase the bending moment capacity due to the tensional strength and high internal moment arm. Therefore, they increase the story shear capacity of the frames.

Since this device is made up of traditional materials like steel, thus it is expected that environmental effects such as temperature, humidity, creep, corrosion, and dust may not become important. It is worth pointing out that in steel yielding devices long-term reliability, performance characteristics, and maintenance costs are well established.

3.5.2 Hysteretic behaviour

The proposed Harmonica Damper Plate (HHDP) has a particular form so that it exhibits a stable hysteretic behaviour to cyclic imposed deformations. To illuminating the behavior of the innovative plate, the results of some numerical analysis is presented. Three different specimens with the same material, boundary conditions, and overall dimensions but in different forms of arms as shown in Fig. 3.16-a –c were numerically analyzed in the case of lateral displacement control. According to the Fig. 3.16-d, for analysis of the specimens, only one arm of every specimen was analyzed. Fig. 3.16-d depicts the principal stresses in the

longitudinal direction of the arms. The type alt-10-10 has a uniform width of 10 mm in overall length of the arm but the others, alt-10-6 and alt-10-7, have 6 and 7 mm widths in the middle of the arms, respectively. The variations of hysteretic diagram are shown in Fig. 3.17. and displacement-strain diagrams for points 1 at the end of the arms and points 2 at the middle of the arms are displayed in Fig. 3.18. As can be seen, the type alt-10-10 has the maximum strength and energy dissipation capacity but the type alt-10-6 has the closest strains at the points of 1 and 2 for -15 mm imposed displacement among the others. Therefore, it can be resulted that in alt-10-6 the strains are uniformly distributed and different parts of the arm simultaneously yield.

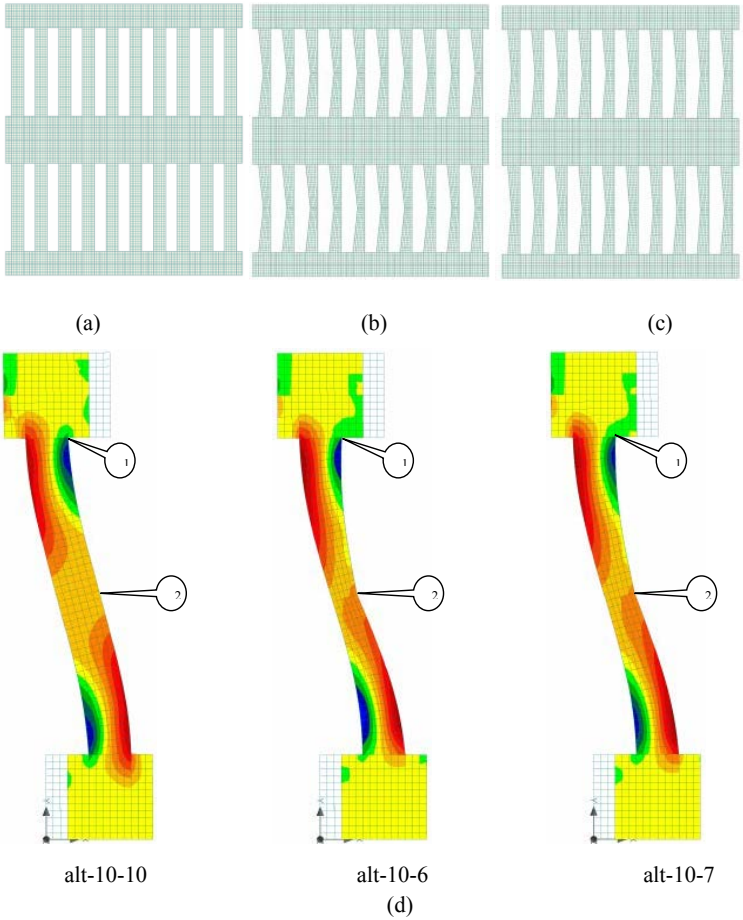

Fig. 3.16: Three different alternatives of innovative Harmonica Damper Plate

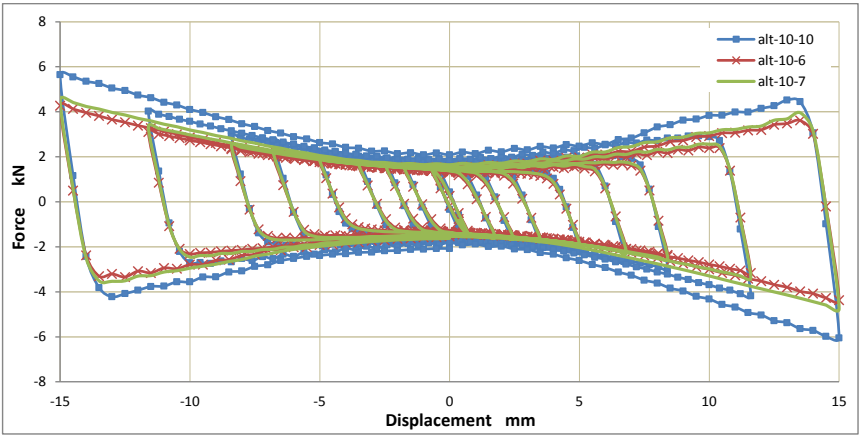

Fig. 3.17: Variations of hysteretic diagram in three different variants of innovative Harmonica Damper Plate (HHDP)

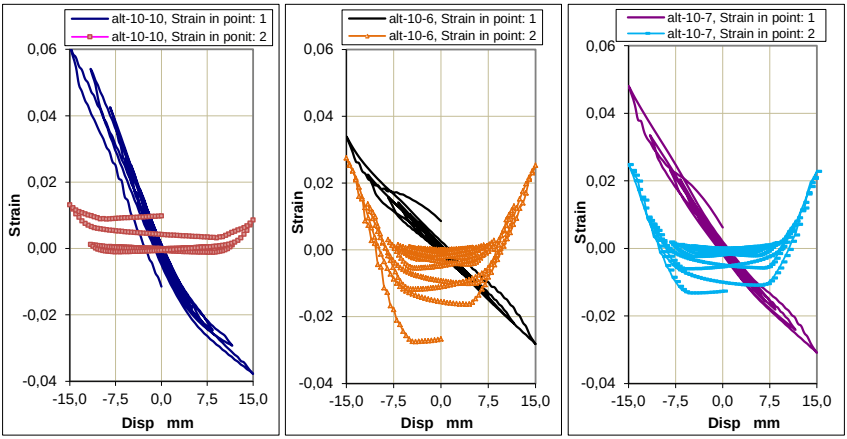

(a) (b) (c)

Fig. 3.17: Displacement-Stain diagrams of three different variants of innovative Harmonica Damper Plate (HHDP) for points 1 and 2

Considering the available possibilities for researcher to calibrate the simulations, it has been conducted a statically compression test on a set of Harmonica Damper Plate (HHDP) with its pod. Fig. 3.18 shows a picture of the experimental test and Fig. 3.19 displays the finite

element model of the specimen. The results of experimental test and numerical analysis are compared in Fig. 3.20. As can be seen, in displacement-force diagram, Fig. 3.20-a, and displacement-strain diagram (strain of a point at the end of the last arm in the main direction, point A), Fig. 3.20-b, the numerical results acceptably match the experimental findings.

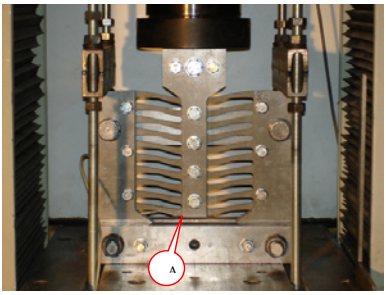

Fig. 3.18: Statically compression test of innovative Harmonica Damper Plate (HHDP)

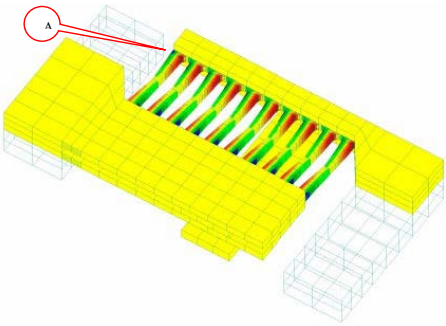

Fig. 3.19: Finite element model of innovative Harmonica Damper Plate (HHDP)

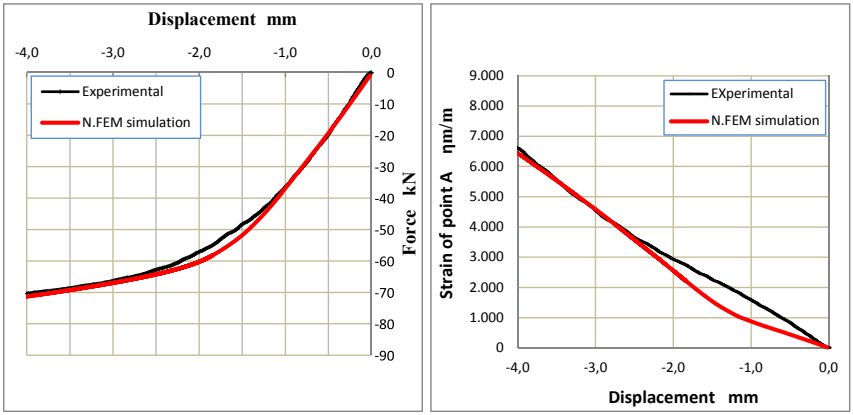

(a) (b)

Fig. 3.20: Experimental and numerical results of test and analysis of innovative Harmonica Damper Plate

3.6 An Innovative strengthening and retrofitting technique through Multi Functional Corbels (HMFC), Retrofitting Technique 1 (RT1)

3.6.1 Approach and modified SFSD

The target is to retrofit the vulnerable existing RC frame structures through the concept of capacity design based on the beam sidesway mechanism and strong column-weak beam performance. By installation of the Multi Functional Corbel system into the existing beam-column joint region, the brittle shear mechanism of the joint is prevented and extra energy absorbed while the failure sequence inverts to form the beam-hinging mechanism. Obviously, the reliable margin of safety should be performed to guarantee the desired failure mechanism and strength hierarchy of the joint subassembly.

When the Multi Functional Corbels, with the length of *a*, height of *b*, and toe angle of $\Theta 1$, are installed above and below the joint region, Fig. 3.21-a and b, the moments of beam and column at the joint zone interfaces can be dramatically reduced, Fig. 3.21-f. On the other hand, the maximum moments in the beam and column are transferred away from the critical joint interfaces, Fig. 3.21-d and f. Consequently, if the system is designed adequately, the reduction of beam-joint moment, M_{bc}, can eliminate the brittle failure of the joint and the migration of the maximum moment in the beam can develop the ductile flexural hinge at a distance *a* from the face of the column.

According to Fig. 3.21-b and c1, the imposed story shear of V_{col} develops the internal forces of F_c and F_e in the chords and edges of the corbels, respectively. The resultant of these forces is F_{re} which has the angle of $\Theta 2$ and passes through the point B, Fig. 3.21-b and b1. The vertical and horizontal components of chord forces, F_c , as well as the edge forces, F_e are shown in Fig. 3.21-c2. The final loads on the beam-column joint subassembly are displayed in Fig. 3.21-c and the moment and shear diagrams of beam and column before and after the retrofitting are depicts in Fig. 3.21-d-g.

To draw the strength and failure sequence diagram (SFSD) in a retrofitted joint in V_{col}- N performance domain, we have to find V_{col} based on the different strengths of joint subassembly such as beam and column shear and bending moment strengths as well as joint shear strength due to the desired limit state of the principal tensile stress of the joint, f_{tj}.

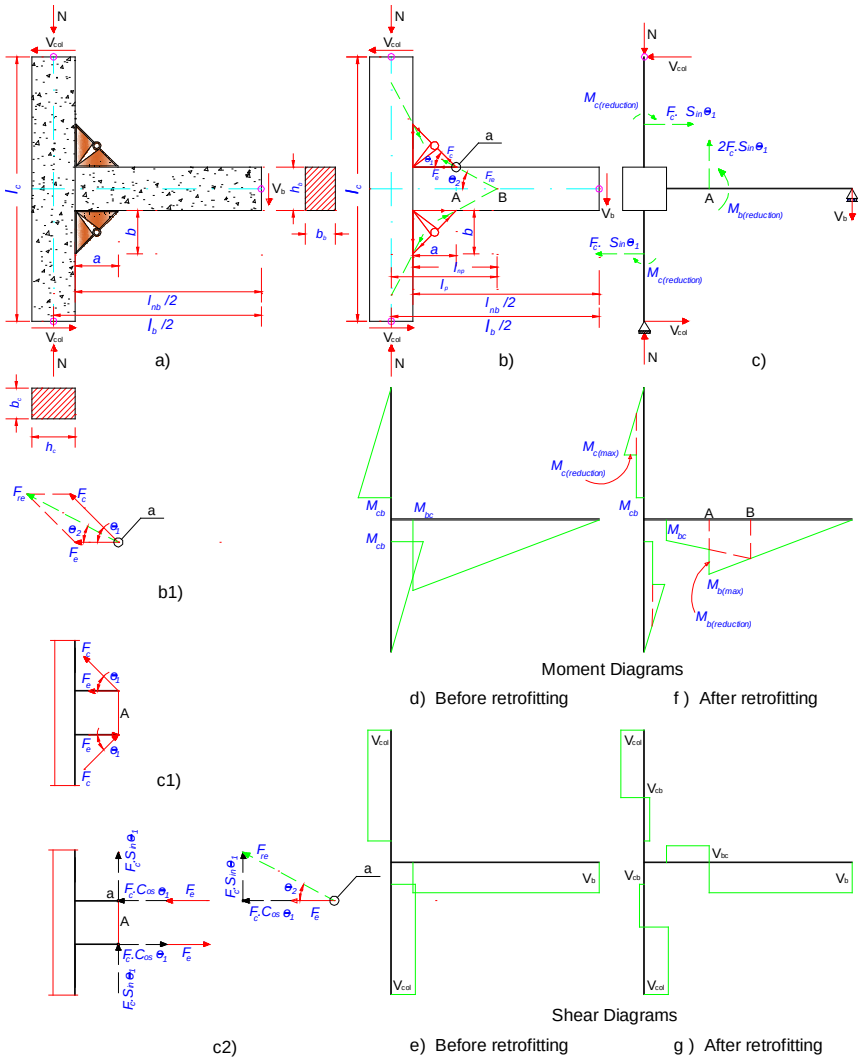

Fig. 3.21: Internal forces in strengthened exterior beam-column joint with Multi Functional Corbel, Retrofitting Technique 1 (RT1)

According to Fig. 3.21-g, the story shear capacity of the retrofitted exterior joint, $\bar{\bar{V}}_{col}$ corresponding to the shear strength of the beam and column and maximum bending moments in the beam and column can be represented as:

$$\bar{\bar{V}}_{col-column\ shear} = V_{nc} \tag{3.17}$$

$$\bar{\bar{V}}_{col-beam\ shear} = V_{nb}.\, l_b/2l_c \tag{3.18}$$

$$V_{col} = M_{b(max)} l_b/l_c(l_{nb} - 2a) \tag{3.19}$$

$$V_{col} = 2M_{C(max)}/(l_c - h_b - 2b) \tag{3.20}$$

The substitution of nominal flexural strength of the beam and column, M_{nb} and M_{nc}, into the $M_{b(max)}$ and $M_{c(max)}$ in Eq. (3.19) and Eq. (3.20), respectively, leads to:

$$\bar{\bar{V}}_{col-beam\ hinge} = M_{nb} l_b/l_c(l_{nb} - 2a) \tag{3.21}$$

and

$$\bar{\bar{V}}_{col-column\ hinge} = 2M_{nc}/(l_c - h_b - 2b) \tag{3.22}$$

To calculate the story shear corresponding to the joint shear strength, the following equations are considered. According to Fig. 3.21-g, the joint horizontal shear force is:

$$V_{jh} = M_{bc}/z_b - V_{cb} \tag{3.23}$$

where:

$$V_{cb} = V_{col} - F_c\, sin\, \Theta 1 \tag{3.24}$$

The beam bending moment at the joint interface will be:

$$M_{bc} = V_b l_{nb}/2 - 2aF_c\, sin\, \Theta 1 - M_{b(reduction)} \tag{3.25}$$

where:

$$M_{b(reduction)} = (F_c\, cos\, \Theta 1 + F_e) z_b \tag{3.26}$$

Therefore, the story shear capacity of the retrofitted exterior joint, $\bar{\bar{V}}_{col}$, based on the joint limit state principal tensile stress of f_{tj} is:

$$\bar{\bar{V}}_{col-joint\ shear} = \frac{A_e\sqrt{{f_{tj}}^2 - f_{tj}N/A_g} + F_c[(2a/z_b - 1)\sin\Theta 1 + \cos\Theta 1] - F_e}{(l_{nb}l_c/l_b z_b - 1)} \quad (3.27)$$

On the other hand, the beam bending moment at the joint interface can be also found as:

$$M_{bc} = V_b\, l_{nb}/2 - 2F_c l_{np}\sin\Theta 1 \quad (3.28)$$

Consequently, the story shear capacity of the retrofitted exterior joint, $\bar{\bar{V}}_{col}$, corresponding to the joint shear strength can be also expressed as:

$$\bar{\bar{V}}_{col-joint\ shear} = \frac{A_e\sqrt{{f_{tj}}^2 - f_{tj}N/A_g} + (2l_{np}/z_b - 1)\,F_c\sin\Theta 1}{(l_{nb}l_c/l_b z_b - 1)} \quad (3.29)$$

Furthermore, the story shear capacity of the retrofitted joint, $\bar{\bar{V}}_{col}$, can be defined according to the joint moment capacity, $\bar{M}_{bc}$ from Eq. (3.12), and the joint limit state principal tensile stress of f_{tj} as:

$$\bar{\bar{V}}_{col-joint\ shear} = \bar{M}_{bc}/z_b - A_e\sqrt{{f_{tj}}^2 - f_{tj}N/A_g} + F_c\sin\Theta 1 \quad (3.30)$$

It is conceivable to distinguish the different strengths of subassemblies and their sequences by drawing SFSD for a retrofitted beam-column joint. It should be arranged the strengths in a sequence that the shear mechanism is avoided in the joint, beam, and column, when the beam flexural yielding (beam flexural hinge) occurs at the end of the Multi Functional Corbel (HMFC) before column reaches its flexural strength (strong column-weak beam behaviour). If the corbels are designed effectively, the induced joint moment, M_{bc}, will be decreased significantly so that the reduced joint horizontal shear forces cannot lead to a shear mechanism. Considering the SFSD, if the beam and column need to shear strengthening, they can be retrofitted by ordinary shear retrofitting methods such as utilising the FRP fabrics.

3.6.2 Upgrading the resistance to bond-slip of the beam bottom bars

As stated before, the slippage of beam bottom positive bars due to inadequate development length or joint confinement is one of the main deficiencies of RC GLD frame structures that contribute to the collapse during an earthquake. The proposed retrofitting technique not only can prevent the joint brittle shear failure but also can rehabilitate the development length of beam positive moment reinforcement at joint region.

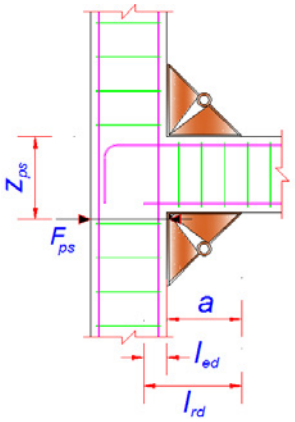

Fig. 3.22: The rehabilitation of development length of beam positive bars

According to Fig. 3.22, the inadequate existent development length of beam positive bars, l_{ed}, can be rehabilitated through the proposed retrofitting technique. As can be inferred, the modified bending moment diagram of the beam in the retrofitted case, Fig. 3.21-f, clarifies that the available length of the beam bottom reinforcement in back side of the corbel toe, l_{rd}, should provide the minimum required development length corresponded to the reduced moment at point A. Therefore, it may be written that:

$$l_{rd} \geq \frac{M_{nb} - M_{b(reduction)}}{M_{nb}} l_d \tag{3.31}$$

where:

l_d development length in tension of deformed bar based on the building codes, mm

and

$$l_{rd} = l_{ed} + a \tag{3.32}$$

Furthermore, to provide the reduced bending moment at the joint interface, M_{bc}, the bottom corbel should be satisfactorily fixed to the column close to the joint region. It can be carried out by different methods for instance post-stressed of threaded rods. In that case the total post-tensioning force may satisfy the following relation:

$$F_{ps} \geq \frac{M_{bc}}{z_{ps}} \tag{3.33}$$

where:

F_{ps} total post-tensioning force of the bottom corbel, N

z_{ps} proper moment arm of the bottom corbel post-tensioning, mm

3.6.3 Procedure for designing and developing

The Procedure for designing and developing of the innovative retrofitting technique through Multi Functional Corbels is based on try-and-error. The proposed procedure is explained through the following steps. The iterations on choosing design parameters are continued to attain the desired retrofitting target (strong column-weak beam behaviour).

Step 1: The strength and failure sequence diagram (SFSD) for the as built joint is drawn and then the weaknesses and deficiencies of subassemblies and their sequences are known.

Step 2: The joint moment capacity ($\bar{M}_{bc}$) from Eq. (3.12) for the as built joint, based on the joint limit state principal tensile stress of f_{tj}, is calculated. According to the literature different limit states for f_{tj} were proposed, for instance by [Pantelides et al.-02] as given in section 2.2, but for the practical use we can assume it equal to $0.29\sqrt{f_c'}$ for the first diagonal shear cracking as it was confirmed by the experimental test during the current research.

Assuming that the first diagonal shear cracking and beginning of the producing beam flexural plastic hinge at the end of HMFC are simultaneously occurred, if the first diagonal shear cracking is chosen as the limit state, there will be a reasonable margin of safety for joint in passing through extensive damage to completely joint shear failure at the strain hardening steps of flexural reinforcement.

Step 3: The design parameters of the Multi Functional Corbel (a, b, $\Theta 1$, and initial sections of the corbel members) are preliminary selected.

Step 4: The simplified model of strengthened beam-column joint is elastically analysed. It should be controlled that under the $\bar{\bar{V}}_{col-beam\ hinge}$ the joint moment M_{bc} is not more than $\bar{M}_{bc}$. If this condition is not satisfied, the design parameters of the corbels should be redefined and modified and subsequently, the model must be reanalysed. The iteration process should be reviewed until the assumed condition is provided.

Step 5: In the case of bond deficiency due to the slippage of beam bottom positive bars, the horizontal length of the corbel through Eqs. (3.31) and (3.32) should be checked and finally the Eq. (3.33) must be satisfied.

Step 6: The SFSD for the retrofitted joint is prepared and the strengths of subassemblies and their hierarchies are checked. If $\bar{\bar{V}}_{col-column\ hinge}$ is not satisfied the required conditions, first of all it should be tried to improve it by changing the design parameter b of the corbel otherwise the column needs to a local supplementary moment strengthening to properly invert the strength hierarchy. If it is needed, the capacities of $\bar{\bar{V}}_{col-beam\ shear}$ and $\bar{\bar{V}}_{col-column\ shear}$ can also be qualified by supplementary shear strengthening.

Obviously, the desired strength sequences of subassembly will be ensured, if the reasonable margins of safety are practically established among the different strengths of the joint subassembly to resolving the unpredictable events and material and models uncertainties. Apparently, to achieve the logical safety factors independent investigations are needed.

As mentioned before, moreover the dissipated energy through the beam flexural hinge, the Multi Functional Corbels are also capable to absorb extra imposed energy by exhibiting the elasto-plastic hysteretic behaviour. To attain this property, the corbel set system should be designed so that its yield strength reaches before the beam flexural hinge occurs and joint system exits from elastic domain. Consequently, any increasing in story shear enhances the internal forces of the elastic joint system to reach the plastic hinge at the end of corbels while the elasto-plastic behaviour is appeared in the corbels and dissipates energy.

3.7 An Innovative strengthening and retrofitting technique through HMFC and Harmonica Damper Plates (HHDP), Retrofitting Technique 2 (RT2)

3.7.1 Approach and modified SFSD

Similar to the last innovative retrofitting technique, the aim is to upgrade the vulnerable existing RC frame structures through the concept of capacity design based on the beam sidesway mechanism and strong column-weak beam performance. By installation of the Multi Functional Corbel (HMFC) system as well as Harmonica Damper Plates into the joint region, the joint brittle shear mechanism is avoided, the story shear capacity is desirably increased, and energy dissipation in the innovative corbels and harmonica plates is extra obtained while the failure sequence inverts to form the beam-hinging mechanism. Obviously, the logical margin of safety can guarantee the desired failure mechanism and strength hierarchy of the joint subassembly.

When the strengthening complex of Multi Functional Corbels (with the length of a, height of b, and toe angle of $\Theta 1$) and Harmonica Damper Plates (with the overall length of c and additional height of h) are installed above and below the joint region, Fig. 3.23-a and b, the moments of beam and column at the joint zone interfaces can be dramatically reduced, Fig. 3.23-f while the Harmonica Damper Plates contribute to the beam bending moment between points A and C and enhance the overall moment capacity in this segment. The overall increased bending moment capacity at the end of corbels leads to enhancement of story shear and energy dissipation through the beam hinge and elsto-plastic behaviour of Harmonica Damper Plates. Moreover, the maximum moments in the beam and column are transferred away from the critical joint interfaces, Fig. 3.23-d and f. Consequently, if the system is designed adequately, the beam-joint moment, M_{bc}, is reduced and subsequently the brittle failure of the joint is eliminated, furthermore, the maximum moment of the beam and column is migrated inside the members away from the critical points and the ductile flexural hinge is developed at the end of the corbels.

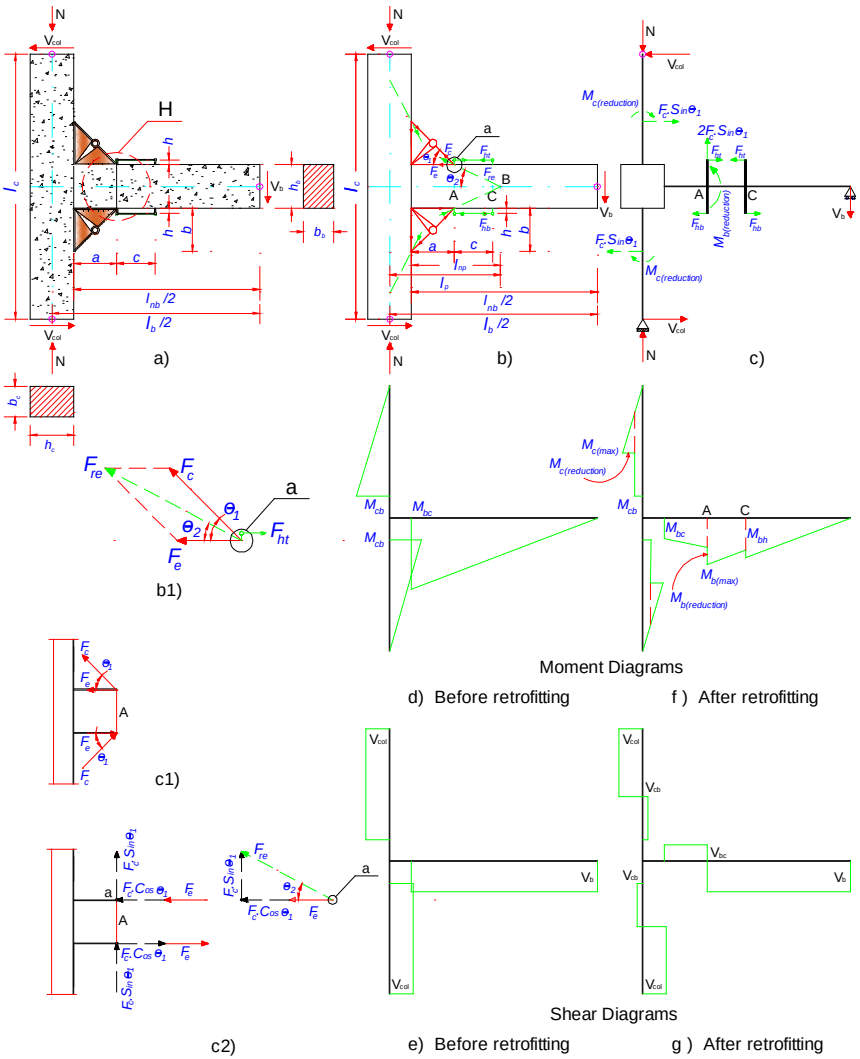

Fig. 3.23: Internal forces in strengthened exterior beam-column joint with Multi Functional Corbel (HMFC) and Harmonica Damper Plates (HHDP), Retrofitting Technique 2 (RT2)

The imposed story shear of V_{col} develops the internal forces of F_c and F_e in the chords and edges of the corbels, respectively, and force of F_h in the harmonica plates, Fig. 3.23-b, b1 and c1. The resultant of corbel forces is F_{re} which has the angle of $\Theta 2$ and passes through the

point B, Fig. 3.23-b and b1. The vertical and horizontal components of chord forces, F_c , as well as the edge forces, F_e are shown in Fig. 3.23-c2. The internal forces of harmonica plates, F_h, are applied at the distance of h from the upper and lower levels of the beam. The final loads on the beam-column joint subassembly are displayed in Fig. 3.23-c and the moment and shear diagrams of beam and column before and after the retrofitting are depicts in Fig. 3.23-d to Fig. 3.23-g.

The strength and failure sequence diagram (SFSD) in a retrofitted joint in V_{col}- N performance domain is drawn by finding V_{col} based on the different strengths of the joint subassembly such as beam and column shear and bending moment strengths as well as the joint shear strength due to the desired limit state of the principal tensile stress of the joint, f_{tj}. Since the installing of Harmonica Damper Plates increases the bending moment capacity of the beam at the end of the corbels, the story shear capacity of the system due to the capacities of the beam at the point C should be also considered.

As shown in Fig. 3.23-g, the story shear capacity of the retrofitted exterior joint, $\bar{\bar{V}}_{col}$, corresponding to the shear strength of the beam and column can be obtained from Eq. (3.17) and Eq. (3.18), respectively.

Fig. 3.24 displays the detail of H (as referred to in Fig. 3.23), a section of the beam at the end of HMFC along with HHDP, and assumed stain distribution. For simplicity, it is assumed a linear distribution of strain across the section, although it may not be exactly correct, because of probable shear lag between HHDP and concrete section. According to Fig. 3.24-c, the strains of top and bottom HHDP in the balanced strain condition of the beam under a negative moment will be ε_{shb} and ε'_{shb}, respectively. As it is known, in balanced condition, tension reinforcement reaches the strain corresponding to f_y just as concrete in compression reaches its assumed ultimate strain (ε_{cu}) and the neutral axis is located at a distance x_b from extreme compression fiber. It can be seen that the stain amounts of HHDP are more than the maximum strains in concrete and reinforcement. As it is known, in practical cases because of tension-controlled concept, the neutral axis height (x) is less than x_b, therefore the strain distribution such as Fig. 3.24-d can be expected in which the strain amounts of reinforcement (ε_s) and HHDP (ε_{sh} and ε'_{sh}) are much more than the strains corresponding to yield strength. Consequently, it can be supposed that in practical issues the HHDP is completely shows a

plastic behaviour, on condition that the HHDP form provides yield state at the defined strain, Fig. 3.20, and also the beam shear failure is avoided.

On the other hand, in the conditions that the strain in HHDP reaches the yield strain ε_{shy} and ε'_{shy}, Fig. 3.24-e, the strains of reinforcement and concrete are much smaller than the yield and ultimate strain, respectively. Consequently, although the RC section is in elasto-plastic domain, the plastic behaviour is exhibited by HHDP and therefore the energy dissipation is started through hysteretic performance while the main RC section shows elasto-plastic behaviour. This is a unique performance of HHDP to dissipation of imposed energy through bending moments smaller than the plastic capacity of the main section.

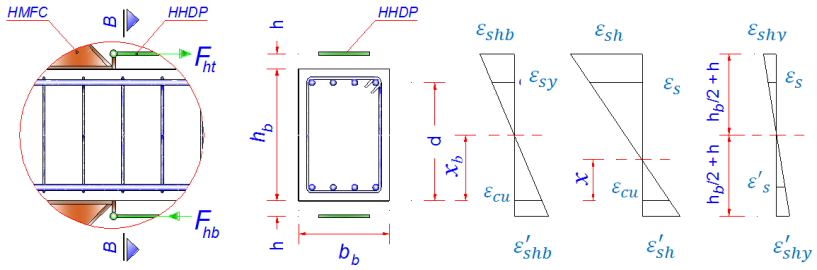

Fig. 3.24: Detail of H as referred to in Fig. 3.23 and assumed strain distribution in the strengthened beam section at the end of HMFC

To find the relation between the story shear and the maximum bending moment of the beam we have:

$$V_{col} = (M_{b(max)} + M_h) l_b / l_c (l_{nb} - 2a) \tag{3.34}$$

where:

$$M_h = F_{ht}(h_b - x + h) + F_{hb}(x + h) \tag{3.35}$$

is the extra bending moment provided by the twin Harmonica Damper Plates (HHDP) that F_{ht} and $F_{hb}$are the forces corresponding to the strains of the HHDP at the top and bottom of the beam, respectively. If the shear failure of the beam is avoided, then it is expected that the

strain condition of Fig. 3.24-d is available, therefore, the nominal flexural strength of the beam and HHDP can be simultaneously occurred in which the corresponding flexural capacity of twin HHDP will be:

$$M_{nh} = F_{hy}(h_b + 2h) \tag{3.36}$$

Where F_{hy} is the force corresponding to the yield state of HHDP, provided that the strain distribution is like the Fig. 3.24-d. The substitution of the nominal flexural strength of the beam, M_{nb}, and flexural capacity of twin Harmonica Damper Plates, M_{nh}, into the $M_{b(max)}$ and M_h in Eq. (3.34), respectively, leads to the story shear capacity corresponding to the overall flexural strength as:

$$\bar{\bar{V}}_{col-beam\ \&\ HHDP\ hinge} = (M_{nb}+M_{nh})l_b/l_c(l_{nb} - 2a) \tag{3.37}$$

As can be seen, the story shear capacity is increased by installing of the harmonica plates.

The maximum shear carrying capacity of the story due to column bending strength is found by Eq. (3.22).

According to Fig. 3.23-c, f and g, the story shear capacity corresponding to the joint horizontal shear strength can be obtained by Eqs. (3.27), (3.29), and (3.30).

It is possible to find out the different strengths of the joint subassembly and their sequences by drawing SFSD for a retrofitted joint. It should be organized the strengths in a subsequence that the shear mechanism is avoided in the joint, beam, and column, when the beam flexural yielding (beam flexural hinge) and Harmonica Damper Plates yielding occur at the end of the Multi Functional Corbel (HMFC) before column reaches its flexural strength (strong column-weak beam behaviour). In addition the bending moment strength at the end of the corbels, point A, and the bending strength of the beam at the end of Harmonica Damper Plates, point C, should be also controlled because the twin harmonica plates increase the overall bending capacity at the point A and the capacity of the point C may not tolerate the bending enhancement at point A. The same control must be carried out for shear strengths of the beam between the internal harmonica plate segment, A to C, and external parts, if the shear strength of the internal segment is upgraded. Consequently, as can be inferred, the number of control

points in SFSD (Fig. 3.7) through this retrofitting technique may be increased more than five. If the corbels are designed efficiently, the induced joint moment, M_{bc}, will be decreased considerably so that the reduced joint horizontal shear forces cannot lead to a joint shear mechanism. Considering the SFSD, if the beam and column need to shear retrofitting, they can be strengthened by common shear retrofitting methods.

3.7.2 Upgrading the resistance to bond-slip of the beam bottom bars

This innovative technique like the last retrofitting method (RT1) is also able to rehabilitate the development length of beam positive moment reinforcement at joint region. According to the Fig. 3.25, as described before, through the selecting an adequate horizontal length for the bottom corbel, a, and consequently providing the minimum required development length for the bottom reinforcement of the beam, l_{rd}, corresponding to the reduced moment at point A and also properly fixing the top of the bottom corbel to the column for providing M_{bc} at the beam joint interface, it will be possible to rehabilitate the slippage of beam bottom positive bars. The design relations are the same with the last retrofitting technique, Eqs. (3.31) to (3.33).

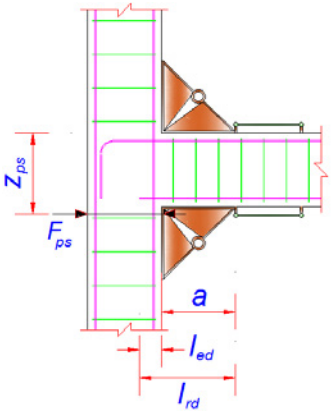

Fig. 3.25: The rehabilitation of development length of beam positive bars

3.7.3 Procedure for designing and developing

The Procedure for designing and developing of the proposed retrofitting technique through Multi Functional Corbels and Harmonica Damper Plates is based on try-and-error. The suggested procedure is described through the next steps. The iterations on selecting design

parameters are continued to achieve the desired retrofitting aim (strong column-weak beam behaviour).

Step 1: The strength and failure sequence diagram (SFSD) for the as built joint is drawn and then the weaknesses and deficiencies of subassemblies and their sequences are known.

Step 2: The joint moment capacity ($\bar{M}_{bc}$) from Eq. (3.12) for the as built joint, based on the joint limit state principal tensile stress of f_{tj}, is calculated. According to the literature different limit states for f_{tj} were proposed, for instance by [Pantelides et al.-02] as given in section 2.2, but for the practical use we can assume it equal to $0.29\sqrt{f_c'}$ for first diagonal shear cracking as it was confirmed by the experimental test during the current research.

Assuming that the first diagonal shear cracking and beginning of the forming beam flexural plastic hinge at the end of HMFC are simultaneously occurred, if the first diagonal shear cracking is chosen as the limit state, there will be a reasonable margin of safety for joint in passing through extensive damage to completely joint shear failure at the strain hardening steps of flexural reinforcement and HHDP.

Step 3: The design parameters of the Multi Functional Corbel (a, b, $\Theta 1$, and initial sections of the corbel members) are preliminary selected.

Step 4: With knowing the nominal flexural strength of the beam at the end of Multi Functional Corbels, M_{nb}, and the required increased story shear capacity, $\bar{\bar{V}}_{col-beam\ \&\ HDP\ hinge}$, the needed bending moment capacity corresponding to the twin Harmonica Damper Plates, M_{nh}, is calculated by Eq. (3.37). Subsequently, the tensile and compression strength of the Harmonica Damper Plate (HHDP), F_{hy}, is obtained by Eq. (3.36) and then the dimensions and geometry of Harmonica Damper Plates can be estimated and through a limited try–and-error process modified.

Step 5: The simplified model of upgraded beam-column joint is elastically analysed. It should be controlled that under the $\bar{\bar{V}}_{col-beam\ \&\ HDP\ \ hinge}$ the joint moment M_{bc} is not more than $\bar{M}_{bc}$. If this condition is not satisfied, the design parameters of the corbels should be redefined and modified and subsequently, through the steps 4 and 5 the changes should be considered and

the model reanalysed. The iteration process should be reviewed until the assumed condition is provided.

Step 6: In the case of bond deficiency due to the slippage of beam bottom positive bars, the horizontal length of the corbel through Eqs. (3.31) and (3.32) should be checked and finally the Eq. (3.33) must be satisfied.

Step 7: The SFSD for the retrofitted joint is prepared and the strengths of subassemblies and their hierarchies are checked. During the drawing of SFSD, the flexural and maybe shear strength of the beam out of the Harmonica Damper Plate (HHDP) segment, at point C, should be considered with their overall corresponding at point A.

The capacity of $\bar{\bar{V}}_{col-column\ hinge}$ must be satisfied the required conditions, otherwise it should be improved by changing the corbel design parameter of b or local supplementary moment strengthening to properly invert the strength hierarchy. If it is needed, the capacities of $\bar{\bar{V}}_{col-beam\ shear}$ and $\bar{\bar{V}}_{col-column\ shear}$ can also be qualified by supplementary shear strengthening.

As stated before, to resolving the material and analytical model uncertainties and also unpredictable events in the practical cases, the reasonable margins of safety should be considered in comparing the different strengths of the joint subassembly with each other through the independent investigations.

As mentioned before, moreover the dissipated energy through the beam flexural hinge and yielding of Harmonica Damper Plates, the Multi Functional Corbels are also capable to absorb extra imposed energy by exhibiting the elasto-plastic hysteretic behaviour. To achieve this property, the corbel set system should be designed so that its yield strength reaches before the beam flexural hinge forms and joint system exits from elastic domain. Consequently, any increasing in story shear enhances the internal forces of the elastic joint system to reach the plastic hinge at the end of corbels while the elasto-plastic behaviour is appeared in the corbels and dissipates energy.

Chapter 4

Experimental Program and Development

4.1 Introduction

This chapter presents the experimental study program and its results. In order to study the behavior of the vulnerable RC beam-column joints built in the 1970s, two kinds of deficiencies have been considered, bond-slip and shear deficiencies. The bond-slip deficiency can cause significant strength degradation and contribute to the collapse of structure because of the inadequate anchorage of beam bottom positive bars and their slippage. The joint shear deficiency causes a brittle shear mechanism of low ductility and leads dramatically to a local and global strength degradation, because the story shear capacity corresponding to the joint shear is less than the capability due to the beam plastic hinge and moreover the joint has inadequate reinforcement. The substandard 2/3-scale one-way exterior beam-column joint specimens and their retrofitted ones are subjected to reversed cyclic loading and constant column axial load. The as-built deficient units are tested as the reference specimens and the upgraded ones are evaluated for the efficiency of the proposed innovative retrofitting techniques. The production process of the test specimens as well as loading setup design and fabrication are described in this chapter. The design of proposed energy dissipation devices, Multi Functional Corbels (HMFC) and Harmonica Damper Plates (HHDP), are explained and their producing and installing are depicted. The instrumentation and measurements of loads,

displacements and strains are presented and estimation of rotations and distortions are described. The Strength and Failure Sequence Diagrams (SFSD) of reference and retrofitted specimens are drawn and finally the test results and their interpretations as well as their behaviours are presented and compared.

4.2 Test specimens, energy dissipation devices and retrofitting

In the following subsections, the design, dimensions, details, and production of the RC test specimens and the innovative strengthening and energy dissipation devices as well as the upgrading process of units are described in detail.

4.2.1 RC beam-column joint specimens

Two shear deficient (SD) and three bond-slip deficient (BD) RC beam-column joint specimens are considered in this study. From every deficiency, one specimen is chosen as the reference or in the other word benchmark unit, (BD-B) and (SD-B), and the others are retrofitted by the two innovative retrofitting techniques (RT1 and RT2) mentioned in the last chapter.

4.2.1.1 Material properties

The concrete of the shear deficient (SD) and bond-slip deficient (BD) specimens which casting in different times had the same strength class (specified compressive strength of concrete, 30/37 MPa). The sample tests and average values of two sample test results for specimens are presented in the Fig. 4.1 and Table 4.1, respectively.

The steel reinforcement consisted of Φ6, Φ8, Φ10, Φ12, and Φ16 mm deformed bars with nominal yield strength of 500 MPa. The average values of three measured tensile strength for every reinforcing steel bar used in the test specimens are displayed in Table 4.2.

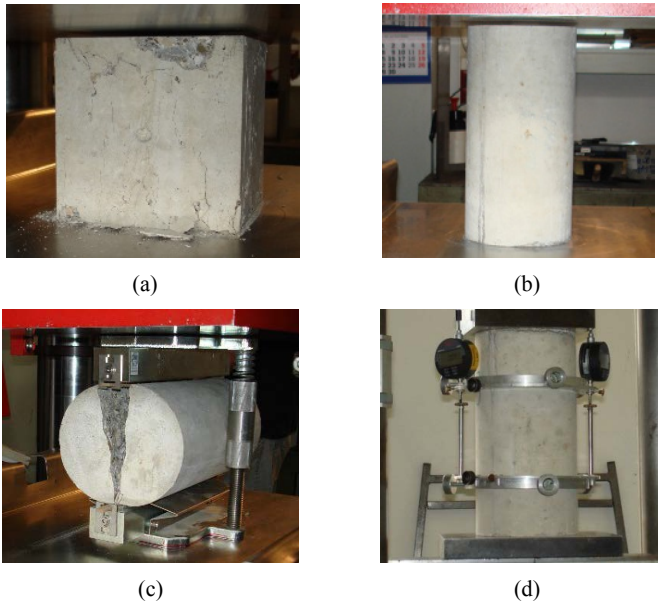

(a) (b)

(c) (d)

Fig 4.1: Test of concrete samples, tests of a) cubic compression, b) cylinder compression c) split, and d) modulus of elasticity

Table 4.1: Average measured properties of concrete

		Specimen	Cylinder (150x300) MPa			Cubic (150x150) MPa
			Compression	Modulus of elasticity	Tension (Split test)	Compression
Laboratory-cured samples (10 Samples)	7 Days	SD	*30.45*	-	-	-
		BD	*32.44*			
	28 Days	SD	*38.80*	*27500*	*3.36*	*46.85*
		BD	*41.60*	*26100*	*3.52*	*47.78*
Field-cured samples (6 Samples)	24 months	SD	*47.75*	*29100*	*3.68*	*54.70*
		BD	*49.15*	*29200*	*3.55*	*58.28*

Table 4.2: Average measured properties of reinforcing steel bars

Bar size (mm)	Φ6	Φ8	Φ10	Φ12	Φ16
Yield strength f_y (MPa)	538	569	564	602	552
Tensile Strength f_u (MPa)	598	675	669	657	649
ε_u	0.165	0.170	0.165	0.158	0.165

4.2.1.2 Design, dimensions and details

The 2/3-scale exterior RC beam-column joint specimens were designed according to the pre-1970s building code of practice, ACI 318-63; including deficient detailing so that the shear and bond slip deficiencies were clearly distinguished in test specimens, [ACI 318-63]. Fig. 4.2 shows the geometry and overall dimensions of the test specimens and Fig. 4.3 and 4.4 display the reinforcement details of the shear deficient (SD) and bond-slip deficient (BD) specimens, respectively. As can be seen, there is no joint shear reinforcement in both kinds of the specimens and BD test specimens have the beam bottom bars with an embedment length of only 150 mm into the joint.

To find out the design requirements of different building codes of practice for the assumed joint test specimens to seismic resistant, Table 4.3 is provided considering the Table 2.1. According to the Table 4.3, the development length of the beam hooked bars into the joint is satisfied based on the ACI 318-11 and ACI 352-02 but Eurocode 8 needs to a more column height to satisfactorily anchor the beam bars. The ACI codes require the small amount of minimum joint horizontal reinforcement and on the other hand predict low nominal joint shear strength in comparison to the Eurocode 8. Furthermore, providing the joint vertical reinforcement is suggested by Eurocode 8 while the others don't claim. To prevent column hinging during the test and concentrate on the deficiencies of the joint, the flexural strength ratio of columns to beam should be chosen more than the code requirements. To find proportioning the test modules for flexural strength ratio of columns to beam, section R9.1.2 [ACI 374.1-05] specifies that the column axial load effect should be neglected. Therefore, the flexural strength ratio ($M_R = \sum M_{nc} / \sum M_{nb}$) for the assumed test specimens was obtained equal to 1.53 which was greater that the code requirements. On the other hand, the beam shear

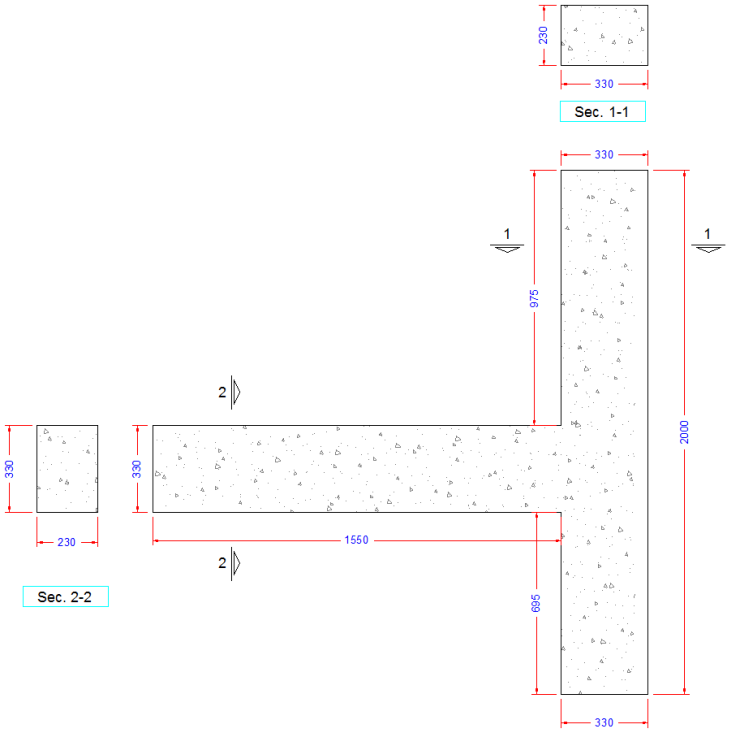

Fig. 4.2: The overall geometry of specimens

strength was intentionally provided lower than the code requirements for seismic resistant so that the existing nominal beam shear strength equal to 83.7 kN is less than the imposed beam shear of 134 kN corresponding to the beam end probable flexural strength. In test specimens, the provided transverse reinforcement of the beam and column close to the joint region does not also satisfy the seismic resistant requirements so that based on ACI 318-11 it should be provided in the beam over a minimum length of 660 mm ($2h_b$) from the face of the column with maximum spacing of 74 mm (Min. d/4 , $6d_b$, and 150 mm) while these amounts for the column transverse reinforcement must be 450 mm (Max. h_c , $l_{cn}/6$, $b_c/4$, 450 mm), and 58 mm ($b_c/4$, $6d_b$, $100 + (350 - h_x)/3$, and 150 mm) respectively, where d is the effective height of the member, d_b is the diameter of the Min. bar, l_{cn} is the clear length of the column, and h_x is the Max. center-to-center spacing of crosstie legs on all faces of the column in mm.

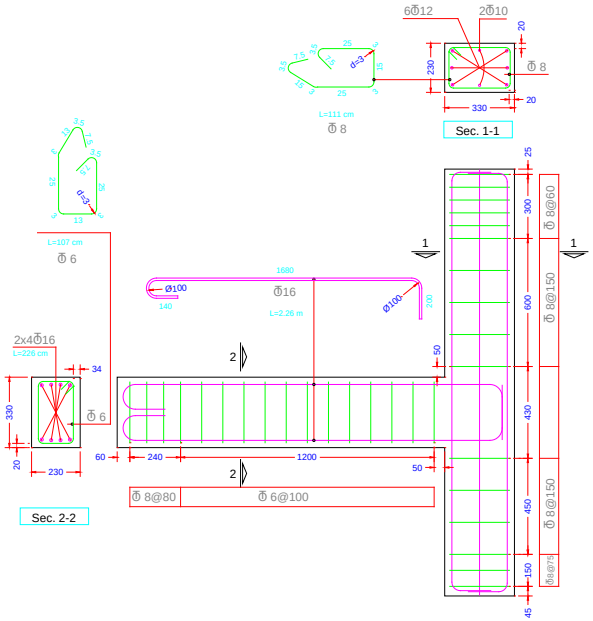

Fig. 4.3: Reinforcement details of specimens SD

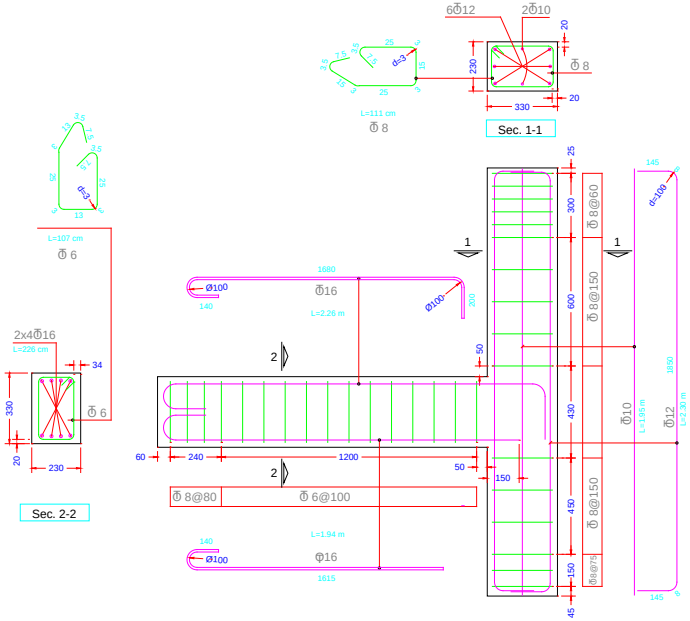

Fig. 4.4: Reinforcement details of specimens BD

Table 4.3: Summary of the design requirements for the test specimens based on the codes of practice for seismic resistant

	ACI 318M-11	ACI 352R-02	Eurocode 8 EN 1998-1:2004
Development length of hooked bars	$l_{dh} \geq 270\ mm$	$l_{dh} \geq 264\ mm$	$h_c \geq 409\ mm$
flexural strength ratio of columns to beams $(\sum M_{nc} / \sum M_{nb})$	≥ 1.2	------	≥ 1.3
Nominal shear strength of the joint	415 kN	415 kN	687 kN
Required Min. joint horizontal reinforcement	$A_{Tjh} \geq 516\ \ mm^2$	$A_{Tjh} \geq 516\ \ mm^2$	$A_{Tjh} \geq 887\ \ mm^2$
Joint vertical reinforcement	-----	------	$A_{sv,i} \geq 592\ \ mm^2$

On the other hand, in the assumed specimens (BD and SD), the nominal strengths of beam-column joint subassemblages can be predicted based on ACI 318-11 as the table 4.4. It should be noted that the column axial compressive load of 300kN (nearly $0.13A_g f'_c$) was considered in the represented table and according to articles 21.5.4.2 and 21.6.5.2 of ACI 318-11 [ACI 318M-11], the contribution of concrete to shear strength of beam and column, because of cyclic loading, should be eliminated.

Table 4.4: Summary of the predicted nominal strengths of beam-column joint specimens' subassemblages

	Positive flexural strength $(+M_n)$ kN.m	Negative flexural strength $(-M_n)$ kN.m	Shear strength (V_n) kN	
Beam (BD)	20.0 *	108.5	83.7 **	147.1***
Beam (SD)	109.7	109.7		
Column	For N=300 kN $M_n = 119.6$		99.2 **	180.5***

* at the beam-joint interface

** the contribution of the concrete to shear strength is eliminated

*** the contribution of the concrete to shear strength is not eliminated

4.2.1.3 Production of test specimens

The test specimens have been produced through the following stages.

- Preparing of reinforcements through cutting and bending them into the desired lengths and shapes, Fig. 4.5:

  Although the steel bars were cut by angle grinder and bent by simple handmade devices (Fig. 4.5-a, c) the dimensions and bend diameters (Fig. 4.5-b) were desired according to the ACI 318-63.

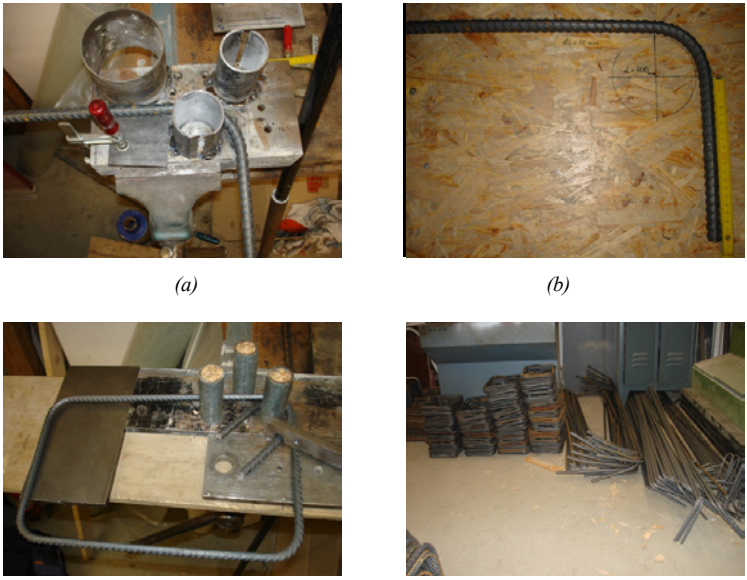

(a) *(b)*

(c) *(d)*

Fig. 4.5: Preparing of reinforcing bars

- Preparing of reinforcing bars to attaching and sticking the strain gauges, connecting the cables, and covering strain gauges with water resistant materials, Fig. 4.6:

  The bar surfaces were prepared with flap discs and abrasive papers and then were cleaned with acetone and after that the strain gauges were attached by adhesive (Fig. 4.6-a). The cables were soldered to the terminals and fixed to the bars (Fig. 4.6-b) then

the gauges were covered with waterproof liquid material (Fig. 4.6-c) and finally the places were covered with waterproof tapes (Fig. 4.6-d).

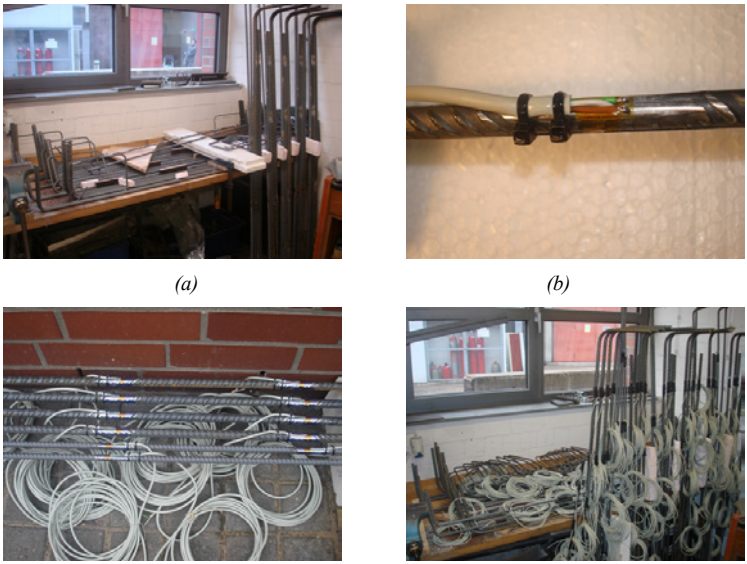

(a) *(b)*

(c) *(d)*

Fig. 4.6: Attaching strain gauges to reinforcing bars

- Producing of reinforcement cages, Fig. 4.7:

According to the drawings (Figs. 4.3 and 4.4) the reinforcement cages were produced on a wooden template.

(a) *(b)*

Fig. 4.7: (continued)

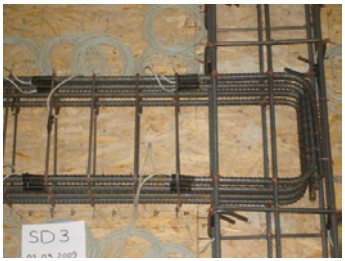

(c) *(d)*

Fig. 4.7: Production of reinforcement cages

- Producing of formworks, Fig. 4.8:

The formwork walls were from plywood and the bottom side was from chipboard covered with plastic film. The top side of formwork walls was anchored to each other by U shape steel tie rods to supporting formwork deformation and sagging during casting.

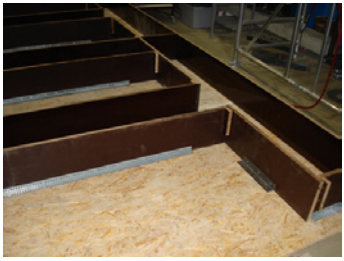

(a) *(b)*

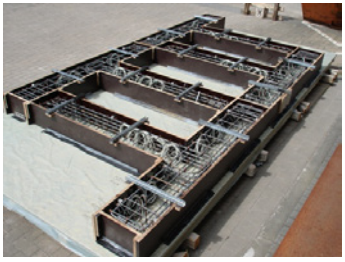

(c) *(d)*

Fig. 4.8: Production of formwork

- Placing reinforcement cages into the formworks, adjusting, wiring the strain gauges, and installing temporary steel bracings to the test specimens, Fig. 4.9:
  To avoid any probable cracking in the joints during transportations and erections, a bracing of steel flat strip was temporarily fixed between end of the beam and column top for every test specimen.

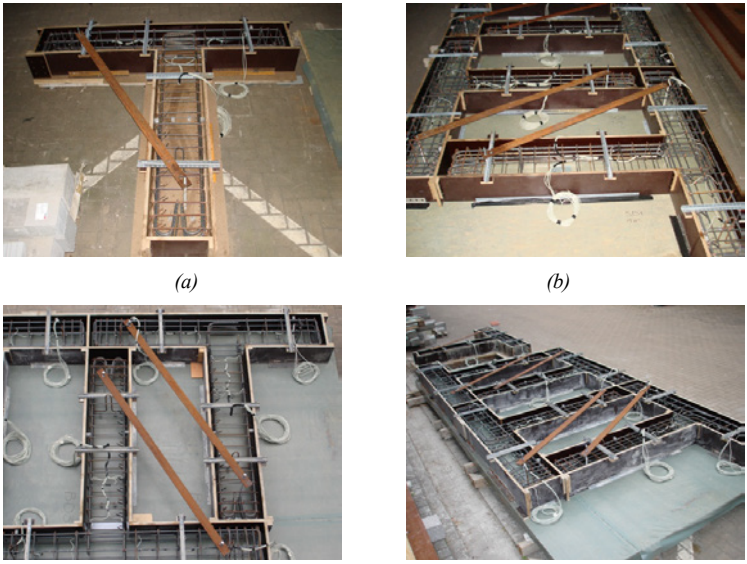

(a) *(b)*

(c) *(d)*

Fig. 4.9: Wiring the strain gauges and temporary bracing the test specimens

- Casting of the specimens and preparing the cylinder and cubic samples for testing the concrete properties, Fig. 4.10:

  The concrete was provided by the commercial plant as a ready mixed concrete C30/37 and transported to the casting place by a truck mixer (Fig. 4.10-a). The maximum size of coarse aggregate was 16 mm. The concrete was compacted by electrical vibrators during the casting concrete (Fig. 4.10-c). To test the concrete properties at different ages some cylinder and cubic samples were provided during the casting.

- Curing of the specimens for at least one week, Fig. 4.11:

After the concrete casting, the specimens and field-cured cylinder and cubic samples (Fig. 4.11-a) were cured for at least one week by water and covering with plastic film (Fig. 4.11-b).

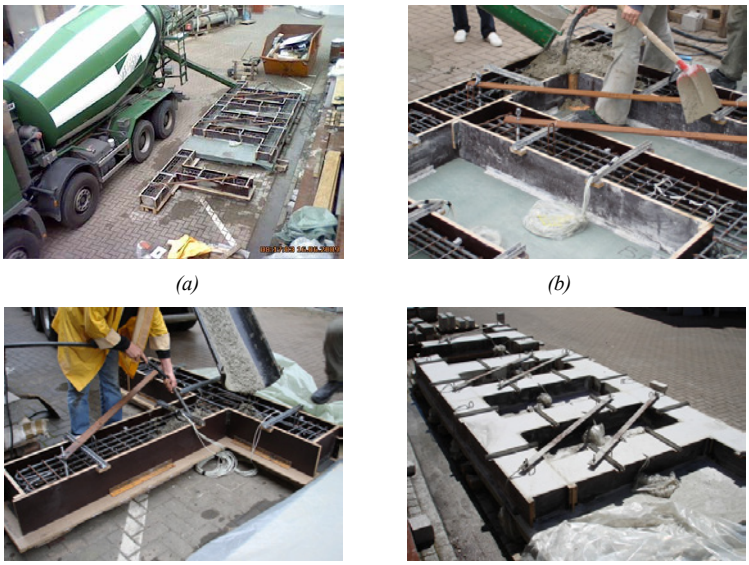

(a) *(b)*

(c) *(d)*

Fig. 4.10: Casting of test specimens

(a) *(b)*

Fig. 4.11: Curing the test specimens for at least one week

- Removing out the specimens from the formworks and transfer them to depot, and preserving them and concrete controlling samples until the test time, Fig. 4.12:

The cured test specimens were removed out from the formworks by a lift truck through the three prepared anchors at the end of the members and transferred to the depot (Fig. 4.12-a). In depot, the specimens were put on each other with polyurethane foam spacers and the field-cured samples were located beside them (Fig. 4.12-b). Finally, the whole was covered by plastic films and preserved until the test time, (Fig. 4.12-c,d).

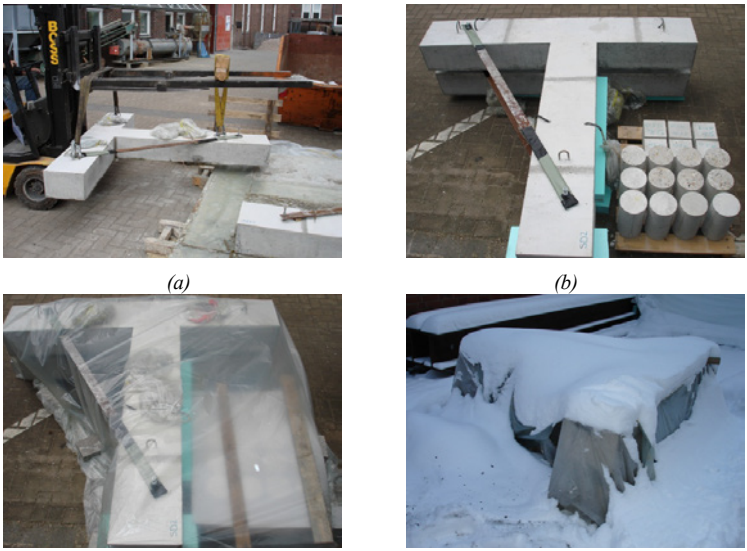

(a) *(b)* *(c)* *(d)*

Fig. 4.12: Transferring the test specimens to depot and preserving them until the test time

4.2.2 Multi Functional Corbels, HMFC

Three pairs of Multifunctional Corbels, HMFC, were designed to use in the retrofitting techniques 1 and 2 (RT1 and RT2). Two bond-slip deficient specimens (BD) were strengthened by retrofitting techniques 1 and 2 (RT1 and RT2) and one shear deficient specimen (SD) was upgraded though retrofitting technique 2 (RT2). The BD category retrofitted specimens through RT1 and RT2 are named BD-H1 and BD-H3-D, respectively and the upgraded of SD specimen through RT2 is named SD-H2-D. Therefore, the Multi Functional Corbel (HMFC) used in BD-H1 and BD-H3-D are named H1 and H3, respectively and the other that used in SD-H2-D is named H2. Table 4.5 displays the summary of the retrofitted specimen's nomination.

Table 4.5: Summary of the retrofitted specimen's nomination

As built specimen	Retrofitting Technique	HMFC	HHDP	Name of retrofitted specimen
BD	RT1	H1	-	BD-H1
SD	RT2	H2	D	SD-H2-D
BD	RT2	H3	D'	BD-H3-D

4.2.2.1 Design, dimensions and details

The design of Multi Functional Corbels, H1, H2 and H3 for BD-H1, SD-H2-D and BD-H3-D specimens, respectively, was carried out according to the conceptual design procedure outlined in the last chapter. As a result, according to the Figs. 4.13, 4.14 and 4.15 for H1, H2 and H3, respectively, assuming $a = b = 330\ mm\ and\ \Theta\Theta 1 = 60°$ as well as geometry and dimensions were satisfied to achieve the target that under the $\bar{\bar{V}}_{col-beam\ hinge} = 79.78\ kN$ the joint moment M_{bc} is not more than $\bar{M}_{bc} = 68.17\ kN.m$. The detail process of design will be described in the next sections. In Figs 14.13, 14.14 and 4.15, (a) and (b) display the dimensions and overall form of HMFCs and (c) presents welding details, Meanwhile, (d) and (e) depict the details of components. The plates and pipes were from S355.

According to Fig. 4.13, in case of H1, the energy absorber element (P1) is diagonally located at the bisector of the angle between edge plates (h1 and h2) and the imposed loads are transmitted to it through the transmitter web plates (h4). The chord plates (h3) prevent the lateral sidesway of the energy dissipation device (P1) and participate in the energy dissipation by inelastic deformation at the chord tip in the middle.

Figs. 4.14 shows that in case of H2, the energy dissipation device (P1) is at the tip point of the external chord plates, h11, and imposed loads are transmitted to it through a levering action around the tip point of the internal chord plates, h8. In contrast, in case of H3 (Fig. 4.15), P1 is at the tip point of the internal chord plates, h6, and levering action is around the tip point of the external chord plates, h3. To avoid of lateral sidesway under compression, the moment of inertia around the main axis of the external and internal cord plates (h11 and h8 in H2 and h3 and h6 in H3) can satisfy the required stability. On the other hand, the stiffened web plates (h10 in H2 and h5 in H3) by internal plates (h9 in H2 and h7 in H3) can effectively improve the concentration of imposed levered loads on the energy absorber element (P1).

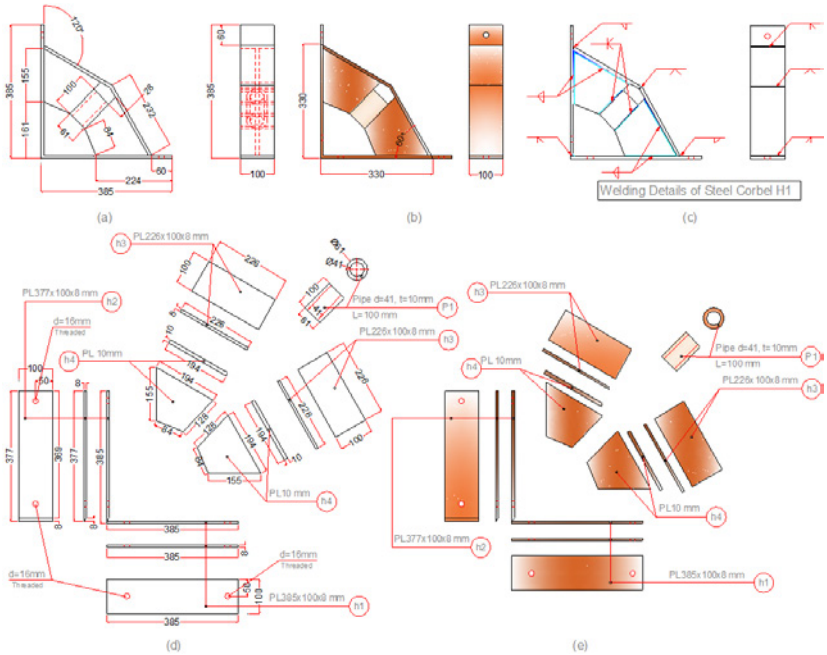

Fig. 4.13: Dimensions and details of Multi Functional Corbel (HMFC) case H1

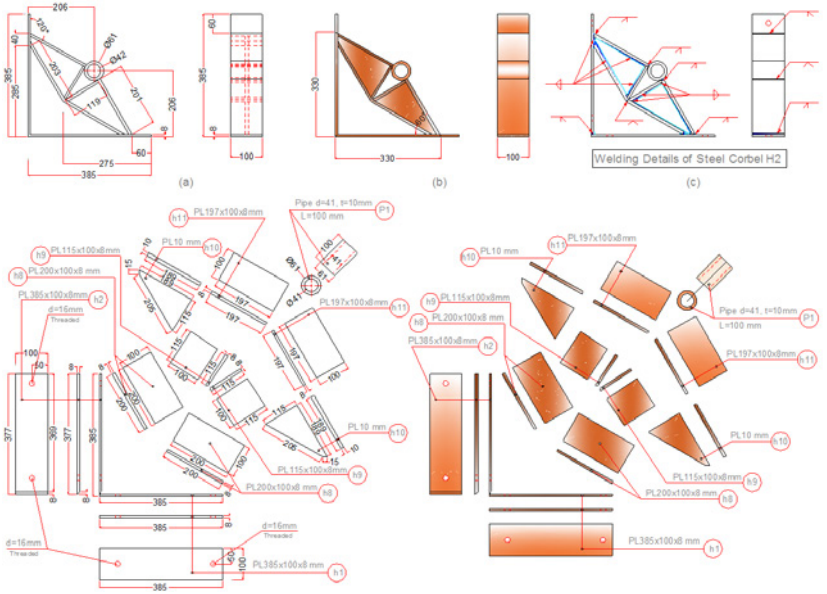

Fig. 4.14: Dimensions and details of Multi Functional Corbel (HMFC) case H2

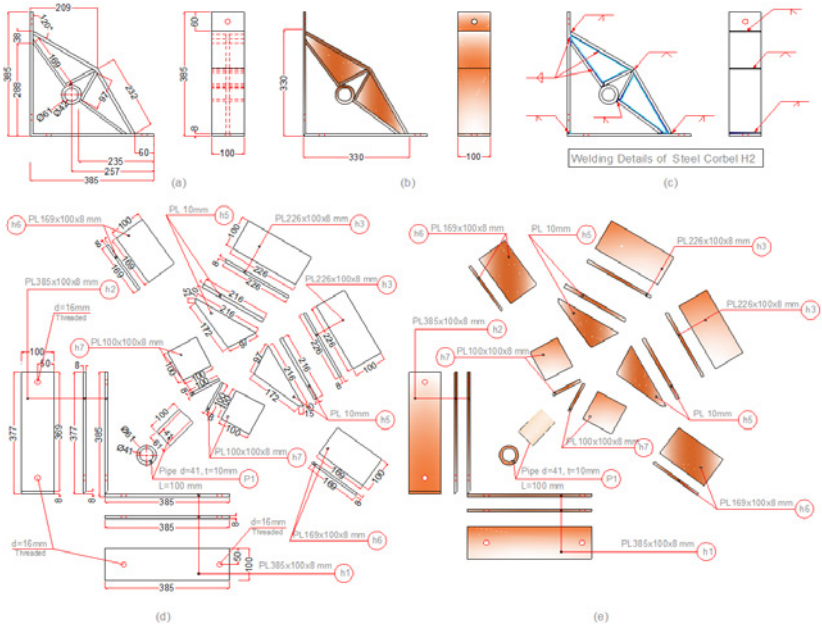

Fig. 4.15: Dimensions and details of Multi Functional Corbel (HMFC) case H3

4.2.2.2 Fabrication of H1, H2 and H3

A same method of fabricating for Multi Functional Corbels (HMFC) has been utilized which are described through the following stages.

- The plates and pipes were cut into desired dimensions by angle grinder and electric band saw machine, respectively (Fig. 4.16-a). The edges of some plates which should be connected to the pipes, were prepared by cutting back along the joint lines for achieving the more continuity by welding (Fig. 14.16-b and 14.17-a).
- To achieve the exact angle between the beam and column at top and bottom of the joint, the HMFC components were assembled at their places in the beam-column joint of test specimen by temporary supports and F-clamps and then were temporarily joined to each other by tack welding to hold the pieces in position (Fig. 4.17-h). Fig. 14.16-c to f, Fig. 14.17-b to i and Fig. 4.18-a show the mentioned process for cases H1, H2 and H3, respectively.
- The assembled components in the last step were released and completed with the complementary plates to form the whole shape of the HMFC (Fig. 4.16-g) and fixed

with additional temporary holders and supports by F-clamps to minimize risk of warping and deforming the joints during the welding process (Fig. 4.17-j and Fig. 4.18-b).

- The completed sets in the last stage were entirely welded and the final forms were obtained and tested to fit in their places, Figs. 14.16-i to j and 14.17-l.

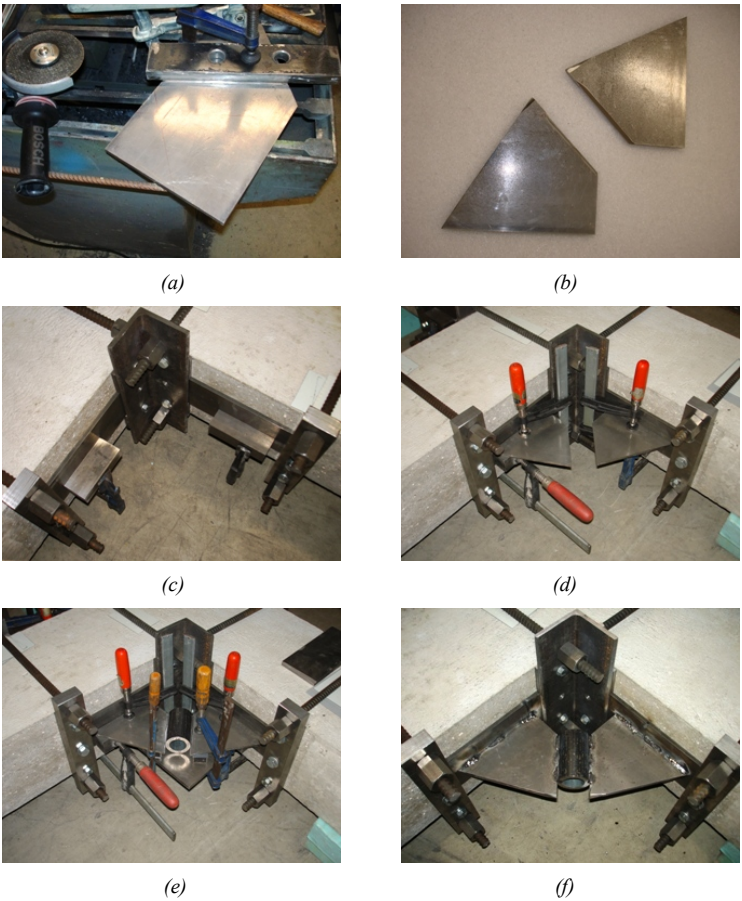

(a) *(b)*

(c) *(d)*

(e) *(f)*

Fig. 4.16: (continued)

(g)

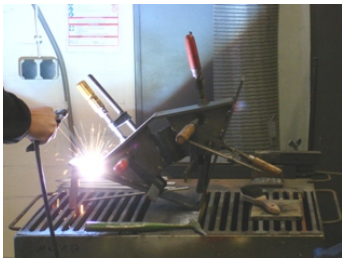

(h)

(i)

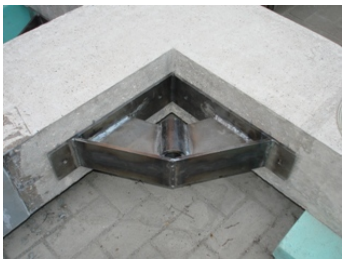

(j)

Fig. 4.16: Production process of Multi Functional Corbel (HMFC) case H1

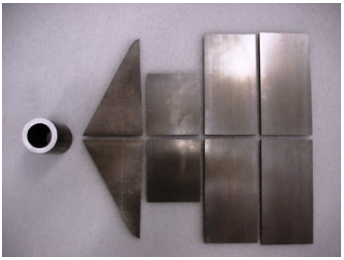

(a)

(b)

(c)

(d)

Fig. 4.17: Production process of Multi Functional Corbel (HMFC) case H2

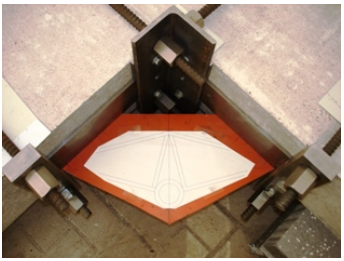

(e)

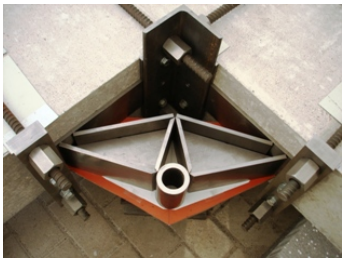

(f)

(g)

(h)

(i)

(j)

(k)

(l)

Fig. 4.17: (continued)

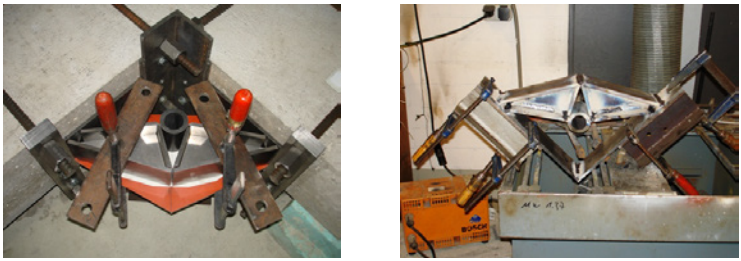

(a) *(b)*

Fig. 4.18: Produced Multi Functional Corbel (HMFC) case H3

4.2.3 Harmonica Damper Plates, HHDP

The harmonica Damper Plates (HHDP) were used to upgrading of one SD and one BD specimen through retrofitting technique 2 (RT2). The used HHDP in two specimens was the same dimensions but there was a difference between their connector plates of their pods to the main test specimen and HMFCs. The set of HHDP and its pod used in SD-H2-D and BD-H3-D is shortly named D and D', respectively.

4.2.3.1 Design, dimensions and details

The design of Harmonica Damper Plate (HHDP) was performed in accordance with the conceptual design procedure sketched out in the chapter 3. The story shear corresponding to the beam flexural plastic hinge at the end of H2 or H3 is $\overline{\overline{V}}_{col-beam\ hinge} = 79.78\ kN$. If it is assumed that the story shear strength is raised to about 20% through retrofitting technique 2 (RT2) with respect to RT1, it should be reached to $\overline{\overline{V}}_{col-beam\ \&\ HHDP\ hinge} = 95.74\ kN$. Therefore, according to Eq. (3.37) and Table (4.5), the required nominal flexural strength of HHDP must be $M_{nh} = 21.35\ kN.m$. Subsequently, considering Eq. (3.36) and moment arm of 430 mm for HHDPs, the required yield strength of HHDP should be at least $F_{hy} = 49.65\ kN$.

To find out the initial dimensions of the HHDP, it is assumed a strip of S355 with thickness of 8 mm and width of 10 mm fixing at the ends of a 75 mm span while the ends are circular haunched with a radius of 10 mm. To develop a plastic bending moments at the ends of the desired strip, the plastic analysis of this strip over a nearly effective clear span of 70 mm and average width of 11.3 mm at the ends of the strip leads to about 2.59kN lateral strength.

Considering 10 parallel strips in two rows, generally provides 20 strips and overall 51.80kN lateral strength which is approved by the diagram of Fig. 3.20. According to Fig. 3.20, the assumed HHDP is nearly completely yielded at 50kN corresponding to 1.5 mm displacement. Consequently, the considered Harmonica Damper Plate can satisfy the requirements. To support and connect the designed HHDP to the RC beam-column joint test specimen, a special pod was analysed and designed so that the simply hysteretic behaviour of the HHDP is safely provided.

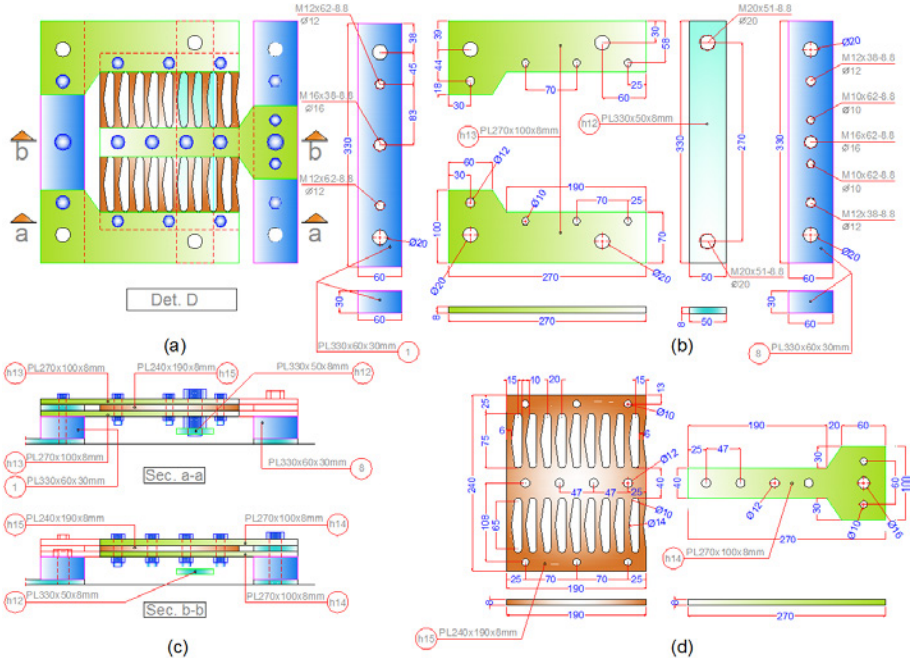

Fig. 4.19: Dimensions and details of Harmonica Damper Plate (HHDP) and its pod, D, (First alternative)

Fig. 4.19 and Fig. 4.20 display the dimensions and overall form of the designed D and D', respectively. In these figures the details of the designed D and D' and their components are depicted. Figures (a) show the overall top view of the HHDPs inside of the pods and figures (c) represent two longitudinal sections through middle and lateral arms of the pod. The forms and dimensions of the pod components are displayed though figures (b) and (d) in detail. The h12 plate as a lateral bracing of side pod arms was designed to support the lateral component of reaction on the side pod arms due to the longitudinal distributed bending moments imposed

by the strips, and avoid of torsional reaction of the left and right supports of side pod arms in D and D', respectively. Finally, the dimensions and form of the designed HHDP is shown in figure (d) in detail.

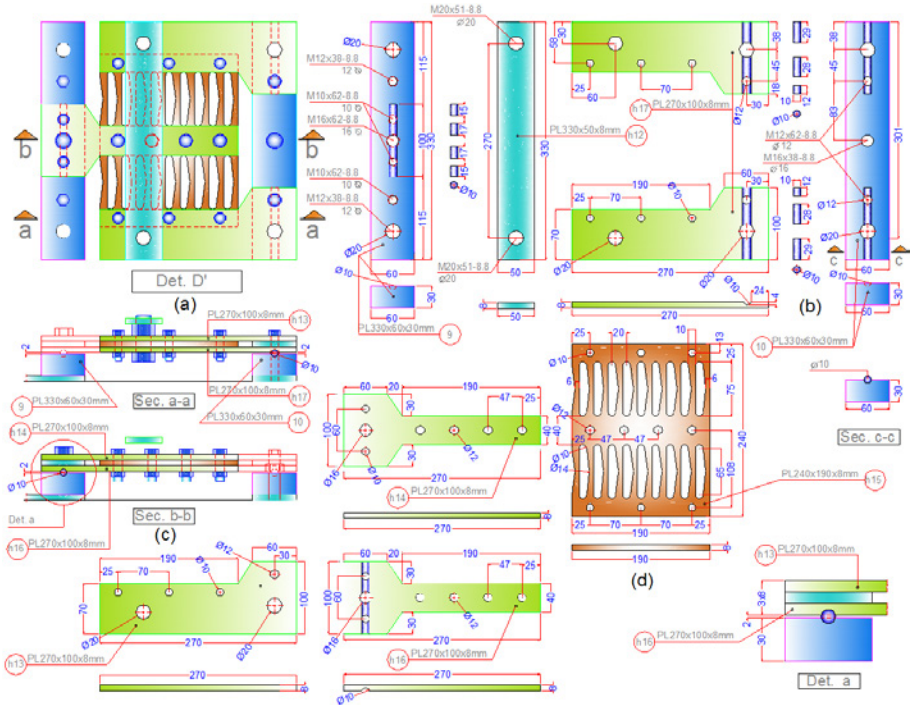

Fig. 4.20: Dimensions and details of Harmonica Damper Plate (HHDP) and its pod, D', (Second alternative)

4.2.3.2 Fabrication of D

The fabrication of D and D' sets can be shortly described in two parts, a) production of Harmonica Damper Plates (HHDP) and b) fabrication of pods. To produce HHDPs, 8 mm steel plates were cut according to the drawing by water jet cutter at Institut für Werkstoffkunde, Unterwassertechnikum Hannover (UWTH). The slicing was carried out using a jet of a mixture of water and an abrasive substance at high velocity and pressure. Figs. 4.21(a) and (b) display the jet cutting stage and produced HHDP, respectively.

Fabrication of pods was manually performed through angle grinder, electric band saw machine, drill press, and hand threading tools by the researcher. The used screws were Hex

Head Cap Class 8.8 DIN931 and DIN933. Fig. 4.22 shows different views of the D set. After testing the specimen SD-H2-D, a few changes was carried out in connector plates of the pods to provide a relatively free rotation at the ends of D and therefore case of D' was produced (Fig. 4.23). According to Fig. 4.23, in connector plates, the 4mm slots were milled by a manually operated universal milling machine to hold steel rods of 10mm diameter.

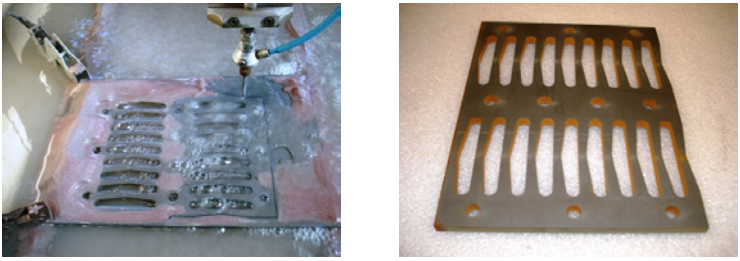

(a) *(b)*

Fig. 4.21: Harmonica Damper Plate (HHDP): a) cutting the plate by water jet, b) HHDP

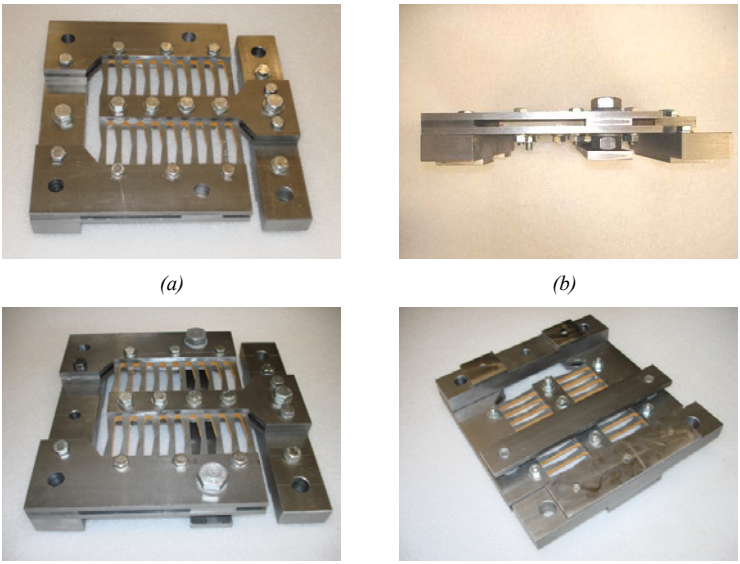

(a) *(b)*

(c) *(d)*

Fig. 4.22: Harmonica Damper Plate (HHDP) with its pod (case D)
a) D set without lateral bracing of side pod arms, b) side view of D set,
c) view of top side, d) view of bottom side

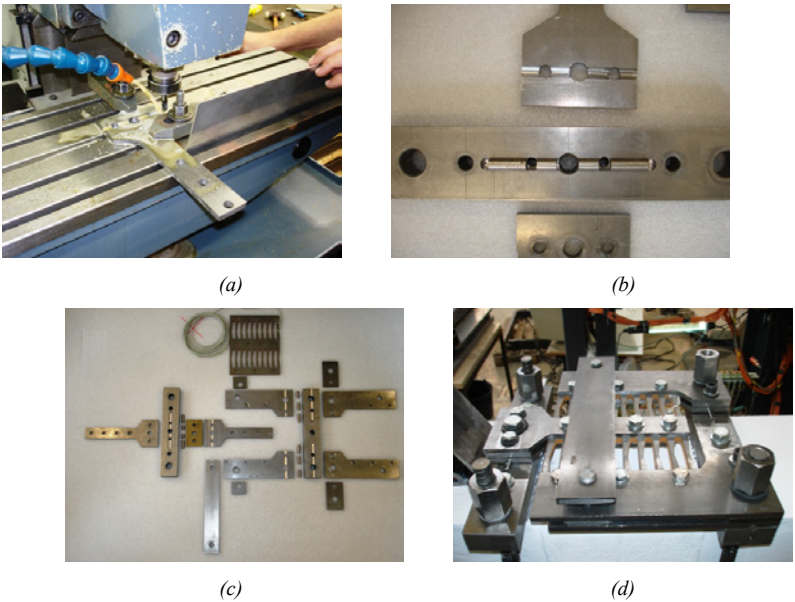

(a) *(b)*

(c) *(d)*

Fig. 4.23: Harmonica Damper Plate (HHDP) with its pod (case D')
a) milling a slot into the connector plates by a universal milling machine , b) milled plates
c) components of D' set, d) connected D' set to the main test specimen and H3

4.2.4 Retrofitted specimens

According to Table 4.5, the retrofitted BD units through RT1 and RT2 were named BD-H1 and BD-H3-D, respectively and the upgraded SD specimen by RT2 was named SD-H2-D. In the following two sections, the retrofitted specimens are described in details.

4.2.4.1 Retrofitted specimen BD-H1

4.2.4.1.1 Design of retrofitted specimen BD-H1

The design of specimen BD-H1 through RT1 is described according to the proposed design procedure which was explained in article 3.6.3. The design steps are presented as follows.

Step 1: Considering the strength of beam-column joint subassemblages (Table 4.4), the expected strength and failure sequence diagram (SFSD) of the as-built BD specimen is drawn such as Fig. 4.24. It is worth mentioning that the column is continuously under compressive load of 300kN.

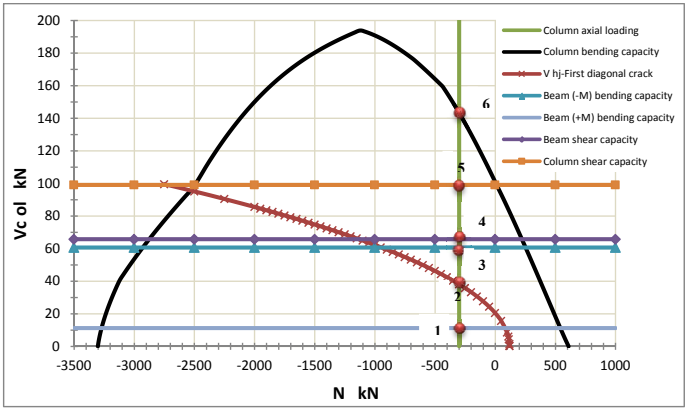

Fig. 4.24: Expected Strength and Failure Sequence Diagram (SFSD) for as-built BD specimen

As can be seen, considering the constant column axial load of 300 kN, the failure mechanisms are expected to be formed: 1: slippage of beam bottom bars; 2: joint first diagonal shear cracking; 3: beam flexural failure due to the negative moment; 4: beam shear failure; 5: column shear failure, and 6: column flexural failure, respectively. It is clear that to upgrading the specimen and reach to the raised story shear, the beam bottom bars should be sufficiently anchored and then joint shear cracking delayed. Meanwhile, the shear strength of the beam must be considered.

Step 2: The joint moment capacity ($\bar{M}_{bc}$) from Eq. (3.12) for the as-built specimen (BD) based on the joint first diagonal cracking limit ($f_{tj} = 1.59MPa$) is equal to 68.17kN.m.

Step 3: The form of H1 according to Fig. 4.13 is selected as the Multi Functional Corbel (HMFC) in which the design parameters are $a = b = 330\ mm$ and . $1 = 60°$.

Step 4: According to the analysis of simplified retrofitted model through RT1 (Fig. 4.25) it is observed that under $\bar{\bar{V}}_{col-beam\ hinge} = 79.78\ kN$ the joint moment M_{bc} is equal to 65.50 kN.m which is less than $\bar{M}_{bc} = 68.17\ kN.m$.

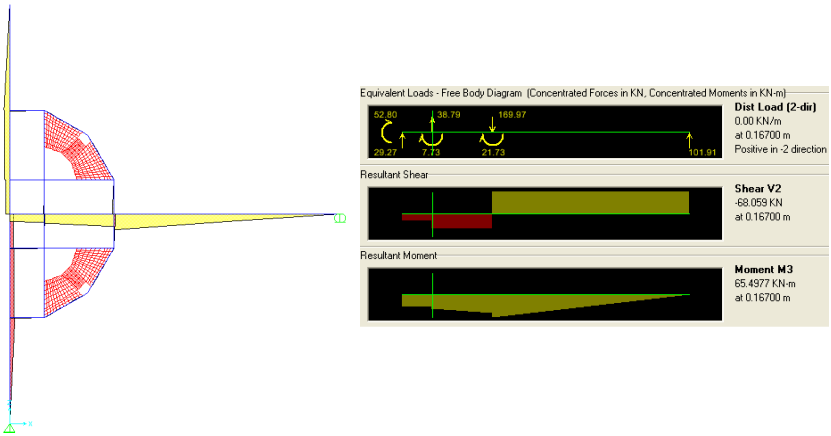

a) *b)*

Fig. 4.25: Analysis of simplified structural retrofitted model BD-H1 under $V_{col} = 79.78\ kN$, a) Moment diagram of structural model; b) The results of beam analysis

Step 5: To overcome the slippage of beam bottom bars, in accordance with Eq. (3.32), the existent development length of $l_{rd} = 480\ mm$ satisfies the required development length (Eq. (3.31) equal to 454 mm. According to Eq. (3.33), the total post-tensioning force of threaded rods with $z_{ps} = 351\ mm$ should be greater than 187kN then for two rods; the post-tensioning force for every rod should be at least 94kN.

Step 6: Retrofitting of the as-built BD specimen through RT1 (BD-H1) upgrades the related Strength and Failure Sequence Diagram (SFSD) (Fig. 4.24) so that the contribution of H1 elements can raise the story shear capacity upper than the strength corresponding to the beam hinge development at the distance of $a = 330\ mm$ away from the column face ($\bar{\bar{V}}_{col-beam\ hinge} = 79.78\ kN$). According to Fig. 4.24, to achieve this capacity, it should be also upgraded the shear strength of the beam.

Shear strengthening of the beam: The shear strength of the beam is upgraded by externally bonded Steel Reinforced Polymer (SRP) sheets. This composite consists of steel wires forming cords which are assembled into a fabric and embedded in either a polymeric resin or a cementitious grout. The reinforcing cords are formed by twisted high strength steel wires. For shear strengthening of the beam, the unidirectional fabrics of 3X2-12-12 Hardwire sheets

and polymeric resin of Sikadur 330 are used. Referring to the manufacturer catalogue, the steel wires have a tensile strength of 3199 MPa (approximately 9 times more than the strength of conventional structural steel), an elastic modulus of 206843 MPa, and a brass coating to providing a long-term durability. The tensile testing of SRP 3X2-12-12 Hardwire sheet displayed the failure mode and force-elongation diagram as Fig. 4.26 (a) and (b), respectively. Furthermore, the manufacturer manual and test results provide the properties of the used SRP composite as the Table 4.6.

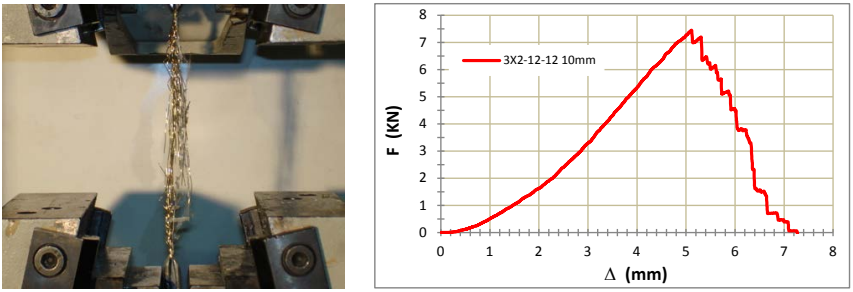

(a) (b)

Fig. 4.26: Tension test of 3X2-12-12 Hardwire composite for 10 mm width

Table 4.6: Properties of 3X2-12-12 Hardwire composite

Reference	Description	No. Of cords /1 cm sheet width	Wire area in each cord (mm^2)	Effective thickness (mm)	Tensile strength/1 cm sheet width (N)	Wire ultimate stress (Mpa)
Catalogue	3X2-12-12	4.7244	0.481	0.2272	7271	3199
Test		-	-	-	7413	3262

Based on ACI 440.2R-02, [ACI 440.2R-02], the one layer completely wrapped of SRP 3X2-12-12 Hardwire sheet over the beam provides 78.7kN shear strength. The coincidence of the test conditions (fully cyclic-induced shear forces along with axial compressive forces less than $A_g f_c'/20$) and requirements of ACI 21.5.5.2 [ACI 318M-11] represents that the

contribution of the concrete to shear strength should be eliminated and therefore the accountable shear strength of the upgraded beam would be resulted of shear reinforcement and wrapped composite. Consequently, according to Table 4.4, the overall shear strength of the upgraded beam section will be 161.98kN and subsequently, the relevant story shear capacity will be 127.9kN. If due to the lateral confining effects of SRP wrapping some parts of this strength is considered, the total shear strength of the beam would be significantly increased. However, since this opinion is not clearly recognized in the literature and on the other hand it seems that it is not needed to have shear strength more than 161.98kN, the concrete contribution is eliminated. Similarly, the contribution of concrete to shear strength of the column, as proposed by the code requirements (ACI 21.6.5.2 [ACI 318M-11]) due to the conditions of the test specimen, has not been taken into account. On the other hand, since the flexural strength of the column is the highest strength, it is expected that a considerable plastic deformation will not be detected in the column and therefore the cracking that leads to elimination of the concrete contribution to shear strength will not be occurred. However, the experimental observations can lead us to a logical conclusion.

A particular prestressed threaded steel bars to prevention of local shear failure at the beam:
Although, as can be seen, the provided shear strength satisfies the produced shear forces in the beam, for more assurance to preventing shear failure during the forming beam plastic hinge in at the end of HMFC particularly when the reinforcement is in strain hardening step, a particular prestressed threaded steel bars close to the end of HMFC are used to protect the beam from localized shear failure at this point. The shear strengthening of the beam at the end of H1 by one layer completely wrapped of the composite along with two pairs of threaded rods provides locally extra shear strength more than 801kN and subsequently 631kN story shear capacity without concrete contribution. This amount is resulted through considering the total strength of materials which are located in the track of 45° probable shear crack passed from the end of H1 toward the beam span.

Continuing the step 6: According to the globally retrofitting of the specimen through RT1 and locally shear strengthening of the beam by SRP external wrapping the expected Strength and Failure Sequence Diagram (SFSD) of the retrofitted specimen (BD-H1) is represented by Fig. 4.27. As can be seen, the expected strength hierarchy is: 1: nearly simultaneously forming the beam flexural plastic hinge and first joint diagonal shear cracking; 2: column shear strength; 3: beam shear strength, and 4: column flexural strength, respectively.

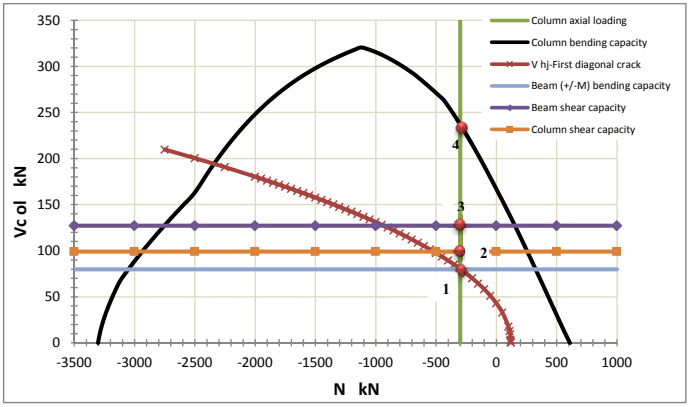

Fig. 4.27: Expected Strength and Failure Sequence Diagram (SFSD) for retrofitted specimen, BD-H1

4.2.4.1.2 Retrofitting details of specimen BD-H1

The general forms of specimen BD-H1 and its details are illustrated in Fig. 4.28. As can be seen, HMFCs are connected to the specimen by prestressed threaded rods. The H1 corbels are assembled to the top and bottom of the joint region through the tip points and corners of the corbels by thick plates and prepared steel angle profiles [Fig. 4.30 (b)], respectively. The details of connector components were displayed in Fig. 4.29.

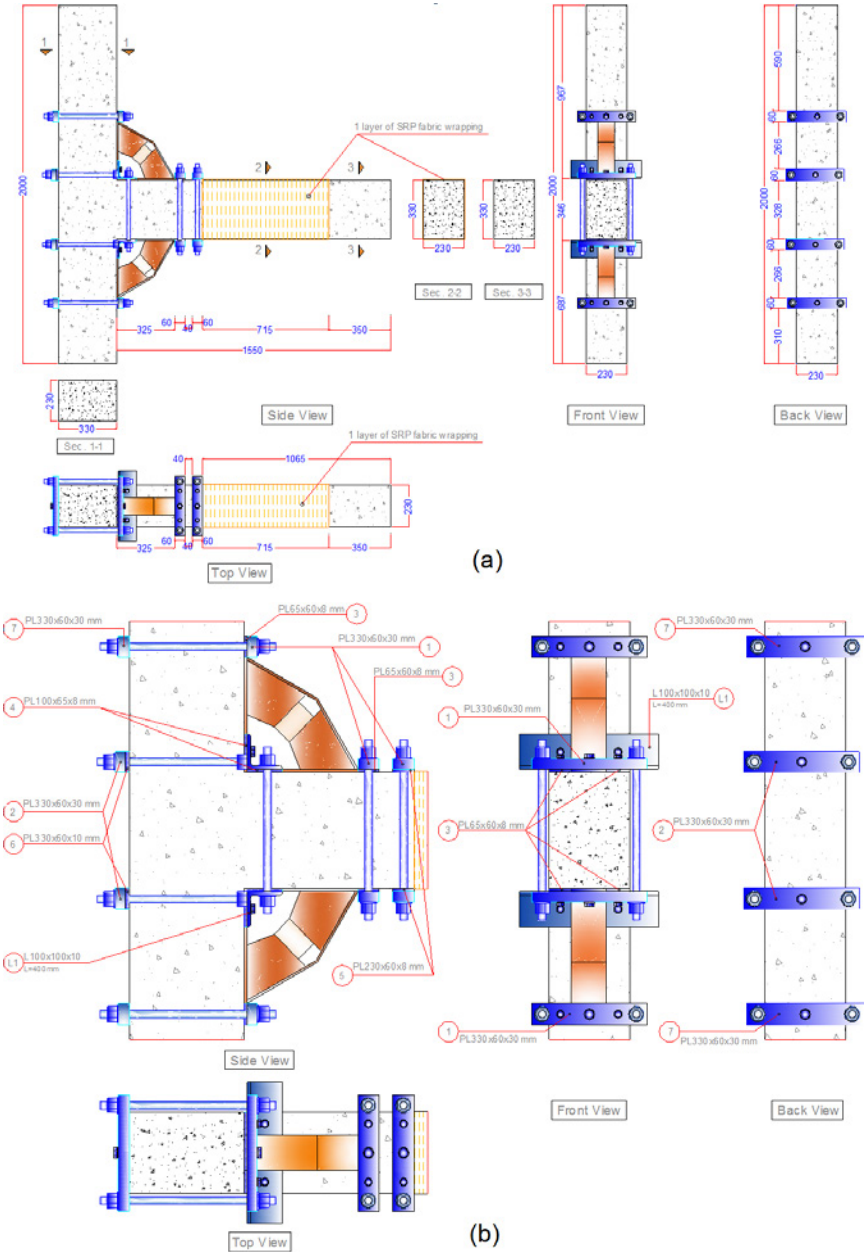

Fig. 4.28: Retrofitting of the Bond Deficient specimen (BD) by Multi Functional Corbel (HMFC) H1 through RT1, (BD-H1)

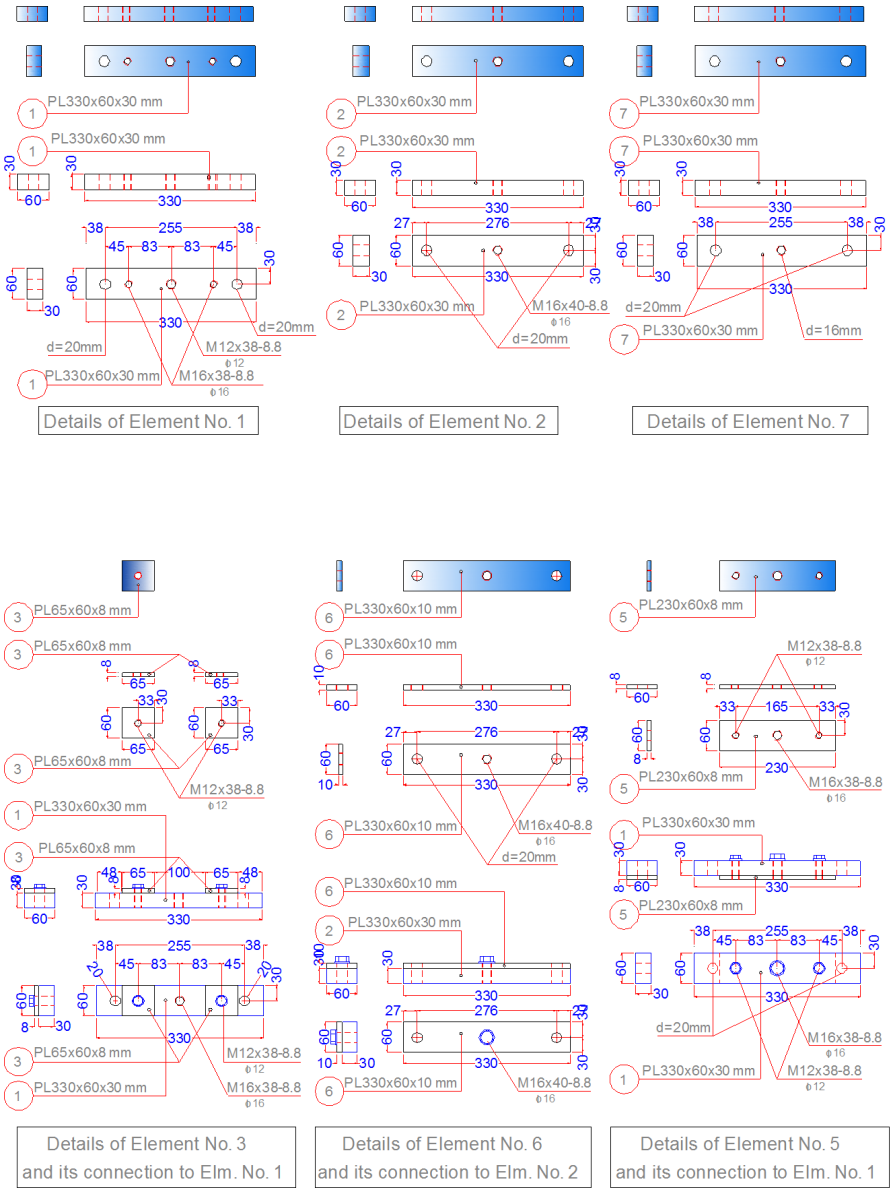

Fig. 4.29: (continued)

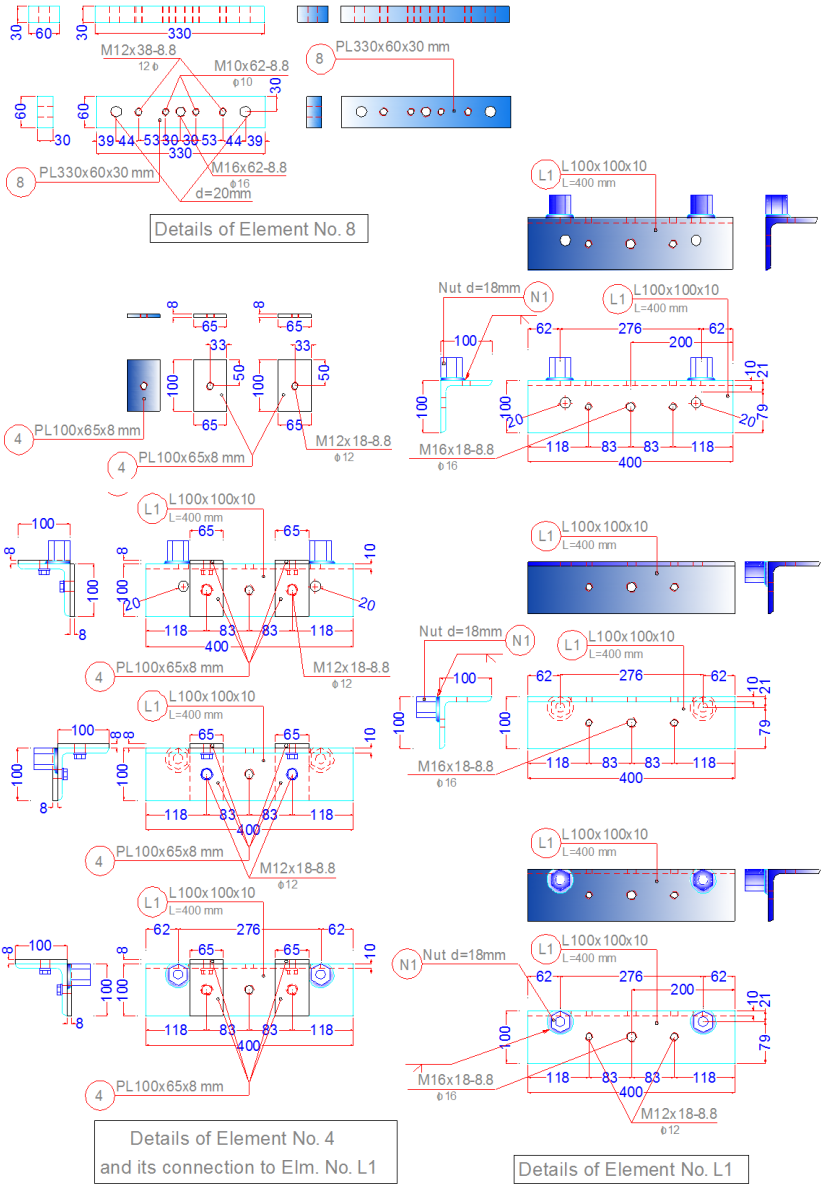

Fig. 4.29: Details of connector components

The high strength hot rolled, ribbed-right hand threaded SAS 670/800-Stahlwerk Annahütte with characteristic yield and ultimate strength of 670 and 800 MPa, respectively, and 18 mm

diameter was used as prestressed threaded steel bars, Fig. 4.30 (a). The length of the anchor nuts was 45 mm.

(a) *(b)*

Fig. 4.30: a) SAS 670/800-Stahlwerk Annahütte threaded steel bar with anchor nuts; b) Prepared angle connector (L1) with welded anchor nuts

As described in the last section step 6, the intentionally considered beam shear weakness was planned to upgrade with externally wrapped SRP fabrics. Fig. 4.31 displays the preparation application procedure of SRP 3X2-12-12 Hardwire sheets on the specimen beam. According to Fig. 4.31 the application procedure is: a) cutting the fabric with a hydraulic guillotine shearing machine into a correct length with considering the overlapping equal to the beam width, b) over bending the fabric to 120° to have the material at 90° after spring-back using sheet metal hand brake machine, c) placing the as-built specimen under a pavilion to application of composite fabric, d and e) substrate preparation of concrete surface by electric hand angle grinder and cleaning the surface with compressed air (according to the manufacturer catalogue, for SRP wraps, because of ability to bent the cords into a sharp angle with a very small cornered radius, no corner rounding of the concrete member is required), f) mixing Sikadure-330 2-part epoxy impregnation resin with mixing ratio 4:1 by weight, g) coating the concrete surface with epoxy by wide spatula and applying the bended sheet on it and then repeating the epoxy coating, h) placing the wooden plates covered with plastic film around the beam and clamping opposite sides with F-clamps for at least 24 hours to fixing the composite, i) removing the F-clamps and wooden plates and repairing the surfaces and corners, j) curing the specimen for at least 7 days in a temperature more than +10°C. After curing, the SRP upgraded specimen was carried to the depot outside the structural laboratory and covered with a wide plastic film and remained there until transferring to the laboratory for test.

(a)

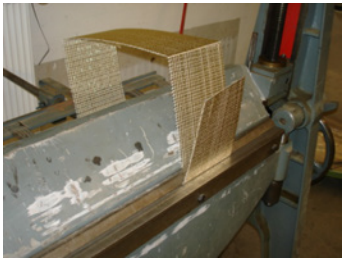

(b)

(c)

(d)

(e)

(f)

(g)

(h)

Fig. 4.31: (continued)

(i) *(j)*

Fig. 4.31: Application procedure of SRP 3X2-12-12 Hardwire sheet on the concrete for the shear strengthening of the specimen beam

The Multi Functional Corbels were assembled to the specimen placed in the loading setup, Fig. 4.32. To reduce safety concerns about slippage of corbels on concrete surface, the contact surfaces were scratched and then smeared with Sikadur-330 epoxy. Subsequently, the connector plates and prepared steel angles were placed and the threaded steel bars were prestressed to about 400 MPa.

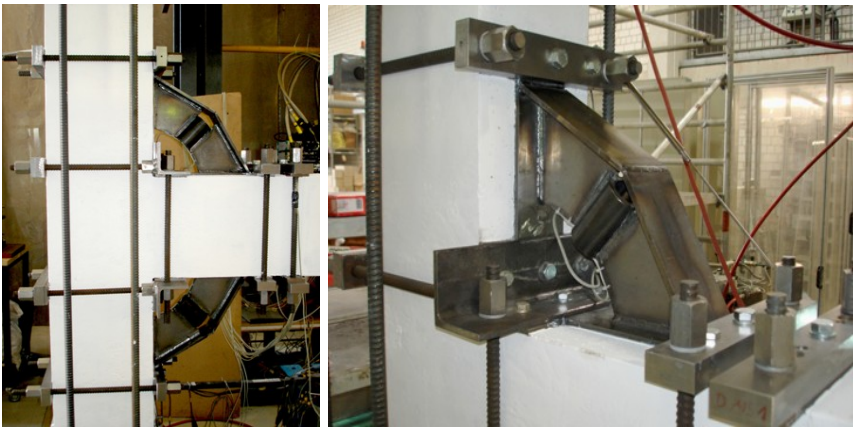

(a) *(b)*

Fig. 4.32: Retrofitted specimen BD-H1 placed in loading setup1H

4.2.4.2 Retrofitted specimen SD-H2-D

4.2.4.2.1 Design of retrofitted specimen SD-H2-D

The design of specimen SD-H2-D through RT2 is described according to the proposed design procedure which was explained in article 3.7.3. The design steps are presented as follows.

Step 1: Considering the strength of beam-column joint subassemblages (Table 4.4), the expected strength and failure sequence diagram (SFSD) of the as-built SD specimen is drawn such as Fig. 4.33. It is worth mentioning that the column is continuously under compressive load of 300 kN.

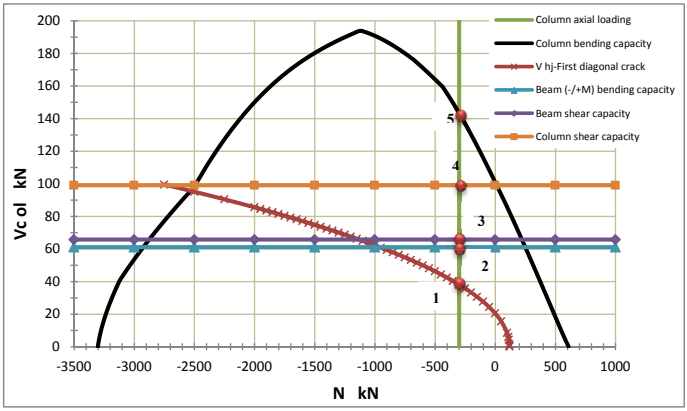

Fig. 4.33: Expected Strength and Failure Sequence Diagram (SFSD) for as-built SD specimen

As shown in Fig. 4.33, the expected failure mechanisms under the constant column axial load of 300 kN are: 1: joint first diagonal shear cracking; 2: beam flexural failure of negative and positive moment; 3: beam shear failure; 4: column shear failure, and 5: column flexural failure, respectively. AS can be seen, to upgrading the specimen and reach to the raised story shear, the joint shear cracking should be delayed and then shear strength of beam must be reasonably increased.

Step 2: For the SD as-built specimen, the limit state of the first diagonal cracking ($f_{tj} = 1.59\ MPa$) will be occurred, if the beam-joint interface moment, according to Eq. (3.12), is going to be more than $\bar{M}_{bc} = 68.17\ kN.m$.

Step 3: According to Fig. 4.14, the form of H2 is selected as the Multi Functional Corbel (HMFC) in which the design parameters are *a= b=330 mm* and *Θ1=60°*.

Step 4: Referring to section 4.2.3.1, if it is assumed that the story shear strength is increased to 20% more ($\overline{\overline{V}}_{col-beam\,\&\,HHDP\,hinge} = 95.74\ kN$), the designed Harmonica Damper Plate (HHDP) can be like as D in Fig. (4.17).

Step 5: The analysis of simplified retrofitted model, Fig. 4.34, shows that the story shear of $\overline{\overline{V}}_{col-beam\,\&\,HHDP\,hinge} = 95.74\ kN$ develops bending moment of $M_{bc} = 66.87\ kN.m$ in the beam-column interface which is smaller than the limit state amount of $\overline{M}_{bc} = 68.17\ kN.m$.

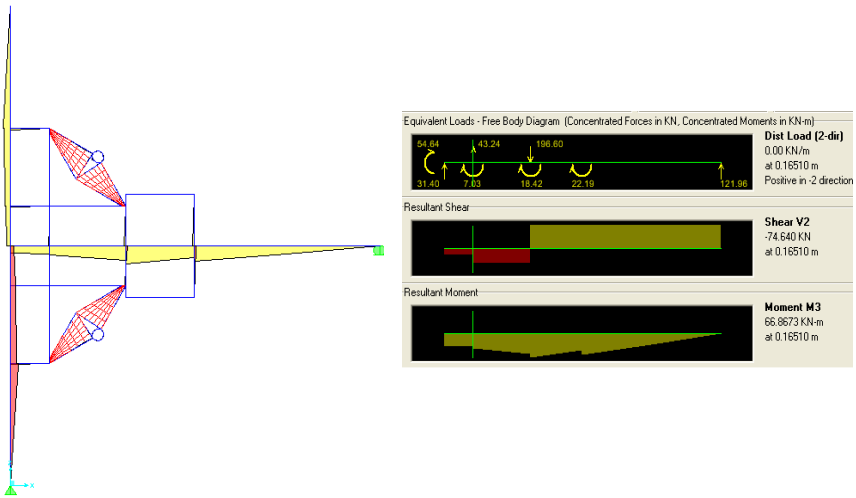

a) *b)*

Fig. 4.34: Analysis of simplified structural retrofitted model SD-H2-D under $V_{col} = 95.74\ kN$, a) Moment diagram of structural model; b) The results of beam analysis

Step 6: Since the beam bottom bars are ended to the standard hooks and development length is satisfied, therefore bond deficiency cannot be determinative.

Step 7: According to section 4.2.3.1, the story shear of as-built SD specimen is raised through RT2 (SD-H2-D) to upper than $\overline{\overline{V}}_{col-beam\,\&\,HHDP\,hinge} = 95.74\ kN$. Therefore, the Strength

and Failure Sequence Diagram (SFSD) of the as-built SD specimen (Fig. 4.33) shows that to achieve this capacity the shear strength of the beam should be upgraded. As described in the section 4.2.4.1.1 step 6, the shear strength of the beam is upgraded by externally bonded unidirectional fabrics of SRP 3X2-12-12 Hardwire sheets. The one layer completely wrapped of the composite over the specimen beam out of the D zone (place of installing the Harmonica Damper Plates) provides 78.7kN shear strength more and therefore it raises the shear strength of the beam up to 225.38kN and 161.98kN with and without concrete contribution to shear strength, respectively.

On the other hand, shear strengthening of the beam in the D region by two layers completely wrapped of the same composite over 90 mm length along with two pairs of threaded rods provides locally extra shear strength more than 472kN and subsequently 372kN story shear capacity without concrete contribution. This amount is resulted through considering the total strength of materials which are located in the track of 45° probable shear crack passed from the end of H2 toward the beam span.

The expected Strength and Failure Sequence Diagram (SFSD) of the retrofitted SD specimen through RT2 can be displayed as Fig. 4.35. Apparently, the contribution of concrete to shear strength of the beam and column according to code requirements is not considered and the probable local shear strength of the beam at the D region is not shown. Obviously, as described for the BD-H1 specimen, the global shear strength of the beam and column due to the concrete contribution and lack of plastic deformations in whole length of the column and length of the beam out of the D region will be certainly close to the case of concrete contribution.

As can be seen, on the condition of elimination the concrete contribution to shear strength of the column and beam, the expected strength hierarchy is: 1: nearly forming simultaneously the beam flexural plastic hinge and yielding of D with first joint diagonal shear cracking; 2: column shear strength; 3: beam hinge at C (at the end of the D zone); 4: beam shear strength; and 5: column flexural strength, respectively. Since the story shears corresponding to the flexural and shear strength of the beam at the point C are greater than the same values at the point A, therefore the flexural plastic hinge will be formed at the predicted point A and the D elements will function.

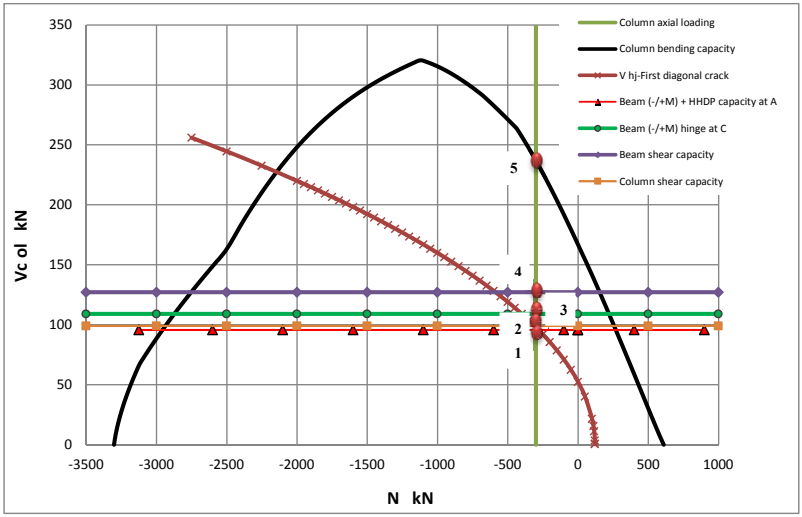

Fig. 4.35: Expected Strength and Failure Sequence Diagram (SFSD) for retrofitted specimen, SD-H2-D

4.2.4.2.2 Retrofitting details of specimen SD-H2-D

The overall views of specimen SD-H2-D and its details are displayed in Fig. 4.36. As can be seen, HMFCs and HHDPs are fixed to the specimen by prestressed threaded rods. The H2 corbels are assembled to the top and bottom of the joint region through the tip points and corners of the corbels by thick plates and prepared steel angle profiles [Fig. 4.30 (b)], respectively. On the other hand, D elements are located on the top and bottom of the beam at the end of H2 so that one side is connected to the test specimen through H2 and the other side is directly attached to the beam. The details of connector components were displayed in Fig. 4.29.

The used materials and erection methods were the same with RT1. The Multi Functional Corbels (HMFC) and Harmonica Damper Plates (HHDP) were assembled to the specimen placed in the loading setup, Fig. 4.37. Furthermore, the application of two layers completely wrapped SRP in the middle part of the D zone were carried out when the specimen was installed in the loading setup, Fig. 4.37 (a), (b).

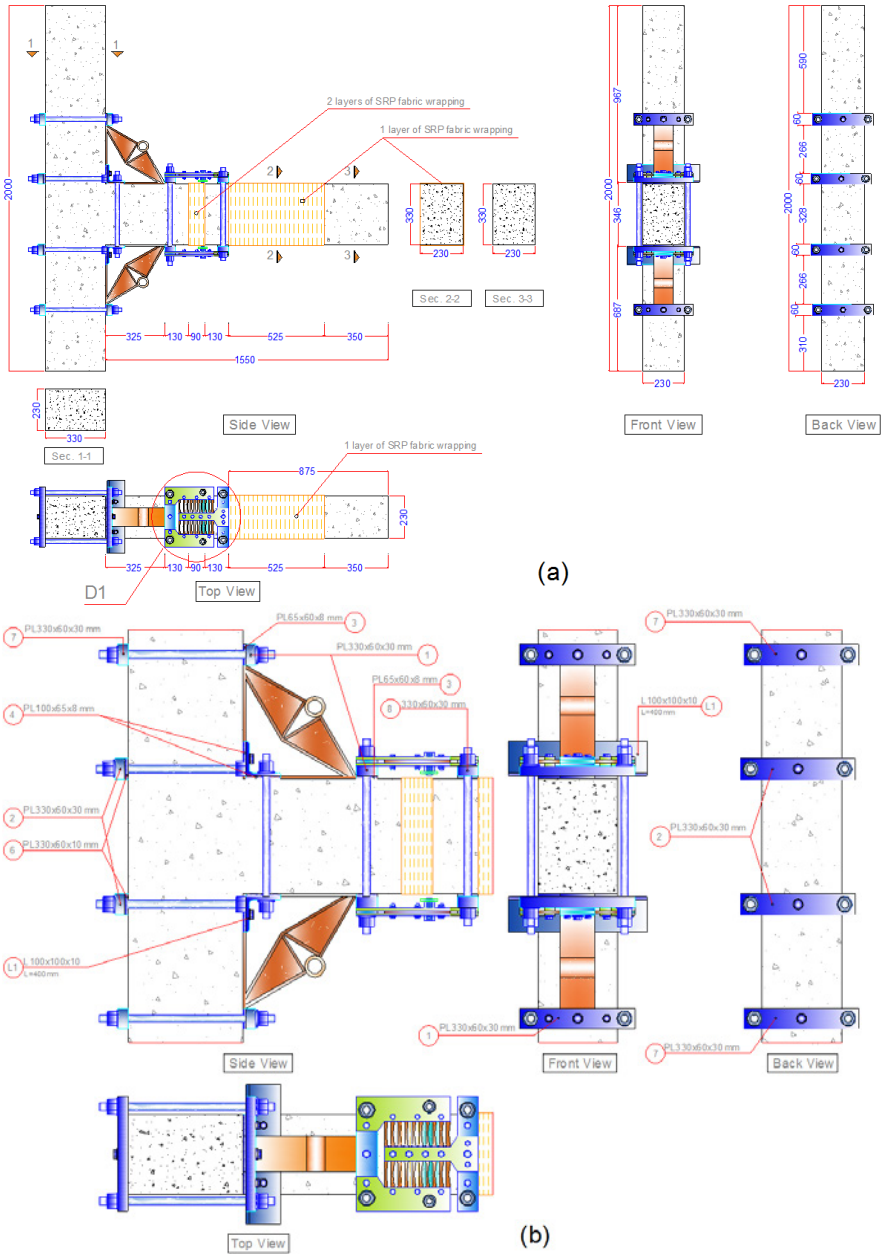

Fig. 4.36: Retrofitting of the Shear Deficient specimen (SD) by Multi Functional Corbels (HMFC) H2 and Harmonica Damper Plates (HHDP) D through RT2, (SD-H2-D)

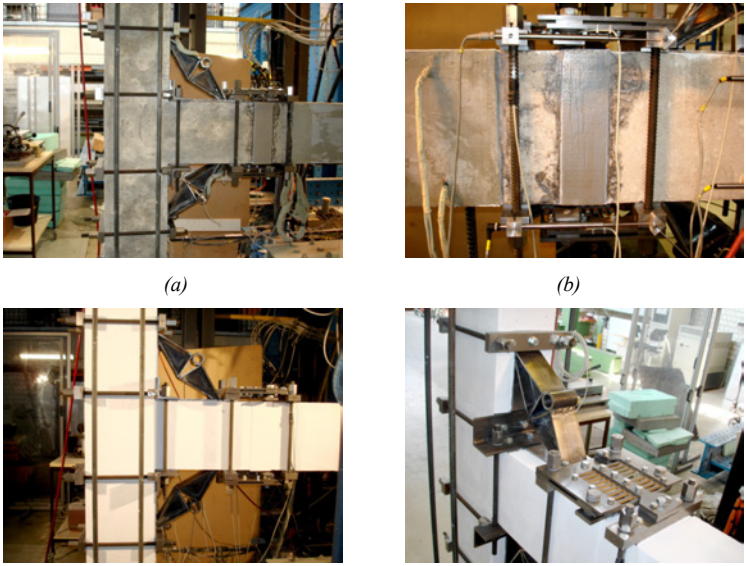

(a) *(b)*

(c) *(d)*

Fig. 4.37: Retrofitted specimen SD-H2-D

4.2.4.3 Retrofitted specimen BD-H3-D

4.2.4.3.1 Design of retrofitted specimen BD-H3-D

The design of specimen BD-H3-D through RT2 is the same with the last specimen SD-H2-D with some differences include of changing the main test specimen from SD to BD, increasing the width of the composite and number of layers in D zone to avoiding or delaying the shear failure modes in this region, and finally changing the types of HMFC and HHDP from H2 and D to H3 and D', respectively. The design steps are presented as follows.

Step 1: The expected strength and failure sequence diagram (SFSD) of the as-built BD specimen is the same with Fig. 4.24.

Step 2: Based on the joint first diagonal cracking limit state ($f_{tj} = 1.59\ MPa$), the joint moment capacity ($\overline{M}_{bc}$) is equal to 68.17kN.m.

Step 3: According to Fig. 4.15, the form of H3 is selected as the Multi Functional Corbel (HMFC) in which the design parameters are $a = b = 330\ mm$ and $\Theta 1 = 60°$.

Step 4: Assuming the increasing of 20% RT1 in story shear strength through RT2 with respect to RT1 (section 4.2.3.1), it will be $\overline{\overline{V}}_{col-beam\ \&\ HHDP\ hinge} = 95.74\ kN$, and therefore the type of D' (Fig. 4.20) can be selected for Harmonica Damper Plate (HHDP).

Step 5: The analysed simplified retrofitted model (Fig. 4.38) shows that imposing the story shear of $\overline{\overline{V}}_{col-beam\ \&\ HHDP\ hinge} = 95.74\ kN$ leads to the joint moment of $M_{bc} = 69{,}78\ kN.m$ which is nearly equal the limit state amount of $\overline{M}_{bc} = 68.17\ kN.m$.

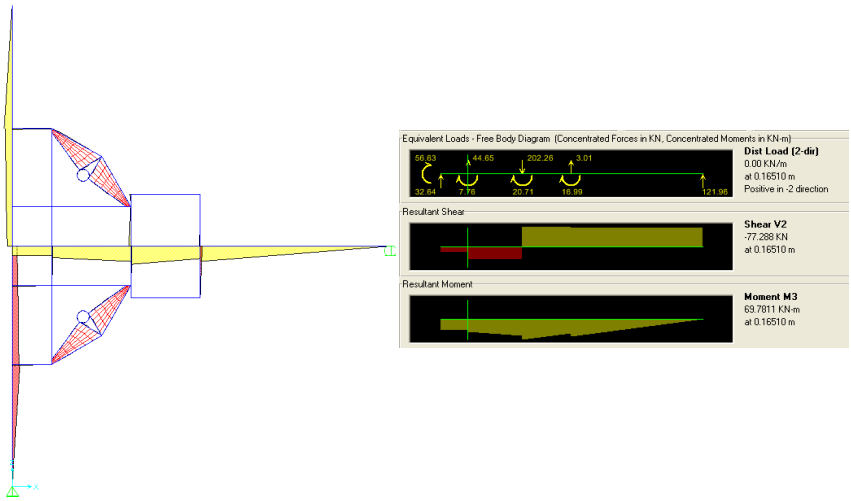

a) *b)*

Fig. 4.38: Analysis of simplified structural retrofitted model SD-H2-D under $V_{col} = 95.74\ kN$, a) Moment diagram of structural model; b) The results of beam analysis

Step 6: According to Eq. (3.32), the required development length of 454 mm [Eq. (3.31)] is satisfied by existent development length of $l_{rd} = 480\ mm$ [Eq. (3.32)] to evident the slippage of the beam bottom bars with only 150mm embedment length into the joint. On the other hand, to preserve the integrity of the joint connection for supporting M_{bc} at the beam-column interface, the treaded rods with moment arm of $z_{ps} = 351\ mm$ should be post-

tensioned with a force (F_{ps}) more than 200kN then for two rods, the post-tensioning force for every rod should be at least 100kN.

Step 7: Upgrading the story shear capacity of the as built BD specimen though RT2 to $\overline{\overline{V}}_{col-beam\,\&\,HHDP\,hinge} = 95.74\ kN$ (section 4.2.3.1) needs to improvement the shear strength of the beam in inside and outside of the D zone. The one layer complete wrapping of the beam with externally bonded unidirectional fabrics of SRP 3X2-12-12 Hardwire sheets in outside length of D zone can increase the story shear capacity to 127.15kN (without contribution of concrete to shear strength) and 176.92kN (with concrete contribution). On the other hand, three layers of complete wrapping of the beam over the 2x100mm length in inside of D region along with two pairs of threaded rods used to fixing HHDPs can locally provide the extra shear strength more than 583kN and subsequently 459kN story shear capacity without concrete contribution. This amount is resulted through considering the total strength of materials which are located in the track of 45° probable shear crack passed from the end of H3 toward the beam span. The expected Strength and Failure Sequence Diagram (SFSD) of the upgraded BD specimen through RT2 will be the same with retrofitted specimen SD-H2-D which was displayed in Fig. 4.35.

4.2.4.3.2 Retrofitting details of specimen BD-H3-D

The general forms and details of the retrofitted specimen BD-H3-D are depicted in Fig. 4.39. Apparently, HMFCs and HHDPs are fixed to the specimen by prestressed threaded rods. The H3 corbels are assembled to the top and bottom of the joint region through the tip points and corners of the corbels by thick plates and prepared steel angle profiles [Fig. 4.30 (b)], respectively. On the other hand, D elements are located on the top and bottom of the beam at the end of H3 so that one side is connected to the test specimen through H3 and the other side is directly assembled to the beam. The details of connector components were displayed in Fig. 4.29.

The H3 and D' elements were assembled to the test specimen placed in the loading setup, Fig. 4.40. Furthermore, the application of three layers completely wrapped composite in the middle part of the D zone were carried out when the specimen was installed in the loading setup.

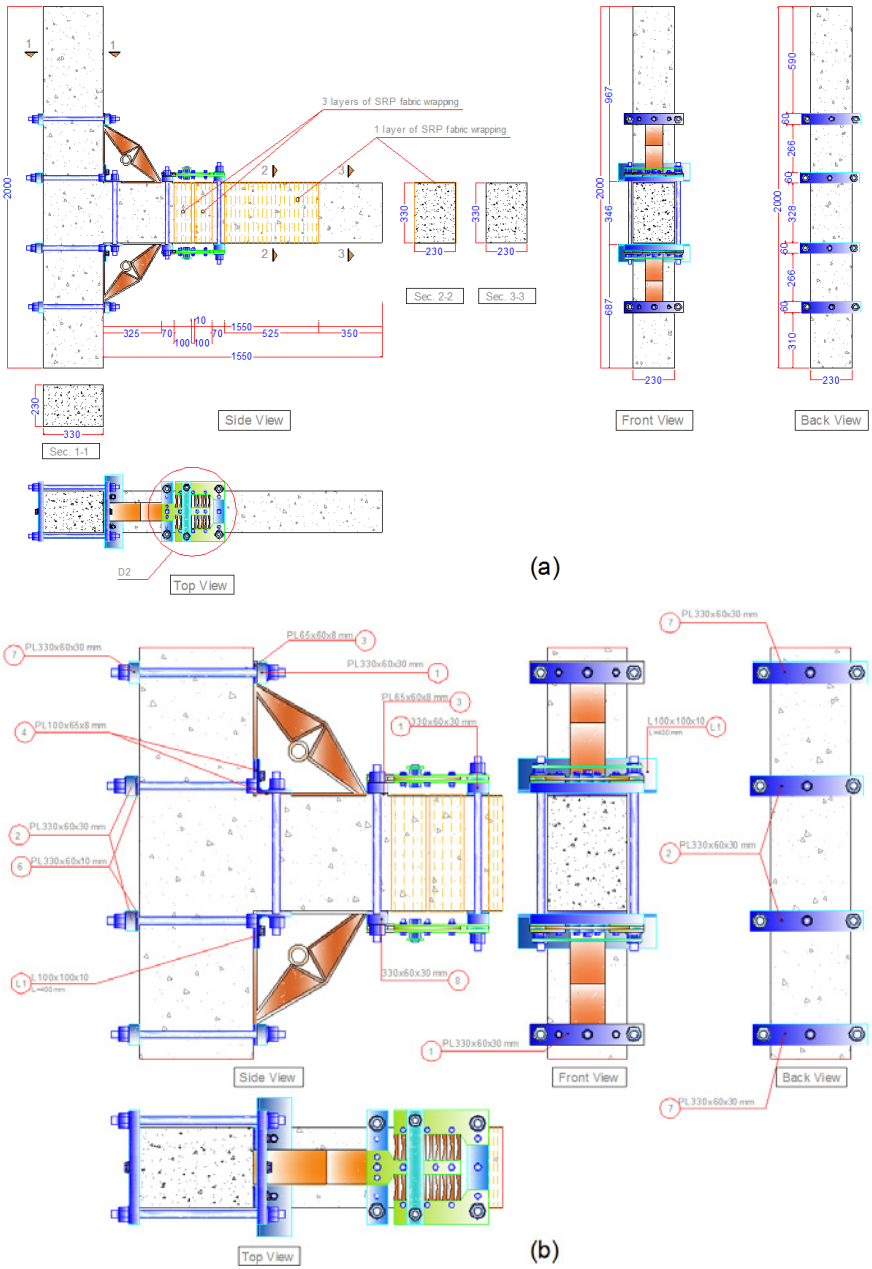

Fig. 4.39: Retrofitting of the Bond Deficient specimen (BD) by Multi Functional Corbels (HMFC) H3 and Harmonica Damper Plates (HHDP) D' through RT2, (BD-H3-D)

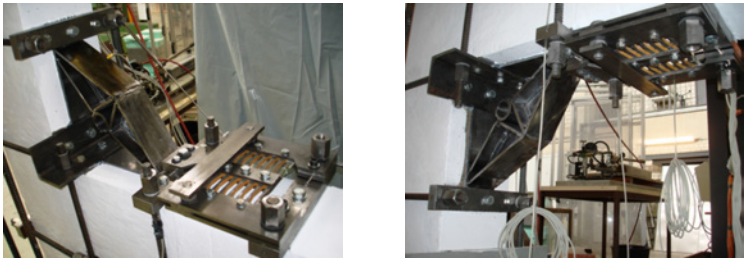

Fig. 4.40: Retrofitted specimen BD-H3-D

4.3 Loading setup

4.3.1 General specifications

A particular loading setup was designed and fabricated for simulating the displacement-controlled cyclic lateral loading sequence of a building carrying service gravity loads, Figs. 4.41 and 4.42. The system was designed to impose up to 200 kN dynamic lateral load and 580 kN static vertical load. The cyclic lateral story shear force was applied by a servo-hydraulic double acting test cylinder (walter & bai ag) up to dynamic capacity of 480 kN compression and 320 kN tension, and the column axial static load of nearly 10% of the column's compressive designed load capacity (300 kN) was applied by manually operated hydraulic cylinder (Lukas) up to 500 kN. The horizontal cyclic load actuator was installed on a braced reaction frame and the vertical static actuator setting-up on the specimen column was clamped by tie rods to apply axial load. A pin support at the column base allowed free rotation while a roller support at the end of the beam prepared also free horizontal displacement. To providing free rotation at the top of the column, in addition to the standard fabricated hinge of the dynamic actuator, it was needed to have another mechanical hinge in the line of the horizontal actuator. Therefore, considering the tight space to place a new hinge, the proposed second mechanical hinge was designed to locate at the top of the column to applying lateral placements from the center line of the column. The imposed horizontal and vertical loads were measured by two load cells and the travelling distance of the dynamic actuator (column top) was gauged by its internal equipped transducer. The whole system was set-up and fixed on the 1000 mm depth strong floor of the structural laboratory.

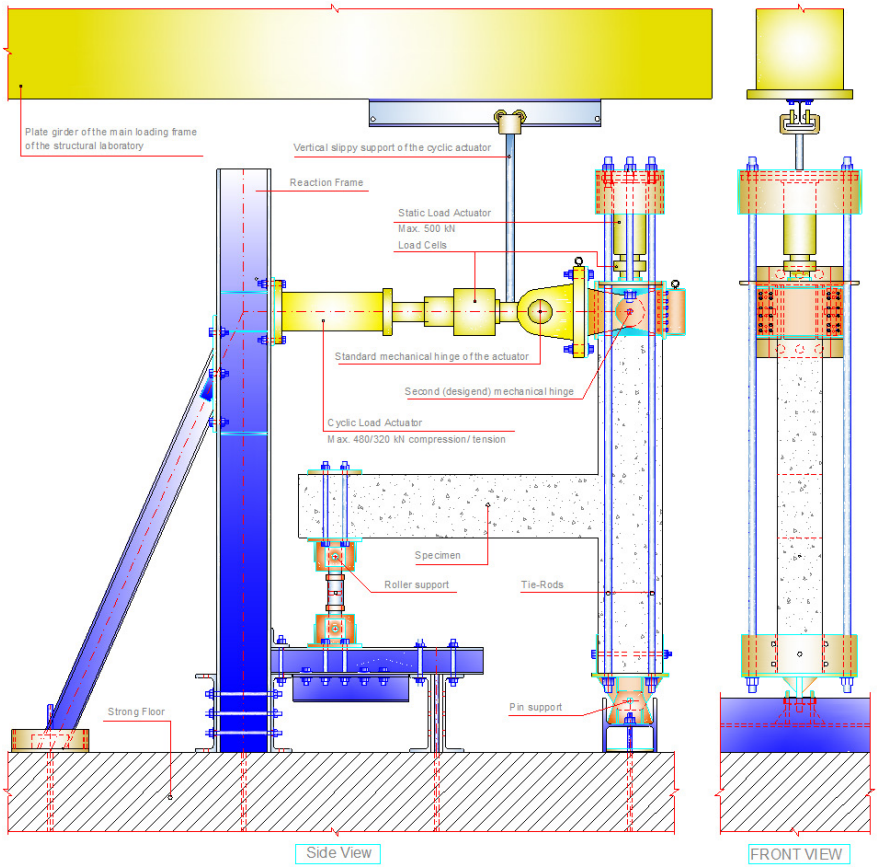

Fig. 4.41: Designed loading setup

Fig. 4.42: Fabricated loading setup

4.3.2 Details and fabrication of the loading setup

Considering the limitations and conditions that the researcher has been faced during the research, the design and fabrication of the loading setup has been a considerable part of the experimental work. The details and fabrication process of the loading frame is depicted in appendix B.

4.3.3 Testing procedure and loading history

To study the seismic performance of specimens, they were imposed under quasi-static simulated seismic load in accordance with [ACI 374.1-05]. The displacement-controlled loading sequence for each specimen consisted of three cycles (push and pull) at a particular drift level and series of progressively increasing displacement amplitudes so that the displacements were increased gradually in steps that were neither too large nor too small. The initial drift ratio (0.2%) were within the linier elastic response range for the specimens and the subsequent drift ratios were not less than 1.25 times, and not more than 1.5 times, the prev-

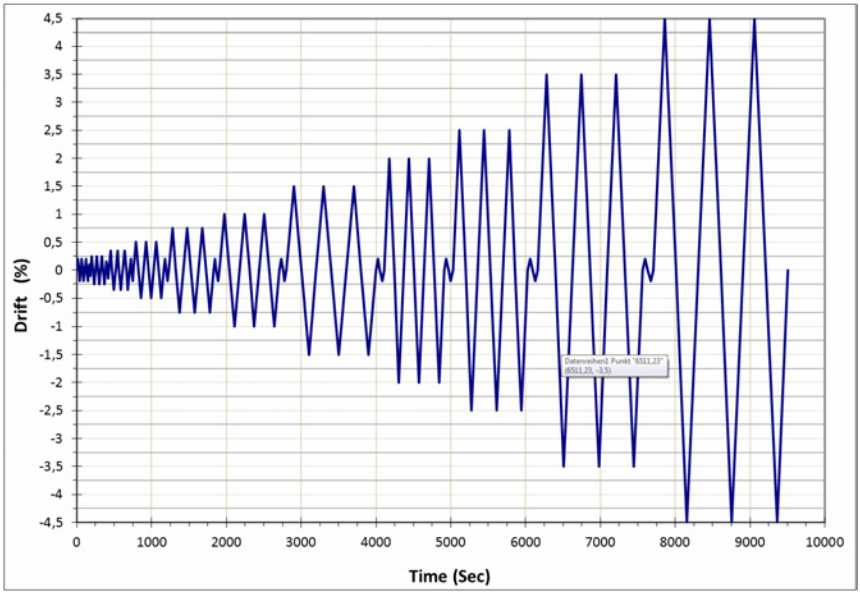

Fig. 4.43: The applied cyclic drift history

-ious drift ratio. Consequently, the applied main cyclic drift ratios were 0.2%, 0.25%, 0.35%, 0.5%, 0.75%, 1.0%, 1.5%, 2%, 2.5%, 3.5%, and 4.5%. Moreover, as required by the current code through example of a test sequence, a cycle of secondary small drifts followed each main drift level to close the gaps between aggregates in the concrete. They were 0.1% and 0.15% after the main drift levels of 0.2% and 0.25%, respectively, and 0.2% after the other larger main drift levels. The applied cyclic drift history is illustrated in Fig. 4.43.

The specimens were simultaneously imposed by column axial compression and lateral cyclic loads. First, an axial load of 300 kN (nearly 10% of the column axial capacity) was applied axially to the column and maintained constant throughout the test and then the displacement-controlled loading system was applied horizontally as a story shear force to the top of the column. The applying of loading system was continued until the lateral drift of column top reached the particular drift level.

4.4 Instrumentation

Considering the limitations and possibilities, the loading setup and specimens were instrumented to monitor the applied loads, displacements, deformations, and strains. The monitored subjects were as follows:

- Monitoring the loads: The applied column axial load and horizontal story shear force were measured by two load cells of 100 kN (Fig. 4.44, LC1) and 600 MPa (Fig. 4.44, LC2) capacity, respectively.
- Monitoring the displacements: The horizontal displacement of the column top was measured by using a Linear Variable Distance Transducer (LVDT) of +/- 125 mm travelling capacity which was integrated within the dynamic actuator (Fig. 4.44, La).
- Monitoring the deformations of loading setup: To modify the recorded displacements, the critical points of the loading setup were also monitored by four different LVDTs of +/- 10 mm travelling capacity (Fig. 4.44, Ls1-4).
- Monitoring the deformations of as-built specimens (reference units): The deformations of the joint subassemblages were measured by twelve LVDTs (Fig. 4.44, Ln) of +/- 200 mm (L7 and L9) and +/- 150 mm (L1-6, L8, and L10-12) travelling capacity. The fixed end rotations of the column were estimated through measuring the deformations recorded by each pair of LVDTs connected between the joint and column on top and

bottom (L1, L4, and L3, L6). The joint shear deformations were evaluated by the joint vertical, horizontal and diagonal LVDTs (L2 and L5, L8 and L10, L11 and L12).

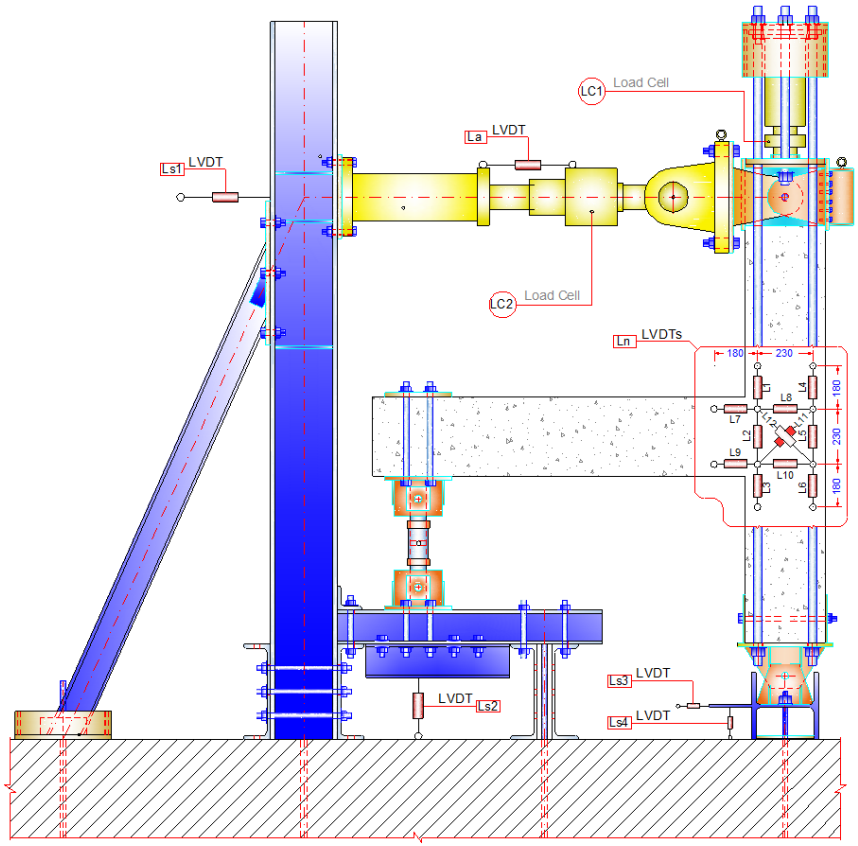

Fig. 4.44: Location of load cells and Linear Variable Distance Transducers (LVDTs) for loading setup and as-built specimens (reference units)

- Monitoring the deformations of the retrofitted specimen BD-H1: The deformations of the joint subassemblages were measured like the reference units by twelve Ln LVDTs (Fig. 4.45). The diagonal displacements of the Multi Functional Corbels (HMFC), H1, were recorded by two LVDTs (Lm1-2), and the rotation of the beam plastic hinge at the end of H1 was measured by two LVDTs (Lm3-4) of +/- 10 mm and +/- 20 mm travelling capacity, respectively.
- Monitoring the deformations of the retrofitted specimen SD-H2-D: The deformations of the joint components were measured like the reference units by twelve Ln LVDTs

(Fig. 4.46). The diagonal displacements of the Multi Functional Corbels (HMFC), H2, were recorded by two LVDTs (Lm1-2), and the displacements of the Harmonica Damper Plates (HHDP), D, were measured by two LVDTs (Lm3-4) of +/- 10 mm and +/- 20 mm travelling capacity, respectively.

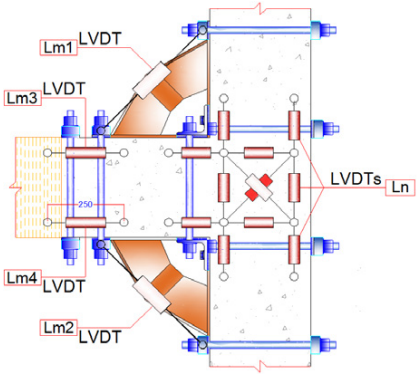

Fig. 4.45: Location of LVDTs for the retrofitted specimen BD-H1

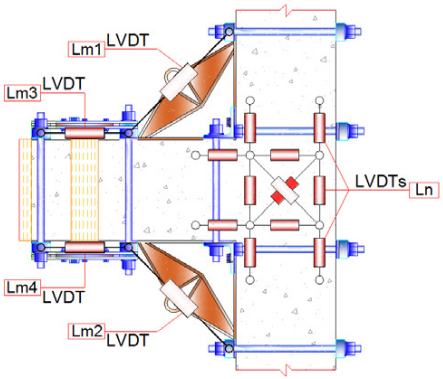

Fig. 4.46: Location of LVDTs for the retrofitted specimen SD-H2-D

- Monitoring the deformations of the retrofitted specimen BD-H3-D: Like the retrofitted specimen SD-H2-D, the deformations of the joint and its components, HMFCs (H3), and HHDPs (D') were measured by LVDTs including twelve Ln, two Lm1-Lm2, and two Lm3-Lm4, respectively, (Fig. 4.47).

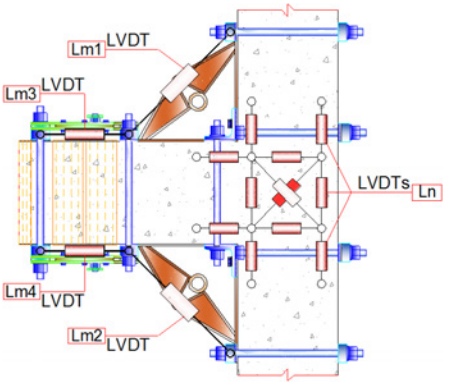

Fig. 4.47: Location of LVDTs for the retrofitted specimen BD-H3-D

- Monitoring the strains in as-built specimens (reference units): The strains of the specimen reinforcing bars in the critical regions were locally measured by strain gauges. According to Fig. 4-48, ten strain gauges were used in each reference units of SD-B and BD-B.

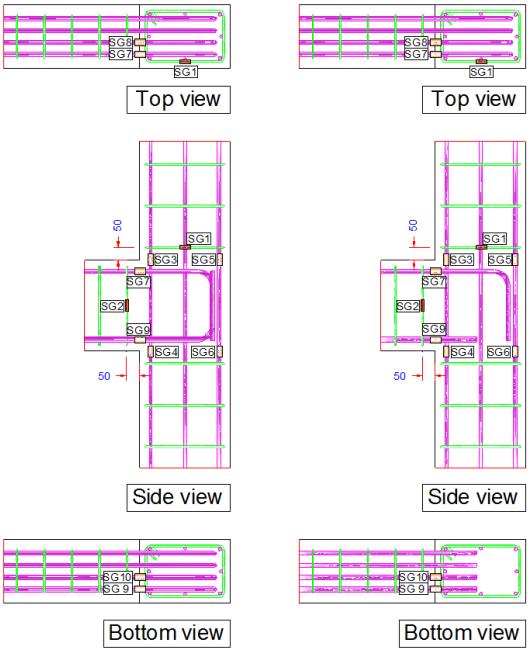

(SD-B) *(BD-B)*

Fig. 4.48: Location of strain gauges of reinforcing bars for the reference specimens

- Monitoring the reinforcing bars of retrofitted specimens: Sixteen strain gauges were used in every retrofitted specimen of BD-H1, SD-H2-D, and BD-H3-D, (Fig. 4.49).

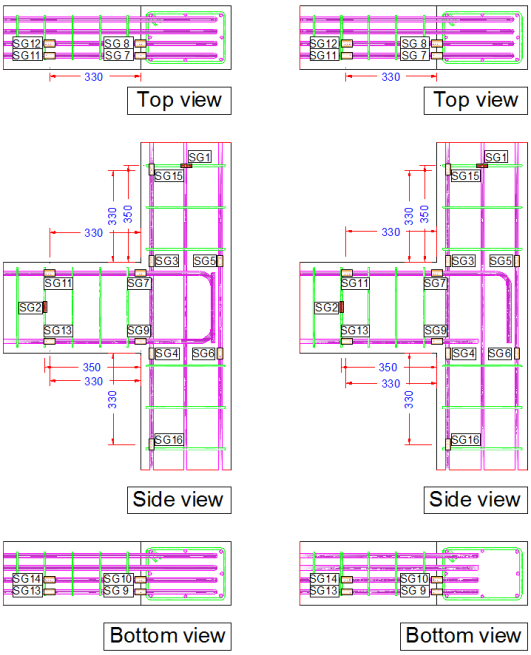

Fig. 4.49: Location of strain gauges of reinforcing bars for the retrofitted specimens: a) for SD-H2-D, b) for BD-H1 and BD-H3-D

- Monitoring the strains of strengthening devices in retrofitted specimens: According to Fig. 4.50 in BD-H1, two strain gauges were used in each Multi Functional Corbel (HMFC) while in SD-H2-D each corbel and Harmonica Damper Plate (HHDP) was monitored by one strain gauge, Fig. 4.51. It is worth mentioning that the strain gauges of HHDPs in specimen SD-H2-D were intentionally located at the neutral position of the arms to avoid of defecting during the test because of low expected strains at these points and obtaining the form of hysteresis loops until the end of the test. Fig. 4.52 shows the location of strain gauges in specimen BD-H3-D to measure the strains of H3 and D' during the test. Apparently, like SD-H2-D every H3 and D' was monitored by one strain gauge but in contrast to position of the strain gauges in D (SD-H2-D),

the strain gauges of D' were located at the end of arms where the stains were expected to be high. Moreover, in both specimens, the strain of two threaded rods was measured to calibrate the prestressing loads and control it during the test.

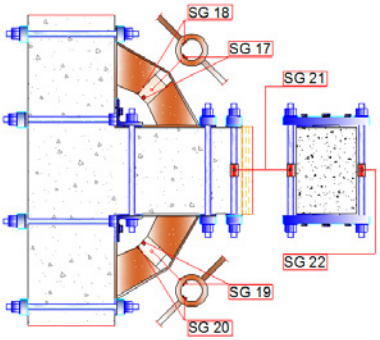

Fig. 4.50: Location of strain gauges of Multi Functional Corbels (HMFC) and threaded roads for the retrofitted specimen BD-H1

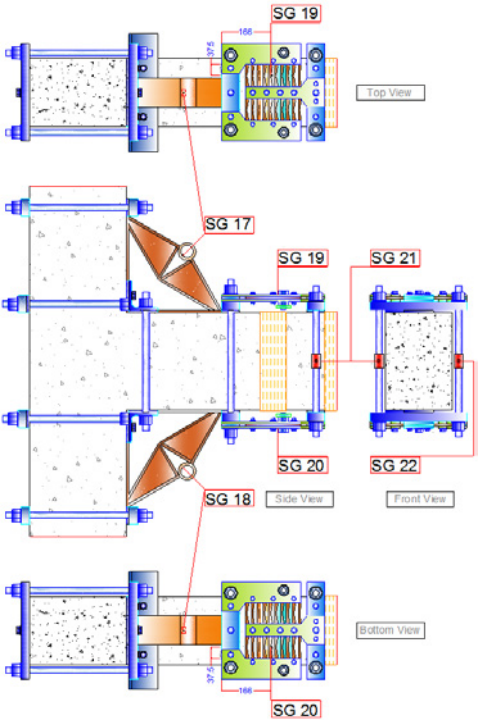

Fig. 4.51: Location of strain gauges of Multi Functional Corbels (HMFC), Harmonica Damper Plates (HHDP), and threaded roads for the retrofitted specimen SD-H2-D

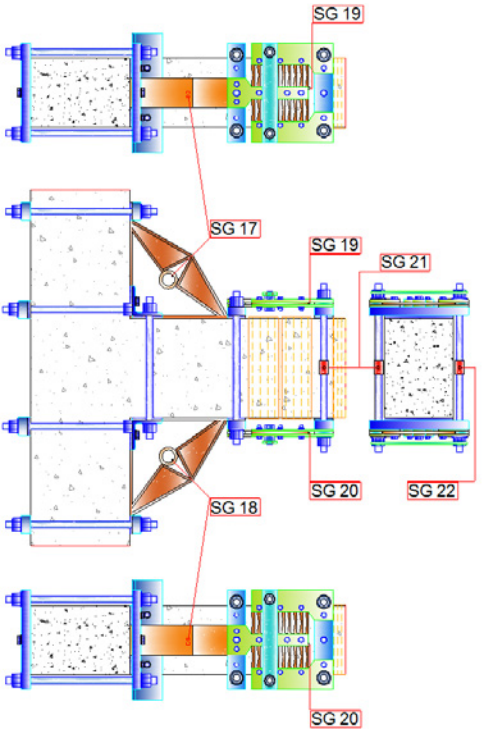

Fig. 4.52: Location of strain gauges of Multi Functional Corbels (HMFC), Harmonica Damper Plates (HHDP), and threaded roads for the retrofitted specimen BD-H3-D

4.5 Experimental tests and results

Here, among the conducted tests are represented the results of experimental assessments on five specimens, two reference units (BD-B, SD-D) and three retrofitted specimens (BD-H1, SD-H2-D and BD-H3-D). The as-built specimens were tested to investigate the behaviour of substandard vulnerable reference units without retrofitting as a benchmark performance and the upgraded specimens were experimented to evaluate the retrofitting methods of RT1 and RT2. To clearly describe the experimental results, the assumed negative and positive loading and displacement are shown in Fig. 4.53. In the following for reasons of simplicity, the joint diagonal cracks which were generated under positive and negative drifts are named the joint diagonal positive and negative cracks, respectively.

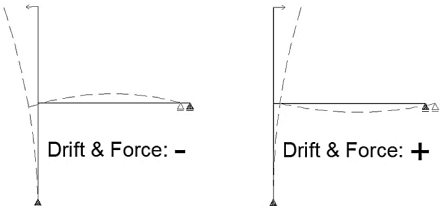

Fig. 4.53: Assumed signs of loading and displacement direction

4.5.1 Tests of reference units

The reference units comprise the two deficiencies, bond deficiency or in the other words beam bottom bars slippage insufficiency (BD-B) and shear deficiency of the joint (SD-B), moreover, there is no joint shear reinforcement in both kinds of the specimens.

4.5.1.1 Test of BD-B

4.5.1.1.1 Specimen description

In specimen BD-B, the beam bottom bars have only 150 mm embedment length into the joint. According to the expected Strength and Failure Sequence Diagram (SFSD) of BD-B (Fig. 4.24), the slippage and pulling-out of the beam bottom bars is expected to be occurred prior to joint first diagonal shear crack.

4.5.1.1.2 Strength sequences and damage mechanisms

Specimen BD-B demonstrated significant vulnerability of the joint panel zone region and critical function of the slippage and pull-out of the beam bottom bars due to inadequate development length into the joint. The spalling of the concrete cover due to pulling-out of the discontinuous beam bottom bars and brittle failure of one-way concrete wedge mechanism because of the interaction of shear cracking and stress concentration at the 90° hook zone was detected in the final failure pattern of specimen BD-B. The final failure mechanism, monitored hysteresis loops of story shear-drift and variation of column axial load during the test are displayed in Fig. 4.54, 4.55, and 4.56, respectively. As can be seen, the overall structural stiffness degradation due to pulling-out of the beam bars and reducing axial load capacity because of the concrete spalling was resulted through the test. Furthermore, it was

observed that the repetition of cycles in each drift level would significantly reduce the maximum lateral resistance and stiffness of the specimen under the same drift demand especially after the drift level of peak load carrying capacity. Meanwhile, because of an electrical problem between the load cell of cyclic actuator and computer, some of lateral loads were estimated and modified through some directly noted amounts of maximum data in every drift level from the monitor of actuator.

Fig. 4.54: Final failure of specimen BD-B after the first cycle of 3.5% drift

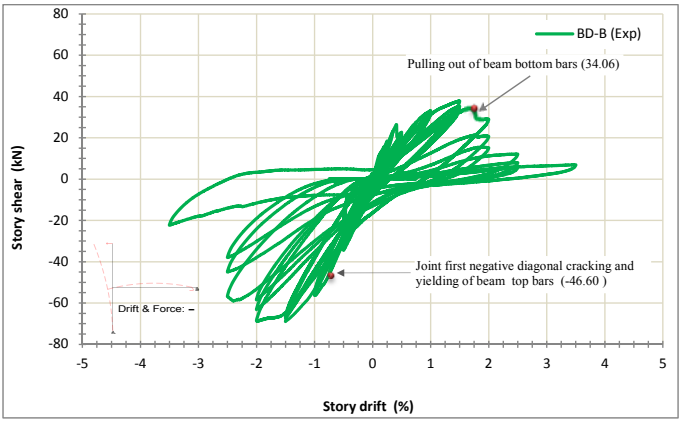

Fig. 4.55: Experimental story shear-drift hysteretic response of specimen BD-B

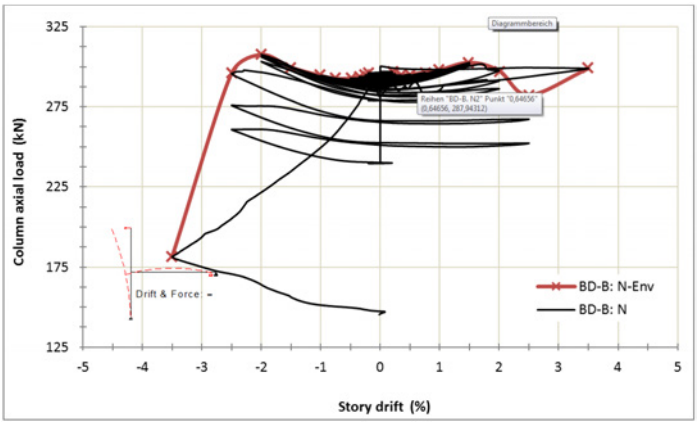

Fig. 4.56: Imposed column axial load versus drift of specimen BD-B

The strain envelope of beam longitudinal bars at the beam column interface versus story drift of the tested specimen BD-B is also illustrated in Fig. 4.57. Evidently, the top bars of the beam yielded under tension after the drift level of 0.75%, while the bottom bars could not achieve the yield point because of inadequate development length into the joint.

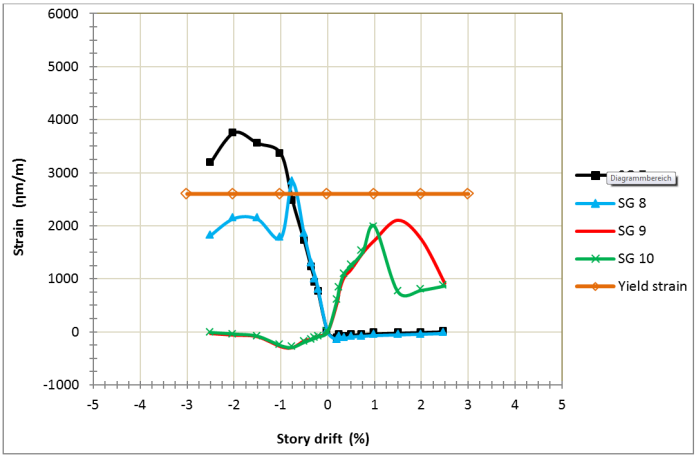

Fig. 4.57: The envelope diagram for Max. strain of beam longitudinal bars at the beam-column interface versus story drift of specimen BD-B

The sequence of observed crack patterns and damage modes after end of each imposed drift

level are illustrated in Fig. 4.58. The observed results during each drift level are shortly discussed as follows.

- *Drift 0.20%:* No crack was observed.
- *Drift 0.25- 0.35%:* The hairline flexural cracks in the beam were observed.
- *Drift 0.50%:* The first positive joint shear diagonal crack was occurred under imposed positive story shear of +26.40kN at +0.41% drift. Meanwhile, a vertical crack at the middle of column side face, nearly end of beam bottom bars, was developed towards the lower part of the column.
- *Drift 0.75%:* The first negative joint shear diagonal crack was occurred under imposed negative story shear of -46.60kN. The developed cracks in the beam and joint were propagated. The joint diagonal positive crack was connected to the column vertical crack (created during the last drift) and expanded to the lower column and the joint diagonal negative cracks were propagated towards the upper column. The beam top bars began to yielding but bottom bars due to inadequate development length cannot raise their stresses to reach to the yield point.
- *Drift 1.0%:* The developed cracks in the beam and joint were propagated and the new joint diagonal positive and negative cracks were generated.
- *Drift 1.5%:* The developed cracks in the beam and joint were propagated and the joint diagonal cracks were increased. The width of the joint main diagonal positive crack was reached to 1.2 mm and a horizontal transverse crack was developed on the back of the column at the lowest level of the beam. Furthermore, a vertical crack was developed on the front face of the lower column under the beam at the middle. At the first cycle, the specimen reached to the maximum positive and negative story shear strength of +37.8 and -68.95kN, respectively, while the negative reinforcement of the beam was in strain hardening step and positive reinforcement illustrated elastic behaviour.
- *Drift 2.0%:* The propagated cracks became wider and new cracks were occurred in the joint and different faces of the column. The slippage of beam bottom bars was clearly demonstrated during the first positive drift (+1.71%) under the story shear of +34.06 kN and pulling-out failure was occurred during the positive drifts of next cycles along with the beginning of concrete spalling at the lower corner of the beam column interface. Meanwhile, the joint negative diagonal cracks were stretched out toward backside of the column, upper than the beam top level. The maximum negative story shear strength of the specimen was the same with the last drift result while the positive strength dramatically decreased due to slippage of beam bottom reinforcement.

- *Drift 2.5%:* The first positive drift led to concrete spalling at the lower corner of the beam column interface. Subsequently, at the continuation of joint negative diagonal cracks towards backside of the upper column, the negative drift developed concrete fracturing as a brittle failure of one-way concrete wedge mechanism. The buckling of column front face corner side longitudinal bars along with deformation of column first tie was observed under the beam. The negative and positive lateral strength of the specimen were decreased 17% and 58% with respect to the last drift results, respectively. As can be seen from Fig. 4.56, the imposed column axial load was declined from nearly 280kN (at the beginning of the drift level) to 240kN during the test.
- *Drift 3.5%:* The concrete in the joint panel zone near to the beam column interface started to fall down and buckling of column middle longitudinal bars (Φ10) at the joint panel zone was observed. The specimen has lost the story shear capacity and the test was stopped after one cycle drift. According to Fig. 4.56, the column axial force was increased to 300kN before starting of the drift level.

a) Drift 0.2%: No cracks

b) Drift 0.25%: Minor hairline cracks in the beam

c) Drift 0.35%: Minor hairline cracks in the beam

d) Drift 0.5%: First positive diagonal crack in the joint

Fig. 4.58: (continued)

e) *Drift 0.75%: First negative diagonal cracking in the joint*

f) *) Drift 1%: Propagation of the cracks*

g) *Drift 1.5%: First crack in the back of column*

h) *Drift 2%: Slippage and pulling-out failure of beam Bot.bars and beginning of concrete spalling*

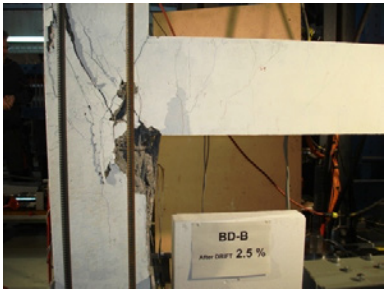

i) *Drift 2.5%: Concrete wedges Spall off*

j) *Drift 3.5%: Concrete in the joint panel falls down*

Fig. 4.58: Crack patterns and damage mode sequence of specimen BD-B at different levels of drifts

4.5.1.1.3 Joint behaviour

The joint behaviour could be investigated in terms of principal tensile stress. Assuming the constant amount of beam moment arm (z_b), column gross area (A_g), and effective joint cross-sectional area (A_e), the plot of normalized conventional joint principal tensile stresses

($f_{tj}/\sqrt{f'_c}$) versus top drifts of the unit BD-B was represented in Fig. 4.59. According to the diagram, the first positive and negative diagonal shear cracking were occurred at principal tensile stresses of $f_{tj} = 0.126\sqrt{f'_c}$ and $f_{tj} = 0.305\sqrt{f'_c}$, respectively. The positive crack was observed during the first cycle of drift level +0.5% at +0.41% and the negative crack was noticed at drift of -0.75% while the beam top bars began to yield in the negative loading direction at -1.0% drift. The providence of column middle longitudinal reinforcement (Φ10) was resulted to increase the principal tensile stress after the first diagonal shear cracks. At the drifts of +1.5% and -1.5%, the maximum conventional principal tensile stresses of joint were measured $0.223\sqrt{f'_c}$ and $0.534\sqrt{f'_c}$, respectively.

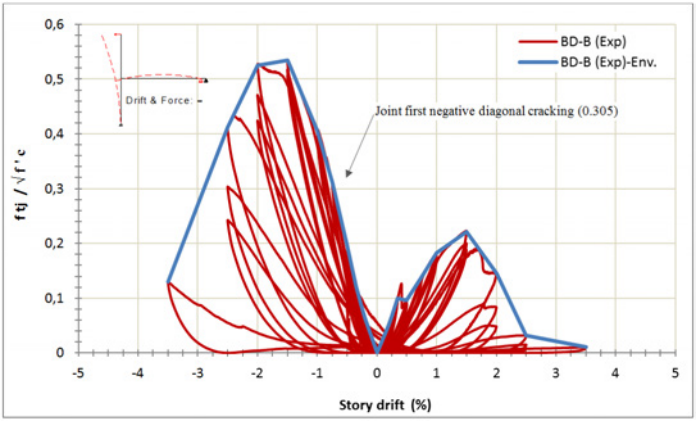

Fig. 4.59: The relationship between joint principal tensile stress ($f_{tj}/\sqrt{f'_c}$) and story drift of specimen BD-B

On the other hand, the scheme of normalized conventional joint horizontal shear stresses ($v_{jh}/\sqrt{f'_c}$) versus story drifts of specimen BD-B, assuming the constant amount of beam moment arm (z_b) and effective joint cross-sectional area (A_e), was represented in Fig. 4.60. As can be seen, the peak value of horizontal joint shear was not able to reach more than $0.777\sqrt{f'_c}$ which is considerably less than the nominal shear strength of the joint proposed by ACI and Eurocode 8 (Table 2.1). The joint shear strength degradation in the positive and negative directions occurred after drift level of ±1.5% while the slippage and finally bond failure of beam bottom bars into the joint didn't allow the joint shear strength to more increase in the positive direction. The maximum conventional horizontal shear stresses of

joint were resulted at the drifts of +1.5% and -1.5% with the amounts of $0.424\sqrt{f_c'}$ and $0.777\sqrt{f_c'}$, respectively.

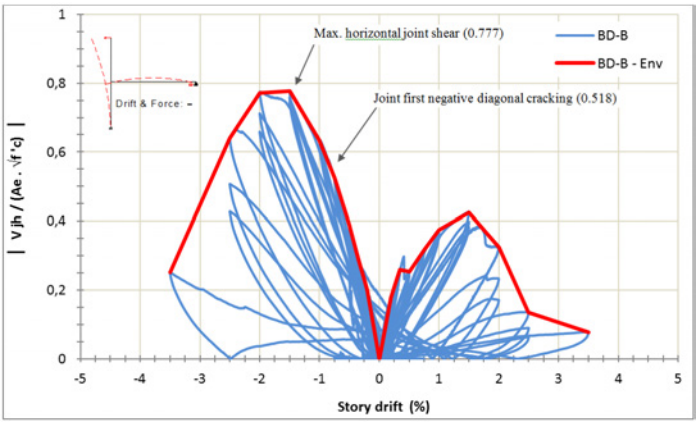

Fig. 4.60: The relationship between absolute value of (joint horizontal shear stress) $\left| V_{jh}/(A_e\sqrt{f'_c}) \right|$ and story drift of specimen BD-B

The joint shear deformations (γ) were obtained by monitoring the installed LVDTs in the joint region, Fig. 4.61. After processing the recorded data from the LVDTs, the joint shear deformation versus the normalized conventional tensile principal stress and story drift can be plotted as Fig. 4.62. The joint shear deformation of first positive and negative diagonal shear cracks were 0.00074 and 0.001 Radian while the joint principal tensile stresses were $f_{tj} = 0.126\sqrt{f_c'}$ and $f_{tj} = 0.305\sqrt{f_c'}$, respectively. The maximum recordable joint shear deformation of 0.0047 and 0.004 Radian under positive and negative loading was measured at ±1.5% drift level, respectively.

Fig. 4.61: LVDT layout for measurement of joint shear deformation and horizontal displacement component

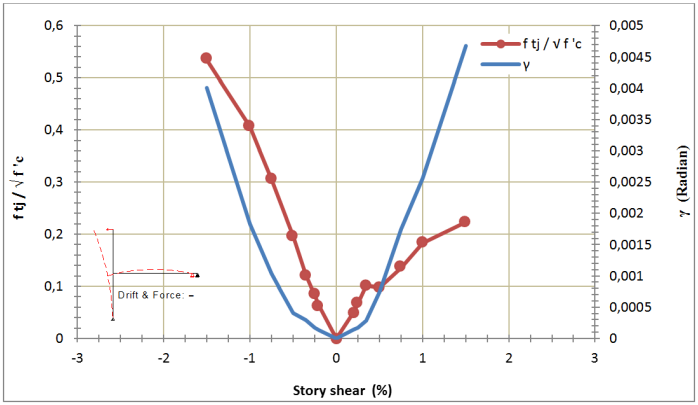

Fig. 4.62: The relationship among joint principal tensile stress ($f_{tj}/\sqrt{f'_c}$), story drift, and joint shear deformation (γ) of specimen BD-B

4.5.1.1.4 Decomposition of lateral displacement

The total lateral displacement components of beam, column and joint in every drift level are represented in Fig. 4.63. As can be seen, the joint contribution increased after joint first diagonal cracks at +0.41% and -0.75%, respectively.

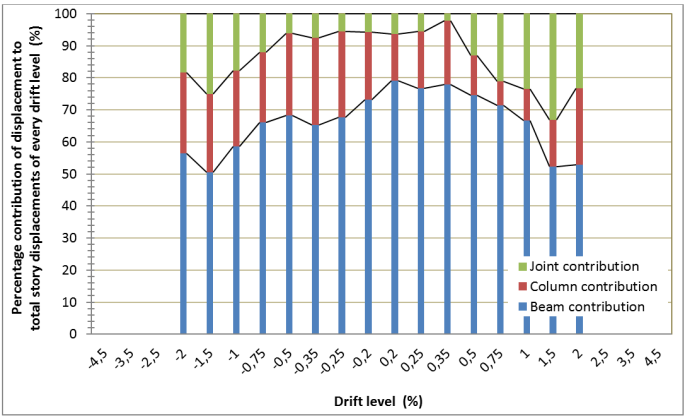

(a)

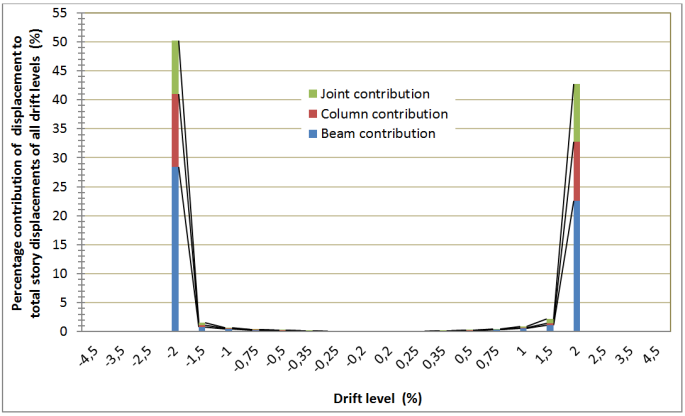

(b)

Fig. 4.63: Percentage contributions of beam, column and joint displacement in specimen BD-B to a) total displacements in every drift level, b)total displacements of all drift levels

4.5.1.2 Test of SD-B

4.5.1.2.1 Specimen description

In specimen SD-B, the beam bars ended to standard 90 degree hook into the joint. According to expected Strength and Failure Sequence Diagram (SFSD) for SD-B (Fig. 4.33), the joint shear diagonal crack is expected to be occurred prior to the yielding of beam longitudinal bars.

4.5.1.2.2 Strength sequences and damage mechanisms

Specimen SD-B demonstrated significant vulnerability of the joint panel zone region due to joint shear failure mode and spalling of the concrete. The concrete spalling due to brittle failure of two-way concrete wedge mechanism was detected in the final failure pattern of specimen SD-B. The final failure mechanism, recorded hysteretic behaviour, and variation of the imposed column axial load are displayed in Fig. 4.64, 4.65, and 4.66, respectively. As can be seen, the joint shear failure didn't provide the conditions to continue the strength after the drift level of ±2.5% and finally the brittle concrete spalling led to the overall failure and losing the axial load capacity. Moreover, it was found that the repetition of cycles in each drift level would considerably reduce the maximum load carrying capacity and stiffness of the unit under the same drift demand especially after the drift level of peak resistance.

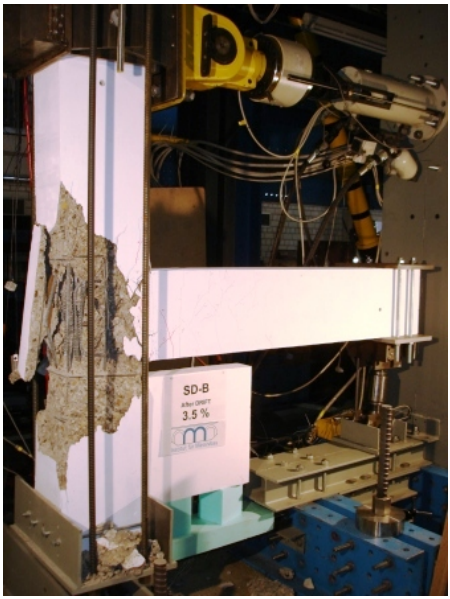

Fig. 4.64: Final failure of SD-B after 3.5% drifts level

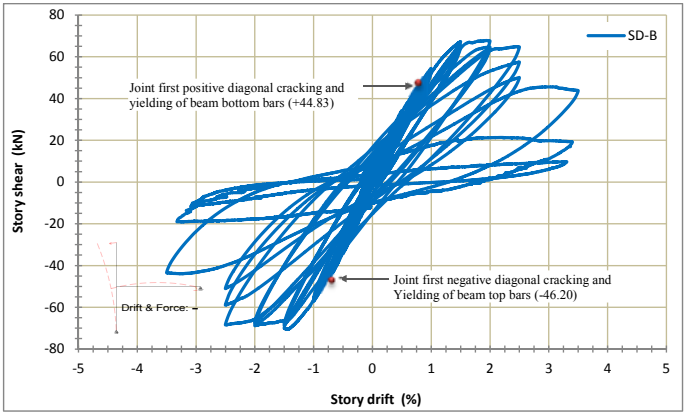

Fig. 4.65: Experimental story shear-drift hysteretic response of specimen SD-B

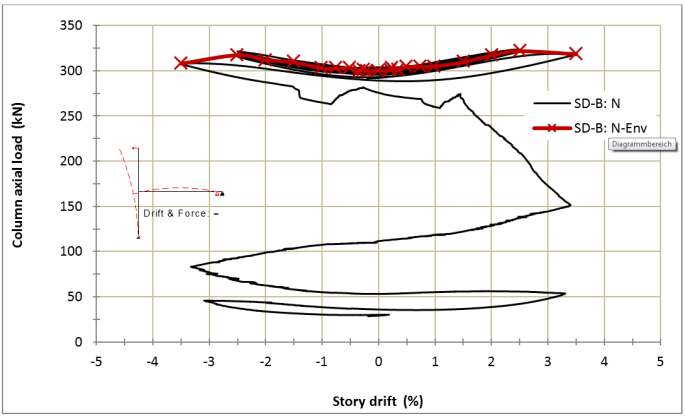

Fig. 4.66: Imposed column axial load versus drift of specimen SD-B

The strain envelope of beam longitudinal bars at the beam column interface versus story drift of the tested specimen SD-B is displayed in Fig. 4.67. As can be seen, the top and bottom bars of the beam have nearly begun to yield under negative and positive moments, respectively, after the drift level of 0.75%.

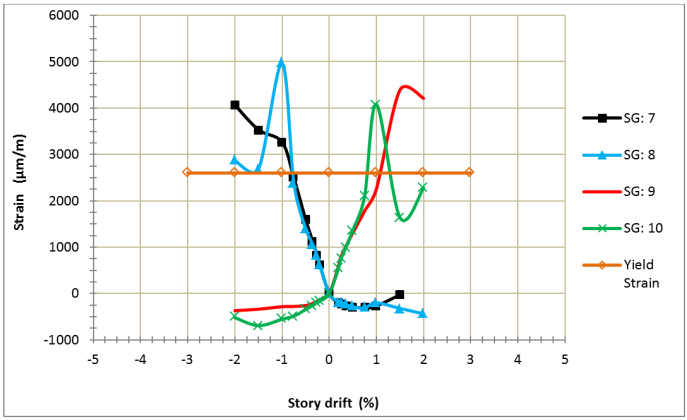

Fig. 4.67: The envelope diagram for Max. strain of beam longitudinal bars at the beam-column interface versus story drift of specimen SD-B

The sequence of observed crack patterns and damage modes after end of every drift level are represented in Fig. 4.68. The monitored results during drift levels are shortly discussed as follows.

- *Drift 0.20%:* No crack was observed.
- *Drift 0.25- 0.35%:* The hairline flexural cracks in the beam were observed.
- *Drift 0.50%:* The first small diagonal cracks were observed at the beam corners of the beam column interface.
- *Drift 0.75%:* The first positive and negative joint shear diagonal cracks were occurred under imposed negative story shears of +44.83kN and -46.20kN, respectively. The developed cracks in the beam and joint were propagated. The beam bottom and top bars began to yield.
- *Drift 1.0%:* The developed cracks in the beam and joint were propagated and the new joint diagonal positive and negative cracks were generated.
- *Drift 1.5%:* The developed cracks in the beam and joint were propagated and the joint diagonal cracks were increased. At the first cycle, the specimen reached to the maximum positive and negative story shear strength of +67.27kN and -69.96kN, respectively, while the beam flexural reinforcement were in strain hardening step. It can be expressed that the beam at the joint interface initiated to hinging.

- *Drift 2.0%:* The propagated diagonal cracks in the joint and flexural crack at the beam column interface became wider. At the first cycle of drift level, the maximum positive and negative story shear capacities were nearly the same with the maximums of the last drift level of 1.5%.
- *Drift 2.5%:* Whilst the maximum story shear capacities of the drift level were nearly the same with drift level of 2%, the joint positive and negative diagonal cracks continued towards bottom and top of the column, respectively, and propagated to the backside of it. The beam flexural crack at the joint interface as well as joint diagonal cracks became wider. Subsequently, the positive and negative drifts developed concrete fracturing as a brittle failure of two-way concrete wedge mechanism.
- *Drift 3.5%:* The concrete of the joint panel zone started to spalling and falling down and subsequently, buckling of column longitudinal bars at the joint panel zone was observed. The story shear capacity was dramatically decreased and according to Fig. 4.65, at the end cycle the system lost significantly the vertical load bearing capacity.

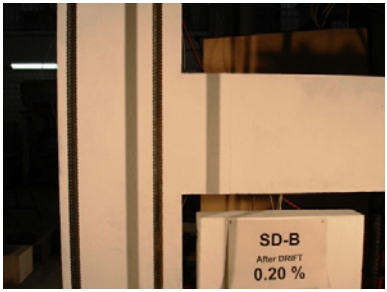

a) Drift 0.2%: No cracks

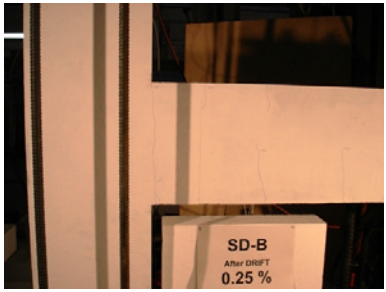

b) Drift 0.25%: Minor hairline flexural cracks in the beam

c) Drift 0.35%: Minor hairline flexural cracks in the beam

d) Drift 0.5%: First small diagonal cracks at the beam corners of the beam column interface

Fig. 4.68 (continued)

e) Drift 0.75%: First diagonal cracks in the joint

f) Drift 1%: Propagation and opening the cracks

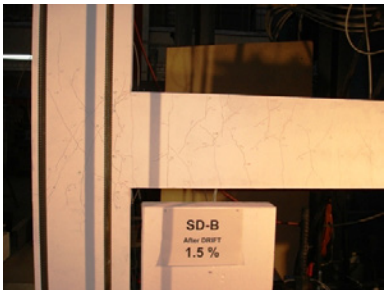

g) Drift 1.5%: Propagation and opening the cracks

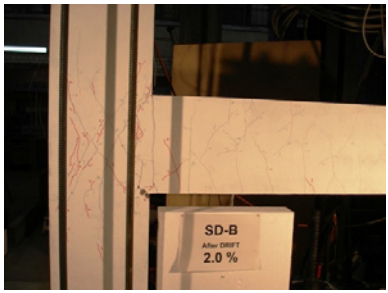

h) Drift 2%: Propagation and opening the cracks

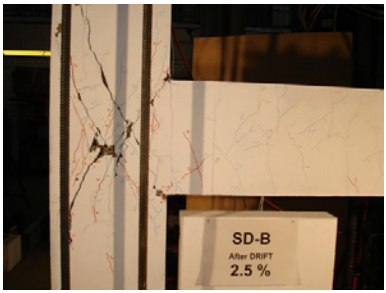

i) Drift 2.5%: forming a concrete wedge by the crack opening

j) Drift 3.5%: spalling and falling down the concrete from the joint panel

Fig. 4.68: Crack patterns and damage mode sequence of specimen SD-B at different levels of drifts

4.5.1.2.3 Joint behaviour

The scheme of normalized conventional joint principal tensile stress versus story drift (Fig. 4.69) shows that the principal tensile stresses of $f_{tj} = 0.293\sqrt{f_c'}$ and $f_{tj} = 0.307\sqrt{f_c'}$ caused the development of the first positive and negative diagonal shear cracking in the joint at 0.75% drift, respectively. As mentioned before, the beam longitudinal bars began to yield at

±1.0% drift and providence of column middle longitudinal bars resulted to preparing the increasing of principal tensile stress after the first shear diagonal cracks. The maximum conventional principal tensile stresses of joint were resulted at the drifts of +1.5% and -1.5% with the amounts of $0.519\sqrt{f_c'}$ and $0.547\sqrt{f_c'}$, respectively.

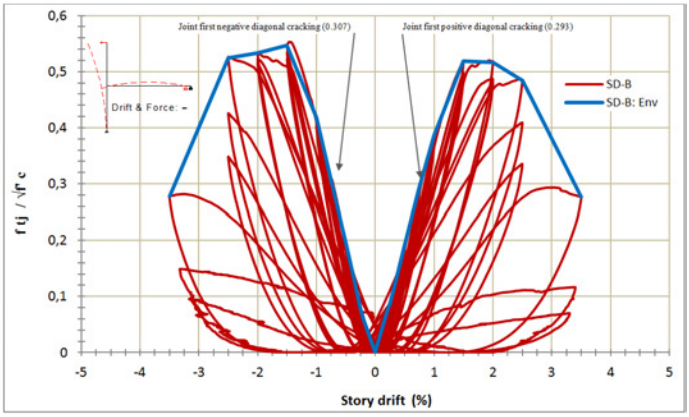

Fig. 4.69: The relationship between joint principal tensile stress ($f_{tj}/\sqrt{f'_c}$) and story drift of specimen SD-B

The plot of normalized conventional joint horizontal shear stresses versus story drifts (Fig. 4.70) displays that the joint first positive and negative diagonal shear cracking occurred at ±0.75% drift with $0.51\sqrt{f'_c}$ and $0.52\sqrt{f'_c}$ horizontal shear stresses, respectively. Meanwhile, the maximum amount of horizontal joint shear stresses at drift of -1.5% and +1.5% could not reach more than $0.789\sqrt{f'_c}$ and $0.758\sqrt{f'_c}$, respectively, which is significantly less than the proposed code requirements of ACI and Eurocode 8 (Table 2.1). As can be seen, the joint horizontal shear strength degradation in the positive and negative directions occurred after drift level of ±1.5%.

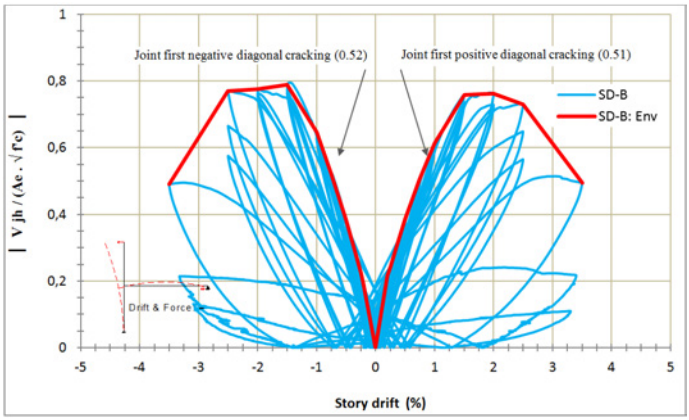

Fig. 4.70: The relationship between absolute value of (joint horizontal shear stress) $\left| V_{jh}/(A_e\sqrt{f'_c}) \right|$ and story drift of specimen SD-B

The diagram of joint shear deformation versus normalized conventional tensile principal stress and story drift (Fig. 4.71) illustrates that the joint shear deformation of 0.00064 and 0.00078 Radian were measured at the first positive and negative joint diagonal shear cracking in ±0.75% drift while the joint conventional tensile principal stresses were $f_{tj} = 0.293\sqrt{f'_c}$ and $f_{tj} = 0.307\sqrt{f'_c}$, respectively. The maximum recordable joint shear deformation of 0.0032 and 0.0028 Radian under positive and negative loading was measured at ±2.0% drift level, respectively.

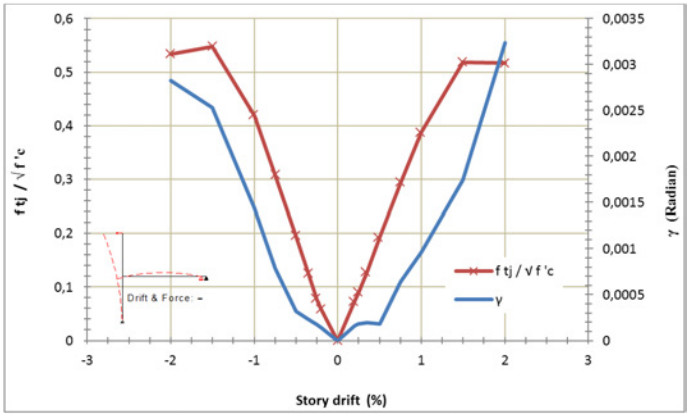

Fig. 4.71: The relationship among joint principal tensile stress ($f_{tj}/\sqrt{f'_c}$), story drift, and joint shear deformation (γ) of specimen SD-B

4.5.1.2.4 Decomposition of lateral displacement

The reviewing of the beam, column and joint contributions in every drift levels (Fig. 4.72) clarifies that the portion of joint contribution was raised after occurring the first diagonal shear cracks at ±0.75%.

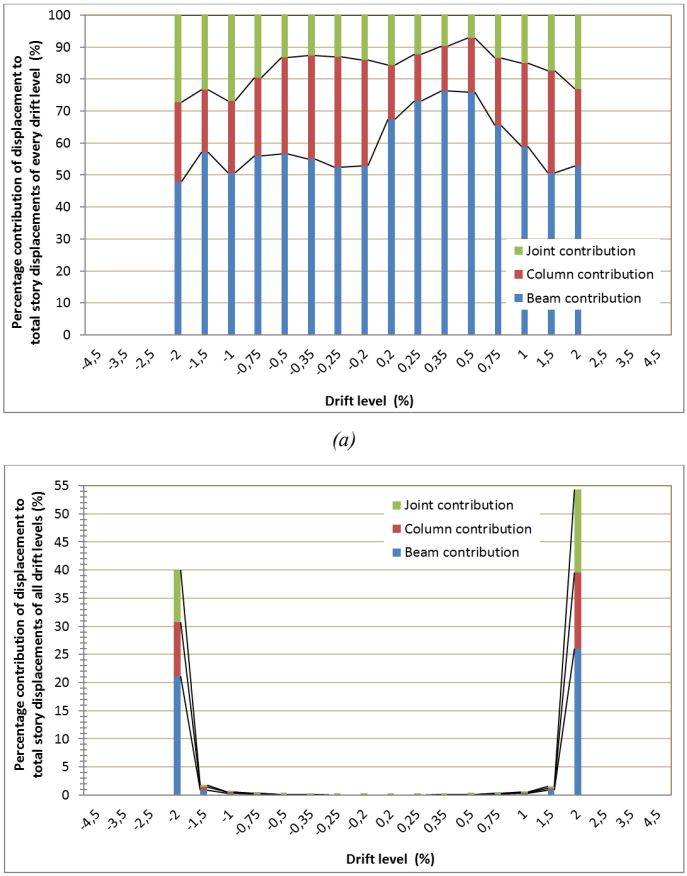

Fig. 4.72: Percentage contributions of beam, column and joint displacement in specimen SD-B to a) total displacements in every drift level, b) total displacements of all drift levels

4.5.2 Tests of retrofitted units

Following the proposed procedures for designing and developing the innovative retrofitting techniques (RT1 and RT2) in chapter 3 and designed solutions in current chapter, the seismic response of the retrofitted units (BD-H1 and SD-H2-D) were studied in this section. Through these techniques, the joint panel zones were protected by relocating the flexural plastic hinge in the beam away from the column face at the end of Multi Functional Corbels (HMFC) and the effectiveness of the proposed retrofit solutions would be experimentally investigated.

4.5.2.1 Test of BD-H1

4.5.2.1.1 Specimen description

The specimen BD (with only 150mm embedment length of the beam bottom bars into the joint) was upgraded through retrofitting technique 1 by two pairs of HMFC (H1). According to the expected Strength and Failure Sequence Diagram (SFSD) (Fig. 4.27), the beam flexural plastic hinge would be simultaneously formed with first joint diagonal shear cracking. Meanwhile, to have the extra energy dissipations through HMFCs set (H1), they would be designed so that their yield strengths reach before the beam flexural hinge occurring.

4.5.2.1.2 Strength sequences and damage mechanisms

Specimen BD-H1 demonstrated significant strength and ductility in comparison with the reference unit BD-B. The pulling-out of the beam bottom bars, brittle shear failure mechanism of the joint, and overall structural stiffness degradation were eliminated and considerable structural strength and energy dissipation were resulted. The final failure mechanism, monitored hysteretic behaviour and imposed column axial load are depicted in Fig. 4.73, 4.74,

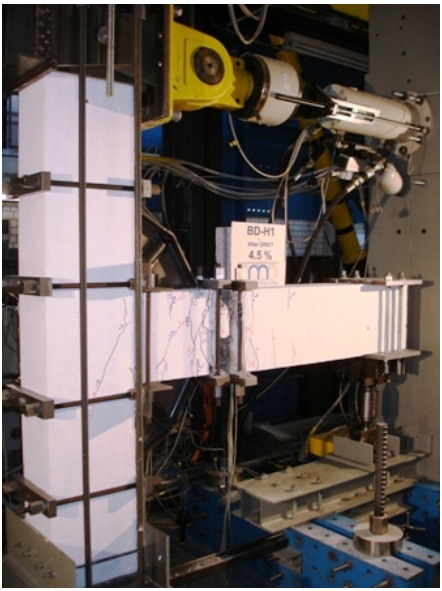

Fig. 4.73: Retrofitted specimen BD-H1 after 4.5% drifts level

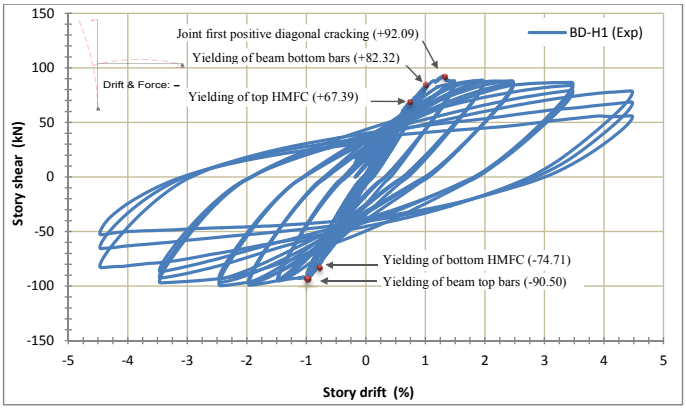

Fig. 4.74: Experimental story shear-drift hysteretic response of specimen BD-H1

and 4.75, respectively. Evidently, the failure sequence inverted to form the beam-hinging mechanism at the end of HMFC and concrete spalling-off was observed in the plastic hinging

region at higher drift level. Furthermore, no crack was appeared in the column and no reducing of column axial capacity was noticed. Meanwhile, it was observed that until the drift level of 2.5%, the repetition of cycles in each drift level was not considerably reduce the story shear resistance and stiffness under the same drift demand but after that, little by little, the demonstration of reduction can be considered.

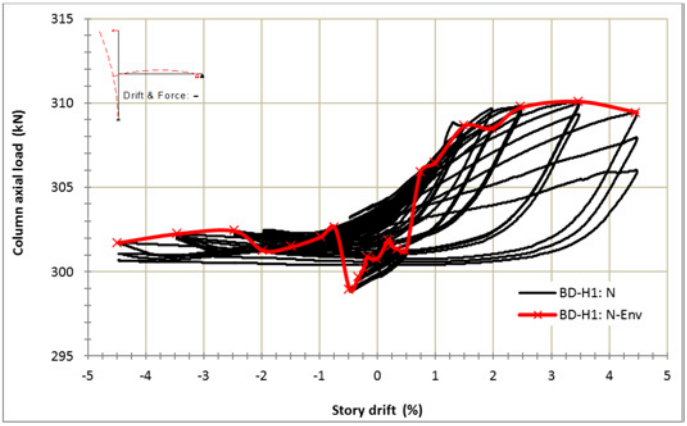

Fig. 4.75: Imposed column axial load versus drift of specimen BD-H1

The strain envelope of beam longitudinal bars at the beam column interface and end of HMFCs versus story drift of the tested specimen BD-H1 are depicted in Figs. 4.76 and 4.77, respectively. As can be considered, at the beam column interface the top bars of the beam yielded under tension nearly after the drift level of -2%, while the bottom bars could not reach to yield point. On the other hand, at the end of HMFCs the beam longitudinal bars yielded after ± 1% drift. That means the retrofitted technique could successfully satisfy the development requirements of the bottom bars with only 150mm embedment length into the joint.

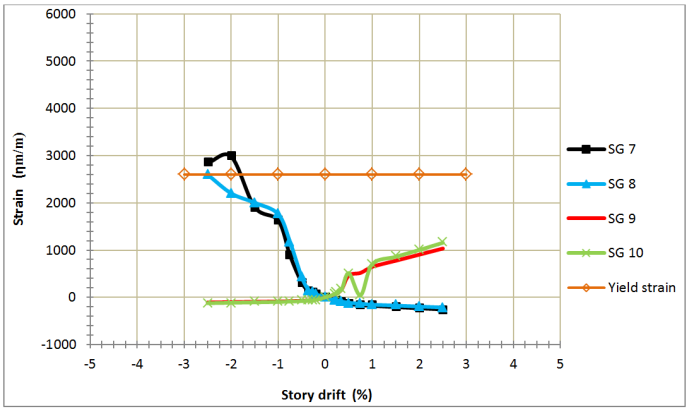

Fig. 4.76: The envelope diagram for Max. strain of beam longitudinal bars at the beam-column interface versus story drift of specimen BD-H1

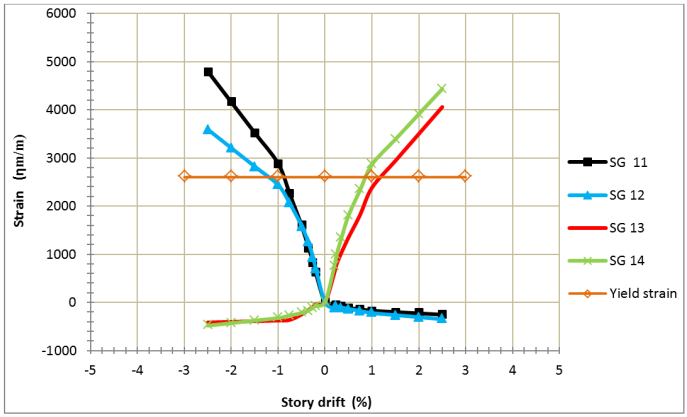

Fig. 4.77: The envelope diagram for Max. strain of beam longitudinal bars at the end of HMFC versus story drift of specimen BD-H1

The progression of observed crack patterns and damage modes after end of every drift level are displayed in Fig. 4.78. The monitored results during drift levels are shortly discussed as follows.

- *Drift 0.20%:* No crack was detected.
- *Drift 0.25%:* The first hairline flexural cracks were observed in the beam at the end of HMFCs.
- *Drift 0.35%:* The flexural cracks of drift level 0.25% were propagated to the middle of the beam.

- *Drift 0.5%:* Flexural cracks were occurred in the beam along the length of HMFC at the top and bottom.
- *Drift 0.75%:* In the beam out of the length of the HMFC, flexural cracks near to the HMFCs were observed. The energy dissipation devices of top and bottom HMFCs began to yield under story shears of +67.39kN and -74.71kN, respectively.
- *Drift 1.0%:* The cracks were propagated and widened. At the end of HMFCs, the beam bottom and top bars began to yield under story shears of +82.32kN and -90.50kN, respectively.
- *Drift 1.5%:* The first positive joint shear diagonal crack was occurred as a hairline under imposed positive story shear of +92.09kN at +1.29% drift. The story shear of the specimen in positive direction reached to the maximum capacity of +92.09kN. The negative joint shear diagonal crack was not clearly detected.
- *Drift 2*.0%: The cracks were propagated and widened, but the deformation was concentrated at the end of HMFCs as a flexural hinge so that the crack width reached to 4mm. The positive joint shear diagonal crack was expanded a little bit towards lower column but did not widen.
- *Drift 2*.5%: While the story shear capacity was nearly the same with the last drift level and no considerable decrease was observed during the current drift level, little by little, the clear plastic deformations in plastic hinge was observed and the specimen reached to the maximum negative shear story capacity of -99.65kN.
- *Drift 3*.5%: The concrete spalling-off was observed in the plastic hinging region of the beam while the maximum story shear capacity was nearly the same
- *Drift 4*.5%: While the rate of concrete spalling-off in the plastic hinging region of the beam was raised, decreasing of about 9% and 14% of maximum story shear capacity was monitored in comparison with the last drift level in positive and negative direction, respectively.

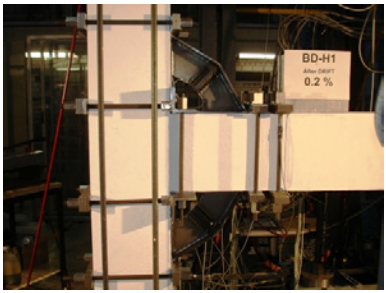

a) Drift 0.2%: No cracks

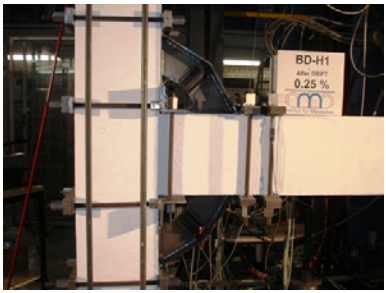

b) Drift 0.25%: The first flexural cracking in the beam at the end of HMFC

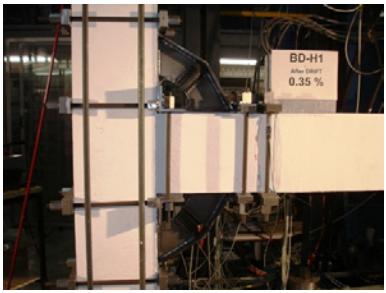

c) Drift 0.35%: Propagation of the flexural cracks in the beam at the end of HMFC

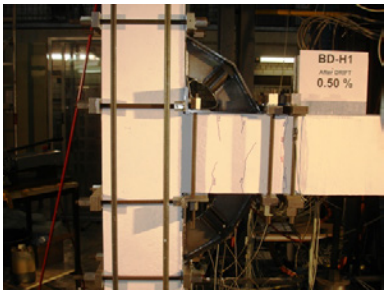

d) Drift 0.5%: Flexural cracking in the beam along the length of HMFC

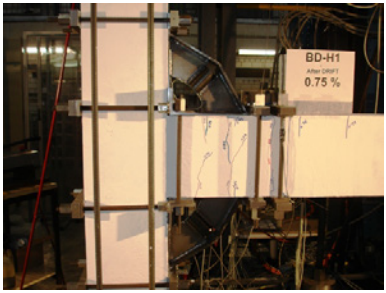

e) Drift 0.75%: Flexural cracking in the beam out of the length of HMFC

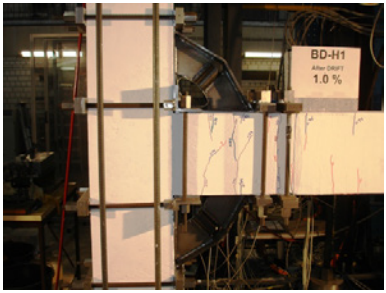

f) Drift 1%: Propagation and opening the cracks

Fig. 4.78: (continued)

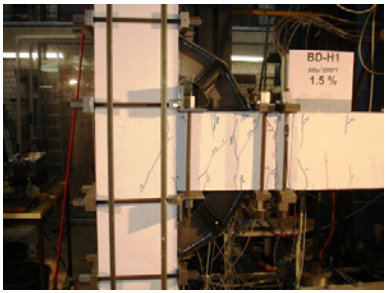

g) Drift 1.5%: First positive diagonal hairline shear crack of the joint

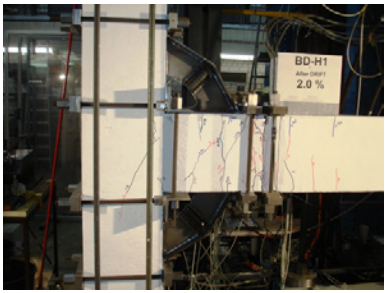

h) Drift 2%: The flexural beam crack at the end of HMFC widened to about 4 mm

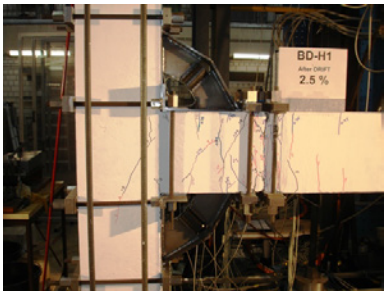

i) Drift 2.5%: Propagation and opening the cracks

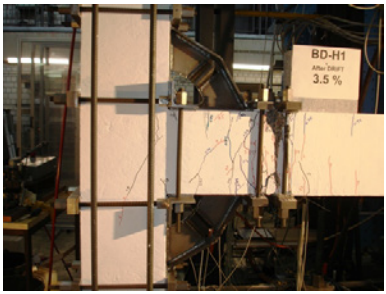

j) Drift 3.5%: Concrete spalling-off in the plastic hinging region

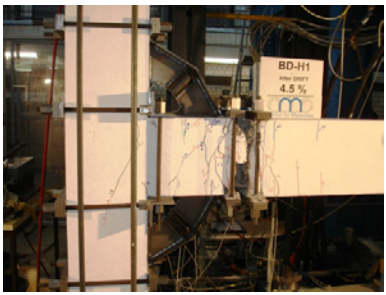

k) Drift 4.5%: Concrete spalling-off in the plastic hinging region

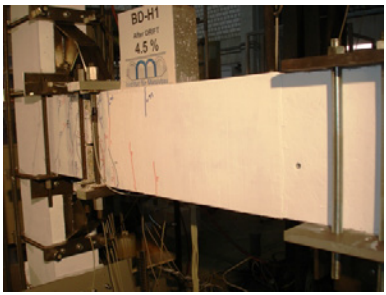

l) Drift 4.5%: Concrete spalling-off in the plastic hinging region

Fig. 4.78: Crack patterns and damage mode sequence of specimen BD-H1 at different levels of drifts

4.5.2.1.3 Joint behaviour

According to the displayed diagram of normalized conventional joint principal tensile stress versus story drift in Fig. 4.79, the principal tensile stress of $f_{tj} = 0.338\sqrt{f_c'}$ is resulted for the first positive diagonal shear cracking in the joint at 1.29% drift. That is the maximum value in the positive direction. But in the negative direction the highest is resulted at the drift of -2.5% with the amount of $0.382\sqrt{f_c'}$.

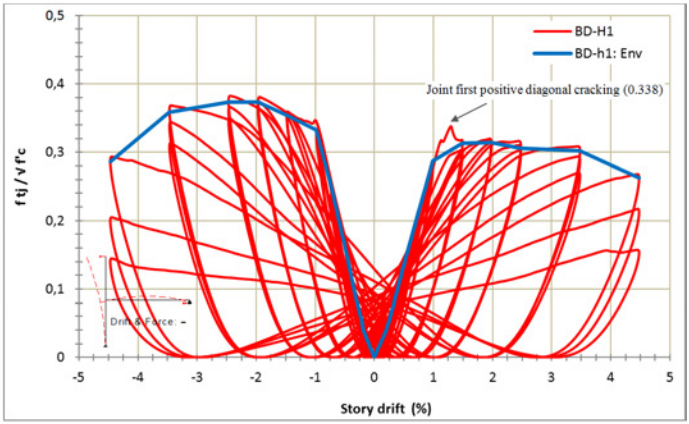

Fig. 4.79: The relationship between joint principal tensile stress ($f_{tj}/\sqrt{f'_c}$) and story drift of specimen BD-H1

The diagram of normalized conventional joint horizontal shear stresses versus story drifts (Fig. 4.80) shows that the joint first positive diagonal shear cracking occurred at +1.29% drift under horizontal shear stress of $0.557\sqrt{f'_c}$. Furthermore, the maximum horizontal shear stress was obtained at 2% and 2.5% drift level with about $0.6\sqrt{f'_c}$ shear stress. Meanwhile, the degradation of joint horizontal shear strength in the positive and negative directions occurred after drift level of ±3.5%.

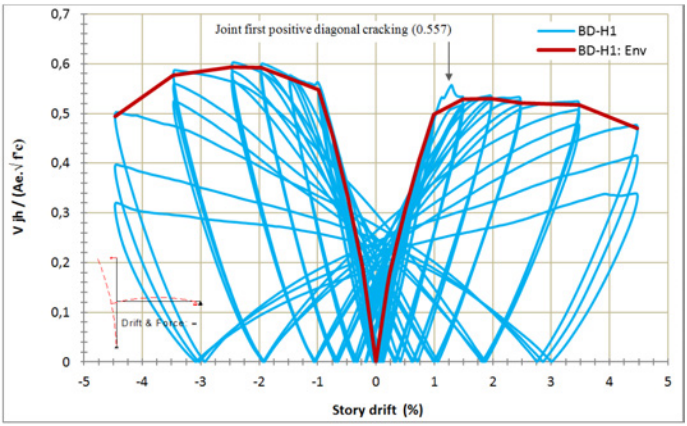

Fig. 4.80: The relationship between absolute value of (joint horizontal shear stress) $\left| V_{jh}/(A_e\sqrt{f'_c}) \right|$ *and story drift of specimen BD-H1*

The processing of the recorded data from LVDTs installed at the joint region (Fig. 4.81) leads to a diagram of joint shear deformation versus the normalized conventional tensile principal stresses and story drifts as plotted in Fig. 4.82. The joint shear deformation of first positive diagonal shear crack was 0.00065 Radian while the joint principal tensile stress was $f_{tj} = 0.338\sqrt{f'_c}$. The maximum joint shear deformation was recorded at +3.5% drift with 0.00132 Radian while at the drift of -4.5% drift, the deformation was 0.00095 Radian.

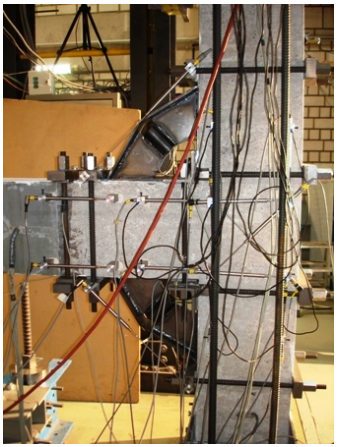

Fig. 4.81: LVDT layout for measurement of joint shear deformation and horizontal displacement component of BD-H1

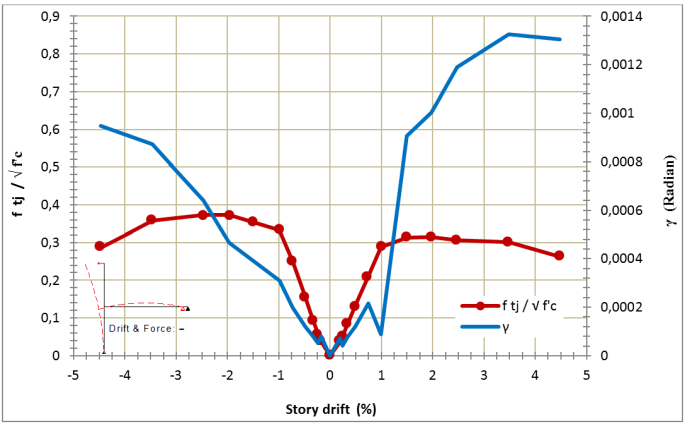

Fig. 4.82: The relationship among joint principal tensile stress ($f_{tj}/\sqrt{f'_c}$), story drift, and joint shear deformation (γ) of specimen BD-H1

4.5.2.1.4 Behaviour of Multifunctional Corbel (HMFC)

The hysteresis loops of strain-story drift as well as strain envelop for energy dissipation devices (pipe) of top and bottom HMFCs (H1) are illustrated in Figs. 4.83 and 4.84, respectively. As expected, the energy dissipation devices in both of HMFCs reached to the yield strain at ±0.75% drift which is less than drift level of ±1% that the longitudinal reinforcement of the beam yielded on it. Moreover, the joint has been elastic until the ±0.75% drift level. According to the design procedure mentioned for retrofitting technique 1 (RT1), to have an effective extra energy dissipation through HMFC system, the corbel set should be designed so that its yield strength reaches before the beam flexural hinge occurs and joint system exits from elastic domain. Consequently, both of these conditions have been satisfied during the test.

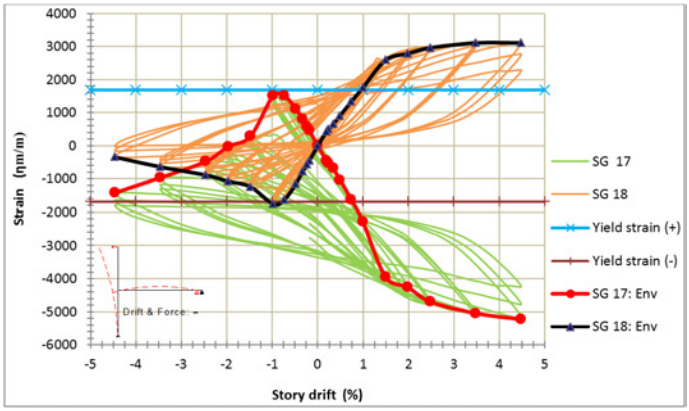

Fig. 4.83: The Hysteretic and envelope diagram for strain of top HMFC versus story drift of specimen BD-H1

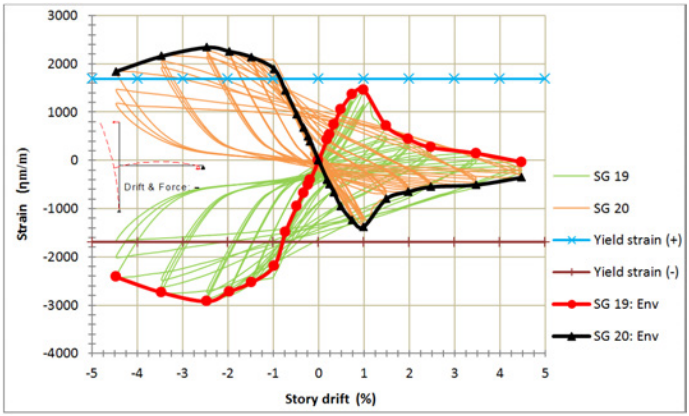

Fig. 4.84: The Hysteretic and envelope diagram for strain of bottom HMFC versus story drift of specimen BD-H1

4.5.2.1.5 Decomposition of lateral displacement

The contribution of the beam, column, and joint from the imposed horizontal displacement to the specimen were achieved by processing monitoring data recorded by LVDTs installed at the joint and end of HMFC on the beam (Fig. 4.45). Fig. 4.85-a and b display the contribution of joint subassemblages from the horizontal total displacement in every drift level and total displacements of all drift levels, respectively. The first diagram shows that the contribution of

beam in every drift level has increased from 25% in ±0.2% drift level to 95% in ±4.5% drift level but by contrast the contribution of column has decreased from 70% in ±0.2% drift level to 3% in ±4.5% drift level. Meanwhile, the part of joint has been changed from 2% in ±0.2% drift level to 5% in -2%-2.5% drift level. On the other hand, the second diagram declares that the contribution of column and joint in comparison with total imposed horizontal displacements during the test were very low while the contribution of the beam was high so that the maximum contributions of the beam, column, and joint were 22.55%, 0.80%, and 0.44% at the drift level of +4.5%, -4.5%, and +4.5%, respectively.

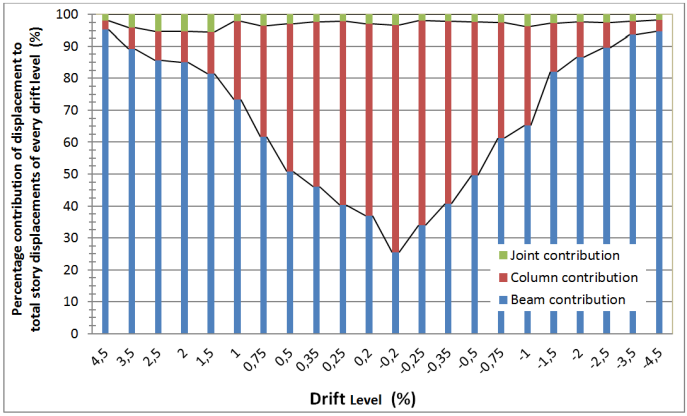

(a)

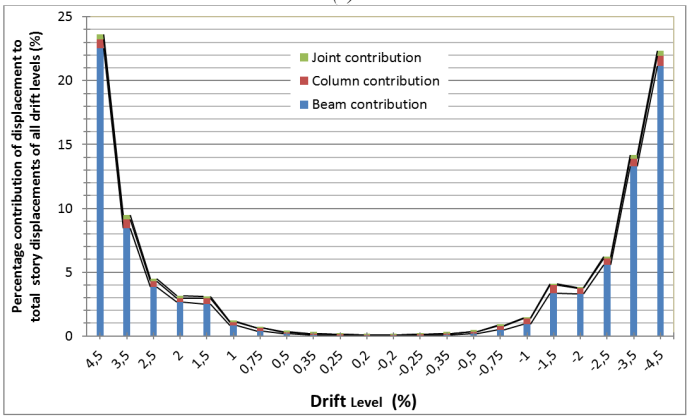

(b)

Fig. 4.85: Percentage contributions of beam, column and joint displacement in specimen BD-H1 to a) total displacements in every drift level, b)total displacements of all drift levels

4.5.2.2 Test of SD-H2-D

4.5.2.2.1 Specimen description

The specimen SD was strengthened through retrofitting technique 2 by two pairs of HMFC (H2) and HHDP (D). According to the expected Strength and Failure Sequence Diagram (SFSD) (Fig. 4.35), the beam flexural plastic hinge and yielding of D would be simultaneously formed with first joint diagonal shear cracking. Meanwhile, to have the extra energy dissipations through HMFCs set (H2), they would be designed so that their yield strengths reach before the beam flexural hinge occurring.

4.5.2.2.2 Strength sequences and damage mechanisms

In comparison with the reference unit SD-B, specimen SD-H2-D demonstrated considerable strength and ductility. During the test the brittle shear failure mechanism of the joint and overall structural stiffness degradation were eliminated and significant structural strength and energy dissipation were resulted. The final failure mechanism, observed hysteretic behaviour and imposed column axial load are depicted in Fig. 4.86, 4.87, and 4.88, respectively. Evidently, the failure sequence inverted to form the beam-hinging mechanism at the end of HMFC and concrete spalling-off was observed in the plastic hinging region at higher drift level. Moreover, no crack was observed in the column and no reducing of column axial capacity was detected. Meanwhile, it was observed that until the drift level of 2.5%, the repetition of cycles in each drift level was not considerably reduce the lateral resistance and stiffness under the same drift demand but after 3.5% drift level, little by little, the demonstration of reduction can be considered.

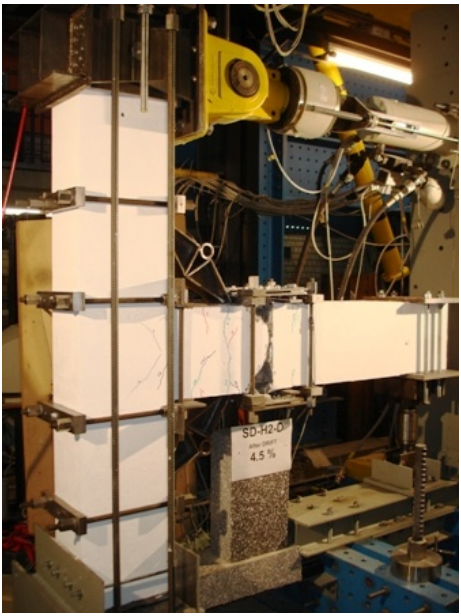

Fig. 4.86: Retrofitted specimen SD-H2-D after 4.5% drifts level

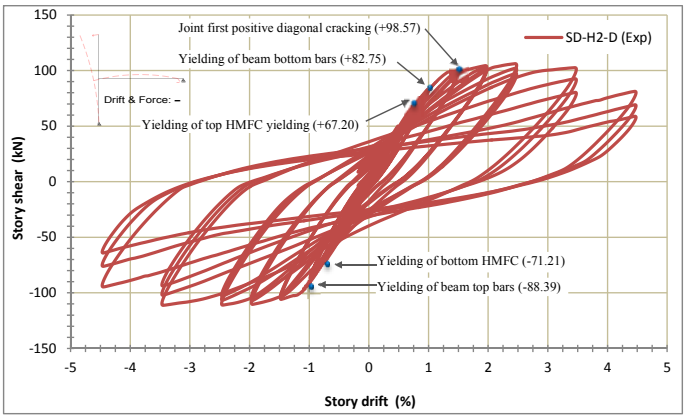

Fig. 4.87: Experimental story shear-drift hysteretic response of specimen SD-H2-D

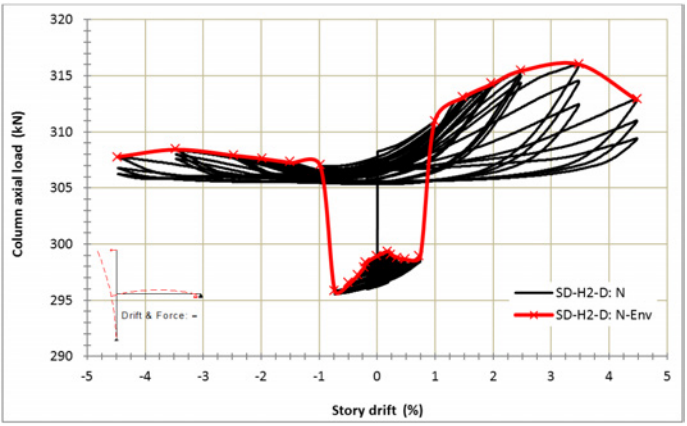

Fig. 4.88: Imposed column axial load versus drift of specimen SD-H2-D

The strain envelope of beam longitudinal bars at the beam column interface and end of HMFCs versus story drift of the tested specimen SD-H2-D are depicted in Figs. 4.89 and 4.90, respectively. As can be observed, at the beam column interface the top and bottom bars of the beam could not reach to the yield point while at the end of HMFCs the beam longitudinal bars yielded after drift level of ± 1%.

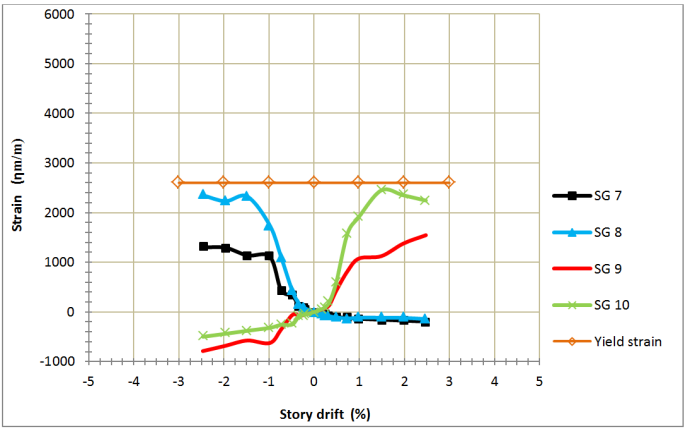

Fig. 4.89.: The envelope diagram for Max. strain of beam longitudinal bars at the beam-column interface versus story drift of specimen SD-H2-D

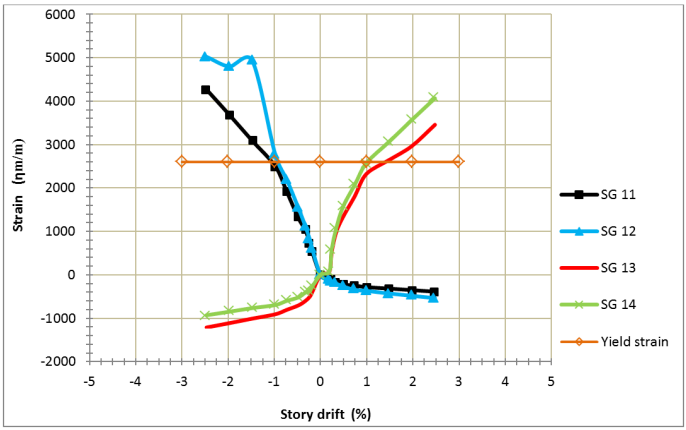

Fig. 4.90: The envelope diagram for Max. strain of beam longitudinal bars at the end of HMFC versus story drift of specimen SD-H2-D

The order of considered crack patterns and damage modes after end of every drift level are illustrated in Fig. 4.91. The observed results during drift levels are shortly discussed as follows.

- *Drift 0.20%:* No crack was detected.
- *Drift 0.25%:* The first hairline flexural cracks were observed in the beam along the first one-third length of HHDP near the end of HMFC.
- *Drift 0.35%:* The flexural cracks of drift level 0.25% were propagated to the middle of the beam.
- *Drift 0.5%:* Flexural cracks were occurred in the beam along the length of HMFC and HHDP at the top and bottom.
- *Drift 0.75%:* The flexural cracks of drift level 0.5% were propagated. The energy dissipation devices of top and bottom HMFCs began to yield under story shears of +67.20kN and -71.21kN, respectively.
- *Drift 1.0%:* The cracks were propagated and widened. At the end of HMFCs, the beam bottom and top bars began to yield under story shears of +82.72kN and -88.39kN, respectively.
- *Drift 1.5%:* The first positive joint shear diagonal crack was observed as a hairline under imposed positive story shear of +98.57kN at +1.5% drift. The negative joint shear diagonal crack was not clearly detected. Inclined shear cracks occurred in D region.

- *Drift 2*.0%: The cracks were propagated and widened, but the deformation was concentrated at the end of HMFCs as a flexural hinge so that concrete cracking was concentrated at the middle and top of the beam in this region. A negative joint shear diagonal crack was observed as a hairline close to the beam column interface.
- *Drift 2*.5%: While the story shear was nearly the same with the last drift level, the lateral strength reached to the maximum positive and negative capacity and little by little, the plastic deformations in plastic hinge were clearly observed.
- *Drift 3*.5%: The concrete spalling-off was observed in the plastic hinging region of the beam while the maximum story shear capacity was the same.
- *Drift 4*.5%: While the rate of concrete spalling-off in the plastic hinging region of the beam was raised, decreasing of about 20% and 14% of maximum story shear capacity was monitored in comparison with the last drift level in positive and negative direction, respectively.

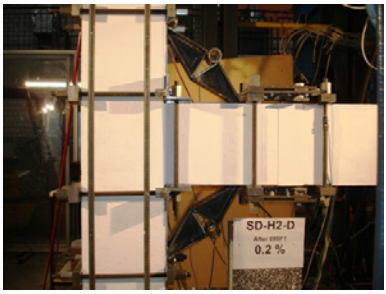

a) Drift 0.2%: No cracks

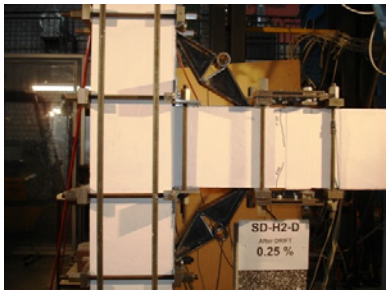

b) Drift 0.25%: The first flexural cracking in the beam along the length of HHDP

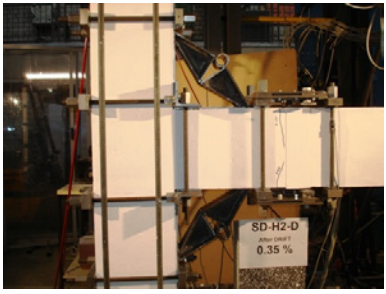

c) Drift 0.35%: Propagation of the flexural cracks in the beam along the length of HHDP

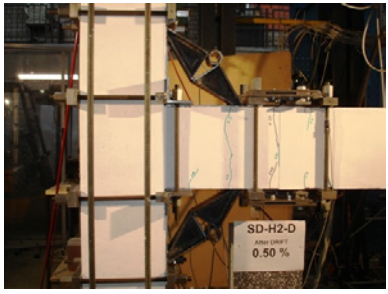

d) Drift 0.5%: Flexural cracking in the beam along the length of HMFC and HHDP

Fig. 4.91: (continued)

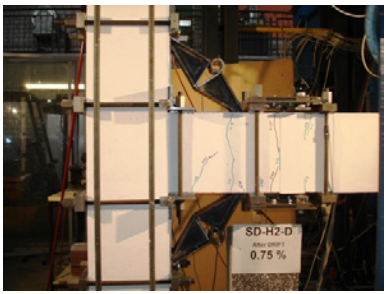

e) Drift 0.75%: Propagation of the flexural cracks

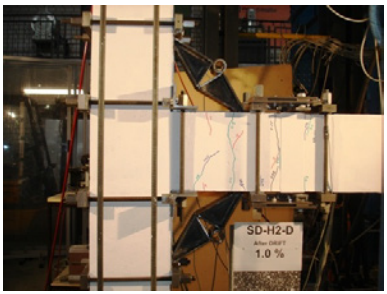

f) Drift 1%: Propagation and opening the cracks

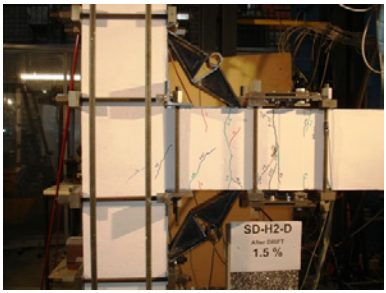

g) Drift 1.5%: First positive diagonal hairline shear crack of the joint

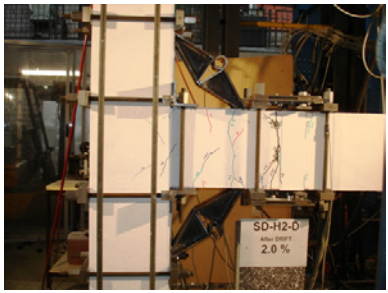

h) Drift 2%: First negative diagonal hairline shear crack of the joint

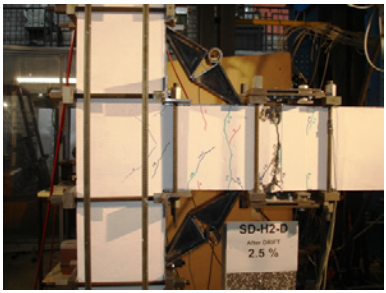

i) Drift 2.5%: Propagation and opening the cracks

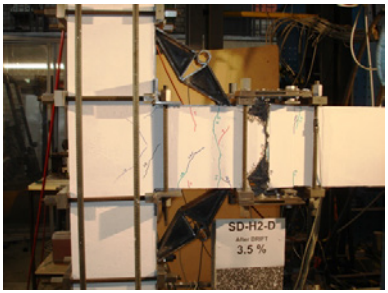

j) Drift 3.5%: Concrete spalling-off in the plastic hinging region

Fig. 4.91: (continued)

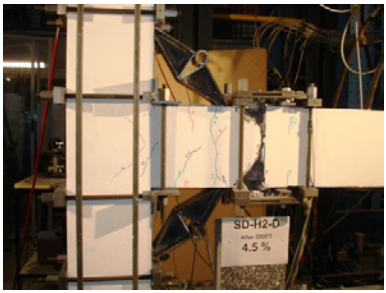

k) Drift 4.5%: Concrete spalling-off in the plastic hinging region

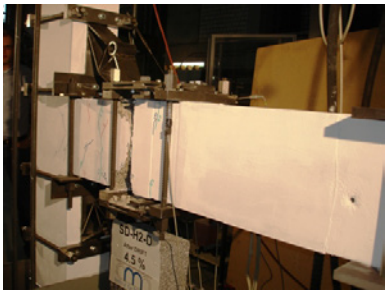

l) Drift 4.5%: Concrete spalling-off in the plastic hinging region

Fig. 4.91: Crack patterns and damage mode sequence of specimen SD-H2-D at different levels of drifts

4.5.2.2.3 Joint behaviour

The diagram of normalized conventional joint principal tensile stress versus story drift in Fig. 4.92 shows that the first positive and negative diagonal shear cracks were occurred by principal tensile stresses of $f_{tj} = 0.293\sqrt{f_c'}$ and $f_{tj} = 0.342\sqrt{f_c'}$, respectively. Furthermore, in ±2.5% drift the maximum principal tensile stresses of $f_{tj} = 0.32\sqrt{f_c'}$ and $f_{tj} = 0.348\sqrt{f_c'}$ were obtained in the positive and negative directions, respectively.

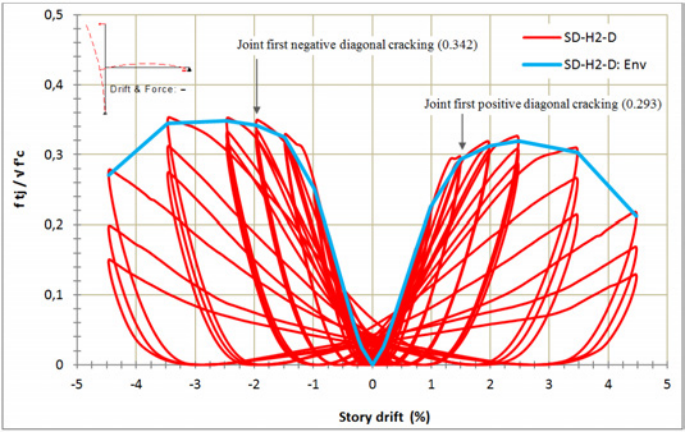

Fig. 4.92: The relationship between joint principal tensile stress ($f_{tj}/\sqrt{f'_c}$) and story drift of specimen SD-H2-D

From the relation of the normalized conventional joint horizontal shear stress to story drift (Fig. 4.93), the joint first positive and negative diagonal shear cracking were resulted under the horizontal shear stresses of $f_{tj} = 0.511\sqrt{f_c'}$ and $f_{tj} = 0.564\sqrt{f_c'}$, respectively, while the maximum stresses in positive and negative directions were obtained at ±2.5% drift with amounts of $f_{tj} = 0.543\sqrt{f_c'}$ and $f_{tj} = 0.571\sqrt{f_c'}$, respectively.

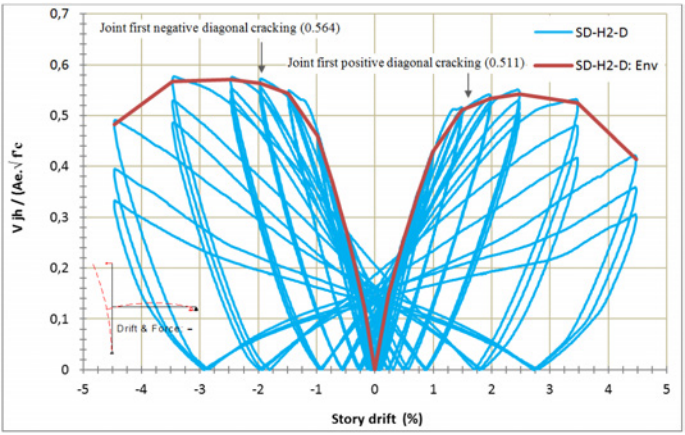

Fig. 4.93: The relationship between absolute value of (joint horizontal shear stress) $\left| V_{jh}/(A_e\sqrt{f'_c}) \right|$ *and story drift of specimen SD-H2-D*

The plot of joint shear deformation versus the normalized conventional tensile principal stress and story drift (Fig. 4.95), which was obtained by processing the monitoring data recorded by LVDTs installed at the joint (Fig. 4.94), shows that the joint shear deformations of first positive and negative diagonal shear cracking were 0.000835 and 0.0017 Radian, while the joint principal tensile stresses were $f_{tj} = 0.293\sqrt{f_c'}$ and $f_{tj} = 0.342\sqrt{f_c'}$, respectively. The maximum joint shear deformation was recorded at -3.5% drift with 0.0031 Radian while at the drift of +3.5%, the deformation was 0.0024 Radian.

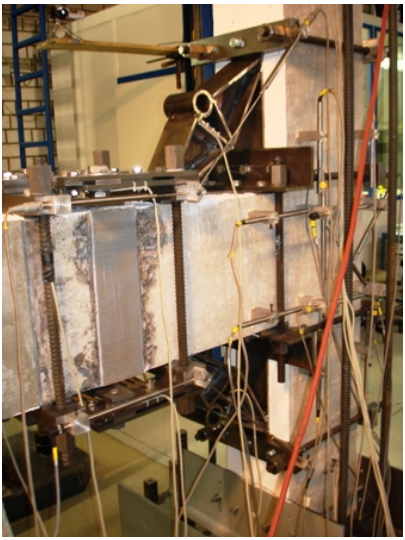

Fig. 4.94: LVDT layout for measurement of joint shear deformation and horizontal displacement component of SD-H2-D

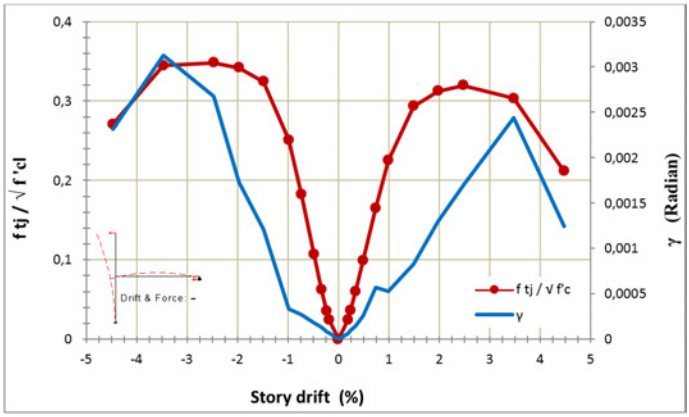

Fig. 4.95: The relationship among joint principal tensile stress ($f_{tj}/\sqrt{f'_c}$), story drift, and joint shear deformation (γ) of specimen SD-H2-D

4.5.2.2.4 Behaviour of Multifunctional Corbel (HMFC)

The plot of hysteresis loops of strain-story drift and strain envelop for top and bottom pipes of H2 (Fig. 4.96) shows that the energy dissipation devices in both of HMFCs reached to the

yield strain at ±0.75% drift which is less than the yielding point of the beam longitudinal reinforcement at the end of HMFCs in 1% drift. Furthermore, the joint demonstrated an elastic behavior until the ±0.75% drift level. Therefore, the design procedure conditions for retrofitting technique 2 (RT2) to have an effective extra energy dissipation through HMFC system with yielding of HMFCs before the yielding of beam longitudinal reinforcement as well as elastic remaining the joint until the HMFCs' yielding have been satisfied in the test.

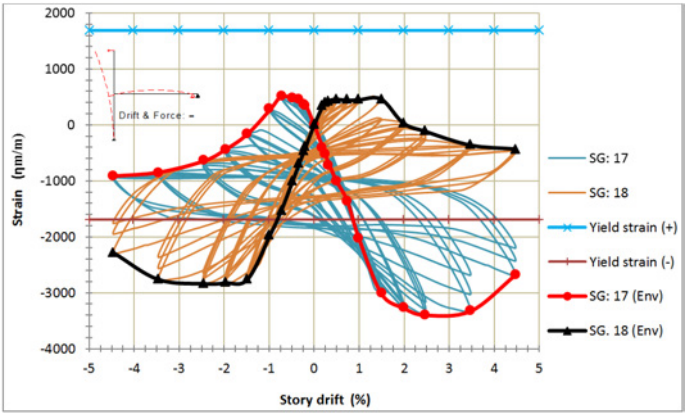

Fig. 4.96: The Hysteretic and envelope diagram for strain of top and bottom HMFCs versus story drift of specimen SD-H2-D

4.5.2.2.5 Behaviour of Harmonica Damper Plate (HHDP)

The hysteresis behavior of the top and bottom HHDPs as a strain-story drift diagram is depicted in Fig. 4.97. As displayed in Fig. 4.51, the recorded strains belong to the points at the middle of the arms where the strains are expected to be very low because of their neutral positions. As expected, the stains are low and the hysteresis loops have been recorded in all of drift levels until the end of the test. Obviously, the strains at the end of the arms could be many times greater than the neutral points at the middle so that their strains could reach to the strains over than the yield strain.

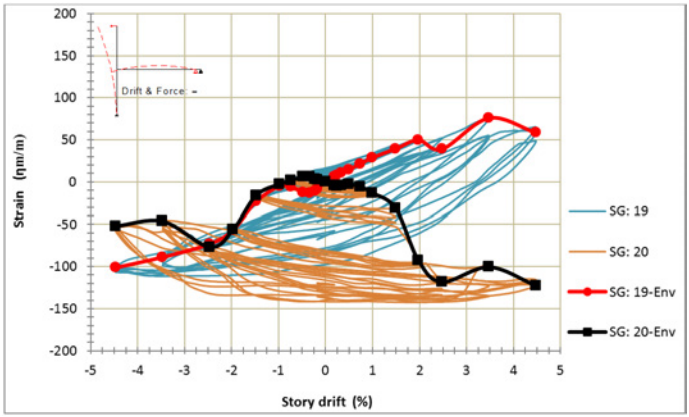

Fig. 4.97: The Hysteretic and envelope diagram for strain of top and bottom HHDPs versus story drift of specimen SD-H2-D

4.5.2.2.6 Decomposition of lateral displacement

The processing monitoring data recorded by LVDTs installed at the joint and sides of HHDPs (Fig. 4.94) leads to the diagrams of Fig. 4.98 that illustrates the contribution of the beam, column, and joint from the horizontal total displacement in every drift level as well as total displacements of all drift levels. Fig. 4.98-a shows that the contribution of the beam in every drift level has increased from 30% in ±0.2% drift level to 90% in ±4.5% drift level but by contrast the contribution of column has decreased from 65% in ±0.2% drift level to 6-8%% in ±4.5% drift level. Furthermore, the joint contribution has changed between 1% in drift level of 4.5% and 10% in drift level of 1%. On the other hand, Fig. 4.98-b displays that the contribution of column and joint in comparison with total imposed horizontal displacements during the test were very low while the contribution of the beam was high so that the maximum contributions of the beam, column, and joint were 19.70%, 1.65%, and 0.81% at the drift level of +4.5%.

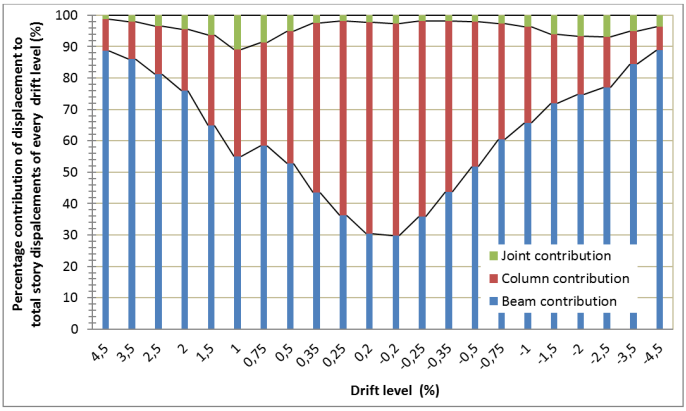

(a)

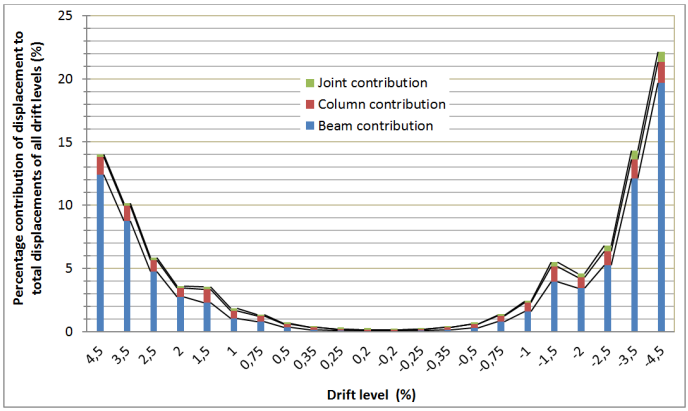

(b)

Fig. 4.98: Percentage contributions of beam, column and joint displacement in specimen SD-H2-D to a) total displacements in every drift level, b) total displacements of all drift levels

4.5.2.3 Test of BD-H3-D

4.5.2.3.1 Specimen description

The specimen BD was strengthened through retrofitting technique 2 by two pairs of HMFC (H3) and HHDP (D) which was modified as described before. According to the expected Strength and Failure Sequence Diagram (SFSD) (Fig. 4.35), the beam flexural plastic hinge and yielding of D would be simultaneously formed with first joint diagonal shear cracking.

Meanwhile, to have the extra energy dissipations through HMFCs set (H3), they would be designed so that their yield strengths reach before the beam flexural hinge occurring.

4.5.2.3.2 Strength sequences and damage mechanisms

The strength and ductility of retrofitted specimen BD-H3-D in comparison with the reference unit BD-B has been significantly increased so that through the test the pulling-out of the beam bottom bars, brittle shear failure mechanism of the joint, and overall structural stiffness degradation were eliminated and considerable structural strength and energy dissipation were obtained. The final failure mechanism, obtained hysteresis loops of story shear-drift and imposed column axial load are illustrated in Fig. 4.99, 4.100, and 4.101, respectively. Finally, the failure sequence inverted to form the beam-hinging mechanism at the end of HMFC and a narrow concrete spalling-off was observed in the plastic hinging region at higher drift level. Additionally, no crack was detected in the column and no reducing of column axial capacity was observed. Although it could not possible to use full capacity of the HHDPs, because of shear failure of the connector bolts (see Art. 4.5.2.3.5), the strength and ductility has been considerably increased. Furthermore, it was observed that until the drift level of 2.5%, the repetition of cycles in each drift level was not considerably reduce the load carrying capacity and stiffness under the same drift demand but after 3.5% drift level, little by little, the demonstration of reduction can be considered.

Fig. 4.99: Retrofitted specimen BD-H3-D after 4.5% drifts level

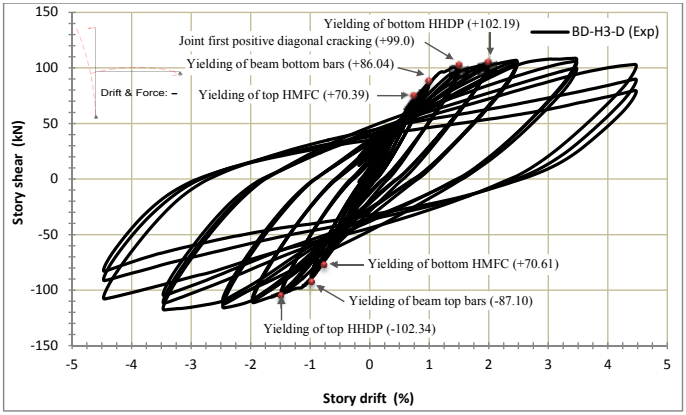

Fig. 4.100: Experimental story shear-drift hysteretic response of specimen BD-H3-D

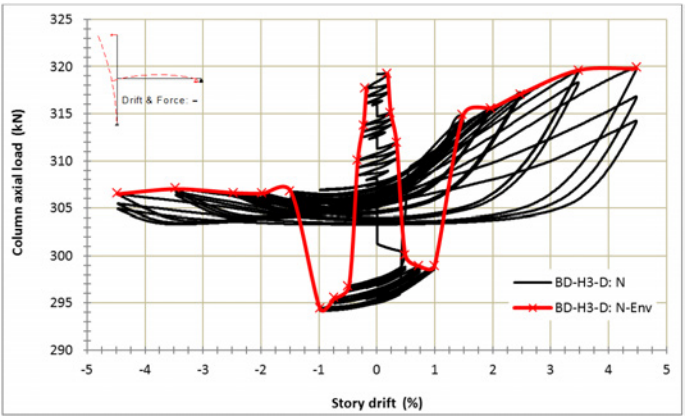

Fig. 4.101: Imposed column axial load versus drift of specimen BD-H3-D

Figs. 4.102 and 4.103 display the strain envelope of beam longitudinal bars at the beam column interface and end of HMFCs versus story drift, respectively. As can be seen, at the beam column interface the top and bottom bars of the beam could reach to the yield point after the 2.5% drift level while at the end of HMFCs the beam longitudinal bars yielded after the drift level of ± 1%. Consequently, the retrofitted technique could successfully satisfy the development requirements of the bottom bars which only had 150mm embedment length into the joint.

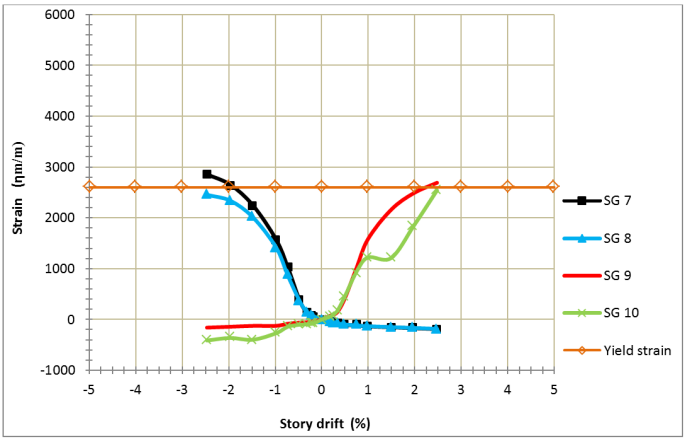

Fig. 4.102.: The envelope diagram for Max. strain of beam longitudinal bars at the beam-column interface versus story drift of specimen SD-H2-D

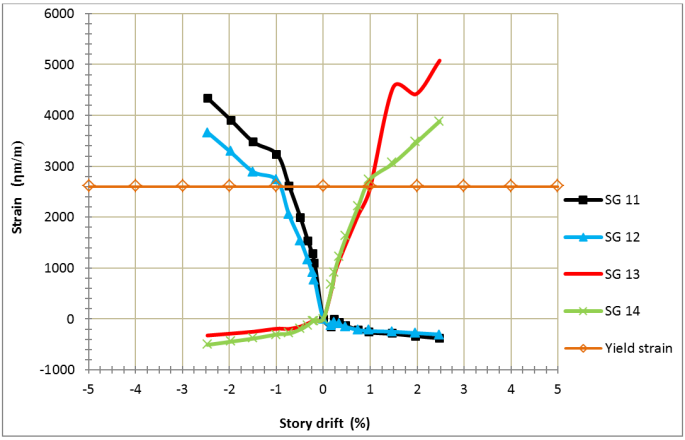

Fig. 4.103: The envelope diagram for Max. strain of beam longitudinal bars at the end of HMFC versus story drift of specimen BD-H3-D

The consecutive crack patterns and damage modes after end of every drift level are displayed in Fig. 4.104. The observed results during drift levels are shortly discussed as follows.

- *Drift 0.20%:* No crack was detected.
- *Drift 0.25%:* The first hairline flexural cracks were observed in the beam at the end of HMFC.
- *Drift 0.35%:* The first cracking at the bottom of the beam was occurred along the length of HMFC close to the end of it.
- *Drift 0.5%:* Another cracking at the top of the beam was occurred opposite to the cracking place of the last drift level.
- *Drift 0.75%:* The flexural cracks of drift level 0.5% were propagated and top of the beam out of the length of HHDP cracked. The energy dissipation devices of top and bottom HMFCs began to yield under story shears of +70.39kN and -70.61kN, respectively.
- *Drift 1.0%:* The cracks were propagated and widened. At the end of HMFCs, the beam bottom and top bars began to yield under story shears of +86.04kN and -87.10kN, respectively.
- *Drift 1.5%:* The first positive joint shear diagonal crack was observed as a hairline under imposed positive story shear of +99.0kN. The negative joint shear diagonal crack was not clearly detected.

- *Drift 2.*0%: The cracks were propagated and widened, but the deformation was concentrated at the end of HMFCs as a flexural hinge.
- *Drift 2.*5%: The plastic deformations at the end of HMFC were clearly observed.
- *Drift 3.*5%: While the story shear was nearly the same with the last drift level, the lateral strength reached to the maximum positive and negative capacity of 110kN and -120kN , respectively.
- *Drift 4.*5%: While the concrete spalling-off was observed in the plastic hinging region of the beam, decreasing of about 4.9% and 8.1% of maximum story shear capacity was monitored in comparison with the last drift level in positive and negative direction, respectively.

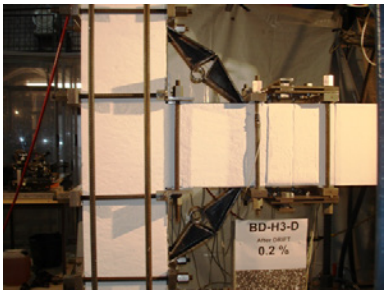

a) Drift 0.2%: No cracks

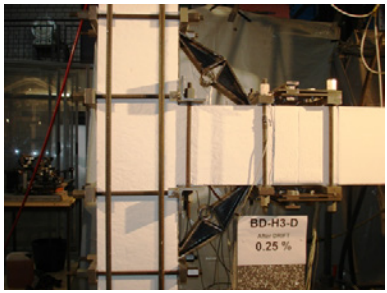

b) Drift 0.25%: The first flexural cracking at the end of HMFC

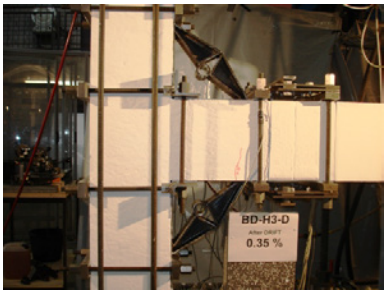

c) Drift 0.35%: First cracking in the beam along the length of HMFC at the bottom

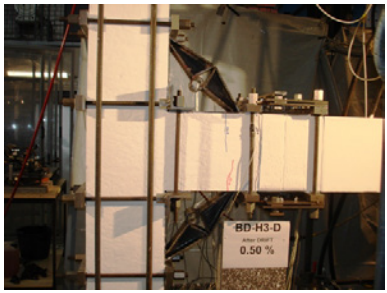

d) Drift 0.5%: Another cracking in the beam along the length of HMFC at the top

Fig. 4.104: (continued)

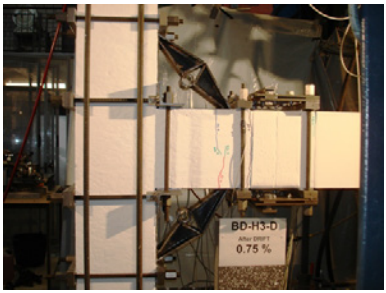

e) Drift 0.75%: Propagation of the flexural cracks

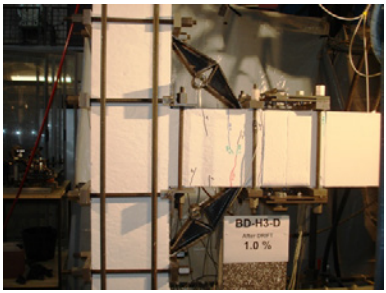

f) Drift 1%: Propagation and opening the cracks

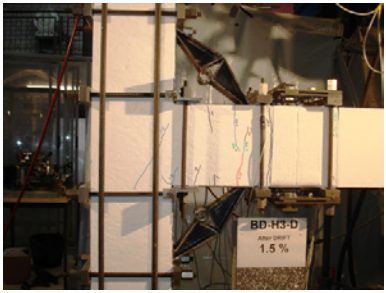

g) Drift 1.5%: First positive diagonal hairline shear crack of the joint

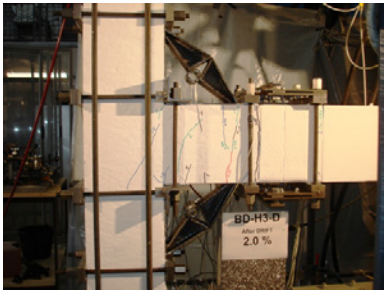

h) Drift 2%: Propagation and opening the cracks

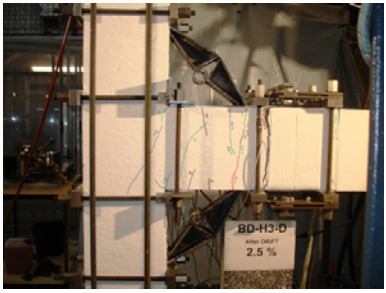

i) Drift 2.5%: Plastic deformation s at the end of HMFC

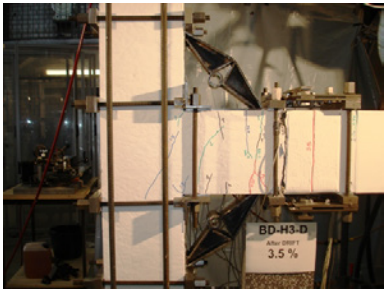

j) Drift 3.5%: Max. story shear was observed

Fig. 4.104: (continued)

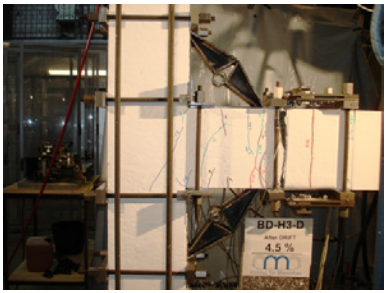

k) Drift 4.5%: Concrete spalling-off in the plastic hinging region

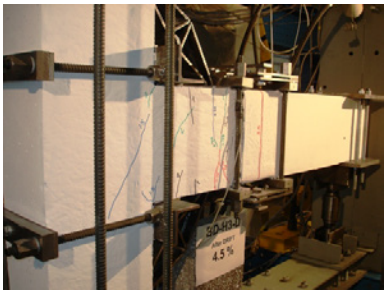

l) Drift 4.5%: Concrete spalling-off in the plastic hinging region

Fig. 4.104: Crack patterns and damage mode sequence of specimen BD-H3-D at different levels of drifts

4.5.2.3.3 Joint behaviour

The plot of normalized conventional joint principal tensile stress versus story drift in Fig. 4.105 illustrates that the principal tensile stress of $f_{tj} = 0.29\sqrt{f_c'}$ caused the first positive diagonal shear cracking. Moreover, in ±3.5% drift the maximum principal tensile stresses of $f_{tj} = 0.324\sqrt{f_c'}$ and $f_{tj} = 0.375\sqrt{f_c'}$ were resulted in the positive and negative directions, respectively.

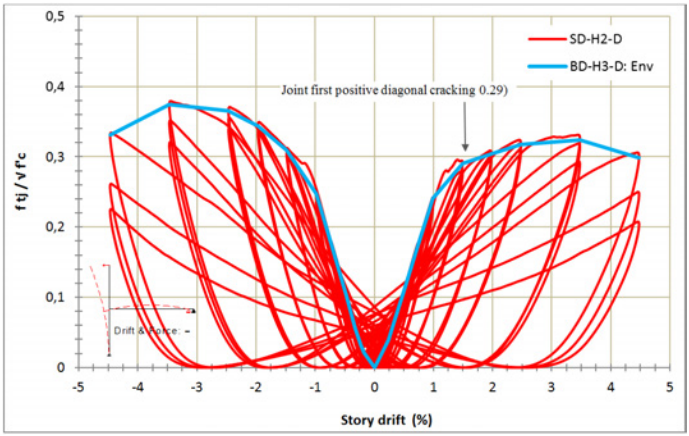

Fig. 4.105: The relationship between joint principal tensile stress ($f_{tj}/\sqrt{f'_c}$) and story drift of specimen BD-H3-D

The normalized conventional joint horizontal shear stress-story drift diagram (Fig. 4.106) shows that the joint first positive diagonal shear cracking was occurred under the horizontal shear stresses of $f_{tj} = 0.506\sqrt{f_c'}$, while the maximum stresses in positive and negative directions were obtained at ±3.5% drift with amounts of $f_{tj} = 0.547\sqrt{f_c'}$ and $f_{tj} = 0.597\sqrt{f_c'}$, respectively.

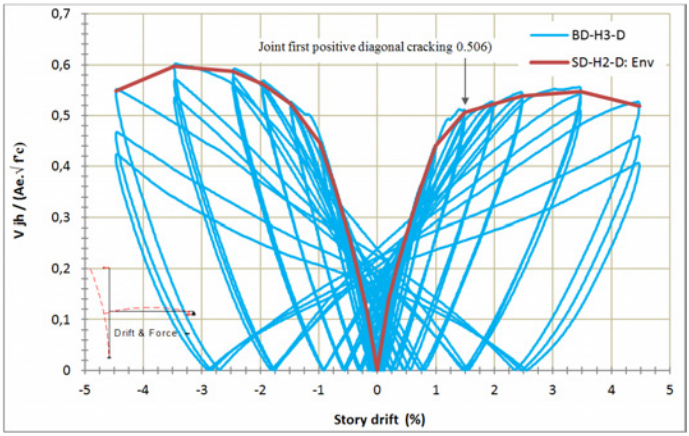

Fig. 4.106: The relationship between absolute value of (joint horizontal shear stress) $\left| V_{jh}/(A_e\sqrt{f'_c}) \right|$ *and story drift of specimen BD-H3-D*

The multiple axis graph of joint shear deformation-normalized conventional tensile principal stress-story drift (Fig. 4.107) illustrates that the joint shear deformations of first positive diagonal shear cracking was 0.00088 Radian, while the joint principal tensile stress was $f_{tj} = 0.290\sqrt{f_c'}$. The maximum joint shear deformations were recorded 0.0016 Radian and 0.0012 Radian at the +3.5% and -3.5% drift, respectively.

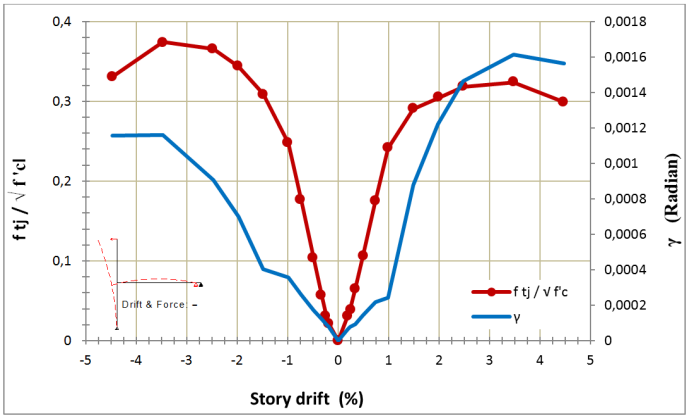

Fig. 4.107: The relationship among joint principal tensile stress ($f_{tj}/\sqrt{f'_c}$), story drift, and joint shear deformation (γ) of specimen BD-H3-D

4.5.2.3.4 Behaviour of Multifunctional Corbel (HMFC)

The monitoring of the strains versus imposed drift levels for top and bottom pipes of H3 (Fig. 4.108) results that the energy dissipation devices in both of HMFCs reached to the yield strain at ±0.75% drift while the yielding point of the beam longitudinal reinforcement at the end of HMFCs was obtained at ±1% drift which is properly greater than those of the HMFCs. As previously explained in design procedure conditions for retrofitting technique 2 (RT 2), this provision provides an effective extra energy dissipation through HMFC system. Meanwhile, the joint demonstrated an elastic behavior until the ±0.75% drift level. Therefore, the design procedure conditions have been satisfied in the test.

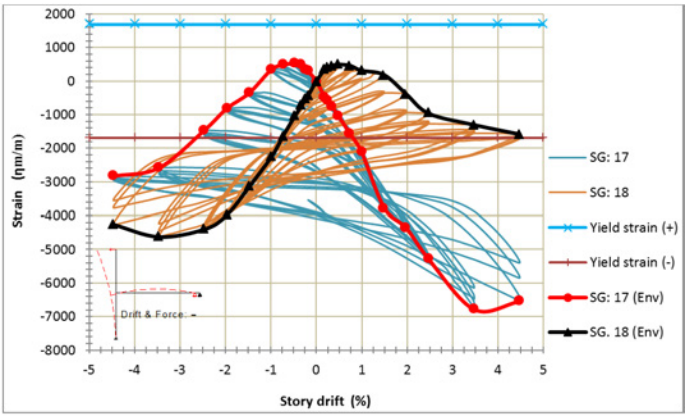

Fig. 4.108: The Hysteretic and envelope diagram for strain of top and bottom HMFCs versus story drift of specimen BD-H3-D

4.5.2.3.5 Behaviour of Harmonica Damper Plate (HHDP)

For top and bottom HHDPs, the hysteresis loops as a strain-story drift graph is displayed in Fig. 4.109. As expected, because of the positions of the strain gauges (Fig. 1), after a few drift levels the deformations and subsequently the strains have been dramatically raised and therefore the strain gauges were damaged. As can be seen, the top and bottom HHDPs passed into the plastic stage after the drift level of -1.5% and +2%, respectively.

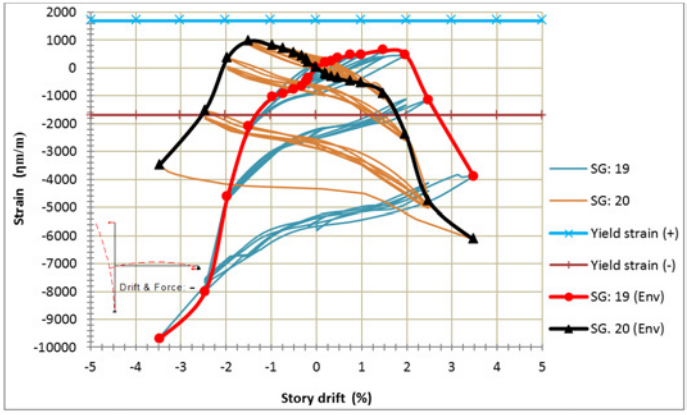

Fig. 4.109: The Hysteretic and envelope diagram for strain of top and bottom HHDPs versus story drift of specimen BD-H3-D

It is worth mentioning that the bolts used to connect the pods of HHDPs to the HMFCs had been damaged during the test because of shear failure (Fig. 4.110) and consequently the HHDPs could not get full capacity.

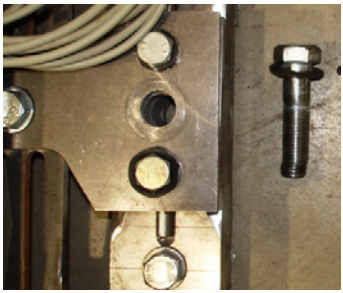

Fig. 4.110: Shear failure of bolts

4.5.2.3.6 Decomposition of lateral displacement

Fig. 4.111 illustrates the contribution of the beam, column, and joint from the horizontal total displacement in every drift level as well as total displacements of all drift levels. Fig. 4.111-a shows that the contribution of the beam in every drift level has increased from 62% in ±0.2% drift level to more than 80% in ±4.5% drift level but by contrast the contribution of column has decreased from 33% in ±0.2% drift level to more than 11% in ±4.5% drift level. Meanwhile, the joint contribution has changed between 3% and 9%. On the other hand, Fig. 4.111-b depicts that the contribution of column and joint in comparison with total imposed horizontal displacements during the test were very low while the contribution of the beam was high so that the maximum contributions of the beam, column, and joint were 12.11%, 2.18%, and 0.88% at the drift level of -4.5%.

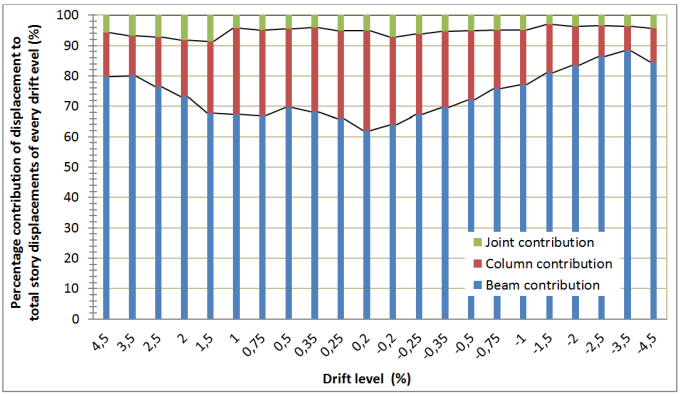

(a)

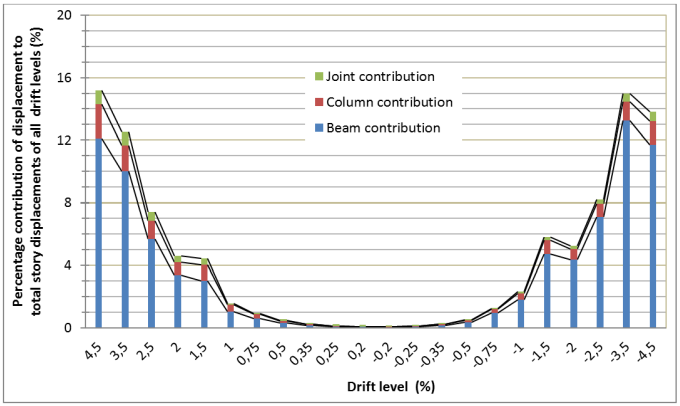

(b)

Fig. 4.111: Percentage contributions of beam, column and joint displacement in specimen BD-H3-D to a) total displacements in every drift level, b)total displacements of all drift levels

4.6 Test results and summary of findings

The findings and results of the experimental study are summarised as follows.

4.6.1 Strength

4.6.1.1 Strengths in the category of BD

The hysteresis loops of the as-built specimen BD-B with the retrofitted ones through retrofitting techniques of RT1 (BD-H1) and RT2 (BD-H3-D) are compared in Fig. 4.112 and Fig. 4.113, respectively. Moreover, to clarifying the comparable performance of the strength

development during the drift levels, envelop lateral strength-drift plot in the category of BD specimens is illustrated in Fig. 4.14. The relative rate of maximum lateral strength in negative and positive directions of every specimen in the category of BD is also displayed in Fig. 4.15. As can be understood:

- The hysteresis behaviours of the as-built specimen (BD-B) in positive and negative direction are not the same because of different embedment conditions of the beam longitudinal bars in the top and bottom. The lateral load-drift hysteresis loops in the negative direction of this specimen can achieve to the higher capacities than the positive direction since the upper longitudinal bars of the beam are ended to the standard hooks and in contrast, the bottom bars have only 150mm embedment length into the joint. On the other hand, the hysteresis behaviours of the retrofitted specimens (BD-H1 and BD-H3-D) are nearly the same in the positive and negative direction. Therefore, the unsymmetrical form of the loops in reference unit is modified to the symmetrical ones of the retrofitted specimens and consequently the proposed retrofitting techniques (RT1 and RT2) can effectively satisfy the development length requirements of beam bottom bars.
- The reference specimen (BD-B) does not show the stable hysteresis behaviour during the test so that after drift levels of +1.5% and -2% the strength increasing rate sharply changes to decreasing phase and finally after +2% and -2.5% drift level the specimen does not practically demonstrate a considerable strength capacity. In contrast, the retrofitted units display practically a stable hysteretic performance so that after ±3.5% drift level the systems have the same response to the displacements. According to 3.2.2 of [ACI 374.1-05], a frame shall be demonstrated as able to retain its structural integrity and support the gravity loads through peak drift ratios of 3.5%. Consequently, the retrofitted techniques could properly satisfy the code requirements.
- Both of retrofitting technique (RT1 and RT2) in the category of BD result to fat hysteresis loops. Therefore, the dissipated energy through these innovative methods should be considerable. In a following section this concept will be discussed independently.

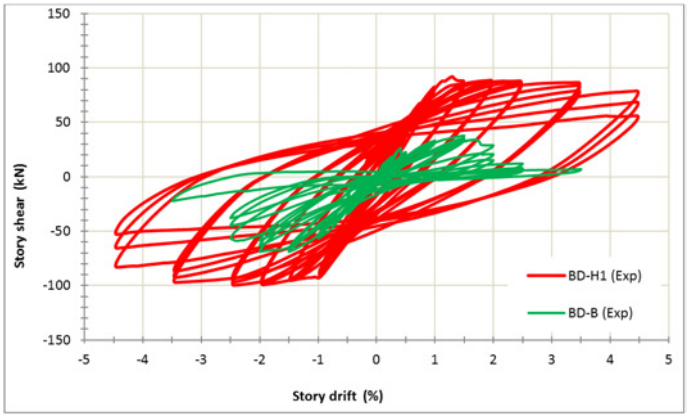

Fig. 4.112: Comparison the hysteresis loops of as-built specimen BD-B with retrofitted unit BD-H1

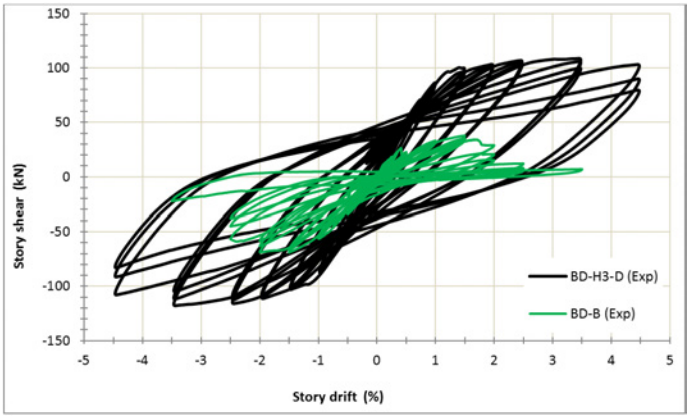

Fig. 4.113: Comparison the hysteresis loops of as-built specimen BD-B with retrofitted unit BD-H3-D

- The envelop lateral strength-drift diagram in Fig. 4.114 shows that the developed strength of the retrofitted specimens in comparison with the reference unit not only dramatically increases but also reasonably stabilizes, meanwhile, the stiffness of retrofitted specimens is also considerably increased. Meantime, between retrofitted units, the upgraded specimen through RT2 (BD-H3-D) illustrates a higher performance.

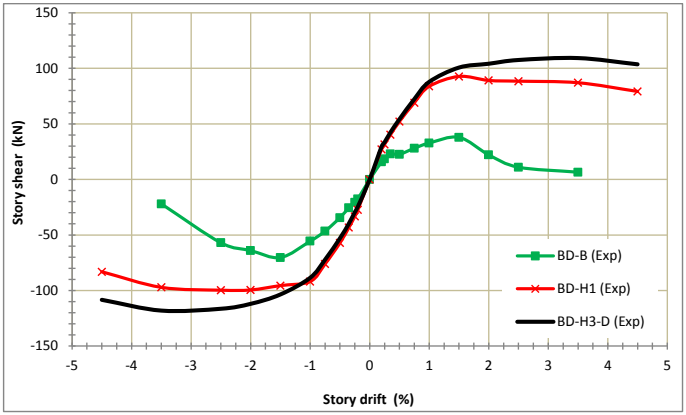

Fig. 4.114: Comparison the envelop strengths in the category of BD

- Individually evaluation of the relative maximum developed lateral strength in the category of BD for negative and positive direction (Fig. 4.115) represents that despite the inadequate development length for the beam bottom bars into the joint, the proposed innovative retrofitting techniques (RT1 and RT2) could reliably provide the required anchoring length for the discontinuous reinforcement to develop strains more than the yielding limit state. As can be seen, the increasing of maximum developed strength in the retrofitted specimen of BD-H1 in comparison with the reference unit of BD-B is 42% and 245% in the negative and positive directions, respectively, while these rates are changed to 68% and 289% in the retrofitted specimen of BD-H3-D, respectively. Furthermore, the increasing rate of maximum strength for BD-H3-D is about 20% more than BD-H1 which is the same with assumed increasing rate during the design process (section 4.2.4.3.1).

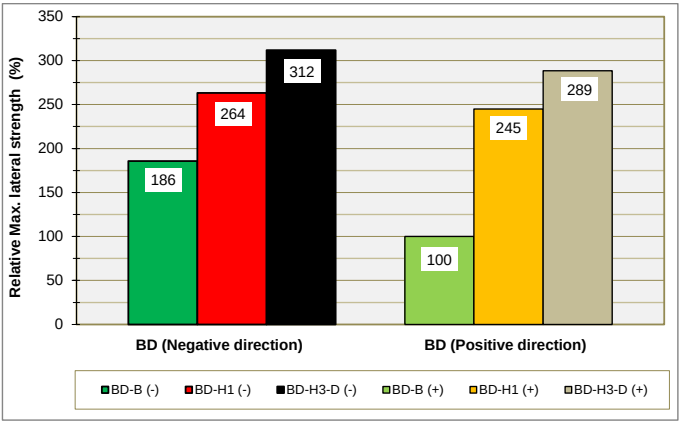

Fig. 4.115: Comparison the relative story shear strength in the negative and positive directions of the category of BD

4.6.1.2 Strengths in the category of SD

The comparable behaviour of reference unit (SD-B) in the category of SD along with retrofitted one through RT2 (SD-H2-D) is depicted in Fig. 4.116. Furthermore, envelop story shear strength-drift diagram and relative change of the maximum lateral strength in negative and positive directions of tested specimens in the category of SD are displayed in Fig. 4.117 and 4.118, respectively. The results can be represented as:

- The unstable hysteresis behaviour of the as-built unit (SD-B) is replaced by a stable performance (SD-H3-D) with maximum strength of more than 50% development, (Fig. 4.116 to Fig. 4.118).
- The strength of benchmark specimen (SD-B) drops sharply with the degradation rate of 35% after ±2.5% drift level, while the retrofitted one (SD-H2-D) shows nearly the same capacity until ±3.5% drift level and strength degradation is observed after that with the rate of 15% and 21% in negative and positive directions, respectively. Consequently, according to 3.2.2 of [ACI 374.1-05], the retrofitted technique could properly satisfy the code requirements.
- The utilized retrofitting technique (RT2) in the category of SD leads to the fat hysteresis loop. Therefore, the dissipated energy through this method would be considerable which will be discussed independently in the following.

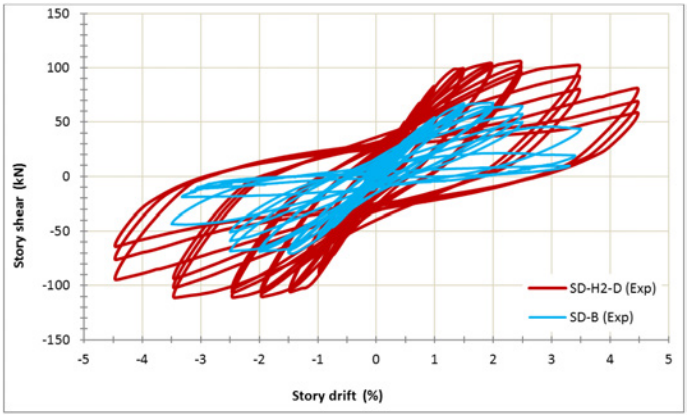

Fig. 4.116: Comparison the hysteresis loops of as-built specimen SD-B with retrofitted unit SD-H2-D

- The significantly enhancement of strength and stiffness in SD-H2-D specimen can be compared from Fig. 4.117.

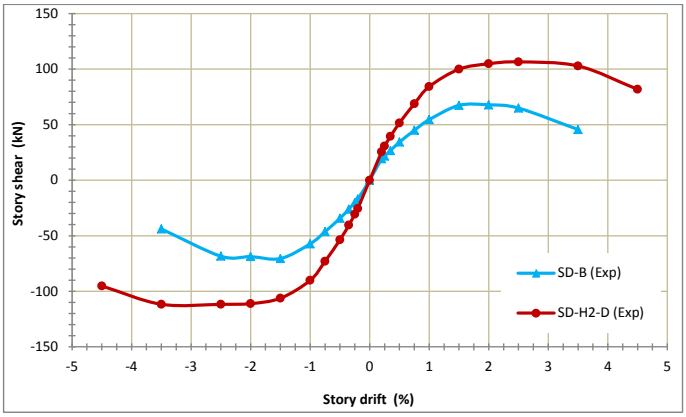

Fig. 4.117: Comparison the envelop strengths in the category of SD

- According to Fig. 4.118, the increasing of maximum developed strength in the retrofitted specimen of SD-H2-D in comparison with the reference unit of SD-B is 59% and 57% in the negative and positive directions, respectively.

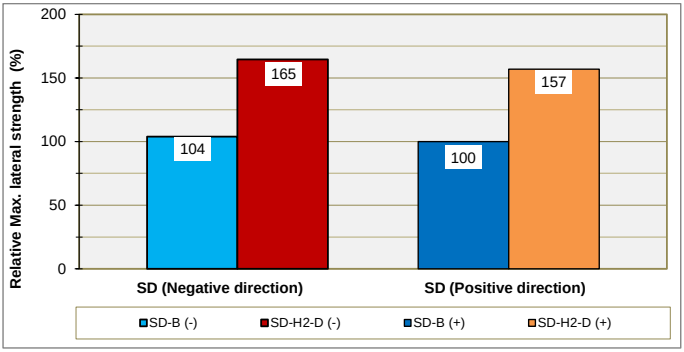

Fig. 4.118: Comparison the relative story shear strength in the negative and positive directions of the category of SD

4.6.1.3 Strengths in all specimens

The envelop story shear strength-drift plot of all specimens (Fig. 4.119) as well as the diagram of retained column axial load at the end of the test (Fig. 4.120) can clearly compare the developed lateral strength in drift levels during the test and column axial capacity at the end. As can be seen, the vulnerable reference units that lost their lateral and vertical carrying capacity after a few initial drift levels are replaced by upgraded ones through retrofitting techniques 1 and 2 (RT1 and RT2) which retain the required strength during the test particularly after the peak drift level of 3.5% which is proposed by ACI Committee 374 in 3.2.2 [ACI 374.1-05].

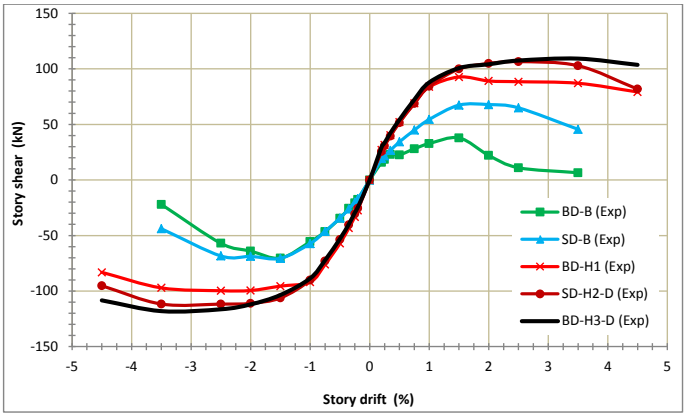

Fig. 4.119: Comparison the envelop strengths of all specimens

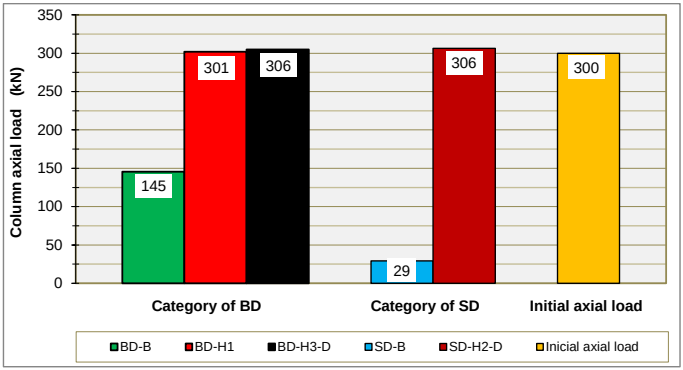

Fig. 4.120: The retained column axial load at the end of last cycle of final drift level (3.5% for reference units and 4.5% for retrofitted specimens)

At high drift levels, strength degradation is inevitable. Therefore, considering the drift level of 3.5% as a conservative limit (3.2.2 and R7.4 [ACI 374.1-05]), the variation of maximum strength degradation with respect to last cycle of 3.5% drift level in the every tested specimen along with the maximum acceptance criteria as 25% (R9.1.3 [ACI 374.1-05]) is illustrated in Fig. 4.121. As can be seen, the reference units can not satisfy the code requirements with demonstration of strength degradation more than 80%. In contrast, the all retrofitted units display the acceptable degradation rate of lateral strength less than 25% so that the maximum degradation rates of 14, 11 and 24% are resulted for specimens of BD-H1, BD-H3-D and SD-H2-D, respectively.

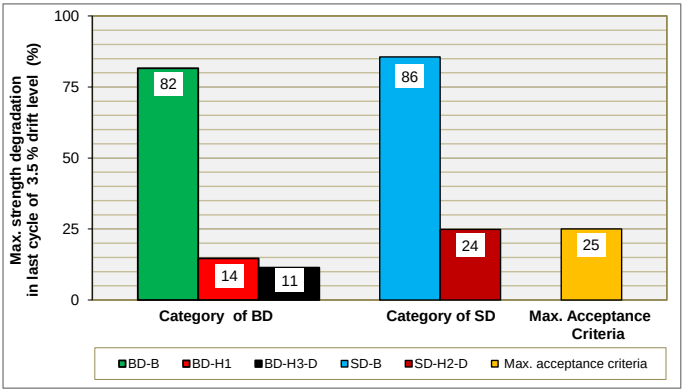

Fig. 4.121: Comparison the maximum strength degradation of all specimens with respect to last cycle of 3.5% drift level

According to R9.1.1 of [ACI 374.1-05], the adequate initial stiffness must be considered to be able to develop nominal strength before the drift ratio exceeds an initial drift ratio consistent with the allowable story drift limitations. Therefore, the higher amounts of initial stiffness will be important to provide the higher nominal strength capacity. For that reason, the variation of initial stiffness for every test specimen is relatively depicted in Fig. 4.122 to compare the result of the tests. As can be seen, in the category of BD with respect to the reference unit, it is observed the development of 56% and 68% for BD-H1 and BD-H3-D, respectively, while in the category of SD, SD-H2-D develops the initial stiffness of SD-B to more than 33%. Furthermore, specimen BD-H3-D displays the initial stiffness 8% more than BD-H1 and 16% over SD-H2-D.

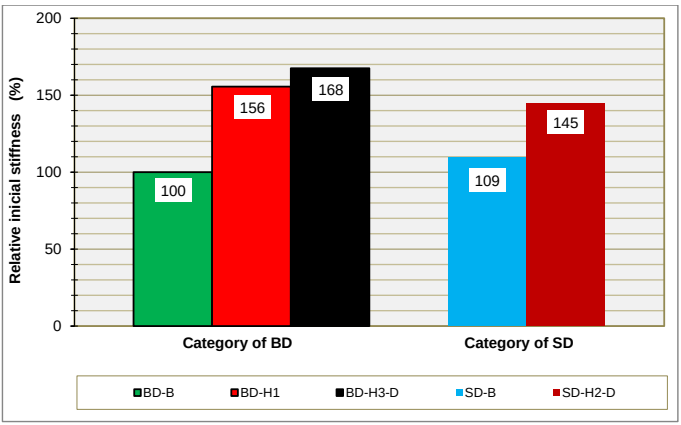

Fig. 4.122: Relatively comparison of initial stiffness in all specimens

4.6.2 Energy dissipation

4.6.2.1 Energy dissipations in the category of BD

Fig. 4.123 displays that the retrofitted specimens of BD-H1 and BD-H3-D that fails by beam flexural hinging mode have 3.91 and 4.17 times more hysteretic energy dissipation rate than the reference unit of BD-B, respectively.

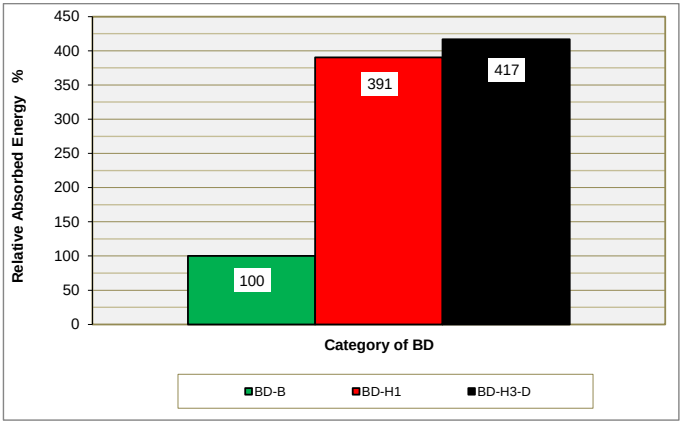

Fig. 4.123: Comparison the energy dissipations in the category of BD

4.6.2.2 Energy dissipations in the category of SD

Fig. 4.124 shows that, in the category of SD, the retrofitted specimen of SD-H2-D, which fails through flexural beam hinging, dissipates energy 2.45 times more than the reference unit of SD-B which fails by joint shear mechanism.

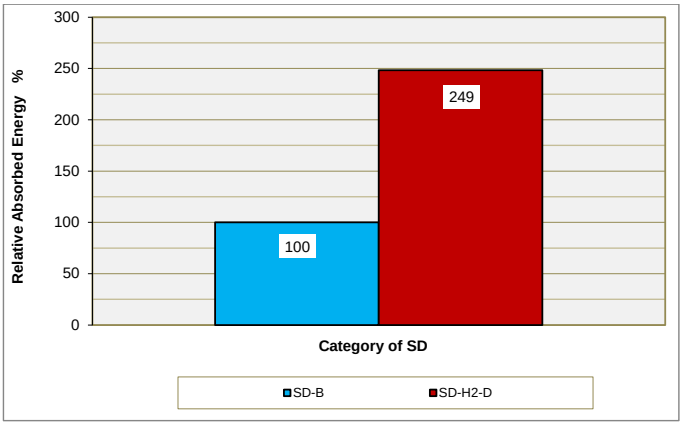

Fig. 4.124: Comparison the energy dissipations in the category of SD

4.6.2.3 Energy dissipation in all specimens

In the all retrofitted specimens, energy dissipation in every cycle is uniformly increased which is not observed in the reference gravity load designed units. The dissipated energy in the all test specimens can be compared with each other by Fig. 4.125. As can be seen, the absorbed energy by SD-B is 58% more than BD-B and the upgraded specimen of BD-H3-D in the category of BD has the highest energy dissipation rate.

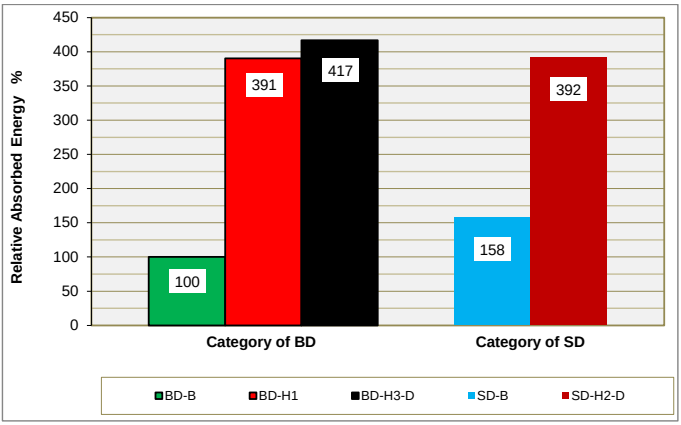

Fig. 4.125: Comparison the energy dissipations in all specimens

The relative dissipated energy of specimens and estimating the contribution of subassemblages are represented in Fig. 4.126. In this diagram, the contribution of Multi Functional Corbels (HMFC) and Harmonica Damper Plates (HHDP) were estimated by simulation of their behavior based on the monitored displacements. Evidently, in every specimen, the major part of absorbed energy was dissipated by the main body of the unit so that in BD-H1, BD-H3-D and SD-H2-D it was about 87.5, 69.0 and 67.0% of the total dissipated energy in every specimen, respectively. The contributions of HMFCs were nearly 12.5, 19.0 and 14.0% and contributions of HHDPs were approximately 0.0, 12.0 and 19.0% for BD-H1, BD-H3-D and SD-H2-D, respectively. Although the total contribution of installed energy dissipation devices for BD-H1, BD-H3-D, and SD-H2-D are 12.5, 31.0, and 33%, respectively, these rates are more than 47, 125, and 81% of the total energy which was dissipated by their reference units in their categories, BD or SD. It is worth mentioning that the role of HMFC in transmitting the flexural plastic hinge far enough away from the joint and providing the conditions that the main body achieves the capability to dissipate major

parts of energy by this way is very important. Consequently, for evaluation of energy dissipation by the proposed retrofitting techniques it should be considered the whole of the designed set, for instance the function of HHDP in preserving the strength degradation in SD-H2-D (Fig. 4.121) is very important.

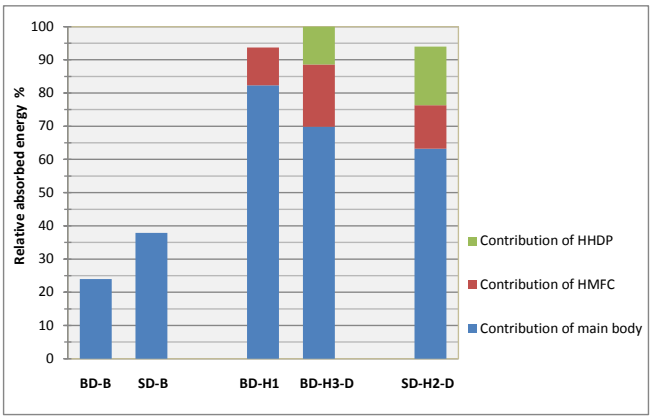

Fig. 4.126: Comparison the energy dissipations in specimens and estimated contribution of subassemblages

To comparison the energy dissipation capability of the retrofitted specimens with each other, the relative energy dissipation ratio based on the concept of R2.4 of [ACI 374.1-05] can be helpful. The concept of relative energy dissipation ratio is illustrated for the third cycle to the drift ratio of 3.5%. According to R9.1.3 of [ACI 374.1-05], the relative energy dissipation ratio should be more than 1/8 otherwise there may be inadequate damping for the frame as a whole and consequently, there may be continuous oscillations for a considerable time after an earthquake, producing low-cycle fatigue effects, and displacements may become excessive. Evidently, Fig. 4.127 illustrates the amounts of relative energy dissipation ratios of retrofitted specimens and compares them with the minimum acceptance criteria proposed by R9.1.3 of [ACI 374.1-05]. As can be seen, the specimens BD-H1 and SD-H2-D with 42.42% and 37.05% of relative energy dissipation ratio have the highest and lowest rates, respectively which are considerably more than the minimum code-conforming rate of 12.5%. Moreover, according to R3.2.1 of [ACI 374.1-05], for reinforced concrete connections, typical relative energy dissipation ratio at 3% drift level have been reported to be 30%. Therefore, the retrofitting techniques led to these specimens can acceptably provide higher amounts of energy abortion.

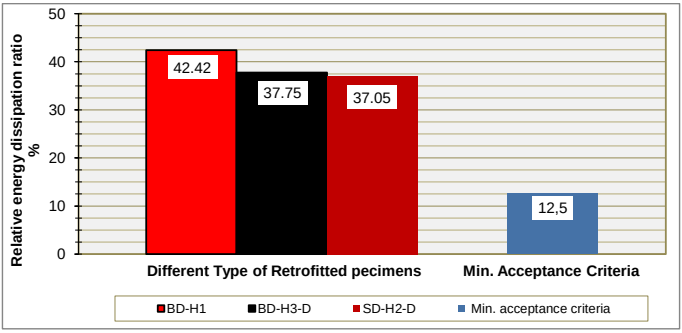

Fig. 4.127: Comparison the energy dissipation ratio of retrofitted specimens in last cycle of 3.5% drift level

4.6.3 Damage mechanisms

The observed failure mode and damage mechanism for every test specimen is shortly illustrated in Table 4.7. Evidently, the undesirable brittle failures of the reference specimens of BD-B and SD-B through the joint shear failure that leads subsequently to the failing of column axial carrying capacity load are replaced by desirable ductile failure mechanism of beam flexural hinge far enough away of the joint in retrofitted specimens. It is worth to mentioning that in the case of BD-B the joint shear failure is preceded by pulling-out of the beam bottom bars too. Moreover, in the retrofitted specimen of SD-H2-D, the plastic shear deformation is also observed at the end of HMFC after drift level of 2.5% because of lack of sufficiently reinforcing for shear deformation and therefore this event leads to the demonstration of shear failure too.

Table 4.7: Failure modes of test specimens

Failure Modes	Test specimens				
	BD-B	SD-B	BD-H1	SD-H2-D	BD-H3-D
Joint shear failure	√	√	-	-	-
Pulling-out of the beam bars	√	-	-	-	-
Failing of axial load carrying capacity of column	√	√	-	-	-
Beam flexural hinge	-	-	√	√	√
Beam shear failure	-	-	-	√	-

4.6.4 Hierarchy of strength

The hierarchy of strength for reference units and retrofitted specimens are tabulated in Table 4.8 and Table 4.9, respectively. Evidently, the desirable adjusted sequence of strength in the retrofitted specimens provides an enhanced seismic resistance performance.

Table 4.8: Hierarchy of strength for reference units

Reference Specimen	BD-B		SD-B	
Displacement Direction	-	+	-	+
Events	Drift level			
Joint first diagonal cracking	-0.75%	-	-0.75%	+0.75%
Yielding the beam bars	-0.75%	-	-0.75%	+0.75%
Max. lateral strength	-1.5%	+1.5%	-1.5%	+2.0%
Beginning of strength degradation	-2.0%	+1.5%	-2.5%	+2.5%

Table 4.9: Hierarchy of strength for retrofitted specimens

Retrofitted Specimen	BD-H1		SD-H2-D		BD-H3-D	
Imposed Displacement Direction	+	-	+	-	+	-
Events	Drift level					
Yielding the HMFC	-0.75%	+0.75%	-0.75%	+0.75%	-0.75%	+0.75%
Yielding the beam bars	-1.0%	+1.0%	-1.0%	+1.0%	-1.0%	+1.0%
Joint first diagonal cracking	-	+1.5%	-	+1.5%	-	+1.5%
Yielding the HHDP	-	-	*	*	-1.5%	+2.0%
Max. lateral strength	-2.5%	+1.5%	-3.5%	+2.5%	-3.5%	+3.5%
Beginning the strength degradation	-3.5%	+3.5%	-3.5%	+3.5%	-	-

** No test result*

4.6.5 Joint behaviour

The joint performance of the tested specimens is briefly tabulated by the normalized conventional joint principal tensile stress ($f_{tj}/\sqrt{f'_c}$) corresponding to the first positive and negative diagonal shear cracking along with their related joint shear deformations (γ) and obtained maximum joint horizontal shear stress in Table 4.10. As can be seen, the corresponding principal tensile stress for the first diagonal shear cracking is averagely equal to $0.310\sqrt{f'_c}$. It is worth mentioning that in the Table 4.10, the maximum joint horizontal shear stress of reference units (BD-B and SD-B) are related to the final joint strength while the presented amounts for the retrofitted specimens correspond to the obtained stresses which are not the final strengths.

Table 4.10: Joint stresses and strains of test specimens

	Joint principal tensile stress at first diagonal shear cracking		Joint shear deformation at first diagonal shear cracking		Max. obtained joint horizontal shear stress	
	$f_{tj}/\sqrt{f'_c}$ *		γ (Radian)		$v_{jh}/\sqrt{f'_c}$ *	
	+	-	+	-	+	-
BD-B	-	0.305	-	0.001	-	0.777
SD-B	0.293	0.307	0.00064	0.00078	0.758	0.789
BD-H1	0.338	-	0.00065	-	0.557	0.6
SD-H2-D	0.293	0.342	0.000835	0.0017	0.543	0.571
BD-H3-D	0.29	-	0.00088	-	0.547	0.597

* *The strength of concrete at 24 months (MPa)*

A comparative diagram is also depicted in Fig. 4.128 for the recorded maximum joint horizontal shear stress and code-conforming nominal shear strength. Evidently, since the recorded amounts for the reference specimens represent the practical joint strengths therefore it can be found that the code-confirmed nominal strengths are not acceptable for the tested as-built specimens.

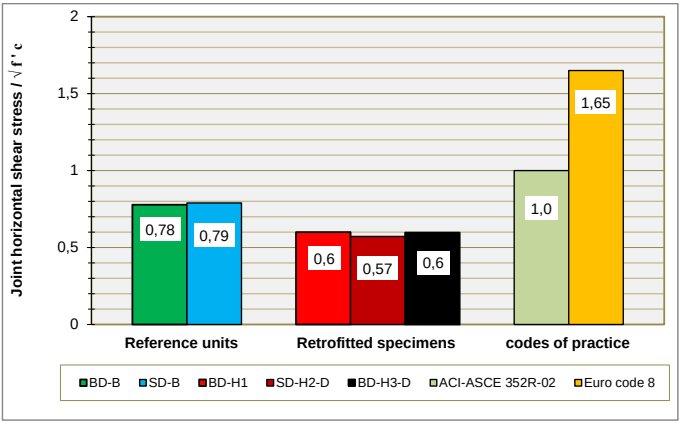

Fig. 4.128: Max. Observed joint horizontal shear stress in test specimens versus code- conforming nominal shear strength of the tested external joint

4.6.6 Decomposition of lateral displacement

The study of component contribution to total lateral displacement of specimen exhibits a clear indication of specimen performance and helps in distinction the possible failure mode. The total lateral displacement components of beam, column and joint in every test specimen are represented in Fig. 4.129. As can be seen, the proportion of 21% (BD-B) and 26% (SD-B) of joint contribution in reference units is replaced by 3% (BD-H1), 4% (SD-H2-D) and 5% (BD-H3-D) in retrofitted specimens. Furthermore, the column contribution is decreased from 24% (BD-B) and 25% (SD-B) in as-built units to 7% (BD-H1), 15% (SD-H2-D) and 14% (BD-H3-D) in upgraded ones. In contrast, the rate of beam contribution is considerably increased from 55% (BD-B) and 51% (SD-B) to 90, 81and 81% in BD-H1, SD-H2-D and BD-H3-D, respectively. Since HHDPs were used in plastic hinge regions, the contribution of beams in SD-H2-D and BD-H3-D in comparison with BD-H1 were decreased. Consequently, the innovative retrofitting techniques (RT1 and RT2) can effectively transmit the deformations from high-risk elements and points (column and joint) to the safety ones and replace the brittle behaviour with desired ductile performance.

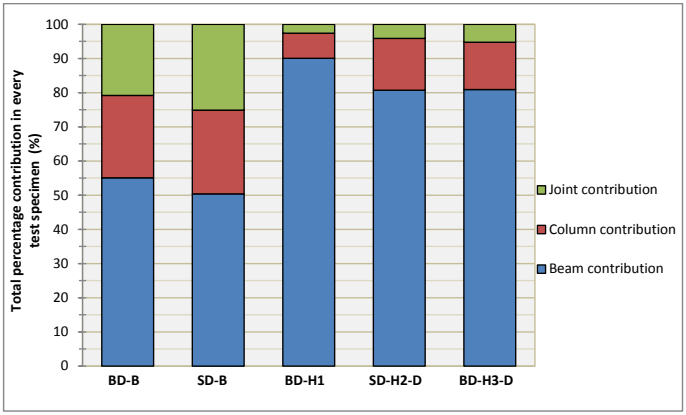

Fig. 4.129: Total percentage contributions of beam, column and joint displacement in every test specimen

Chapter 5

Numerical Analysis and Simulations

5.1 Introduction

This chapter illustrates the numerical study of the beam-column joint specimens including the vulnerable reference units and retrofitted ones. Structural response of specimens was simulated by a nonlinear finite element analysis. In the present study, the nonlinear finite element software ATENA which has been developed for modelling the behaviour of structures with the emphasis on reinforced concrete has been used. The development of fully validated model as an investigation tool that could be used in combination with the experimental study has been targeted. Primarily, before the experimental study, an initial model, which had been calibrated by existing experimental results in the literature, has been developed to simulate the vulnerable units and then validate the proposed innovative retrofitting techniques (RT1 and RT2). The different variety of retrofitting systems has been designed and analysed to establish proposed effective retrofitting models. Then, the final models have been experimentally tested and subsequently the results were used to modifying and calibrating the initial models. Consequently, the validated models were utilized to develop a new simplified innovative retrofitting technique (Retrofitting Technique 3, RT3) with high efficiency that was adopted from both of two proposed Retrofitting Techniques 1 and 2 (RT1 and RT2). Obviously, the calibrated models can be used for further studies on

performance of existing beam-column joints and retrofitted ones; moreover they can contribute on finding the new approaches and methods of upgrading the beam-column joints.

5.2 Implemented constitutive models in ATENA

The assumptions in ATENA for nonlinear analysis of reinforced concrete structures and components including the material models and their behaviour are presented in brief, [ATENA-Theory-06].

5.2.1 Constitutive modelling of concrete

The nonlinear behaviour of concrete is described in ATENA by a constitutive material model based on the concept of smeared cracks, damage and fracture mechanics. The fracture-plastic model combines the constitutive models of tensile (fracturing) and compressive (plastic) behavior. The material model is affected by the behaviour of concrete include the following.

- Non-linear behavior in compression including hardening and softening
- Fracture of concrete in tension based on the nonlinear fracture mechanics
- Biaxial strength failure criterion
- Reduction of compressive strength after cracking
- Tension stiffening effect
- Reduction of the shear stiffness after cracking (variable shear retention)
- Two crack models: fixed crack direction and rotated crack direction

5.2.1.1 The relation of Stress-strain for concrete

The nonlinear behavior of concrete in the biaxial stress state is described by the effective stress σ_c^{ef}, and the equivalent uniaxial strain ε^{eq}. The equivalent uniaxial strain is introduced in order to eliminate the Poisson's effect in the plane stress state.

$$\varepsilon^{eq} = \frac{\sigma_{ci}}{E_{ci}} \tag{5.1}$$

The complete equivalent uniaxial stress-strain diagram for concrete is illustrated in Fig. 5.1. The formula recommended by CEB-FIP Model Code 90 [CEB-FIP-90] has been adopted for the ascending branch of the concrete stress-strain law in compression.

$$\sigma_c^{ef} = f_c'^{ef} \frac{kx - x^2}{1 + (k-2)x} \tag{5.2}$$

where: $x = \varepsilon/\varepsilon_c$, $k = E_0/E_c$, $E_c = f_c'^{ef}/\varepsilon_c$

σ_c^{ef} is concrete compressive stress,

$f_c'^{ef}$ is concrete effective compressive strength,

x is normalized strain,

ε is strain,

ε_c is strain at the peak stress $f_c'^{ef}$,

k is shape parameter,

E_0 is initial elastic modulus, and

E_c is secant elastic modulus at the peak stress.

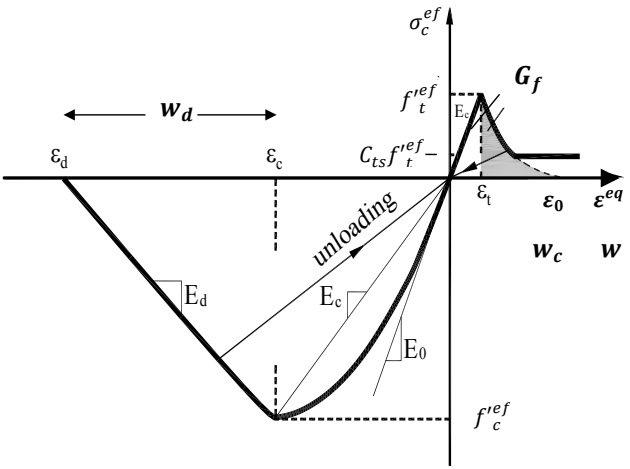

Fig. 5.1: Uniaxial constitutive stress-strain law and softening law for concrete

There are two models of strain softening in compression which are based on dissipated energy and local strain softening. The end point of the softening curve is defined by means of the plastic displacement w_d (Fig. 5.1), therefore, the needed energy for generation of a unit area of the failure plane is indirectly defined. A limit compressive strain ε_d at the zero stress is calculated froma plastic displacement w_d and a band size L'_daccording to the followingexpression:

$$\varepsilon_d = \varepsilon_c + \frac{w_d}{L'_d} \tag{5.3}$$

For normal concrete, the default value of w_d is 0.5 mm. The failure bands (L_t for tension and L_d for compression) are defined as projections of the finite element dimensions on the failure planes as shown in Figure (5.2).

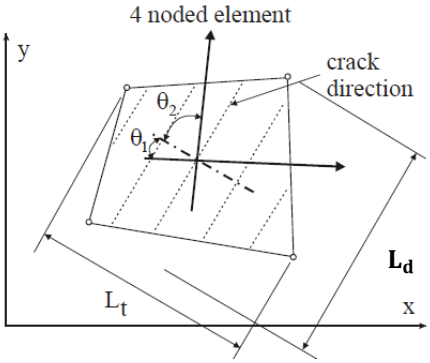

Fig. 5.2: Definition of localization bands

The failure band for skew meshes is obtained by the following formula.

$$L'_t = \gamma L_t \quad , \quad L'_d = \gamma L_d$$
$$\gamma = 1 + (\gamma^{max} - 1)\frac{\theta}{45} \quad , \quad \theta \in < 0\,;45\ > \tag{5.4}$$

An angle θ is the minimal angle [min (θ_1,θ_2)] between the direction of the normal to the failure plane and element sides. The above formula is a linear interpolation between the factor γ=1 for the direction parallel with element sides, and γ=γ^{max}, for the direction inclined at 45°. The recommended (and default) value of $\gamma^{max}$is 1.5.

The behavior of concrete in tension without cracks is assumed linear elastic, Fig. 5.1. E_c is the initial elastic modulus of concrete, f'^{ef}_t is the effective tensile strength derived from the biaxial failure function.

$$\sigma_c^{ef} = E_c \varepsilon^{eq} \quad , \quad 0 \le \sigma_c \le f'^{ef}_t \tag{5.5}$$

$$E_c = \frac{f'^{ef}_t}{\varepsilon_t} \tag{5.6}$$

A fictitious crack model based on a crack-opening law and fracture energy is used for the crack opening formulation. This formulation is suitable for modeling of crack propagation in concrete. The function of crack opening is:

$$\frac{\sigma}{f_t'^{ef}} = \left\{1 + \left(c_1 \frac{w}{w_c}\right)^3\right\} exp\left(-c_2 \frac{w}{w_c}\right) - \frac{w}{w_c}(1 + c_1^3) exp(-c_2) \tag{5.7}$$

$$w_c = 5.14 \frac{G_f}{f_t'^{ef}}$$

where w is the crack opening, w_c is the crack opening at the complete release of stress, σ is the normal stress in the crack (crack cohesion). The values of the constants are, c_1=3, c_2=6.93. G_f is the fracture energy needed to create a unit area of stress-free crack, $f_t'^{ef}$ is the effective tensile strength derived from a failure function. The crack opening displacement w is derived from strains according to the crack band theory in which the crack width w is calculated as a total crack opening displacement within the crack band.

$$w = \varepsilon_{cr} L'_t \tag{5.8}$$

where ε_{cr} is the crack opening strain, which is equal to the strain normal to the crack direction in the cracked state after the complete stress release.

In heavily reinforced concrete structures, or structures with large finite elements, when many reinforcement bars are crossing each finite element, the crack band approach will provide too conservative results, and the calculated crack widths may be overestimated. This is the consequence of the fact that the crack band approach assumes that the crack spacing is larger than a finite element size. In heavily reinforced structures, or if large finite elements are used, it may occur that the crack spacing will be smaller than finite element size. This is especially true if shell/plate elements are used. In this case, typically large finite elements can be used, and they usually contain significant reinforcement. In these cases, it is useful to provide the crack spacing manually, since otherwise the program will overestimate the cracking and due to that also larger deflections may be calculated. The program ATENA allows the user to manually define the crack spacing. This user defined spacing is used as crack band size L_t in cases when the user defined crack spacing is smaller than the L_t that would be calculated by the above mentioned formulas.

In heavily reinforced concrete structures the cracks cannot be fully developed and concrete contributes to the steel stiffness, Fig. 5.1. This effect is called tension stiffening and it can be simulated by specifying a tension stiffening factor. This factor represents the relative limiting value of tensile strength in the tension softening diagram. The tensile stress cannot drop below the value given by the product of $C_{ts}f'^{ef}_{t}$.The recommended default value for C_{ts} is 0.4.

5.2.1.2 Biaxial stress failure criterion for concrete

A biaxial stress failure criterion according to Kupfer et al. (1969) is used as displayed in Fig. 5.3.

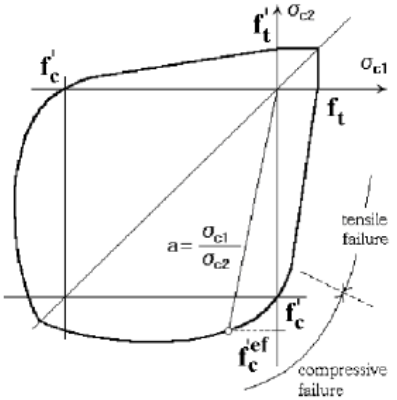

Fig. 5.3: Biaxial failure function for concrete

The failure function for the compressive failure in the compression-compression stress state is:

$$f_c'^{ef} = \frac{1+3.65a}{(1+a)^2} f'_c \ , \qquad a = \frac{\sigma_{c1}}{\sigma_{c2}} \tag{5.9}$$

Where σ_{c1}, σ_{c2} are the principal stresses in concrete and f'_c is the uniaxial cylinder strength. In the biaxial stress state, the strength of concrete is predicted under the assumption of a proportional stress path.

In the tension-compression state, the failure function continues linearly from the point $\sigma_{c1} = 0, \sigma_{c2} = f'_c$ into the tension-compression region with the linearly decreasing strength:

$$f_c'^{ef} = f'_c r_{ec}\ ,\ r_{ec} = \left(1 + 5.3278\frac{\sigma_{c1}}{f'_c}\right),\quad 1.0 \geq r_{ec} \geq 0.9 \tag{5.10}$$

where r_{ec} is the reduction factor of the compressive strength in the principal direction 2 due to tensile stress in the principal direction 1.

The failure function for the tensile failure in the tension-tension state is linear. The tensile strength is constant and equal to the uniaxial tensile strength f'_t.

$$f_t'^{ef} = f'_t \tag{5.11}$$

In the tension-compression state, the tensile strength is reduced by the relation:

$$f_t'^{ef} = f'_t r_{et}\ ,\quad r_{et} = 1 - 0.8\frac{\sigma_{c2}}{f'_c} \tag{5.12}$$

where r_{et} is the reduction factor of the tensile strength in the direction 1 due to the compressive stress in the direction 2. The reduction function has one of the following forms:

$$r_{et} = \frac{A + (A-1)B}{AB}\quad ,\quad B = Kx + A\ ,\ x = \frac{\sigma_{c2}}{f'_c} \tag{5.13}$$

5.2.1.3 Models of smeared cracks

Within the smeared concept, two options are available for crack models: the fixed crack model and the rotated crack model. In both models the crack is formed when the principal stress exceeds the tensile strength. It is assumed that the cracks are uniformly distributed within the material volume. This is reflected in the constitutive model by an introduction of orthotropy.

In the fixed crack model the crack direction is given by the principal stress direction at the moment of the crack initiation. During further loading this direction is fixed and represents

the material axis of the orthotropy. The principal stress and strain directions coincide in the uncracked concrete, because of the assumption of isotropy in the concrete component.
In the rotated crack model, Vecchio (1986) and Crisfield (1989), the direction of the principal stress coincides with the direction of the principal strain. If the principal strain axes rotate during the loading then direction of the cracks rotates as well.

User defined ratio f_{tc}/f_t is used to shift from rotated crack model to fixed crack model.

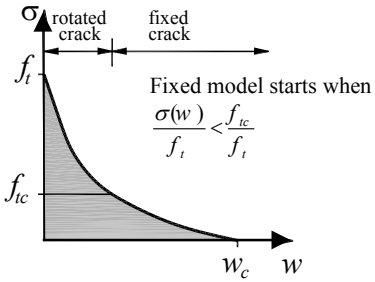

Fig. 5.4: Rotated cracks and fixed crack regions

5.2.2 Constitutive modelling for reinforcement

Available stress-strain laws are bilinear elastic-perfectly plastic or with hardening law; multi-linear law, and cycling reinforcement model based on Menegotto and Pinto (1973).

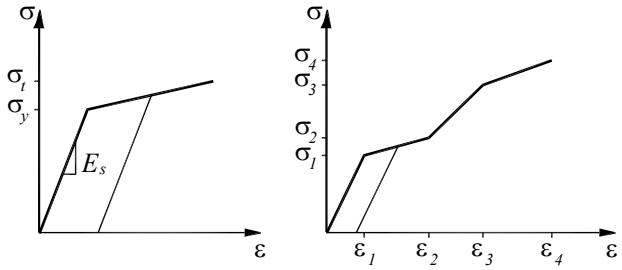

Fig. 5.5: Bilinear and multi-linear stress-strain law for reinforcement

The above described stress-strain laws can be used for the discrete as well as smeared reinforcement.

Bauschinger's effect for reinforcement under cyclic loading is also incorporated by using Menegotto-Pinto model (1973).

5.2.3 Constitutive modelling for reinforcement bond

The basic property of the reinforcement bond model is the bond-slip relationship. This relationship defines the bond strength depending on the value of current slip between reinforcement and surrounding concrete. ATENA contains three bond-slip models: according to the CEB-FIB model code 1990[CEB-FIP-90], slip law by Bigaj (1999) and the user defined law. In the first two models, the laws are generated based on the concrete compressive strength, reinforcement diameter and reinforcement type. The important parameters are also the confinement conditions and the quality of concrete casting.

5.2.3 Constitutive modelling for Von Mises plasticity

The Von Mises plasticity model is often called "J_2 plasticity" is based only on one parameter k. The yield function is defined as:

$$F^p(\sigma_y) = \sqrt{J_2} - k(\varepsilon_{eq}^p) = 0 \quad , \quad k(\varepsilon_{eq}^p) = \sqrt{1/3}\,(\sigma_y)(\varepsilon_{eq}^p) \tag{5.14}$$

where J_2 denote the second invariant of stress deviator tensor, σ_y is the uniaxial yield stress and $k(\varepsilon_{eq}^p)$ is maximal shear stress. The isotropic hardening of the yield criterion can be also controlled by hardening modulus. The cyclic steel behaviour including Bauschinger effect could be defined by Von Mises model which can modify the yield function.

5.2.4 Constitutive modelling for interface

The interface material model can be used to simulate contact between two materials such as a construction joint between two concrete segments or a contact between foundation and concrete structure. The interface material is based on Mohr-Coulomb criterion with tension cut off.

The initial failure surface corresponds to Mohr-Couloumb condition with tension cut-off. After stresses violate this condition, this surface collapses to a residual surface which corresponds to dry friction.

$$\begin{aligned} |\tau| &\le c - \sigma.\emptyset \quad , \quad \sigma \le f_t \\ \tau &= 0 \qquad , \quad \sigma > f_t \end{aligned} \tag{5.15}$$

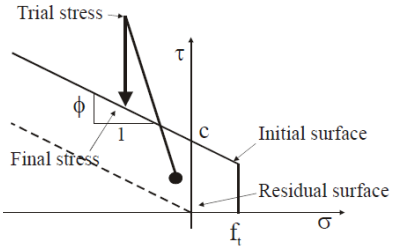

Fig. 5.6: Failure surface for interface elements

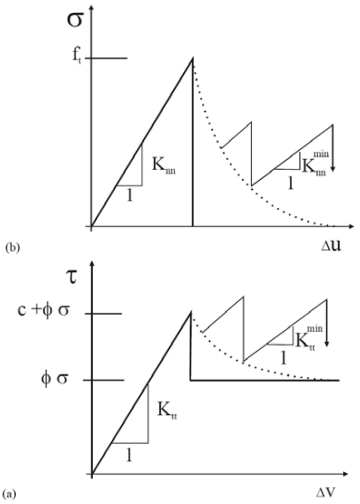

Fig. 5.7: Typical interface model behaviour in: (a) shear, (b) tension

5.3 Element types

Concrete can be modeled by iso-parametric 3D or 2D elements. ATENA finite element library includes iso-parametric tetrahedral elements with 4 to 9 nodes, brick elements with 8 up to 20 nodes, and wedge elements with 6 to 15 nodes. Shell element is a particular case of 3D solid element so that its one dimension (thickness) is very small compared to others. In ATENA shells are modeled by a family of Ahmad finite elements. These elements are reduced from a quadratic 3D brick element with 20 nodes. The element has 9 integration points in shell plane and layers in direction normal to its plane. The total number of integration point is 9x (number of layers). The shell elements can be combined with other 3D elements in one finite element structure.

Reinforcement can be modeled in two distinct forms: discrete and smeared. Discrete reinforcement is in form of reinforcing bars and is modeled by truss elements. The smeared reinforcement is a component of composite material and can be considered either as a single (only one-constituent) material in the element under consideration or as one of the more such constituents. The former case can be a special mesh element (layer), while the later can be an element with concrete containing one or more reinforcements. In both cases the state of uniaxial stress is assumed and the same formulation of stress-strain law is used in all types of reinforcement.

5.4 Solutions of nonlinear equations

Two standard Newton-Raphson and arc-length method are used by ATENA for solution of nonlinear equations. Both solutions are enhanced by the line search method. This method used to accelerate or to damp the speed of analysis of the load-displacement relationship.

For both methods, conditional break criteria can be set to stop the computation if an error exceeds the prescribed tolerance multiplied by the prescribed factor during the iterations or at the end of an analysis step.

5.5 Numerical models for reference units

The three-dimensional iso-parametric brick elements with eight nodes were used to model the concrete and steel parts of reference specimens. Moreover, one-dimensional truss elements were utilized for reinforcement bars. Curvature of beam longitudinal bars inside joint was modelled as truss members in polygons. To model the effect of anchorage at the end bent of beam longitudinal bars, 2-D truss reinforcement was provided by introducing another strut with same element property at the bent corner of reinforcement. For each of longitudinal reinforcement of column and beam, bond-slip relationship was considered as specified by CEB-FIP Model Code 90 [CEB-FIP-90] whereas the stirrups of beam and column were assumed to be perfectly bonded. Due to symmetry in Y axis, one half of the specimen is modelled. According to the experimental tests, the numerical models were analysed under loading history (lateral cyclic displacement and vertical static load) as described in section 4.3.3. Since, these numerical models were computational intensive due to cyclic loading, the overall height and width of members (column and beam) were divided into 4 and 2 FE

elements, respectively; but in the joint region a fine mesh with a special geometry was used to capture the reasonable results.

“3D Nonlinear Cementitious 2’’ and “3D Bilinear Steel Von Mises” material models were used for concrete and steel plates, respectively. The contacts between steel plates and concrete were modelled by “3D Interface” material model. Several models with different ratios of fixed crack coefficient showed that full fixed crack model leads to reasonable results.

Experimental results demonstrated that the reference units were failed by a complex behaviour in joint region. Consequently, to refinement of FE mesh in this region, observing the failure mechanism is necessary. Generated finite element mesh of the numerical model and reinforcement cage for the reference units of BD-B and SD-B are displayed in Fig. 5.8 and Fig. 5.9.

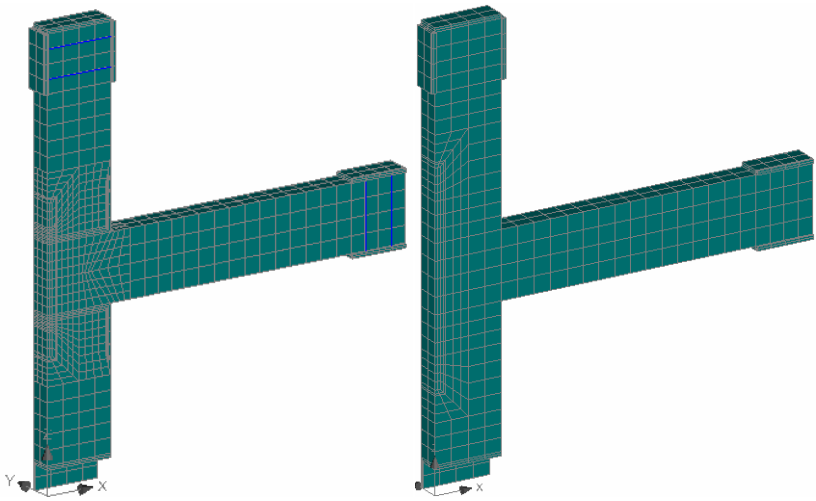

(a) *(b)*

Fig. 5.8: Numerical model for: a) BD-B; b) SD-B

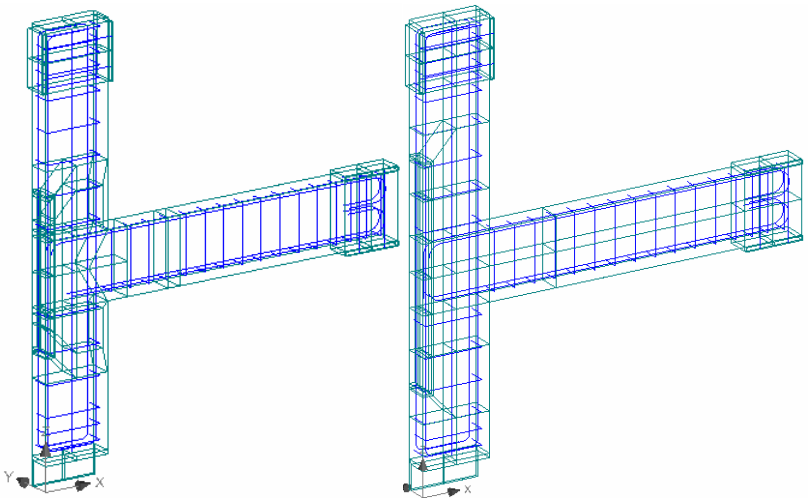

(a) *(b)*

Fig. 5.9: Reinforcement model for: a) BD-B; and b) SD-B

5.6 Sensitivity study

The simulation on structural response through finite element model is affected by varying the user-defined parameters which are used to calibrate the FE model. The sensitivity study investigates the influence of these parameters such as:

- Element size
- Fracture energy
- Reinforcement material
- Tension stiffening
- Cracking model

In the following the influence of every parameter for reference specimen of SD-B is investigated.

5.6.1 Sensitivity of element size

The numerical model of specimen SD-B was analysed using several element sizes to show the sensitivity of mesh sizes on the simulated behaviour. In Fig. 5.10, envelop story shear strength-drift plot of the analysed models are compared with the experimental result. Since the average strains define the element response therefore large elements postpone the

beginning of concrete failure. As can be seen, increasing the mesh size leads to development of peak strength. Evidently, mesh size of 80mm terminated to a reasonable result. Obviously, decreasing the element size results to reduce the crack band, therefore the value of G_f should be modified to obtain the same w_c for different sizes which will be discussed in the next section.

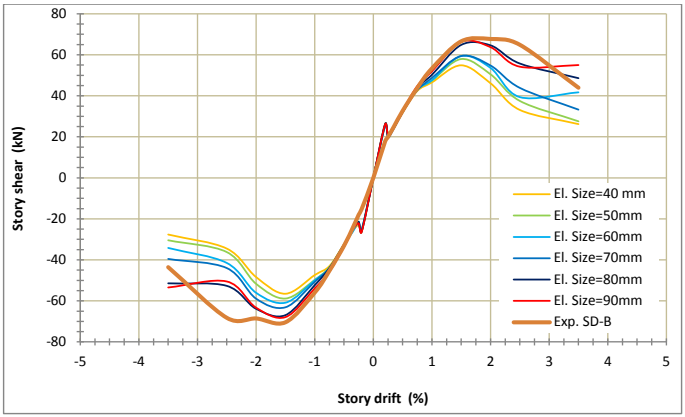

Fig. 5.10: Envelope lateral strength-drift diagram for different FE element sizes

5.6.2 Sensitivity of fracture energy

The fracture energy of concrete G_f which is the energy required to propagate a tensile crack of unit area is estimated by CEB-FIP Model Code 90 [CEB-FIP-90] as:

$$G_f = G_{fo}(f_{cm}/f_{cmo})^{0.7} \tag{5.16}$$

where $f_{cmo} = 10\ MPa$, f_{cm} is the mean axial tensile strength of concrete, and G_{fo} is the base value of fracture energy which depends on the maximum aggregate size $d_{max}$of concrete. For d_{max} equal to 8, 16, and 32mm, G_{fo} is 0.025, 0.03, and $0.058 Nmm/mm^2$, respectively. In ATENA, w_c, the crack opening at the complete release of stress (Fig. 5.1), is defined by specifying the fracture energy. For mesh size of 80mm, envelop lateral strength-drift diagram of numerical models with different amounts of G_f is depicted in Fig. 5.11. As can be seen, the result of $G_f = 0.09 Nmm/mm^2$ is reasonable.

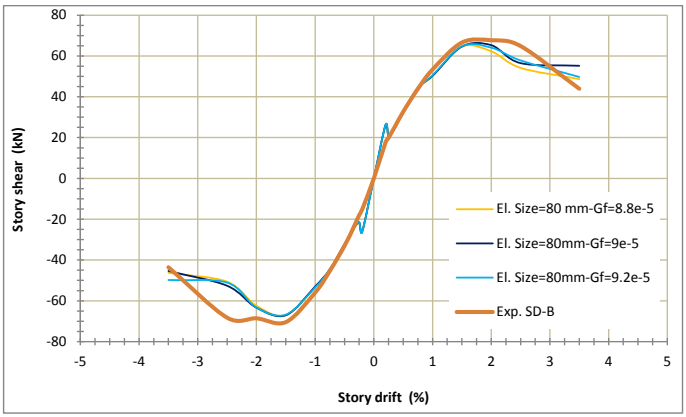

Fig. 5.11: Envelope lateral strength-drift diagram for various values of fracture energy (G_f)

5.6.3 Sensitivity of cyclic reinforcement

Effect of cyclic loading on reinforcement as accounting the isotropic hardening and Bauschinger's effect can be used by cyclic reinforcement model. Fig. 5.12 shows the effects of this model in the resulted envelop lateral strength-drift diagram. Evidently, since, beam longitudinal bars yielded limitedly and subsequently didn't enter to the step of strain hardening, using of normal and cyclic reinforcement model cannot considerably change the behavior.

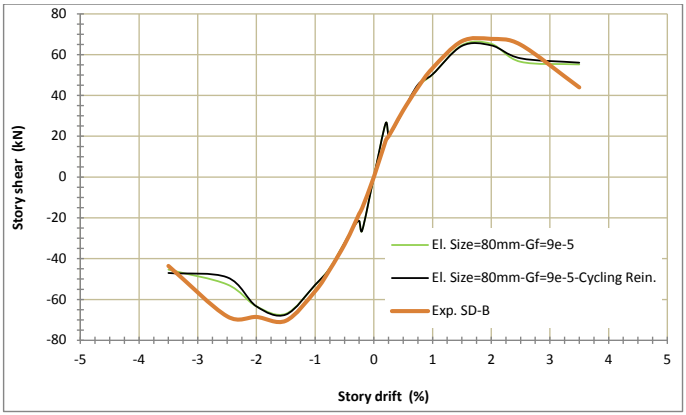

Fig. 5.12: Envelope lateral strength-drift diagram for different reinforcement material

5.6.4 Sensitivity of tension stiffening

The contribution of concrete to steel stiffness in reinforced concrete structures is described by tension stiffening. Furthermore, according to tension softening diagram (Fig. 5.1), the minimum value of tensile stress cannot be less than $C_{ts}f_t'^{ef}$. Fig. 5.13 shows the effect of this parameter in behaviour of numerical models. Evidently, increasing C_{ts} develops the peak load and delays the final failure. It is found that the ratio of 0.45 may be acceptable.

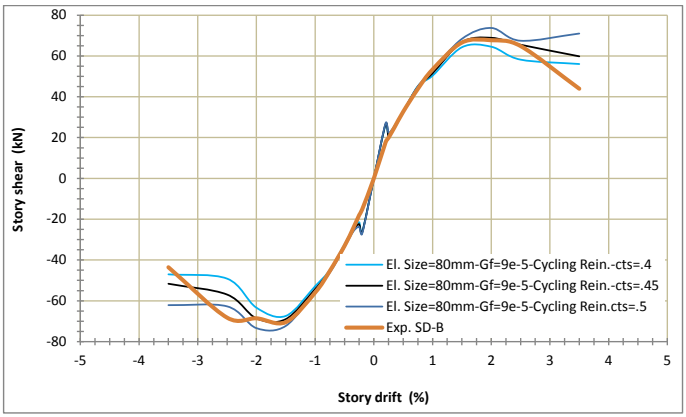

Fig. 5.13: Envelope lateral strength-drift diagram for various values of tension stiffening (C_{ts})

5.6.5 Sensitivity of cracking model

The smeared crack model was changed from fixed crack to rotated crack model by defining a fraction of tensile strength (f_{tc}/f_t) in tension softening regime, Fig. 5.4. The results of analysis are displayed in Fig. 5.14. As can be seen, increasing the tensile strength ratio results to enhancing the failure load and full fixed crack model ($f_{tc}/f_t = 1$) leads to the reasonable behaviour.

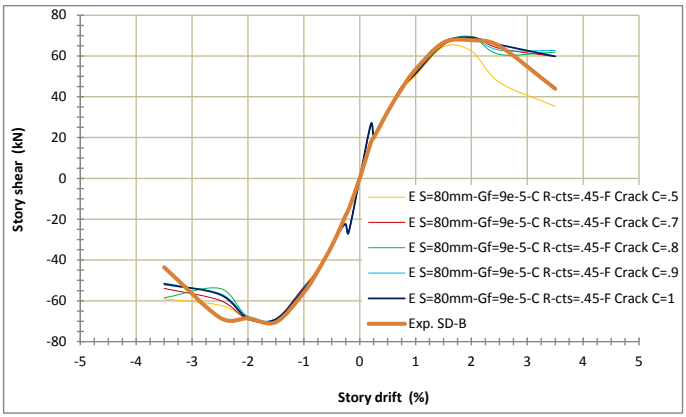

Fig. 5.14: Envelope lateral strength-drift diagram for different smeared cracking models

5.7 Numerical models for retrofitted specimens

In addition to the defined assumptions for the numerical models of reference units (section 5.5), the three-dimensional iso-parametric brick elements with eight nodes were also used to model the Multi Functional Corbels (HMFC) and Harmonica Damper Plates (HHDP) in retrofitted specimens. The pre-stressed threaded bars to fixing the steel plates on the concrete surface and retrofitting devices (HMFC and HHDP) were modelled as external reinforcement with pre-stressing load. The overall height and width of concrete members (column and beam) were divided into 7 and 3 FE elements, respectively. All the SRPs were modelled as 9-noded iso-parametric 6-layered shell elements by considering a single directional reinforcement embedded in epoxy matrix. In wrapped edges, 45° diagonal were created to provide the full contact. Since, these numerical models were computational very intensive due to cyclic loading and numerous elements and materials, the contact type between SRPs and concrete was considered as perfect connection.

According to experimental results the retrofitted specimens were failed by beam flexural hinge at the end of HMFCs and no failure mechanism was observed in joint region. Generated finite element mesh of the numerical model, reinforcement cage and innovative retrofitting devices for the upgraded specimens of BD-H1, SD-H2-D and BD-H3-D are illustrated in Fig. 5.15, Fig. 5.16 and Fig. 5.17, respectively.

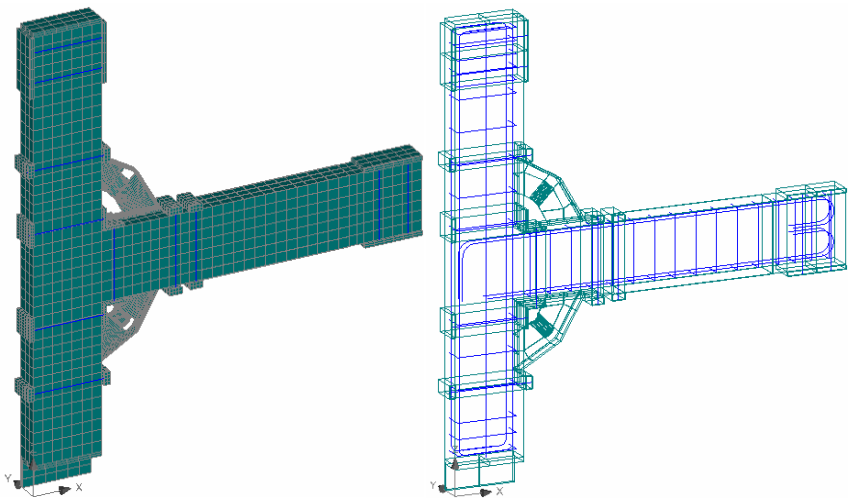

(a) *(b)*

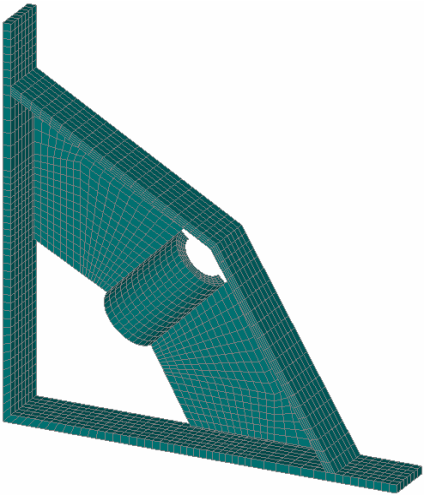

(c)

Fig. 5.15: Numerical model for BD-H1: a) General finite element mesh, b) Reinforcement, c) Multi Functional Corbel , HMFC (H1)

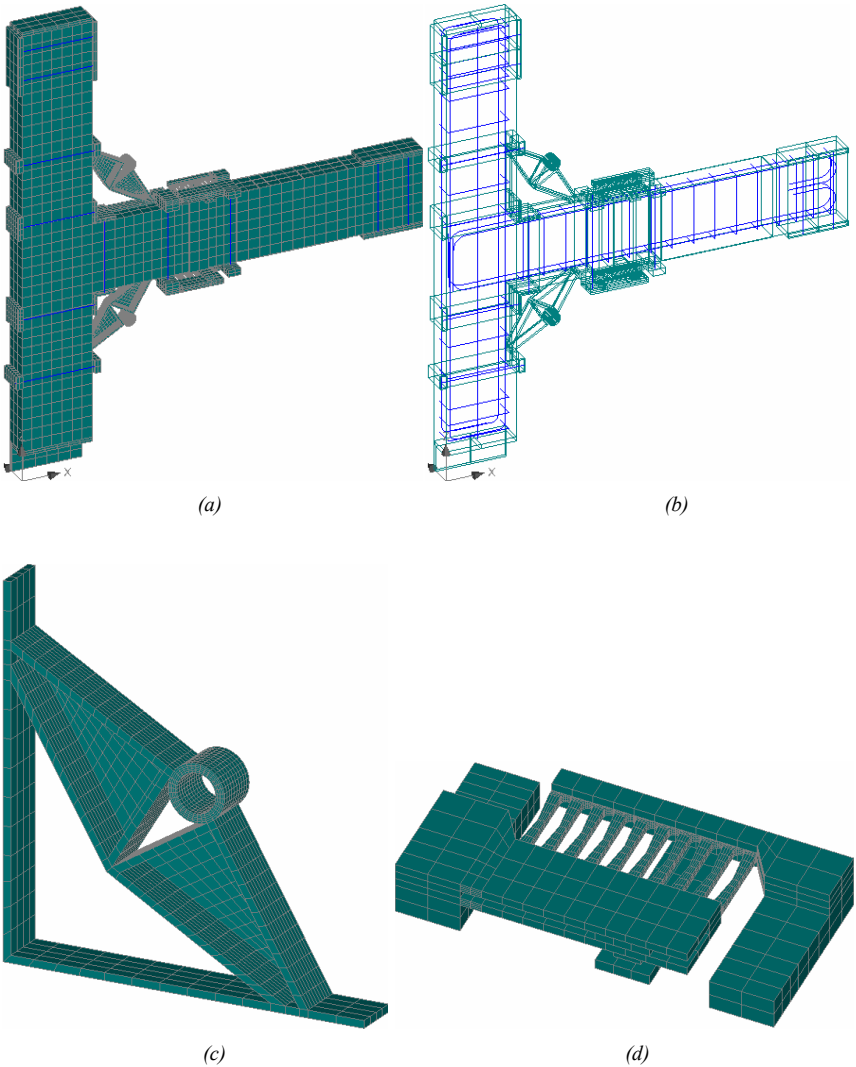

Fig. 5.16: Numerical model for SD-H2-D: a) General finite element mesh, b) Reinforcement c) Multi Functional Corbel HMFC (H2), d) Harmonica Damper Plate HHDP (D)

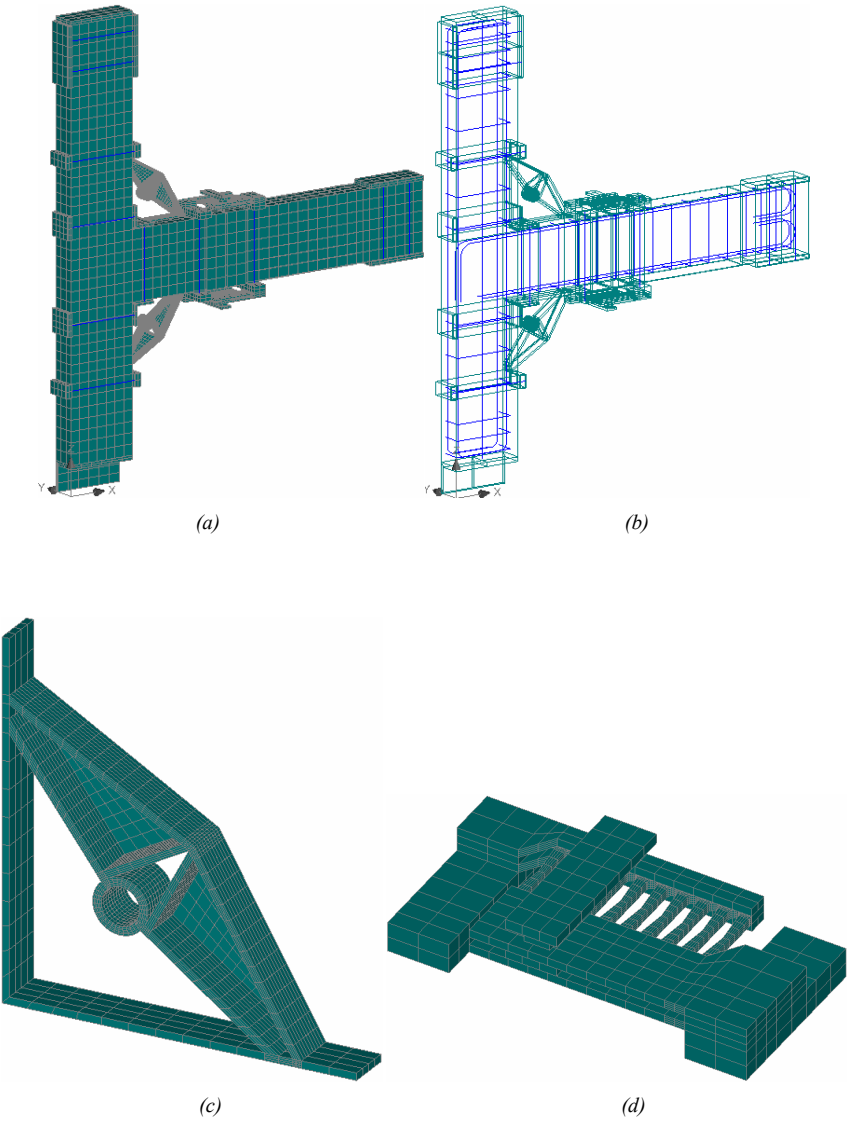

Fig. 5.17: Numerical model for BD-H3-D: a) General finite element mesh, b) Reinforcement c) Multi Functional Corbel HMFC (H3), d) Harmonica Damper Plate HHDP (D')

5.8 Comparison the results of FE analysis and experimental test

The reference units and retrofitted specimens were numerically simulated, analysed and compared with the experimental test results. For each specimen, displacement history was adopted the same as that was used during the experimental test. Before application of the cyclic loading, a constant axial load of 300 kN was applied on the column.

5.8.1 Reference unit BD-B

Story shear-drift hysteresis plot of reference unit BD-B obtained from the numerical analysis is depicted in Fig. 5.18 and envelope lateral shear resistance-drift for numerical study and experimental test can be compared by Fig. 5.19. As can be seen, the load-drift behaviour of investigated specimen in numerical analysis and experimental study are well corroborated. It is observed that the repetition of cycles in each drift level would reduce the maximum load carrying capacity and stiffness under same drift demand.

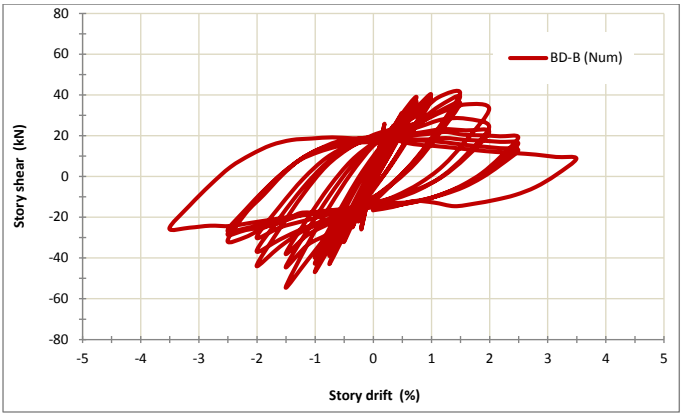

Fig. 5.18: Story shear-drift hysteresis plot of reference unit BD-B from numerical analysis

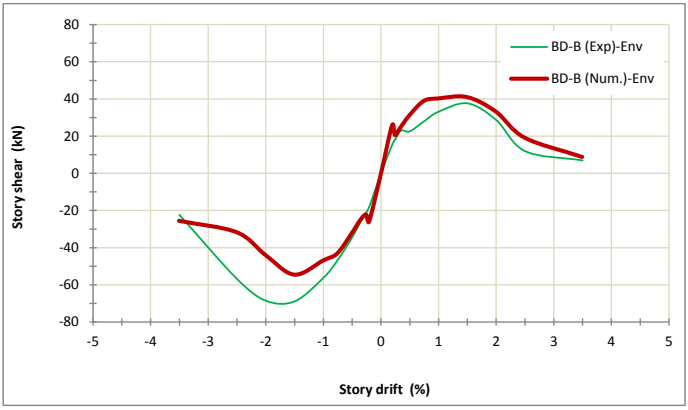

Fig. 5.19: Envelope story shear-drift hysteresis plot of reference unit BD-B from numerical analysis and experimental study

The development of cracks within the model of BD-B is shown in Fig. 5.20. The results obtained from the numerical analysis and experimental test (Fig. 5.21) display that there is a good agreement between the test and analysis. Crack formation and propagation from numerical model shows that the final failure in BD-B is due to failure of bond in beam bottom bars.

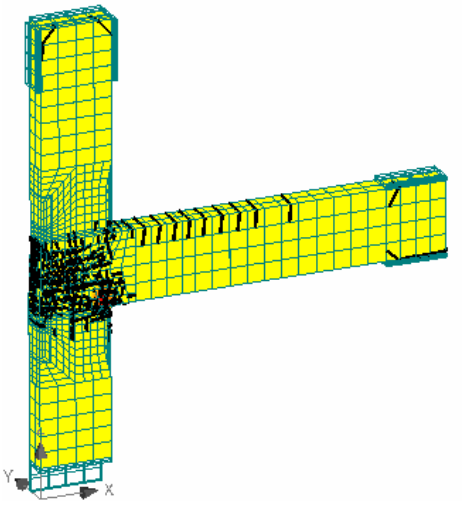

Fig. 5.20: Overall final cracking pattern of reference unit BD-B

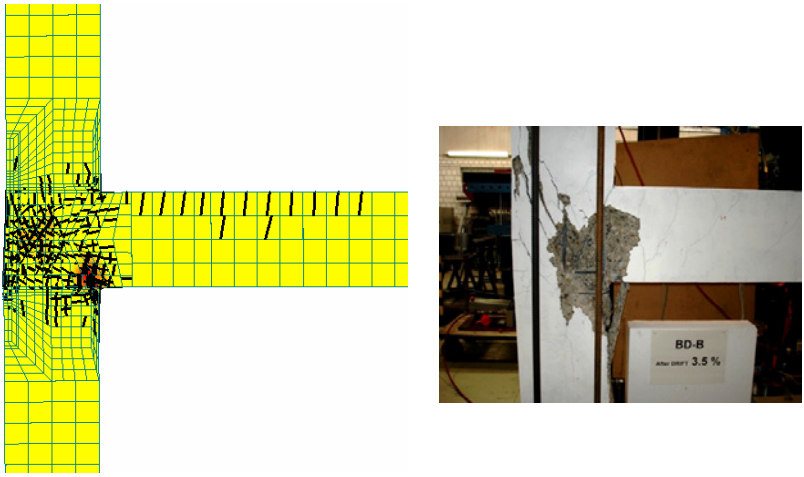

(a) *(b)*

Fig. 5.21: Comparison of crack pattern for reference unit BD-B from a) numerical analysis and b) experimental test

5.8.2 Reference unit SD-B

Story shear-drift hysteresis diagram of reference unit SD-B resulted from the numerical analysis is displayed in Fig. 5.22 and envelope lateral load-drift for numerical study and experimental test can be compared by Fig. 5.23. Evidently, the load-drift behaviour of investigated specimen in numerical analysis and experimental study are well confirmed so that the reduction of load carrying capacity and stiffness in each drift level can be clearly observed by numerical analysis.

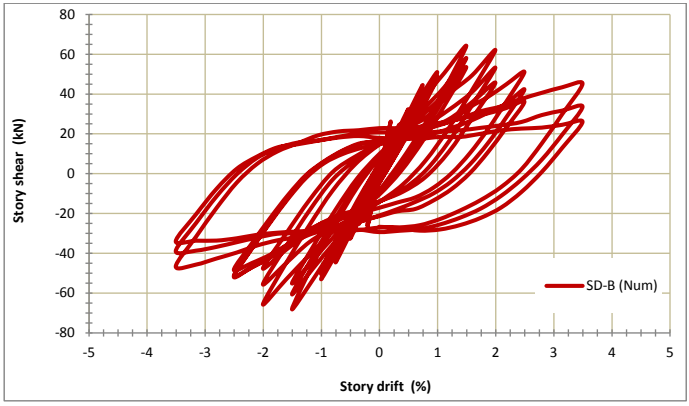

Fig. 5.22: Story shear-drift hysteresis plot of reference unit SD-B from numerical analysis

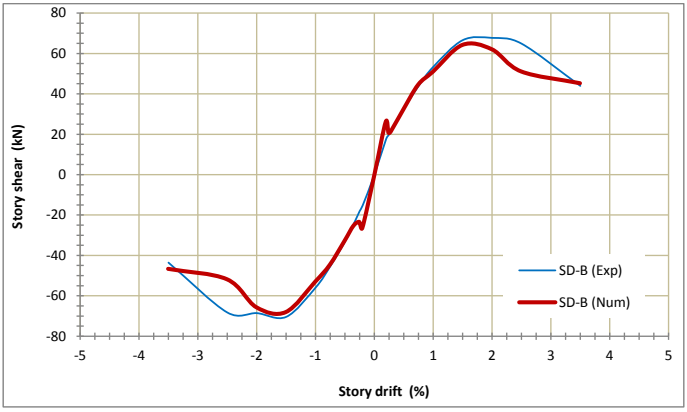

Fig. 5.23: Envelope story shear-drift hysteresis plot of reference unit SD-B from numerical analysis and experimental study

The crack pattern of the SD-B numerical model in Fig. 5.24 and Fig. 5.25 depicts that the numerical analysis and experimental test have a good agreement in crack development and propagation. Crack pattern from numerical model displays that the final failure in SD-B is concentrated in the joint zone and exhibits a brittle non-ductile joint shear failure.

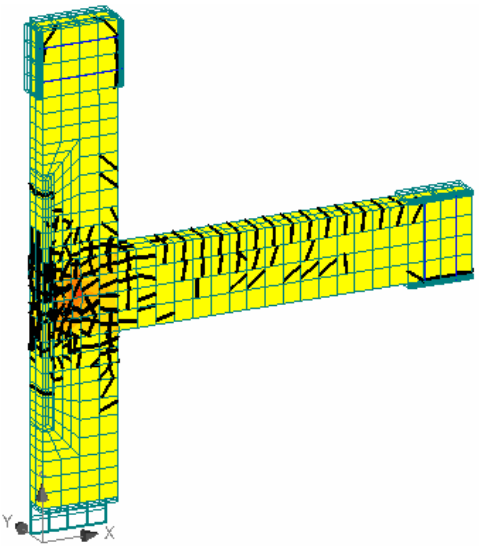

Fig. 5.24: Overall final cracking pattern of reference unit SD-B

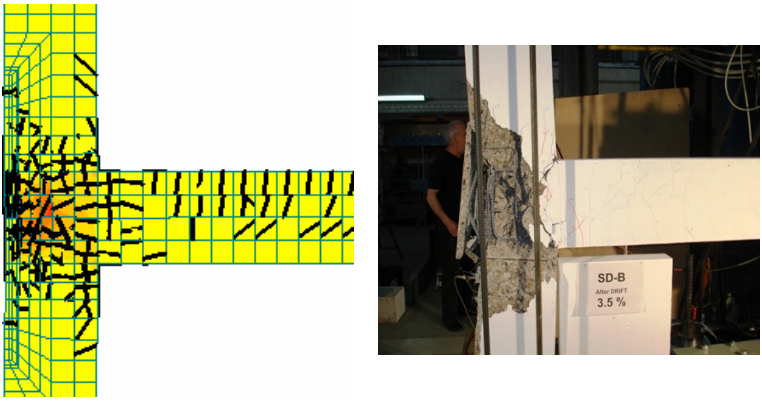

(a) *(b)*

Fig. 5.25: Comparison of crack pattern for reference unit SD-B from a) numerical analysis and b) experimental test

5.8.3 Retrofitted specimen BD-H1

Story shear-drift hysteresis diagram of retrofitted specimen BD-H1 resulted from the numerical analysis is displayed in Fig. 5.26 and envelope lateral load-drift for numerical study and experimental test can be compared by Fig. 5.27. As can be seen, the load-drift behaviour of investigated specimen in numerical analysis and experimental study are well confirmed. It is observed that the repetition of cycles in each drift level would not considerably reduce the maximum load carrying capacity and stiffness.

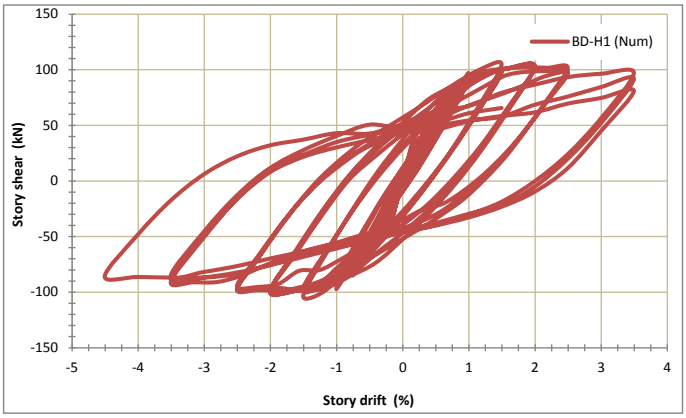

Fig. 5.26: Story shear-drift hysteresis plot of retrofitted specimen BD-H1 from numerical analysis

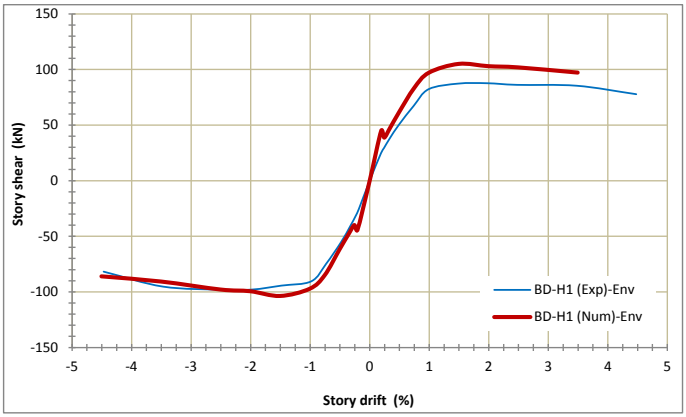

Fig. 5.27: Envelope story shear-drift hysteresis plot of retrofitted specimen BD-H1 from numerical analysis and experimental study

The final crack development within the numerical model and experimental test of BD-H1 is shown in Fig. 5.28. As can be seen, the results of numerical analysis and experimental test illustrate a good agreement between the test and analysis. Crack formation and propagation from numerical model shows that the final failure mechanism in BD-H1 is due to flexural plastic hinge of the beam at the end of H1.

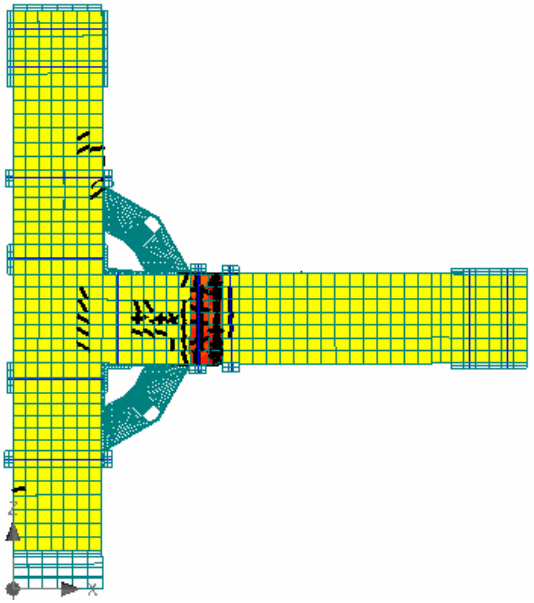

(a)

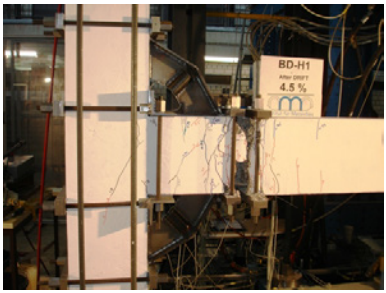

(b)

Fig. 5.28: Comparison of crack pattern for retrofitted specimen BD-H1 from: a) numerical analysis and b) experimental test

Development of principal plastic strain in Multi Functional Corbel HMFC (H1) is represented in Fig. 5.29. As can be observed, different part of the corbel has been reached to yield strain and therefore the domination of energy dissipation is not concentrated to pipe.

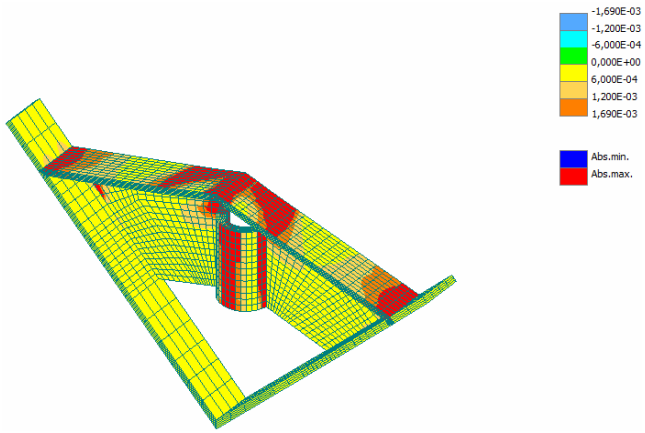

Fig. 5.29: Principal yield strain pattern for HMFC (H1) in retrofitted specimen BD-H1

5.8.4 Retrofitted specimen SD-H2-D

Story shear-drift hysteresis diagram of retrofitted specimen SD-H2-D obtained from the numerical analysis is displayed in Fig. 5.30 and envelope lateral load-drift for numerical study and experimental test can be compared by Fig. 5.31. Evidently, the load-drift behaviour of investigated specimen in numerical analysis and experimental study are well confirmed. It is also observable that like the experimental result the repetition of cycles in each drift level would not significantly reduce the maximum lateral resistance and stiffness.

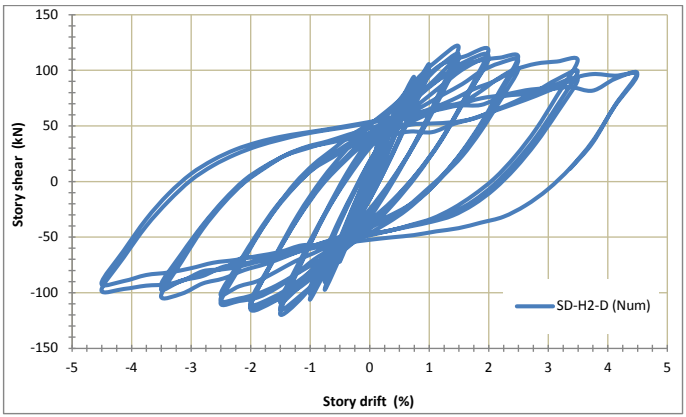

Fig. 5.30: Story shear-drift hysteresis plot of retrofitted specimen SD-H2-D from numerical analysis

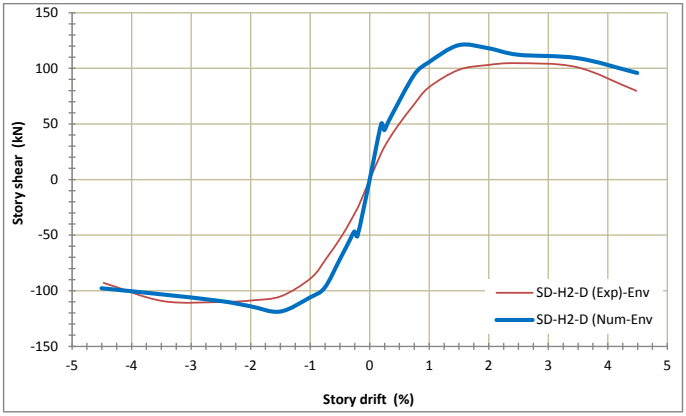

Fig. 5.31: Envelope story shear-drift hysteresis plot of retrofitted specimen SD-H2-D from numerical analysis and experimental study

The final crack pattern within the numerical model of SD-H2-D can be compared to experimental result by Fig. 5.32. The results of numerical model and experimental test illustrate a good agreement so that the crack formation and propagation depicts that the final failure mechanism in SD-H2-D is due to flexural plastic hinge of the beam at the end of H2.

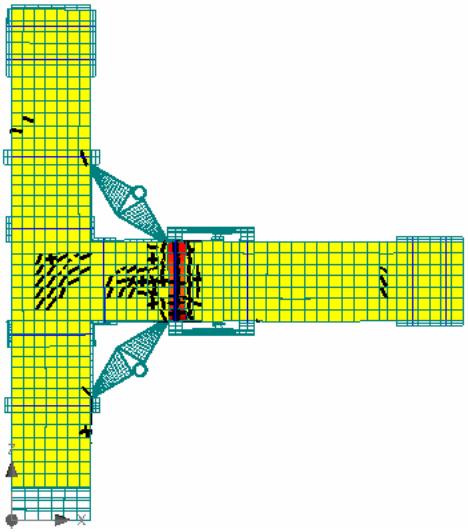

(a)

Fig. 5.32: (continued)

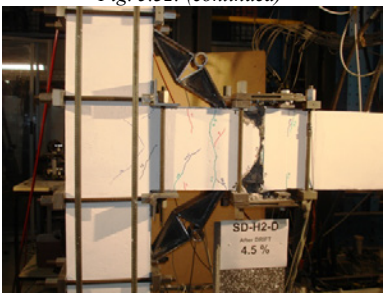

(b)

Fig. 5.32: Comparison of crack pattern for retrofitted specimen SD-H2-D from a) numerical analysis and b) experimental test

Developed principal plastic strain in Multi Functional Corbel HMFC (H2) and Harmonica Damper Plate HHDP is represented in Fig. 5.33 and Fig. 5.34, respectively. As can be observed, not only the pipe reaches to plastic strain, but also the other parts of H2 contribute in energy dissipation by yielding.

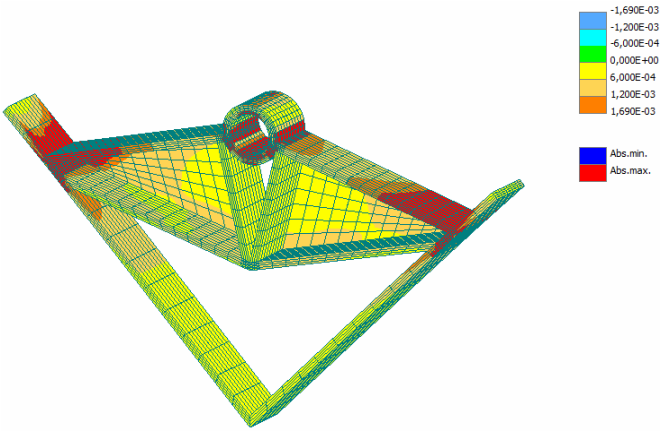

Fig. 5.33: Principal yield strain pattern for HMFC (H2) in retrofitted specimen SD-H2-D

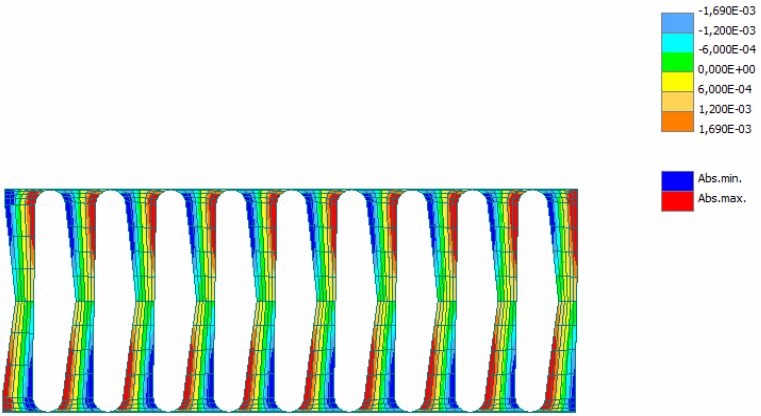

Fig. 5.34: Principal yield strain pattern for HHDP (D) in retrofitted specimen SD-H2-D

5.8.5 Retrofitted specimen BD-H3-D

Lateral resistance-drift hysteresis plot of retrofitted specimen BD-H3-D resulted from the numerical analysis is illustrated in Fig. 5.35 and envelope maximum story shear-drift for numerical study and experimental test can be compared by Fig. 5.36. As can be confirmed, the load-drift behaviour of investigated specimen in numerical analysis and experimental study are well matched. Evidently, the repetition of cycles in each drift level would not considerably reduce the maximum lateral carrying capacity and stiffness.

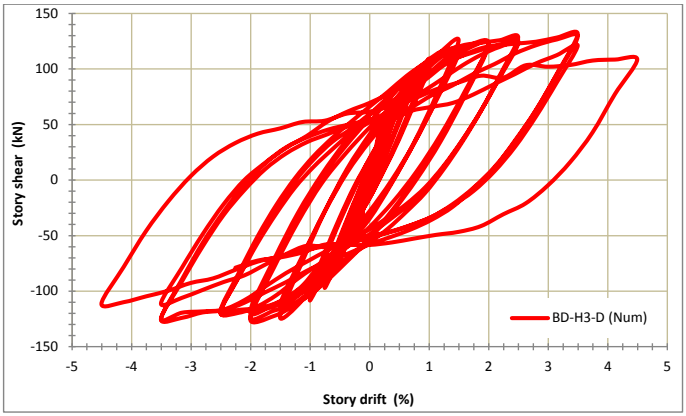

Fig. 5.35: Story shear-drift hysteresis plot of retrofitted specimen BD-H3-D from numerical analysis

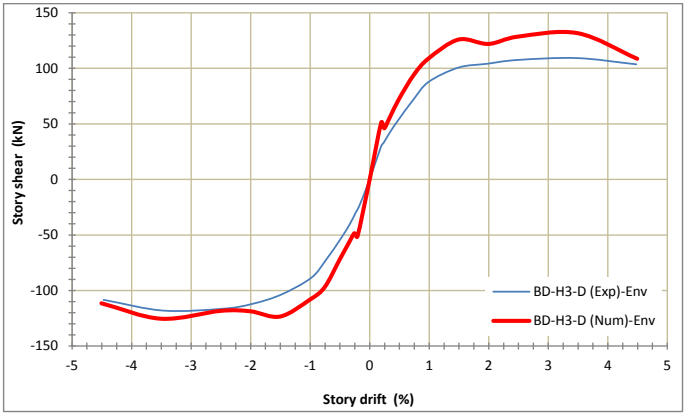

Fig. 5.36: Envelope story shear-drift hysteresis plot of retrofitted specimen BD-H3-D from numerical analysis and experimental study

The comparison of developed final crack pattern within the numerical model and experimental result of BD-H3-D is illustrated in Fig. 5.37. The results of numerical model and experimental test are well matched so that the crack formation and propagation displays that the final failure mechanism in BD-H3-D is due to flexural plastic hinge of the beam at the end of H3.

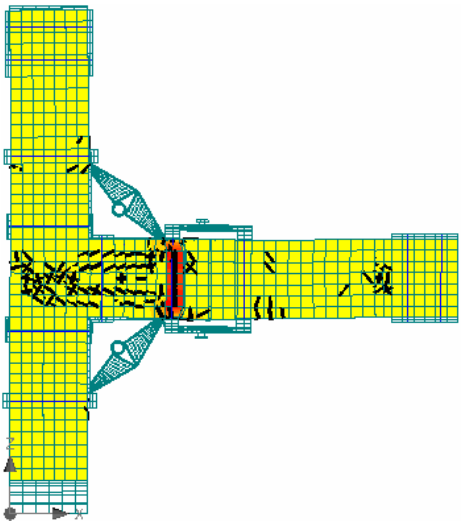

(a)

Fig. 5.37: (continued)

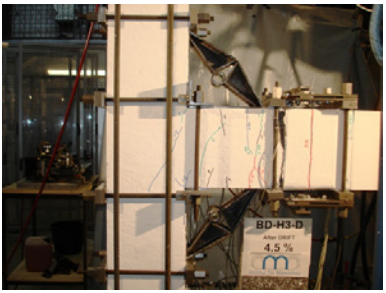

(b)

Fig. 5.37: Comparison of crack pattern for retrofitted specimen BD-H3-D from a) numerical analysis and b) experimental test

Developed principal plastic strain in Multi Functional Corbel HMFC (H3) and Harmonica Damper Plate HHDP (D') is illustrated in Fig. 5.38 and Fig. 5.39, respectively. As can be seen, different parts of H3 contribute in energy dissipation by yielding and full plastic behaviour is developed in arms of HHDP during the analysis.

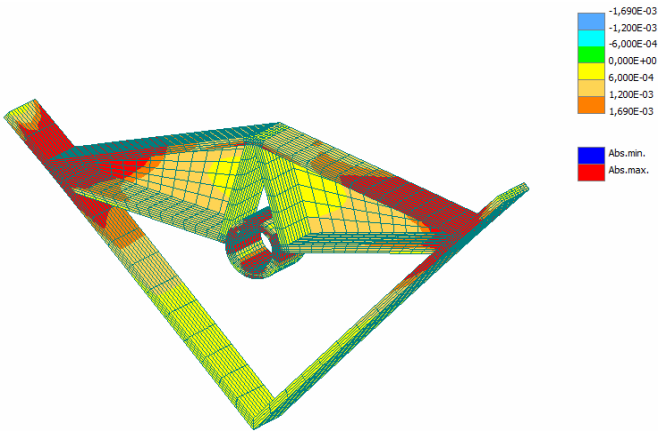

Fig. 5.38: Principal yield strain pattern for HMFC (H3) in retrofitted specimen BD-H3-D

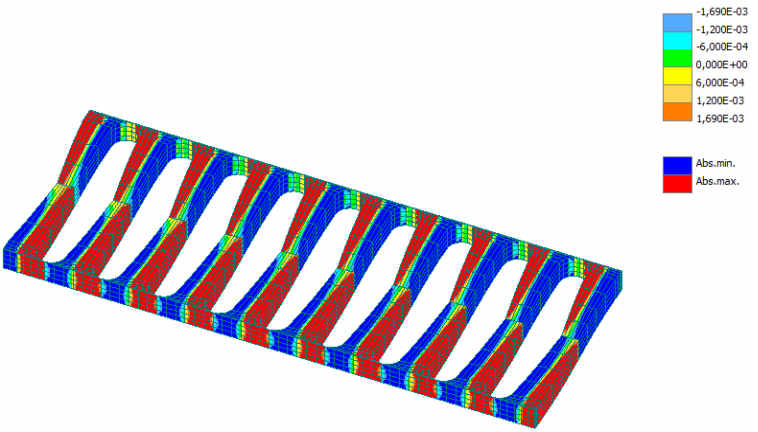

Fig. 5.39: Principal yield strain pattern for HHDP (D') in retrofitted specimen BD-H3-D

5.9 Developing a new upgrading method, Retrofitting Technique 3 (RT3)

Efficiency of Retrofitting Technique 1 (RT1) in effectively dissipate energy in upgraded specimen BD-H1 and performance of Retrofitting Technique 2 (RT2) in preserving the lateral carrying capacity in strengthened specimens SD-H2-D and BD-H3-D during the test illuminated an idea to develop a new innovative upgrading method based on the philosophy of RT1 and RT2 using the concept of friction-bending to increasing the energy dissipation and resistance of the system. According to Fig. 5.40, the new proposed innovative method, Retrofitting Technique 3 (RT3), includes of a Frictional-Bending Damper Plate (HFBDP) which is attached at the end of a Multi Functional Corbel (HMFC) on the beam. As can be found, the new device (HFBDP) is functioned based on friction and bending so that with adjusting the imposed vertical loads on the HFBDP (by prestressing the threaded roads or tightening the screws) the friction between the steel plates from one side and concrete surface from another side becomes active and therefore frictional strength as well as direct flexural bending of the plate at the hinge zone of the beam can proportionally increase the amounts of strength and energy dissipation. Moreover, dowel action of the pate can contribute to the shear strength of the beam.

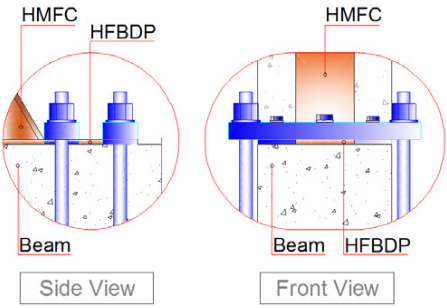

Fig. 5.40: Retrofitting Technique 3 (RT3) by HMFC and HFBDP

To evaluate and measuring the friction characteristics between steel and concrete, an innovative measurement device was designed to test the requirements through the existence tension machine in the laboratory. The designed and fabricated device is shown in Fig. 5.41. As can be seen, by placing a cubic concrete specimen into the device and prestressing the threaded roads which were equipped with strain gauges to measure the prestressing force, the vertical imposed loads on the steel plates is found and by installing the whole system into the tension machine of the structural laboratory the friction characteristics are obtained.

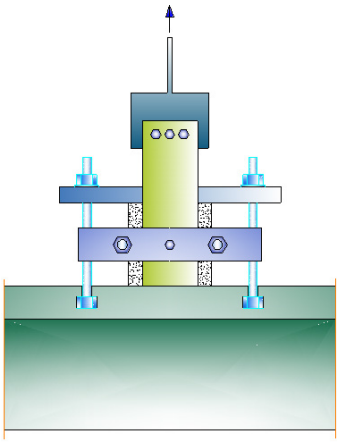

(a)

Fig. 5.41: (continued)

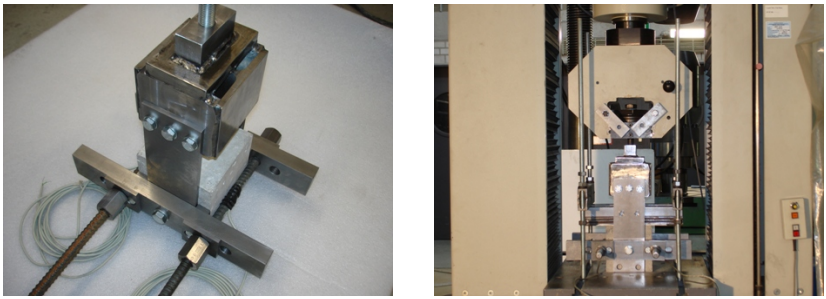

(b) *(c)*

Fig. 5.41: Friction test between steel plates and concrete surface: a) an innovative designed friction test device; b) fabricated test device; c) installation of test device in test machine

The results of experimental test and numerical simulation of the interface in two different cases of the concrete surface, grinded and not grinded, are illustrated in Fig. 5.42. As can be observed, the numerically simulated interface between concrete and steel in both of the cases are well matched with the experimental results. Therefore, the obtained interface characteristics were used in numerically modelling the new retrofitting technique by ATENA.

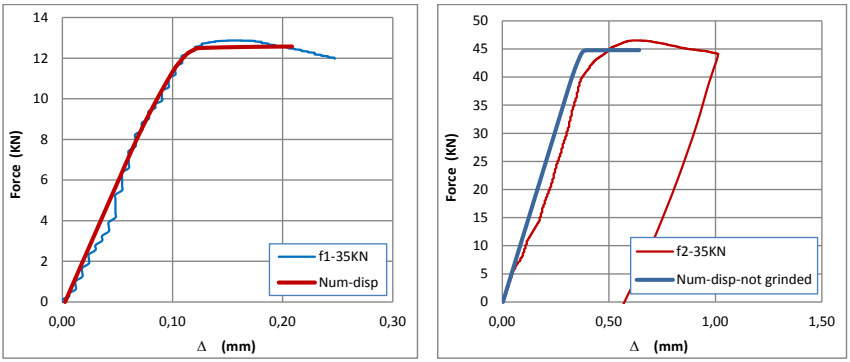

(a) *(b)*

Fig. 5.42: Comparison of load-slip curves of steel-concrete friction in test and simulation: a) for grinded surface of concrete; b) for not grinded surface of concrete

To evaluate the proposed new retrofitting technique, the numerical model of specimen BD-H1 was developed through this technique by perstressing force of 80kN for HFBDP and the model of BD-H1-F was prepared and analysed. The final crack development within the numerical model of BD-H1-F is shown in Fig. 5.43. Crack formation and propagation from

the numerical model shows that the final failure mechanism in BD-H1-F is due to flexural plastic hinge of the beam at the end of HMFC.

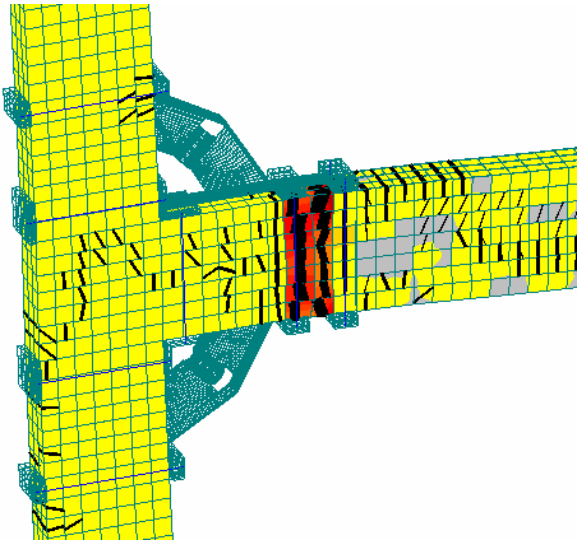

Fig. 5.43: Crack pattern of developed new upgrading method, Retrofitting Technique 3 (RT3) for numerically analysed specimen BD-H1-F

Story shear-drift hysteresis diagram of retrofitted specimen BD-H1-F resulted from the numerical analysis is displayed with experimental results of retrofitted specimen BD-H1 in Fig. 5.44. Moreover, envelope lateral load-drift for numerical study and experimental test of BD-H1 can be compared by Fig. 5.45. As can be seen, the hysteretic behaviour of the retrofitted specimen BD-H1-F though RT3 is significantly better than the retrofitted specimen BD-H1 through RT1. While the friction resistance can be adjusted by controlling the prestressing of the threaded rods, the lateral resistance was considerably increased and sensitivity of the load carrying capacity and stiffness due to repetition of cycles in each drift level was reasonably decreased. Meanwhile, by spreading the diagram surface to the lateral sides, the dissipated energy was also significantly improved. The stable hysteresis performance shows that the used innovative upgrading method (RT3) can be resulted to a practical valuable retrofitting technique.

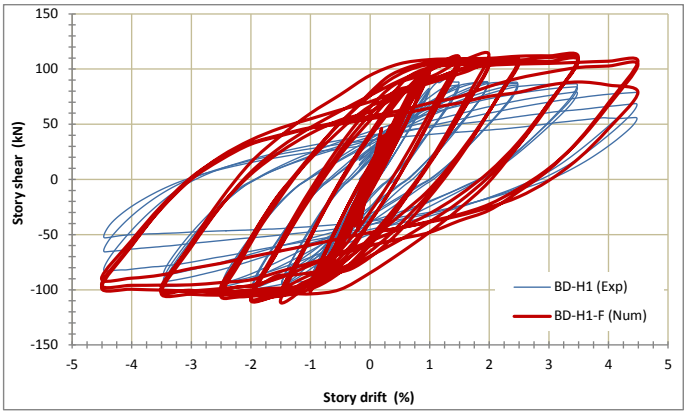

Fig. 5.44: Story shear-drift hysteresis plot of developed new upgrading method, Retrofitting Technique 3 (RT3) for numerically analysed specimen BD-H1-F

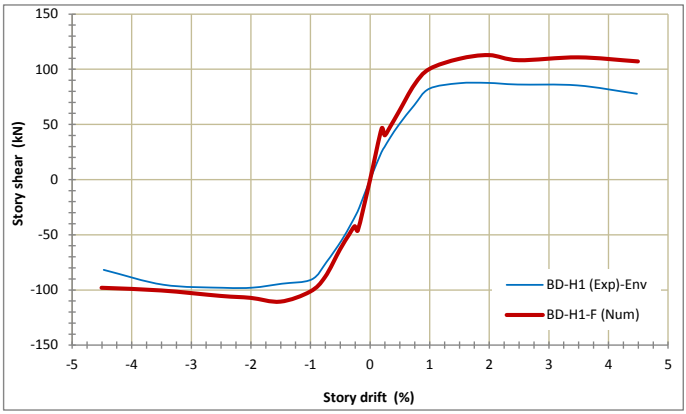

Fig. 5.45: Envelope story shear-drift hysteresis plot of developed new upgrading method, Retrofitting Technique 3 (RT3) for numerically analysed specimen BD-H1-F

Developed principal plastic strain in Multi Functional Corbel HMFC (H1) and Frictional-Bending Damper Plate HFBDP (F) is illustrated in Fig. 5.46 and Fig. 5.47, respectively. As can be seen, different parts of H1 contribute in energy dissipation by yielding and full plastic behaviour is developed in HFBDP during the analysis.

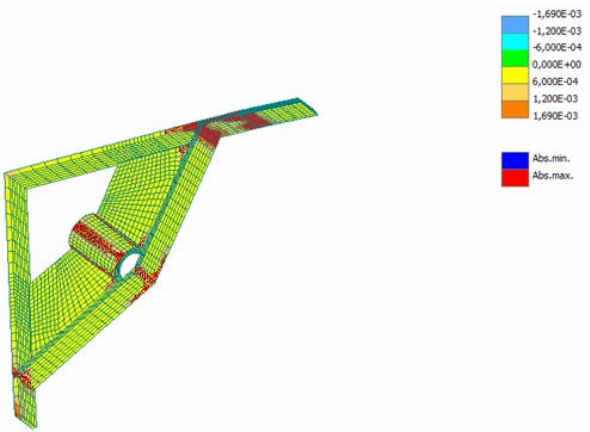

Fig. 5.46: Principal yield strain pattern for HMFC (H1) and HFBDP (F) in retrofitted specimen BD-H1-F

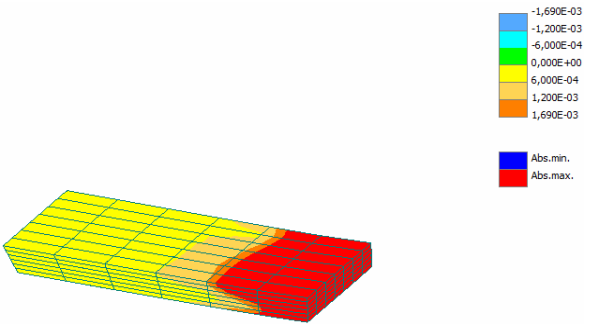

Fig. 5.47: Principal yield strain pattern for HFBDP (F) in retrofitted specimen BD-H1-F

To evaluate the energy dissipation capability of the proposed innovative new retrofitted technique (RT3), the results are compared with the experimental and numerical outcomes of the other specimens. The amounts of relative dissipated energy by different specimens was put side by side is Fig. 5.48. Evidently, specimen BD-H1-F could achieve the highest rate of energy absorption among the others so that the increasing rate in comparison with the reference unit of this category (BD-B) was 525% and BD-H1, BD-H3-D, and SD-H2-D were 34, 26, and 34%.

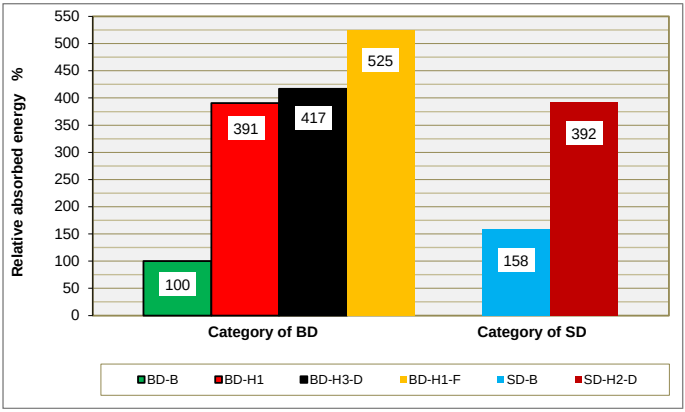

Fig. 5.48: Comparison the energy dissipations in all specimens

The relative energy dissipation ratio in retrofitted specimens can be compared by Fig. 5.49. In this diagram, the results of experimental and numerical studies are put side by side to evaluate the validation of the numerical findings. As can be seen, the experimental outcomes are well matched with the numerical results so that 5, 0.05, and 7% differences are observed for BD-H1, BD-H3-D and SD-H2-D, respectively. Therefore, the new proposed Retrofitting Technique 3 (RT3) provides extra relative energy dissipation in comparison with the other techniques and of course with the minimum code acceptance criteria of 1/8. It is worth mentioning that for reinforced concrete connections, typical relative energy dissipation ratio at 3% drift level have been reported to be 30% [ACI 374.1-05], while the obtained ratios are related to 3.5% drift level. Consequently, it is expected that through the proposed innovative retrofitting techniques RT1 and RT2 and practically RT3 a high rate of damping for RC frames is prepared and subsequently continuous oscillations for a considerable time after an earthquake, excessive displacements, and producing low-cycle fatigue effects is prevented.

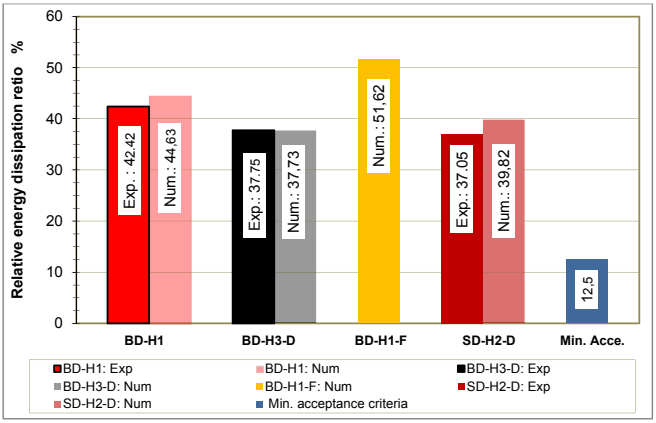

Fig. 5.49: Comparison the energy dissipation ratio of retrofitted specimens in last cycle of 3.5% drift level

The dissipated energy by all specimens and estimated contribution of subassemblages are illustrated in Fig. 5.50. As can be seen, for BD-H1-F, the contribution of main body, HMFC and HFBDP are 65, 15 and 20%, respectively. Accordingly, this specimen has the maximum rate of dissipated energy by installed energy absorption devices among the others therefore it can be claimed that the capability of the devices has been reasonably utilized. Obviously, by increasing the prestressing loads on HFBDP by observing the strength hierarchy to considering the strength of other elements it is possible to achieve the higher amounts of energy dissipation by HFBDP.

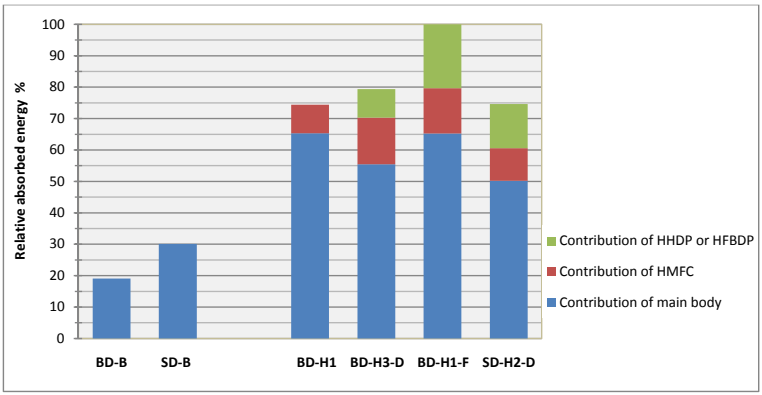

Fig. 5.50: Comparison the energy dissipations in specimens and estimated contribution of subassemblages

Chapter 6

Conclusions and Recommendations

6.1 Conclusions

The main conclusions obtained from the results of a series of experiments and numerical simulations conducted on RC beam-column joint specimens both before and after upgrading with innovative retrofitting techniques are presented below.

6.1.1 Conclusions of experimental study

6.1.1.1 Strength

- In contrast to as-built specimen with shear deficiency (SD-B), bond deficient reference unit (BD-B) had not the same strength in positive and negative direction because of different embedment conditions of the beam longitudinal bars in the top and bottom while the all retrofitted ones of both categories exhibited nearly the same lateral resistance in both directions. Therefore, the unsymmetrical form of the loops in reference unit of BD-B was modified to the symmetrical ones of the retrofitted specimens (BD-H1 and BD-H3-D) and consequently the proposed retrofitting techniques (RT1 and RT2) could effectively provide the development length requirements of beam bottom bars.

- Both of reference units did not demonstrate the stable hysteresis behaviour during the test and in contrast, the retrofitted ones displayed a stable hysteretic performance so that after ±3.5% drift level the systems had the same response to the displacements. Consequently, according to 3.2.2 of [ACI 374.1-05] that a frame shall be demonstrated as able to retain its structural integrity and support the gravity loads through peak drift ratios of 3.5%, the retrofitted techniques could properly satisfy the code requirements.
- The developed strength of the retrofitted specimens in comparison with the reference units not only dramatically increased but also reasonably stabilized so that the increasing of lateral strength in positive direction of BD category was observed to 245 and 289% for BD-H1 and BD-H3-D, respectively and in negative direction of SD category was monitored to 165% for SD-H2-D.
- The retrofitted specimens compared to the reference ones demonstrated a considerable enhancement in stiffness so that the initial stiffness in the category of BD developed to 156 and 168% for BD-H1 and BD-H3-D, respectively and in the category of SD increased to 145% for SD-H2-D. Meantime, the upgraded specimen BD-H3-D illustrated a higher performance. Therefore, according to R9.1.1 of [ACI 374.1-05], the higher nominal strength capacity would be expected to develop before the drift ratio exceeds an initial drift ratio consistent with the allowable story drift limitations.
- The columns of reference units were not able to carry the initial vertical imposed loads of 300kN to the end of the test so that at the end (3.5% drift level) 145 and 29kN was recorded for BD-B and SD-B, respectively, while the all retrofitted ones were capable of support the initial load to the end of the test (4.5% drift level).
- The retrofitted specimens were able to retain the lateral and vertical carrying capacity during the test particularly after the peak drift level of 3.5% which is proposed by ACI Committee 374 in 3.2.2 [ACI 374.1-05].
- The variation of maximum strength degradation in every test specimen with respect to the last cycle of 3.5% drift level (as a conservative limit according to 3.2.2 and R7.4 [ACI 374.1-05]) compared to the maximum acceptance criteria of 25% (R9.1.3 [ACI 374.1-05]) illustrated that the reference units could not satisfy the code requirements with demonstration of strength degradation more than 80%. In contrast, the all retrofitted ones displayed the acceptable degradation rate of lateral strength less than 25% which was 14, 11 and 24% for BD-H1, BD-H3-D and SD-H2-D, respectively.
- Exhibition of shear deformations in plastic hinge region could increase the rate of strength degradation and may provide early failure.

- Finally, the reference gravity load designed units could hardly withstand any lateral cyclic loading along with column static axial load due to poor detailing, insufficient reinforcement and inadequate bond capacity of the beam bottom longitudinal reinforcement and in contrast, the retrofitted ones could reasonably resist the load conditions. Therefore, the shortcomings of the vulnerable reference units were significantly improved by proposed retrofitting techniques (RT1 and RT2) for better performance.

6.1.1.2 Energy dissipation

- Both of retrofitting technique (RT1 and RT2) in the category of BD result to fat hysteresis loops. Therefore, the dissipated energy through these innovative methods should be considerable.
- In the all retrofitted specimens, energy dissipation in every cycle was uniformly increased which was not observed in reference gravity load designed units consequently; the recorded results exhibited a most significant appearance of seismic energy dissipation.
- Enhancement in energy dissipation was observed to be 391 and 417% for BD-H1 and BD-H3-D in the category of BD compared to BD-B and 249% for SD-H2-D in SD category compared to SD-B.
- The retrofitted specimens BD-H1, BD-H3-D and SD-H2-D demonstrated 42.42, 37.75 and 37.05% relative energy dissipation ratio, respectively which were significantly more than the minimum code-conforming rate of 12.5% proposed by R9.1.3 of [ACI 374.1-05]. Therefore, it is expected that an adequate damping for the frame as a whole and consequently, discontinuous oscillations for a considerable time after an earthquake, producing low-cycle fatigue effects, and non-excessive displacements will be resulted [ACI 374.1-05]. Comparison of these results with 30% which was reported by R3.2.1 of [ACI 374.1-05] for typical relative energy dissipation ratio at 3% drift level for reinforced concrete connections shows that the proposed retrofitting techniques (RT1 and RT2) could significantly provide higher amounts of energy abortion for the strengthened joints.
- Energy dissipation in reference gravity load designed units was mainly through the brittle damage in joint region while in retrofitted ones was gathered through ductile

behaviour of beam flexural hinging and energy dissipation devices such as HMFC and HHDP.

- Exhibition of shear deformations in plastic hinge region could decrease the rate of energy dissipation and may reduce the efficiency of installed energy dissipation devices.
-
- Estimating the contribution of the joint subassemblages for dissipation of energy in retrofitted specimens exhibited that for BD-H1, BD-H3-D and SD-H2-D the contribution of main bodies were about 87.5, 69.0 and 67.0%, the portions of HMFCs were nearly 12.5, 19.0 and 14.0%, and the shares of HHDPs were approximately 0.0, 12.0 and 19.0% , respectively.
- The total contribution of HMFCs and HHDPs for absorption of energy for BD-H1, BD-H3-D, and SD-H2-D was more than 47, 125, and 81% of the total energy which was dissipated by their reference units in their categories (BD or SD).
  -
  -

6.1.1.3 Damage mechanisms

- The undesirable brittle failures of the reference units through the joint shear failure and pulling-out of the beam bottom bars that led subsequently to the failing of column axial carrying capacity load were replaced by desirable ductile failure mechanism of beam flexural hinge far enough away of the joint in retrofitted specimens.
  -
  -

6.1.1.4 Hierarchy of strength

- In as-built unit of BD-B, joint first diagonal cracking and yielding the beam top bars were simultaneously occurred in -0.75% drift level and subsequently, maximum lateral strength was observed in $\pm 1.5\%$ drift while strength degradation was monitored after -2% and $+1.5\%$ drift level.
- In reference unit of SD-B, joint first diagonal cracking and yielding the beam bars were observed at the same time in $\pm 0.75\%$ drift level and then maximum lateral strength was recorded in -1.5 and $+2\%$ drift whereas beginning the strength degradation was occurred after $\pm 2.5\%$ drift level.

- The undesirable brittle behaviour of reference units was replaced by ductile performance in upgraded ones so that in all retrofitted specimens, as expected, yielding of HMFCs in ±0.75% drift level surpassed the yielding of the beam bars in ±1% drift. Subsequently, joint first diagonal cracking was observed in +1.5% drift and in BD-H3-D specimen, HHDPs started to yield in -1.5% and +2% drift. While maximum lateral carrying capacity was obtained in ±3.5% drift for BD-H3-D, for BD-H1-D and SD-H2-D was occurred in (-2.5%, +1.5%) and (-3.5%, +2.5%), respectively. The strength degradation for BD-H1 and SD-H2-D was started after ±3.5% while for BD-H3-D was not recorded any degradation of strength.

6.1.1.5 Joint behaviour

- The joint principal tensile stress corresponding to the first diagonal shear crack was averagely obtained equal to $0.310\sqrt{f'_c}$.
- The average amount for joint shear deformation (γ) at first diagonal shear cracking was obtained equal to 0.0008 and 0.001 Radian for reference units and retrofitted ones. Consequently, the average amount for all test specimens was 0.0009 Radian.
- While the average amount of maximum joint horizontal shear stress for reference units was obtained equal to $0.775\sqrt{f'_c}$, the code conforming nominal shear strength of joint proposed by ACI-ASCE 352R-02 and Euro code 8 was equal to $1.0\sqrt{f'_c}$ and $1.65\sqrt{f'_c}$, respectively. Therefore, the proposed code conforming nominal shear strength of joint were less than recorded amount for as-built test specimens and thus could not be acceptable.

6.1.1.6 Decomposition of lateral displacement

- In reference specimens of BD-B and SD-B, the total percentage contributions of beam, column and joint in lateral displacement were about 53, 25, and 24%, respectively.
- In retrofitted specimen BD-H1, the total percentage contributions of beam, column and joint in lateral displacement were 90, 7, and 3%, respectively.

- In retrofitted specimen of SD-H2-D and BD-H3-D, the total percentage contributions of beam, column and joint in lateral displacement were about 81, 14.5, and 4.5%, respectively.
- In upgraded specimens through Retrofitting Technique 2 (RT2) (BD-H3-D and SD-H2-D), because of using HHDPs in plastic hinge regions, the contribution of beams in comparison with the strengthened specimen through Retrofitting Technique 1 (BD-H1) were decreased.
- The retrofitted specimens could effectively transmit the deformations from high risk elements and points (column and joint) to the safety one and replaced the brittle performance with desired ductile behaviour.
- Utilizing of HHDPs or HFBDPs may decrease the contribution of beams in lateral displacement.

6.1.2 Conclusions of numerical study

- The numerical models showed very good correlation with the experimental results.
- The models were developed by ATENA exhibited that the validated models can be reasonably used for further investigations on performance of RC beam-column joints and retrofitted ones.
- To have a full plastic behaviour in HHDP elements, the D zone of the specimens should be effectively preserved against shear deformations.
- Based on the performance of specimens retrofitted through Retrofitting Techniques 1 and 2 (RT1 and RT2) and their efficiencies a new innovative Retrofitting Technique 3 (RT3) was proposed.
- The new numerically developed Retrofitting Technique 3 (RT3) showed that simultaneously activation of friction and bending strength by installation of innovative new device HFBDP at the end of HMFC resulted to a better performance in enhancing the lateral carrying capacity and energy dissipation.
- For retrofitted specimen through RT3 (BD-H1-F), the rate of strength with respect to the reference unit (BD-B) increased to more than 300 and 62% for positive and negative directions, respectively.
- Specimen BD-H1-F in comparison with the reference unit (BD-B) exhibited 525% more energy dissipation rate so that an extra amount of relative energy dissipation ratio was observed for this model equal to 51.62%.

- For BD-H1-F, the contribution of main body, HMFC and HFBDP in energy dissipation were estimated 65, 15 and 20%, respectively.

6.1.3 General conclusion

The upgraded units and subsequently the proposed retrofitting techniques (RT1, RT2 and RT3) demonstrated:

1. Ability to retain the structural integrity and support the imposed column axial loads after the peak drifts of 3.5%
2. The minimum reduction of load carrying capacity and stiffness in every drift level due to repletion of cycles
3. The limited level of strength degradation (<<0.25%) with respect to last cycle of 3.5% as a conservative drift
4. The higher amounts of initial stiffness to provide a higher nominal strength capacity before the drift ratio corresponding to the allowable story drift limitation
5. Significant total energy dissipation and the higher rate of relative energy dissipation ratio (>>1/8)
6. The desired ductile failure mechanism of beam flexural hinge based on the beam sidesway mechanism and strong column-weak beam performance
7. Ability to protect the joint panel by limiting the principal tensile stress demand
8. The transmitting of the deformations from high risk elements and points to the safety ones (from columns and joints to the beams) and replacement the brittle behaviour to the desired ductile performance
9. An excellent performance for innovative RT1, RT2 and particularly RT3.
10. Non-disruption, ease to installation, and practicability techniques for retrofitting the vulnerable RC beam-column joints in comparison with the well known upgrading methods

Consequently, it is claimed that the all acceptance criteria of ACI Committee 374 [ACI 374.1-05], in particular, and constructional issues, in general, were effectively satisfied by the proposed retrofitting techniques.

6.2 Recommendations for further research

In paved way of the above mentioned findings, the following recommendations are suggested for the further study:

- The findings should be compared with the FRP retrofitting strategies for the specimens with the same dimensions and strength.
- An economical study should be carried out amount the proposed retrofitting techniques and FRP retrofitting strategies.
- A study is necessary for investigation of locally confinement at the beam flexural plastic hinge.
- Experimentally and numerically research should be provided on the behavior of different forms of HMFC.
- Experimentally and numerically research should be provided on the behavior of different forms of HHDP.
- The effectiveness of the proposed retrofitting techniques on dynamic characteristics of RC structures is necessary to investigate.
- The presence of floor systems for the proposed retrofitting techniques should be studied.
- The presence of masonry infills for the proposed retrofitting techniques should be studied.
- The proposed retrofitting techniques should be investigated with special configuration of joint for instance joint with eccentric, deep, shallow, and wide beam.
- Different fastening systems for the proposed retrofitting techniques are necessary to study.
- Different alternatives of RT3 including HFBDP between steel-steel, steel-concrete as well as different prestressing loads and methods could be investigated.
- The effectiveness of different architectural configurations on proposed retrofitting techniques could be studied for instance using only bottom HMFCs.
- Experimentally and numerically investigation on the 3D systems of joints using the proposed retrofitting techniques.

References

[ACI 318-63] Committee 318, Building code requirements for structural concrete, American Concrete Institute (ACI), 1963

[ACI 318M-11] Committee 318, Building code requirements for structural concrete and commentary, American Concrete Institute (ACI), 2011

[ACI 352R-02] Joint ACI-ASCE committee 352, Recommendations for design of beam-column connections in monolithic reinforced concrete structures, American Concrete Institute, 2002, Reapproved 2010

[ACI 440.2R-02] Committee 440, Guide for design and construction of externally bonded FRP systems for strengthening concrete structures, American Concrete Institute (ACI), 2005

[ACI 374.1-05] Committee 374, Acceptance criteria for moment frames based on structural testing and commentary, American Concrete Institute, 2005

[ACI-ASCE Committee 326] Joint ACI-ASCE Committee 326, Shear and diagonal tension, ACI journal, Proceedings V. 59, No. 1, Jan. 1962, pp. 1-30, No. 2, Feb. 1962, pp. 277-334, No. 3, Mar. 1962. Pp. 352-396

[Adin et al.-93] Adin, M. A., Yankelevsky, D. Z., and Farhey, D. N., cyclic behavior of epoxy-repaired reinforced concrete beam-column joints, ACI Structural journal, March-April, 1993

[Alcocer et al.-93] Alcocer, S. M., and Jisrsa, J. O.: Strength of reinforced concrete frame connections rehabilitated by jacketing-ACI Structural journal, May-June, 1993

[Alkhrdhaji et al.-99] Alkhrdhaji, T., Nanni, A., Chen, G., and Barker, M., Upgrading the transportation infrastructure: Solid RC deck strengthened with FRP, Concrete international: Design and construction, Vol. 21, No. 10, pp. 37-41, 1999

[Almusallam et al.-09] Almusallam, T. H., Alsayed, S. H., Al-Salloum, Y. A., and Siddiqui, N. A., Seismic response of FRP-strengthened corner RC beam-column joints, Concrete repair, rehabilitation and retrofitting II, Alexander et al. (eds), Taylor & Francis group, London, ISBN 978-0-415-46850-3, pp. 1157-1162, 2009

[Anderson et al.-96] Anderson, D., L., Mitchell, D., and Tinawi, R. G., Performance of concrete bridge during Hyogo-Ken Nanbu (Kobe) earthquake on January 17, Canadian journal of civil engineering, 23(3), 714-726, 1996

[Antonopoulos -03] Antonopoulos, C. P., and Triantafillou, T. C., Experimental investigation of FRP-strengthened RC beam-column joints, Journal of composites for construction, pp. 39-49, Feb. 2003

[ATENA-Theory-06] Cervenka,V., Jendele, L., and Cervenka, J., ATENA program documentation-Part 1- Theory, Cervenka Consulting, Sep. 2006

[Aycardi et al.-92] Aycardi, L. E., Mander, J. B. andReinhorn, A. M.: Seismic resistance of reinforced concrete structures designed only for gravity loads: Part II-Experimental performance of subassemblages, Technical report NCEER-92-0028, SUNY/Buffalo, 1992

[Aycardi et al.-94] Aycardi, L. E., Mander, J. B. andReinhorn, A. M.: Seismic resistance of reinforced concrete frame structures designed only for gravity loads: Experimental performance of subassemblages, ACI Structural journal, Sep.-Oct. 1994

[Beres et al.-92] Beres, A., El-Borgi, S., White, R. N., and Gergely, P.: Experimental results of repaired and retrofitted beam-column joint tests in lightly reinforced concrete frame buildings, Technical report NCEER-92-0025, SUNY-Buffalo, 1992

[Biddah et al.-97] Biddah, A., Ghobarah, A., and Aziz, T. S., Upgrading of nonductile reinforced concrete frame connections, Journal of structural engineering, August, 1997

[Biddah-04] Biddah, A., and Ghobarah, A., Strengthening of inadequate anchorage of beam reinforcement in beam-column joints, Emirates journal for engineering research, 9 (2), 83-89, 2004

[Bracci et al.-95-1] Bracci, J. M., Reinhorn, A. M. andMander, J. B.: Seismic resistance of reinforced concrete frame structures designed for gravity loads: Performance of structural system, ACI Structural journal, Sep.-Oct. 1995

[Bracci et al.-95-2] Bracci, J. M., Reinhorn, A. M. andMander, J. B.: Seismic retrofit of reinforced concrete buildings designed for gravity loads: performance of structural model, ACI Structural journal, Nov.-Dec. 1995

[Calvi et al.-02] Calvi, G. M., Magenes, G. andPampanin, S.: Relevance of beam-column joint damage and collapse in RC frame assessment, Journal of earthquake engineering, Vol. 6, special issue 1 (2002) 75-100, Imperial college press

[Calvi et al.-Sep. 02] Calvi, G. M., Magenes, G. andPampanin, S.: Experimental test on a three story R.C. frame designed for gravity only, 12th European conference on earthquake engineering, paper reference 727, London, UK, Sep. 2002

[CEB-FIP-90] Comite Euro-International Du Beton,: CEB-FIP MODEL CODE 1990, Design code, Thomas Telford Service Ltd, 1993

[Chaimahawan-09] Chaimahawan, P., Pimanmas, A., Seismic retrofit of substandard beam-column joint by planar joint expansion, Material and structures, 42: 443-459, 2009

[Chen et al.-96] Chen, S.J., Yeh, C.H., and Chu, J.M., Ductile steel beam-to-column connections for seismic resistance, Journal of structural engineering, pp.1292-1299, 1996

[Chen-06] Chen, T. H., Retrofit strategy of non-seismically designed frame systems based on a metallic haunch system, MSc dissertation, University of Canterbury, 2006

[Choudhuri et al.-92] Choudhuri, D., Mander, J. B., and Reinhorn, A. M., Evaluation of seismic retrofit of reinforced concrete frame structures: Part I- Experimental performance of retrofit subassemblages, Technical report NCEER-92-0030, SUNY/Buffalo, 1992

[Clyde et al.-00] Clyde, C., Pantelides, C., and Reaveley, L. D.: Performance –based evaluation of exterior reinforced concrete building joints for seismic excitation, PEER report 2000/05, Pacific earthquake engineering research center, College of engineering, University of California, Berkeley, July 2000

[Corazao -89] Corazao, M, Durrani, A. J., Repair and strengthening of beam-to-column connections subjected to earthquake loading, Technical report NCEER-89-0013, SUNY/ Buffalo, 1989

[Costa-03] Costa, J. L. D., Reinforced concrete under large seismic action, DanmarksTekniskeUniversitet, Report BYG.DTU, R-076, 2003

[D'Ayala et al.-03] D'Ayala, D., Penford, A., Valentini, S., Use of FRP fabric for strengthening of reinforced concrete beam-column joints, 10th international conference on structural faults and repair, London, 2003

[De Lorenzis et al.-00] De Lorenzis, L., Nanni, A., La Tegola, A., Strengthening of reinforced concrete structures with near surface mounted FRP rods, International meeting on composite materials, PLAST 2000, Proceedings, Advanced with composites 2000, Ed. I. Crivelli-Visconti, Milan, Italy, May 9-11, pp. 419-426, 2000

[Durrani-87] Durrani, A. J., and Zerbe, H. E.: Seismic resistance of R/C exterior connections with floor slab, Journal of structural engineering, 113(8): 1850-64, 1987

[Ehsani-85-1] Ehsani, M. R. ,and Wigh, J., K.: Effect of transverse beams and slabs on behavior of reinforced concrete beam-to-column connections, ACI journal, March-April 1985

[Ehsani-85-2] Ehsani, M. R. ,and Wigh, J., K.: Exterior reinforced concrete beam-column connections subjected to earthquake type loading, ACI journal, July-August 1985

[El-Amoury-02] El-Amoury, T., Ghobarah, A., Seismic rehabilitation of beam-column joint using GFRP sheets, Engineering structures 24- 1397-1407

[Engindeniz et al.-05] Engindeniz, M., Kahn, L. F., and Zureick, A.-H.: Repair and strengthening of reinforced concrete beam-column joints: State of the art, ACI structural journal, March-April, 2005

[Engindeniz-08] Engindeniz, M., Repair and strengthening of pre-1970 reinforced concrete corner beam-column joints using CFRP composites, PhD dissertation, Georgia institute of technology, 2008

[EN 1998-1:2004] EN 1998-1:2004, Eurocode 8: Design of structures for earthquake resistance- Part 1: General rules, seismic actions and rules for buildings, The European standard, 2004

[Fardis-09] Fardis, M. N., Seismic design, assessment and retrofitting of concrete buildings based on EN-Eurocode 8, ISBN 978-1-4020-9841-3, Springer Dordrecht Heidelberg London New York, 2009

[Filiatrault-96] Filiatrault, A., and Lebrun, I.: Seismic rehabilitation of reinforced concrete joints by epoxy pressure injection technique, Seismic rehabilitation of concrete structures, SP 160, Amexcrican concrete institute, pp 73-92, June 1, 1996

[French et al.-90] French, C. W., Throp, G. A., and Tsai, W.-J., Epoxy repair techniques for moderate earthquake damage, ACI Structural journal, Jul.-Aug. 1990

[Geng et al.-98] Geng, Z.-J., Chajes, M. J., Chou, T.-W., and Yen-Cheng-Pan, D., The retrofitting of reinforced concrete column-to-beam connections, Composites science and technology 58, 1297-1305, 1998

[Ghobarah-01] Ghobarah, A., Said, A., Seismic rehabilitation of beam-column joints using FRP laminates, Journal of earthquake engineering, Vol. 5, No. 1, pp. 113-129, Imperial college press, 2001

[Ghobarah-02] Ghobarah, A., Said, A., Shear strengthening of beam-column joints, Engineering structures, 24, pp. 881-888, 2002

[Ghobarah-05] Ghobarah, A., El-Amoury, T., Seismic rehabilitation of deficient exterior concrete frame joints, Journal of composites for construction, ASCE, Sep.-Oct., 2005

[Grünthal-04] Grünthal, G.: Erdbeben und Erdbebengefährdung in Deutschland sowie im europäschen Kontext-Geographie und Schule, 151, 14-23, 2004

[Hegger et al.-03] Hegger, J., Sherif, A., and Roeser, W.: Nonseismic design of beam-column joints, ACI Structural journal, Sep.-Oct. 2003

[Ilki et al.-11] Ilki, A., Bedirhanoglu, I., and Kumbasar, N., Behavior of FRP-retrofitted joints built with plain bars and low-strength concrete, Journal of composite for construction, ASCE, May-June, 2011

[Karayannis et al.-98] Karayannis, C. G., Chalioris, C. E., and Sideris, K. K., Effectiveness of RC beam-column connection repair using epoxy resin injections, Journal of earthquake engineering, V. 2. No. 2, pp. 217-240, 1998

[Lee-76] Lee, D. L. N., Original and repaired reinforced concrete beam-column subassemblages subjected to earthquake type loading, Report No. UMEE 76R4, Department of civil engineering, The university of Michigan, Ann Arbor, Michigan, U.S.A., April 1976

[Li-11] Li, B., Kai, Q., Seismic behavior of reinforced concrete interior beam-wide column joints repaired using FRP, Journal of composite for construction, May-June, 2011

[Megget-74] Megget, L. M.: Cyclic behaviour of exterior reinforced concrete beam-column joints, Bull. Of the New Zealand national society for earthquake engineering 7(1), 1974

[Mahini-07] Mahini, S. S., Ronagh, H. R., A new method for improving ductility in existing RC ordinary moment resisting frames using FRPS, Asian journal of civil engineering (Building and housing) Vol. 8, No. 6, pp. 581-595, 2007

[Moehle] Moehle, J. P.: State of research on seismic retrofit of concrete building structures in the US, US-Japan symposium and workshop on seismic retrofit of concrete structures-
State of research and practice

[Moehle-91] Moehle, J. P., and Mahin, S. A.: Observation on the behavior of reinforced concrete buildings during earthquakes, Earthquake-resistant concrete structures inelastic response and design, ACI SP-127, ed. Ghosh, S. K., Detroit, 1991

[Mosallam-00] Mosallam, A. S., Strength and ductility of reinforced concrete moment frame connections strengthened with quasi-isotropic laminates, Composites: Part B, 31-481-497, 2000

[Muguruma et al.-95] Muguruma, H., Nishyiyama, M., and Watanabe, F., Lessons learned from the Kobe earthquake-a Japanese perspective, PCI Journal, 40(4), 28-42, 1995

[Mukherjee-05] Mukherjee, A., and Joshi, M., FRPC reinforced concrete beam-column joints under cyclic excitation, Composite structures, 70, 185-199, 2005

[NPO, Geologischer Dinst NRW-07] NPO, Geologischer Dienst NRW-www.scinexx.de-Das Wissenschaftmagazin, 12.07.2007

[Pampanin et al.-04] Pampanin, S., Bolognini, D., Pavese, A., Magenes, G., and Calvi, G.M., Multi-level seismic rehabilitation of existing frame systems and subassemblies using FRP composites, Adelaide, Australia: CICE2004, 2nd International conference on FRP composites in civil engineering, Dec. 2004

[Pampanin et al.-06] Pampanin, S., Christopoulos, C., and Chen, T.-H. , Development and validation of a metallic haunch seismic retrofit solution for existing under-design RC frame buildings, Earthquake engineering and structural dynamics, 35:1739-1766, 2006

[Pampanin et al.-07] Pampanin, S., Akguzel, U., and Attanasi, G., Seismic upgrading of 3-D exterior R.C. beam column joints subjected to bi-directional cyclic loading using GFRP composites, FRPRCS-8, University of Patras, Patras, Greece, July 16-18, 2007

[Pantazopoulou-92] Pantazopoulou, S., and Bonacci, J.: Consideration of questions about beam-column joints, ACI Structural journal, Jan.-Feb. 1992

[Pantelides et al.-02] Pantelides, C. P., Hansen, J., Nadauld, J., and Reaveley, L. D.: Assessment of reinforced concrete building exterior joints with substandard details, PEER report 2002/18, Pacific earthquake engineering research center, College of engineering, University of California, Berkeley, May 2002

[Paulay et al.-78] Paulay, T., Park, R., and Priestley, M. J. N., Reinforced concrete beam-column joints under seismic actions, Journal ACI, Vol. 75, No. 11, pp. 585-593, 1978

[Paulay and Priestley-92] Paulay, T., Priestley, M. J. N., Seismic design of reinforced concrete and masonry buildings, ISBN 0-471-54915-0, John Wiley & Sons, Inc., 1992

[Prota et al.-04] Prota, A., Nanni, A., Manfredi, G., and Cosenza, E., Selective upgrade of underdesignedreinforced concrete beam-column joints using carbon fiber-reinforced polymers, ACI Structural journal, Sep.-Oct., 2004

[Saatcioglu et al.-01] Saatcioglu M., Mitchell, D., Tinawi, R., Gardner, N. J., Gillies, A. G., Ghobarah, A., Anderson, D., L., and Lau, D., The August 17, 1999 Kacaeli (Turkey) earthquake-damage to structures, Canadian journal of civil engineering, 28(4), 715-737, 2001

[Said-04] Said, A., Nehedi, M., Use of FRP for RC frame in seismic zones: Part I. Evaluation of FRP beam-column joint rehabilitation techniques, Applied composite materials, 11: pp. 205-226, Kluwer academic publishers, 2004

[Said-08] Said, A., Nehedi, M., Rehabilitation of RC frame joints using local steel bracing, Structure and infrastructure engineering, Vol. 4, No. 6, 431-447, Dec. 2008

[Shannag-05] Shannag, M. J., and Alhassan, M. A., Seismic upgrade of interior beam-column subassemblages with high-performance fiber-reinforced concrete jackets, ACI Structural journal, Jan.-Feb., 2005

[Shih et al.-01] Shih, M.-H., Cheng, C.-T., and Tung, H.-Y., Experimental validation of retrofitted or repaired beam-column joints by using concrete jacket, First international conference on planning and design, p. 37, Tainan, Nov. 3-4, 2001

[Townsend-77] Townsend, W. H., and Hanson, R. D.: Reinforced concrete connection hysteresis loops, ACI SP53-13, Reinforced concrete structures in seismic zones, 351-70, 1977

[Tsonos-99] Tsonos, A. G., Lateral load response of strengthened reinforced concrete beam-to-column joints, ACT Structural journal, Jan.-Feb., 1999

[Uma and Jain] Uma, S. R., and Jain, S. K, Seismic behaviour of beam column joints in reinforced concrete moment resisting frames, Document No.: IITK-GSDMA-EQ32-V1.0, Final report: A-Earthquake codes, IITK-GSDMA Project on building codes

[Uzumeri -77] Uzumeri, S. M.: Strength and ductility of cast-in-place beam-column joints, ACI SP 53, Reinforced concrete structures in seismic zones, 1977

[Wang-09] Wang, Y.-C., Hsu, K., Shear strengthof RC jacketed interior beam-column joints without horizontal shear reinforcement, ACI structural journal, March-April, 2009

Appendix A: Supplementary Reviews of Laboratory Activities

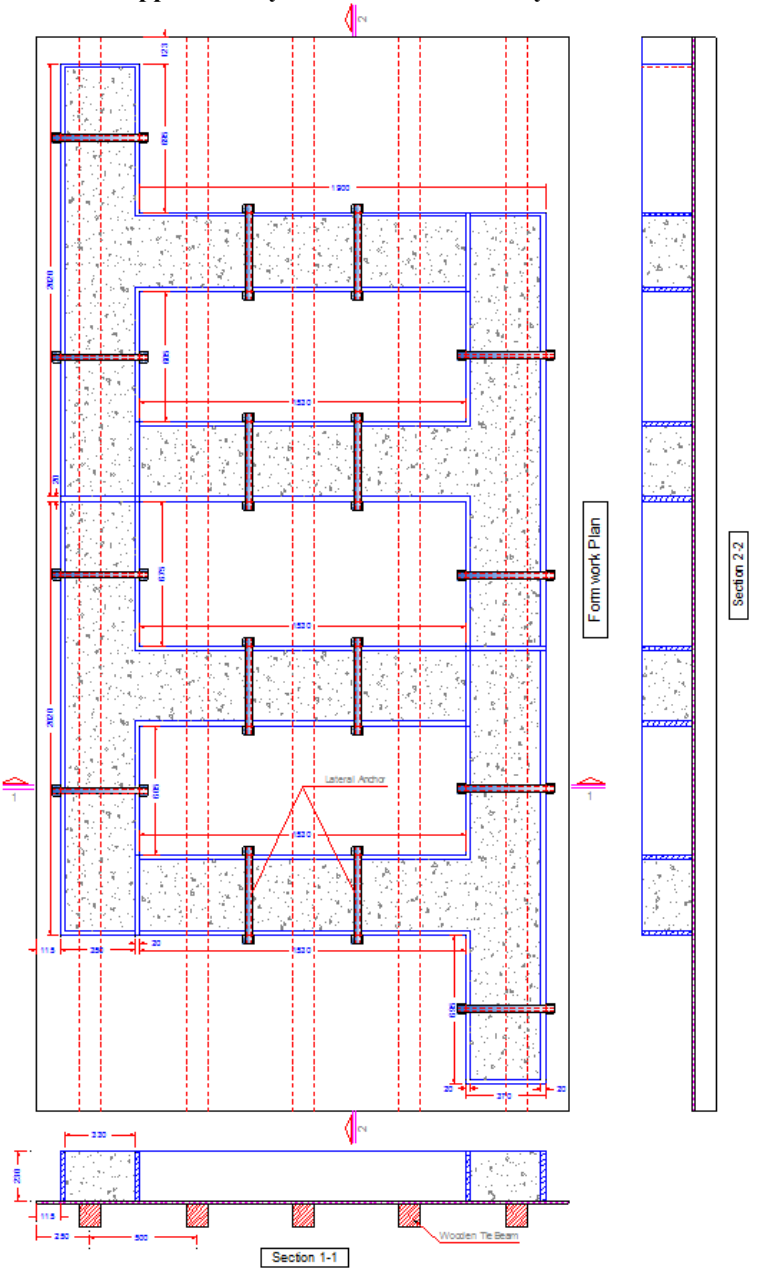

Fig. A.1: Formwork Plan

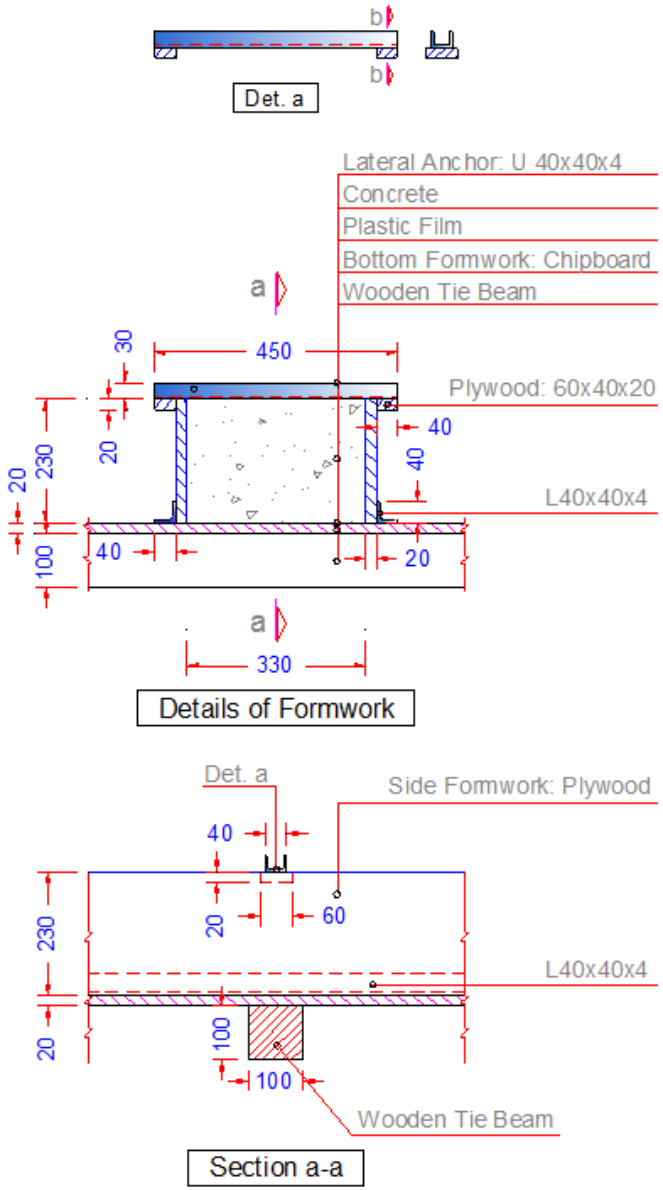

Fig. A.2: Details of formwork

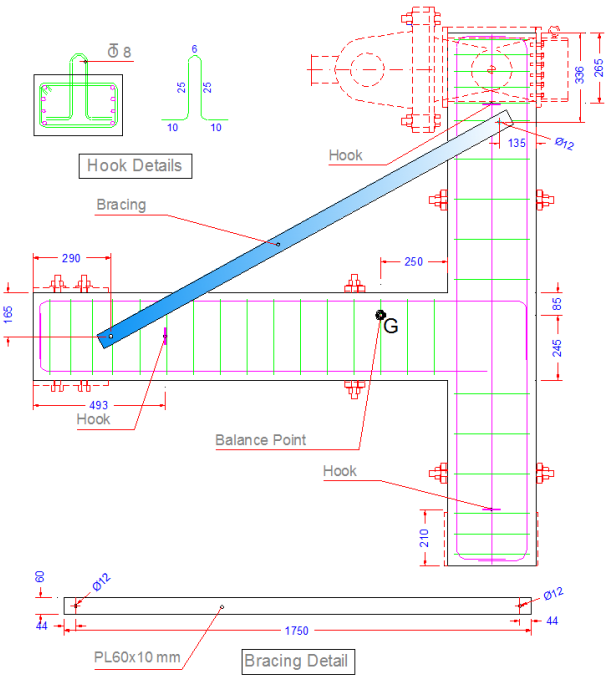

Specimen bracing, hooks and balance point

(a)

(b)

Fig. A.3: a) Specimen bracing, b) Formwork and bracing

Appendix B: Scheme and Details of Loading Setup

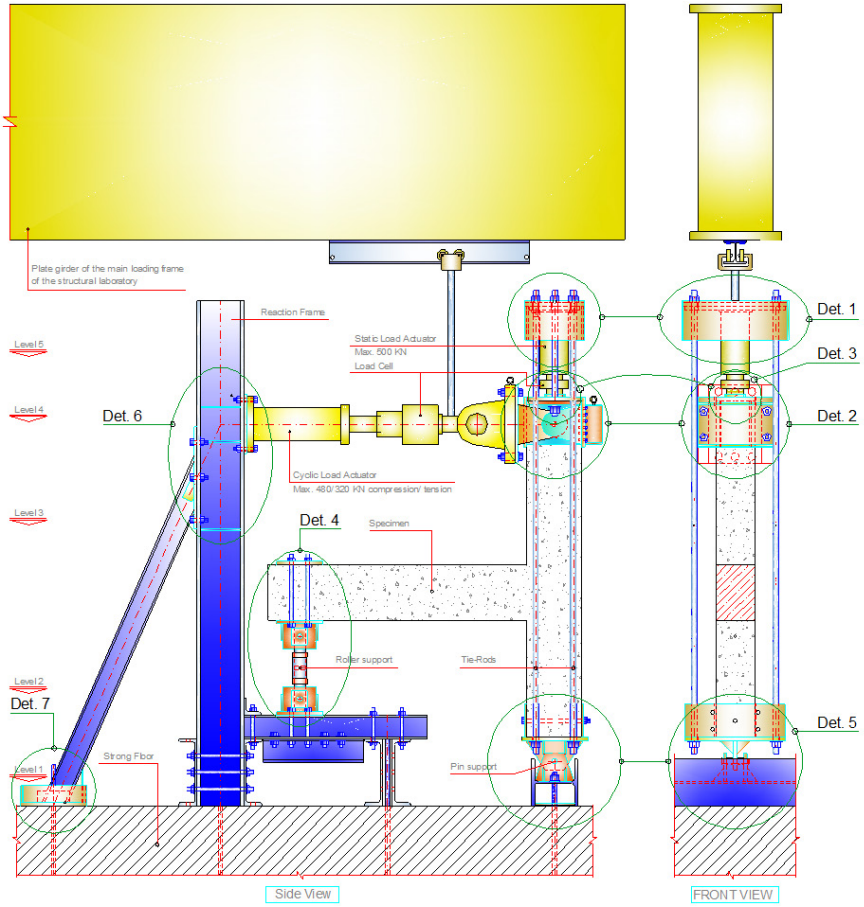

Fig. B.1: Designed loading setup

Fig. B.2: Fabricated loading setup

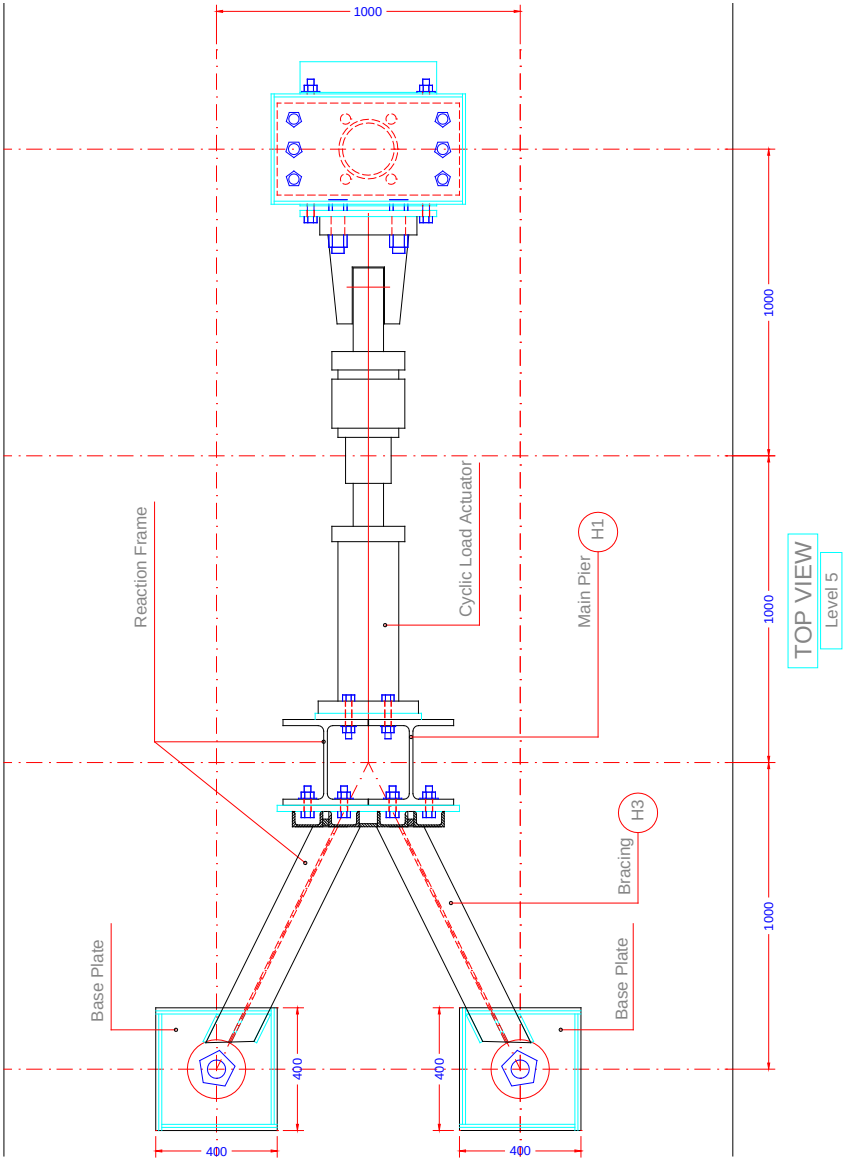

Fig. B.3: Loading setup: Top view of level 5

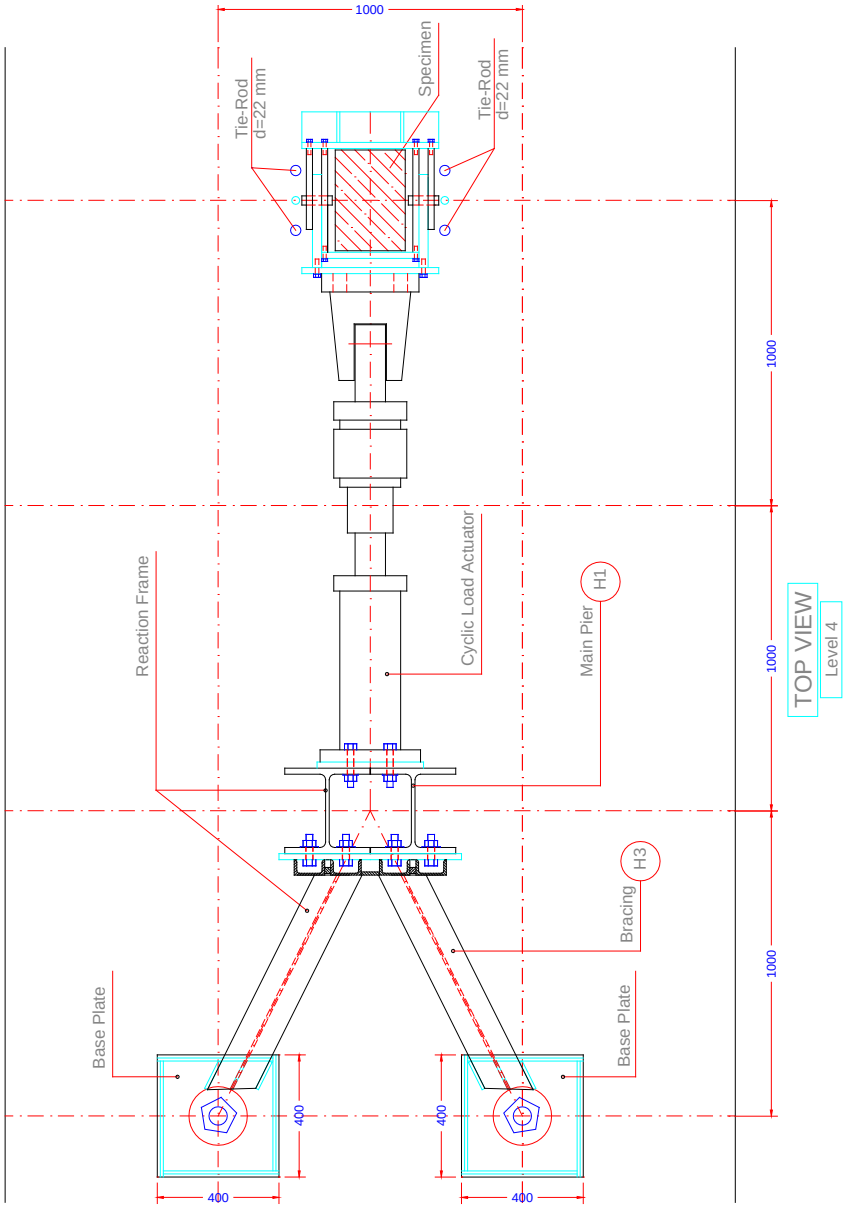

Fig. B.4: Loading setup: Top view of level 4

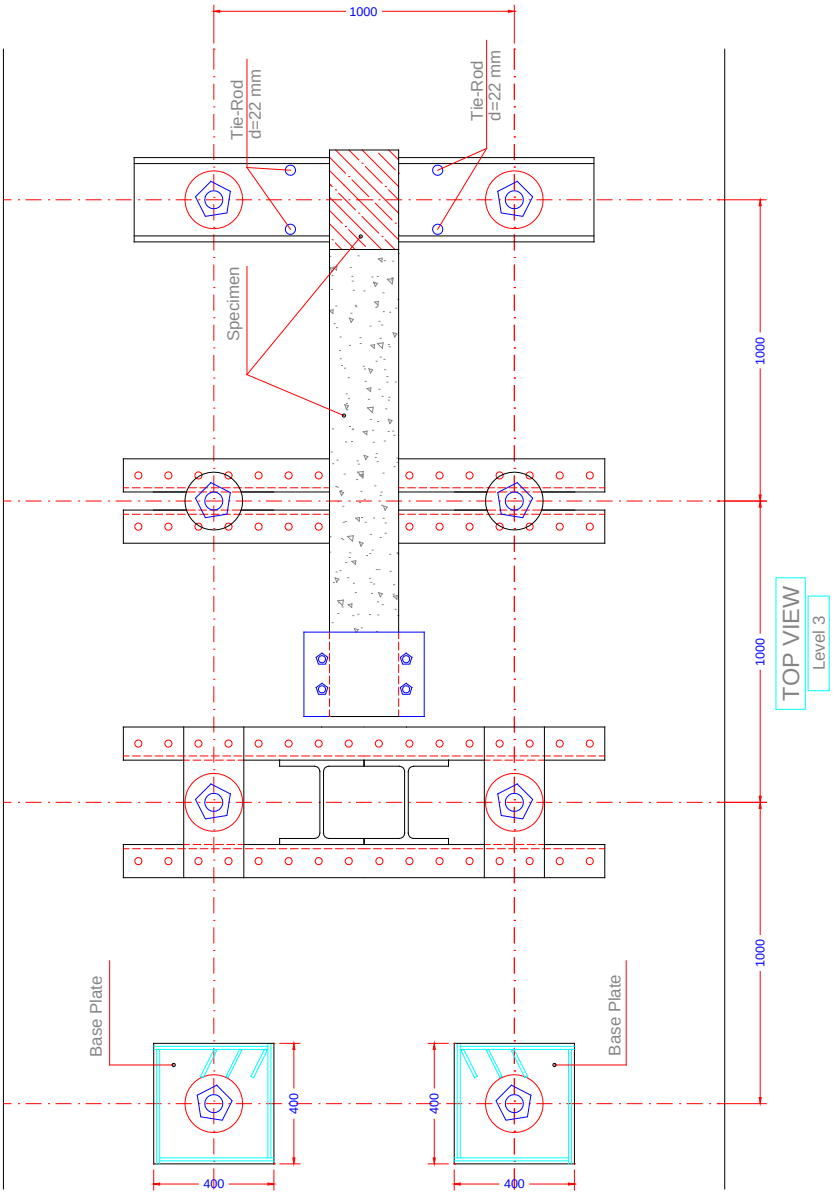

Fig. B.5: Loading setup: Top view of level 3

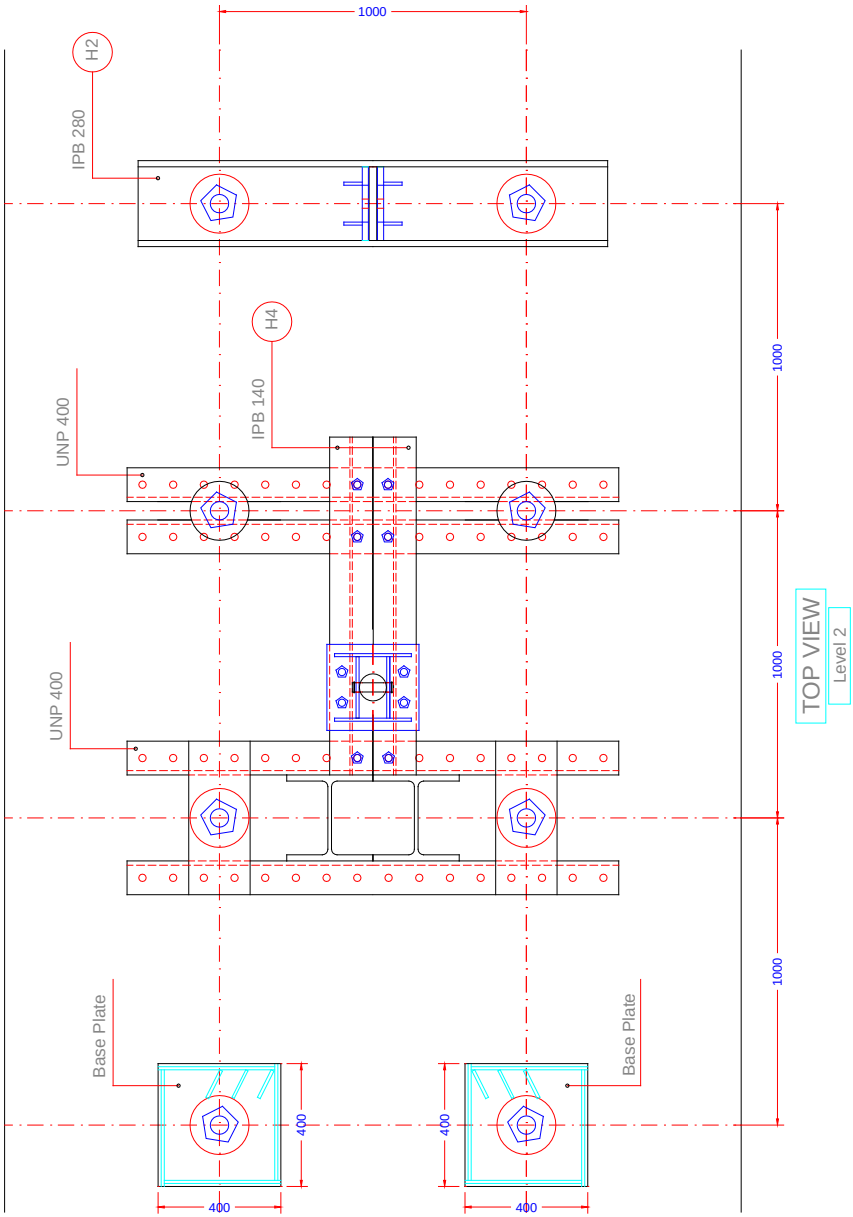

Fig. B.6: Loading setup: Top view of level 2

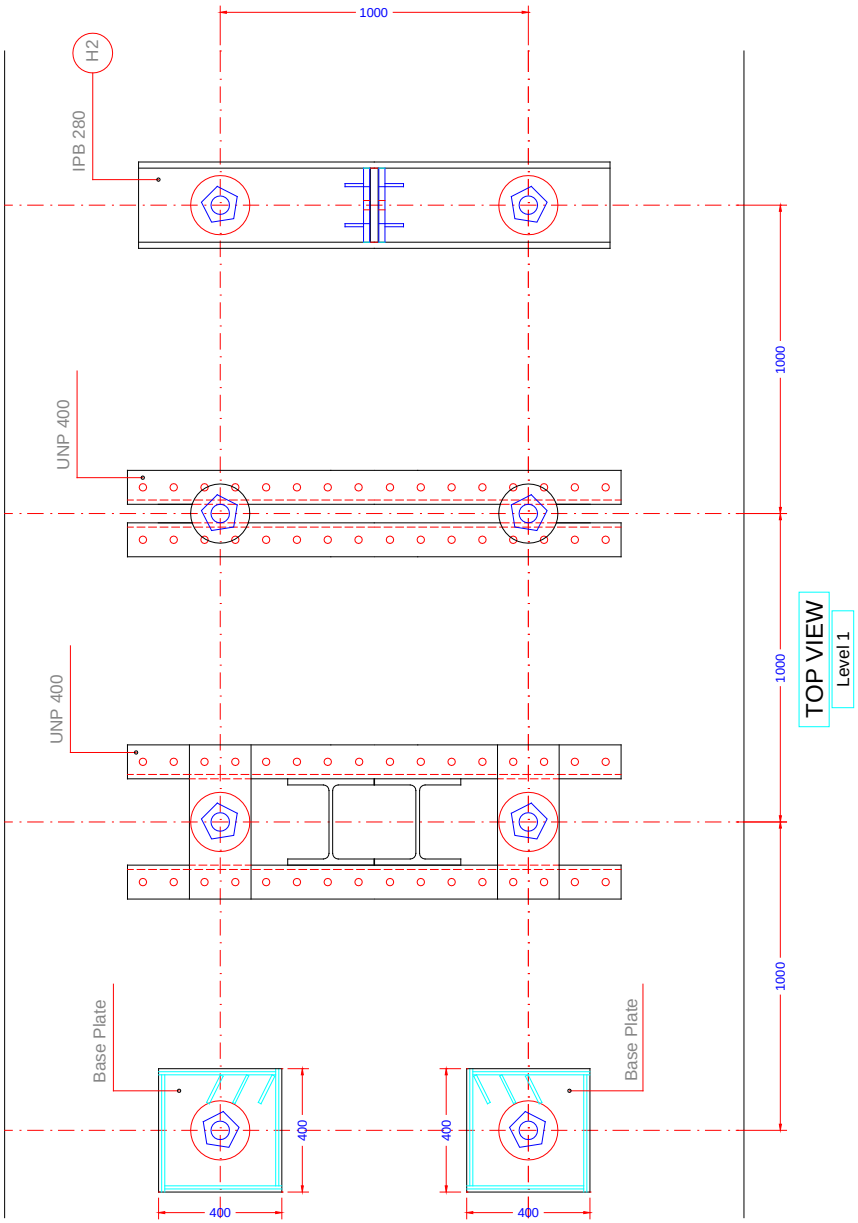

Fig. B.7: Loading setup: Top view of level 1

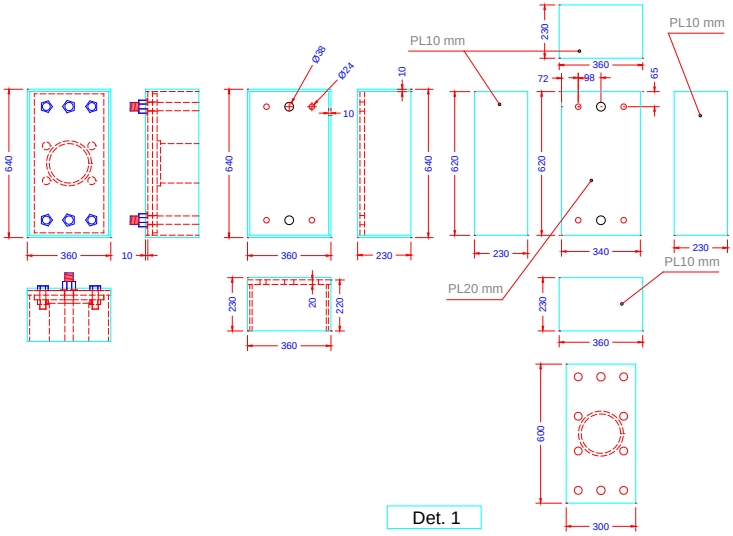

Fig. B.8: Loading setup: Details of top compartment (Det. 1)

Fig. B.9: Loading setup: Fabricated top compartment

Considering that the cyclic actuator of the structural laboratory had only one mechanical hinge, it was investigated that another one is needed to avoid the risks of unexpected lateral loads on cyclic actuator and satisfy the free rotation at the top of the column. Therefore because of limited space to locate second hinge it was decided to fabricate it in the intersection axis of cyclic actuator and column. The necessity justifications of the second mechanical hinge are displayed in Fig.B.10 to B.12.

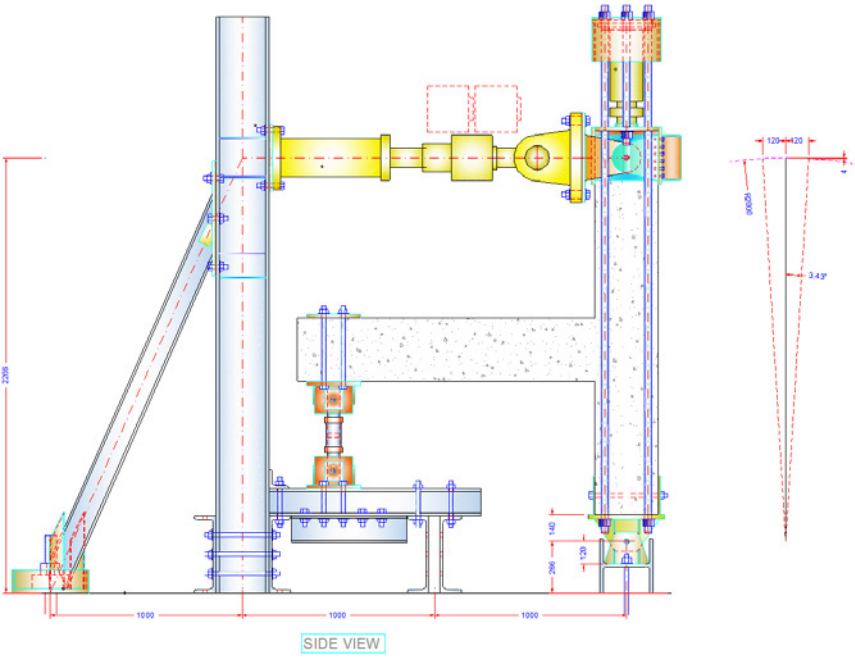

Fig. B.10: Loading setup: Checking the necessity of second mechanical hinge, balance case

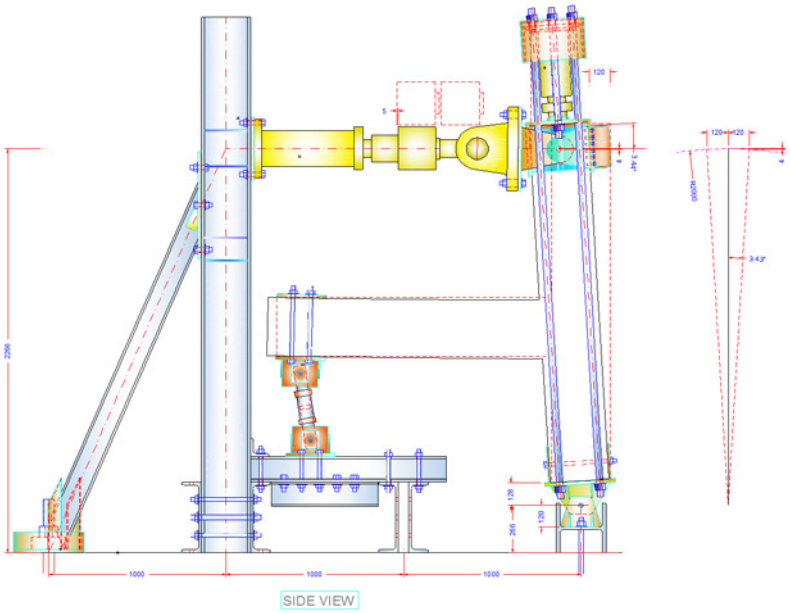

Fig. B.11: Loading setup: Checking the necessity of second mechanical hinge, side sway to left

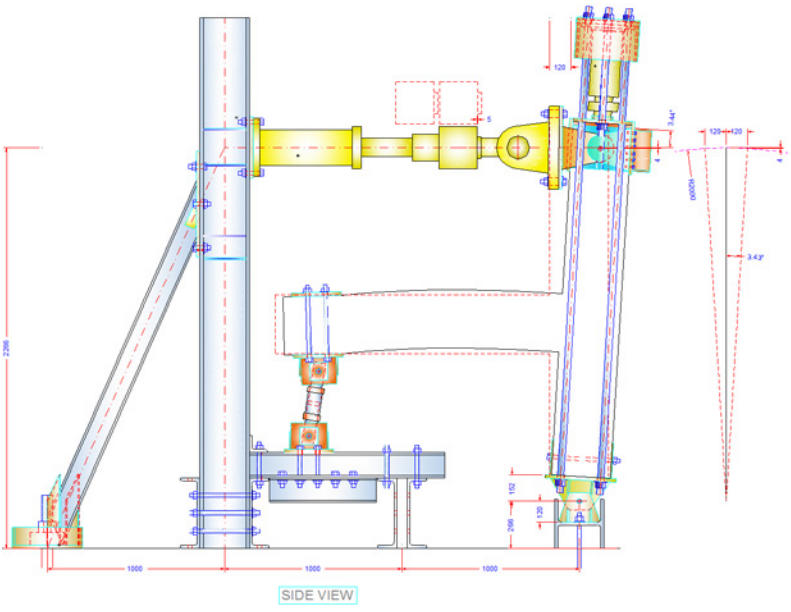

Fig. B.12: Loading setup: Checking the necessity of second mechanical hinge, side sway to right

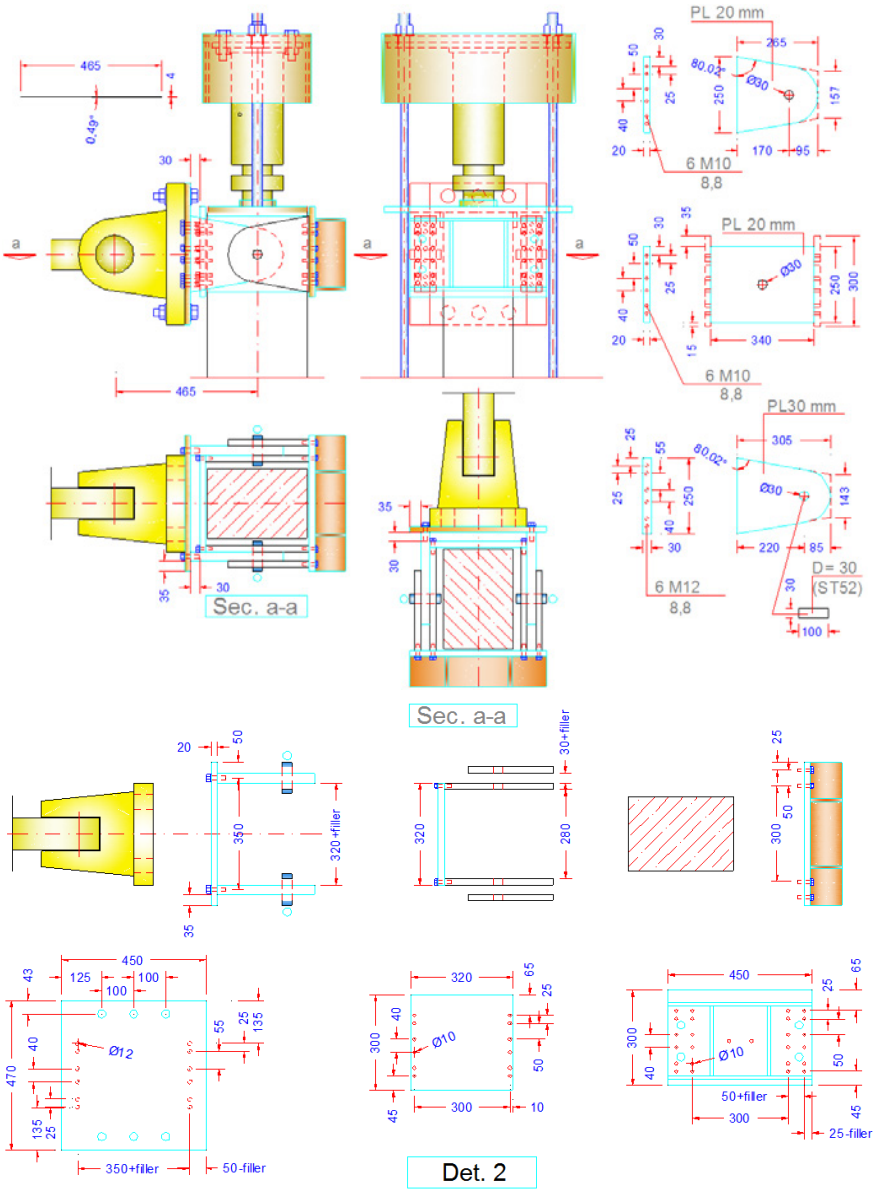

Fig. B.13: Loading setup: Details of designed second mechanical hinge

Fig. B.14: Loading setup: Fabrication of second mechanical hinge

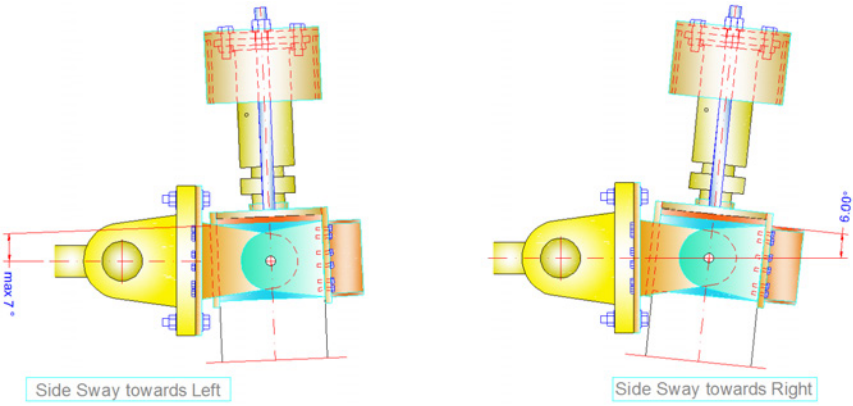

Fig. B.15: Loading setup: Second mechanical hinge, Max. allowable rotation

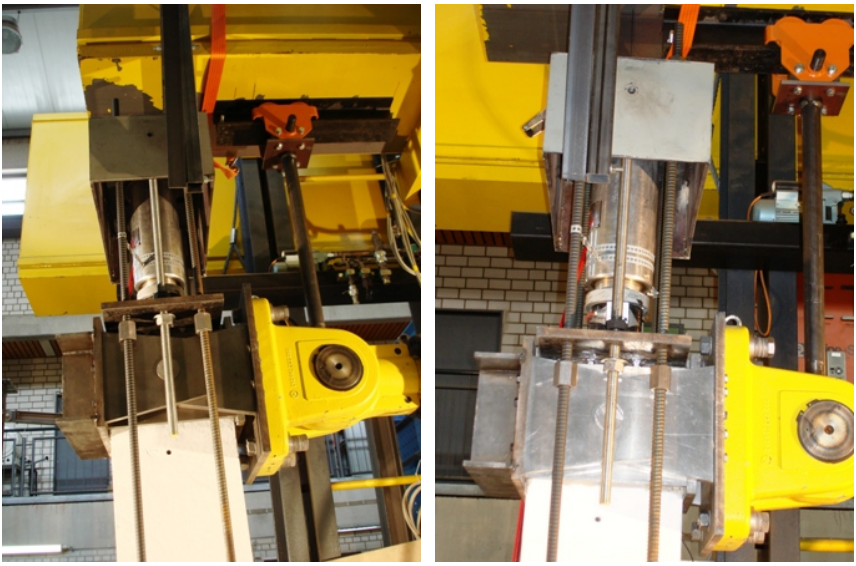

Fig. B.16: Loading setup: Rotation of second mechanical hinge

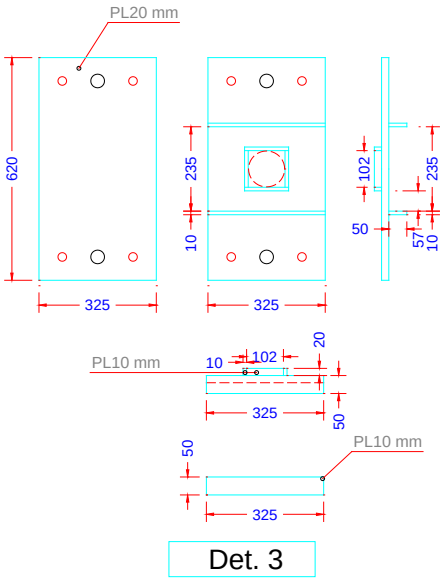

Fig. B.17: Loading setup: Details of top compartment (Det. 3)

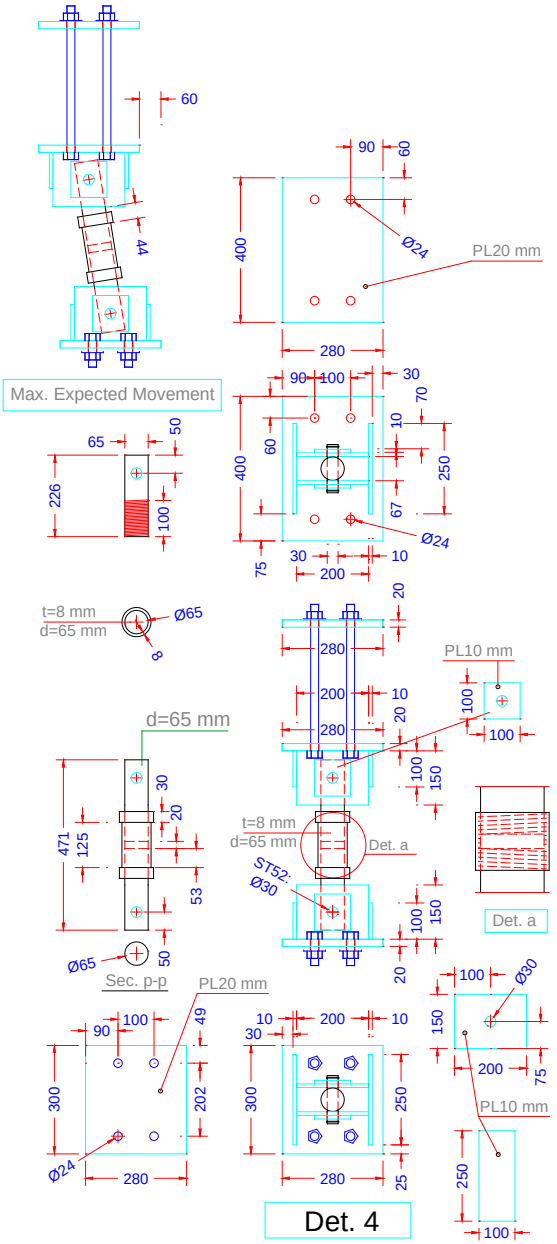

Fig. B.18: Loading setup: Details of movable support (Det. 4)

Fig. B.19: Loading setup: Fabrication of movable support (Det. 4)

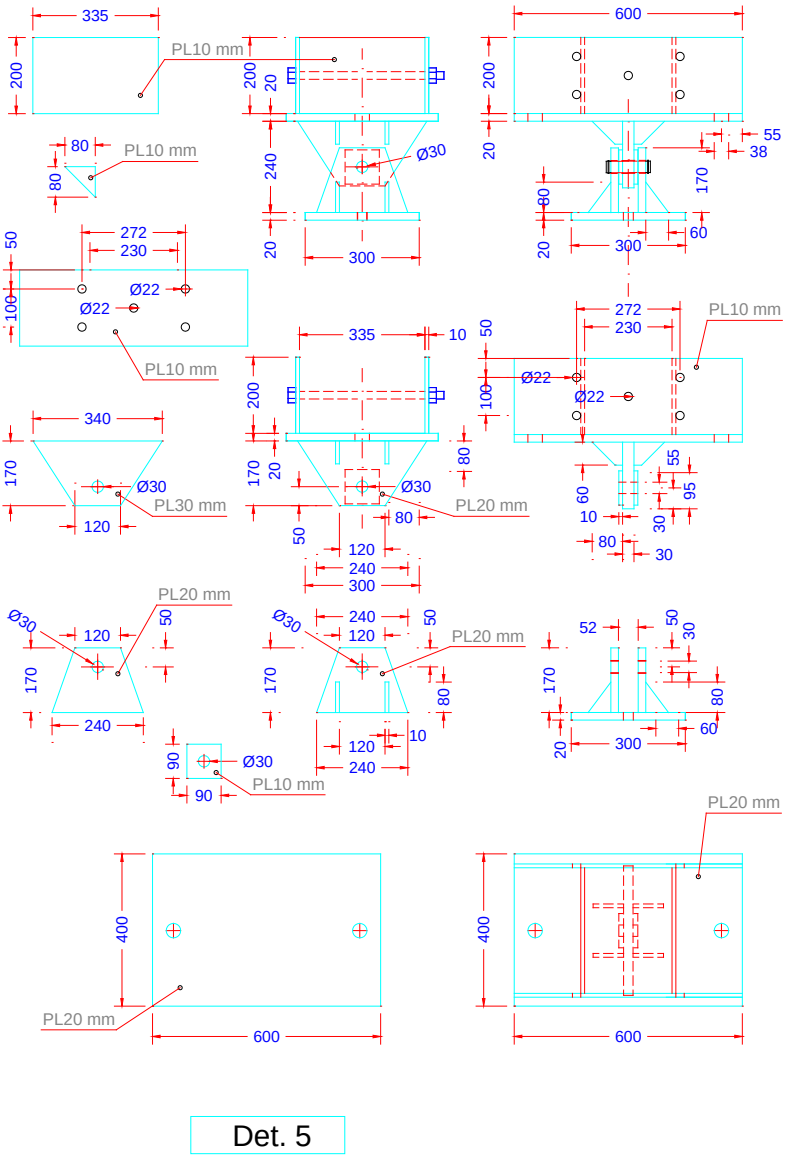

Fig. B.20: Loading setup: Details of fixed hinge (Det. 5)

Fig. b.21: Loading setup: Fabrication of fixed support (Det. 5)

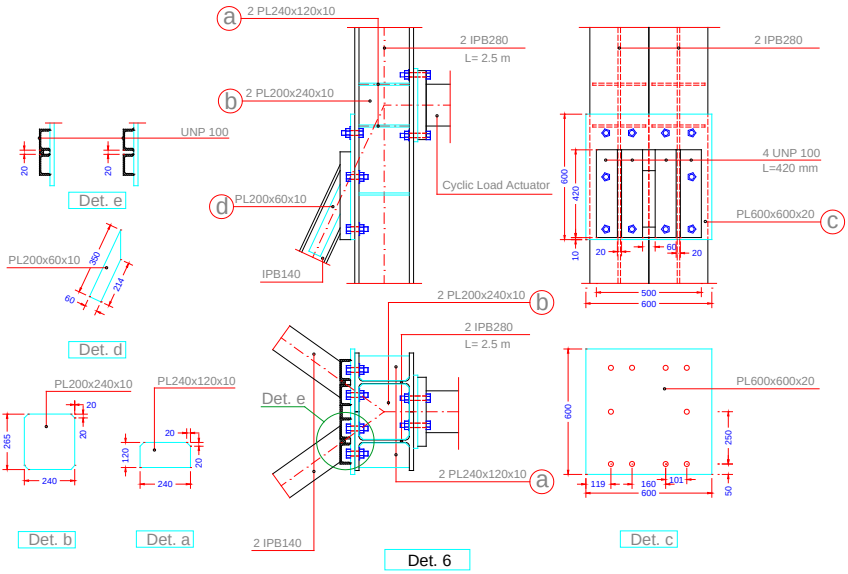

Fig. B.22: Loading setup: Details of reaction frame (Det. 6)

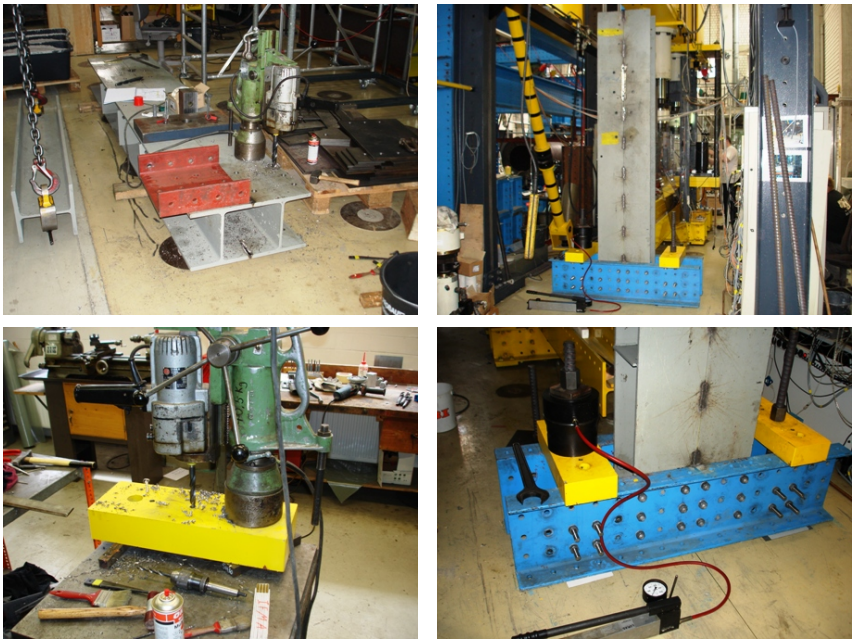

Fig. B.23: (continued)

Fig. B.23: (continued)

Fig. B.23: Loading setup: Fabrication of reaction frame and its connection (Det. 6)

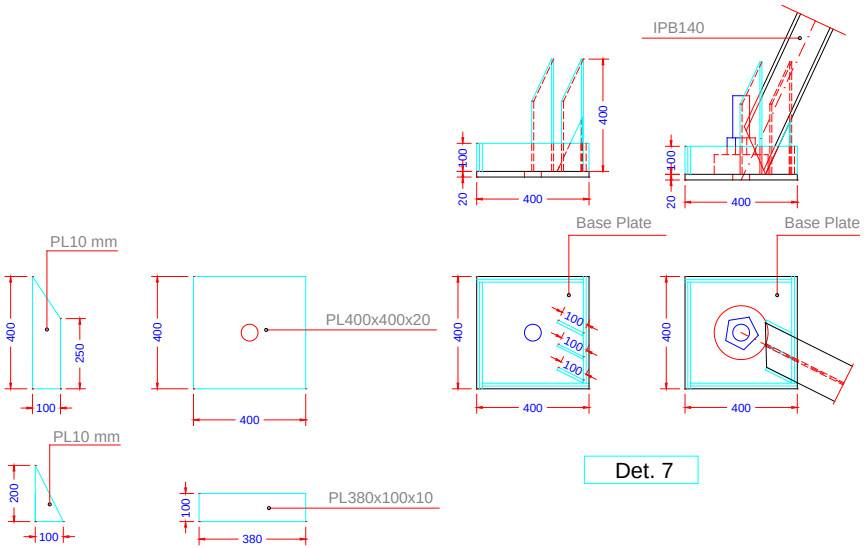

Fig. B.24: Loading setup: Details of base plates (Det. 7)

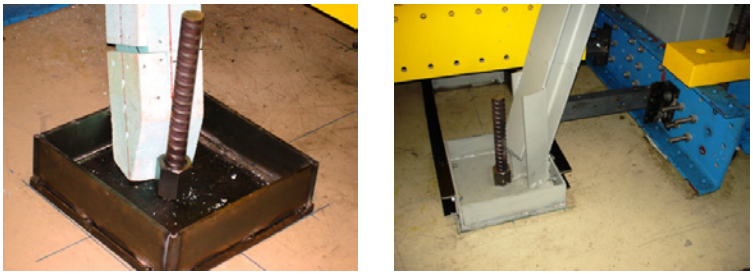

Fig. B.25: Loading setup: Fabricated base plate (Det. 7)

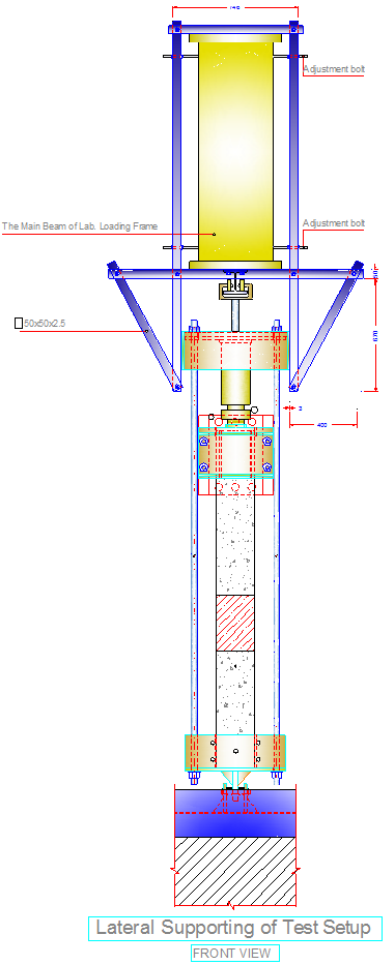

Fig. B.26: Loading setup: Designed lateral support of test specimens

Fig. B.27: Loading setup: fabricated lateral support of test specimens

(a) (b)

Fig. B.28: Loading setup: a) overhead horizontal traveling support of cyclic actuator, b) cyclic actuator

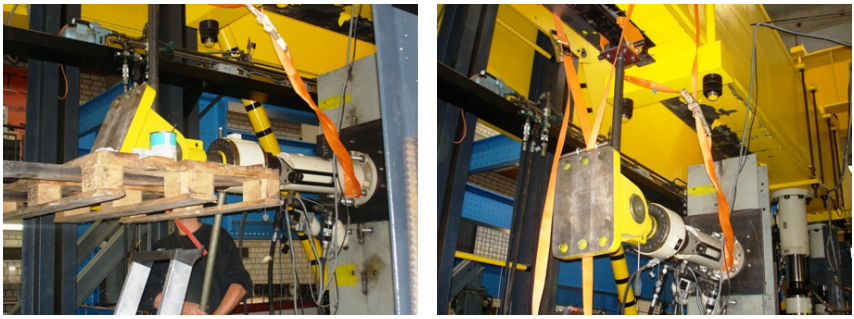

(a) (b)

Fig. B.29: Loading setup: a) installation of cyclic actuator to loading setup, b) installed cyclic actuator

(a) (b)

Fig. B.30: Loading setup: a) loading setup, b) hydraulic jack for static loads

Appendix C: Installation of Specimens into the Loading Setup

Since the place of loading setup was closely limited from the lateral and top sides, it was necessary to check the different alternatives to install test modules in the loading setup and select the best one. Therefore after checking different schemes, the final one was selected as Fig. C.1. Fig. C.1 displays different steps of installation and Fig. C.2 shows some practical process of it in the structural laboratory.

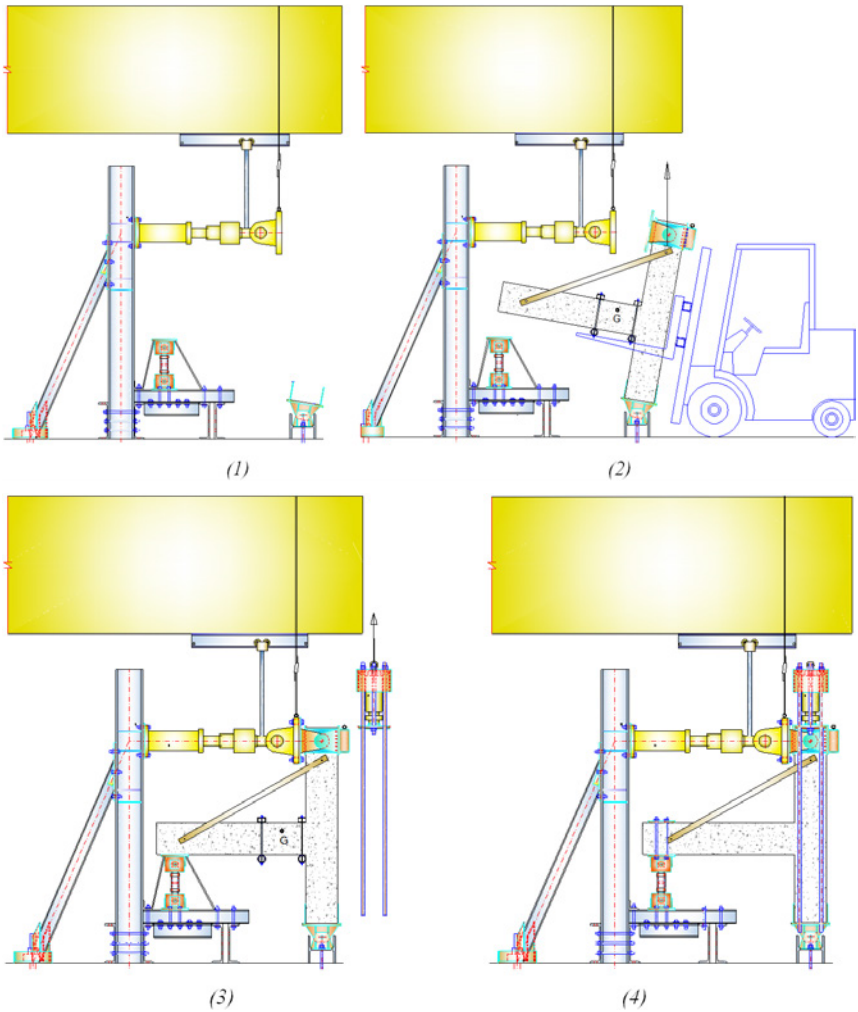

Fig. C.1: (continued)

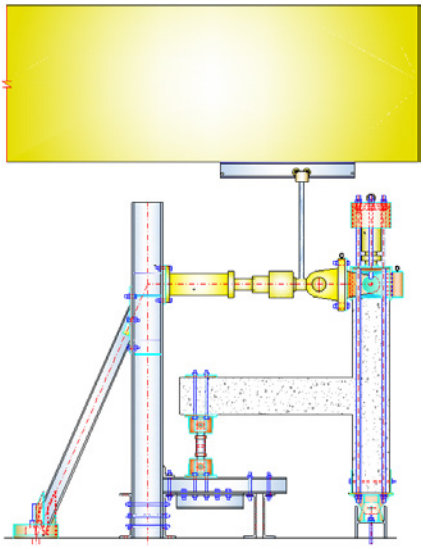

(5)

Fig. C.1: Loading setup: Proposed installation process of specimens in loading setup

Fig. C.2: Loading setup: Installation of specimens in loading setup

Appendix D: Decomposition of Specimen Deformation

D.1 Fix-end rotation of beam and column

The location of installed LVDTs at the end of beam and column in joint interfaces (Fig. D.1) indicates that the fix-end rotation of the beam, top and bottom column can be estimated by Eq. (D.1), (D.2), and (D.3), respectively.

$$\theta_b = \frac{(D_t - D_b)}{h_v} \qquad (D.1)$$

$$\theta_{ct} = \frac{(D_{rt} - D_{lt})}{h_h} \qquad (D.2)$$

$$\theta_{cb} = \frac{(D_{rb} - D_{lb})}{h_h} \qquad (D.3)$$

where:

D_i is measured change in gage length of LVDT,

h_v is vertical distance of horizontal LVDTs at the end of beam, and

h_h is horizontal distance of vertical LVDTs at the end of column.

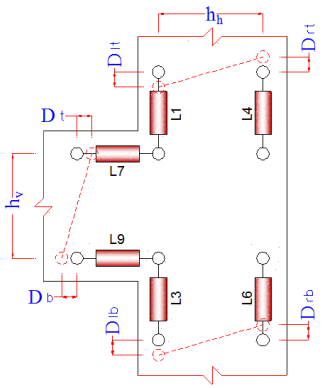

Fig. D.1: Measurement of beam and column fix-end rotation

D.2 Joint deformation

Referred to Fig.D.2 (a), the joint shear distortion can be estimated by the monitoring of installed LVDTs at the joint panel and using a plane-strain transformation as follows.

$$\gamma_{xz} = \frac{\varepsilon_\varphi - \varepsilon_x cos^2\varphi - \varepsilon_z sin^2\varphi}{sin\,\varphi\,\cos\varphi} \qquad (D.4)$$

where:

γ_{xz} is the shear strain of joint panel,

ε_x and ε_z are the normal strains in the x and z directions, respectively, and

ε_φ is the strain in an arbitrary direction (diagonal) with an angle of φ measured counter clockwise from the x axis.

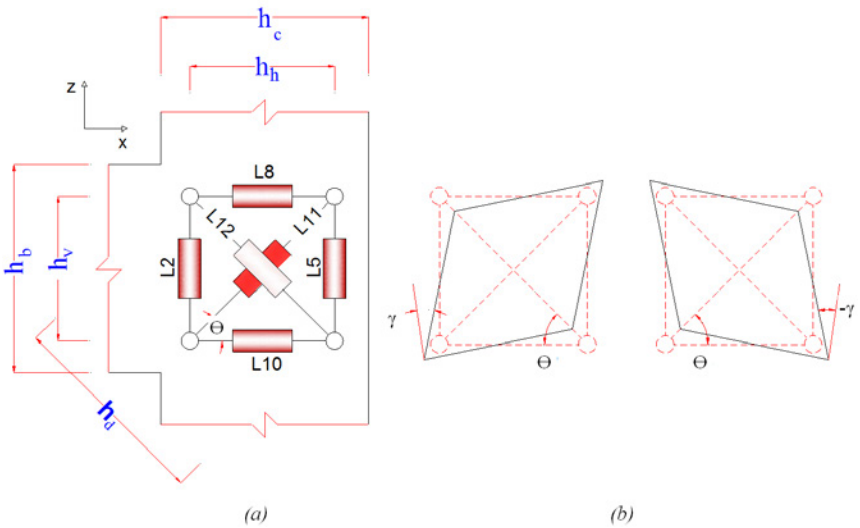

Fig. D.2: Measurement of joint deformation: a) LVDT layout for joint shear strain measurement, b) Sign conventions for joint shear strain

Four estimates of the joint shear strain are extended by forming triangular strain rosettes in the joint panel [Eq. (D.4)] as follows.

$$(\gamma_{xz})_1 = \frac{\varepsilon_{12} - \varepsilon_{10}cos^2\varphi - \varepsilon_2 sin^2\varphi}{-sin\,\varphi\cos\varphi} \quad (D.5)$$

$$(\gamma_{xz})_2 = \frac{\varepsilon_{11} - \varepsilon_{10}cos^2\varphi - \varepsilon_5 sin^2\varphi}{sin\,\varphi\cos\varphi} \quad (D.6)$$

$$(\gamma_{xz})_3 = \frac{\varepsilon_{11} - \varepsilon_8 cos^2\varphi - \varepsilon_2 sin^2\varphi}{sin\,\varphi\cos\varphi} \quad (D.7)$$

$$(\gamma_{xz})_4 = \frac{\varepsilon_{12} - \varepsilon_8 cos^2\varphi - \varepsilon_5 sin^2\varphi}{-sin\,\varphi\cos\varphi} \quad (D.8)$$

where $\varepsilon_i = \Delta L_i / L_i$ that ε_i, ΔL_i and L_i are the resulted strain of i^{th} LVDT, the measured change in gage length and initial gage length, respectively. The final joint shear strain (γ), as suggested by [Engindeniz-08], is estimated by an average of these shear strains as follows.

$$\gamma = \sum_{i=1}^{4} (\gamma_{xz})_i \Big/ 4 \quad (D.9)$$

The sign convention for shear strain as displayed in Fig. D.2 (b) is selected to be consistent with the direction of loading (Fig. 4.53).

D.3 Component contribution to specimen deformation

As displayed in Fig. D.3, the total lateral displacement of the top column can be decomposed to the partial lateral displacements caused by the deformation of beam, column and joint. The beam and column deformations are estimated by the elastic deformations and the fix-end rotation at the joint connections but the joint deformation is contributed by the shear distortion of the joint only.

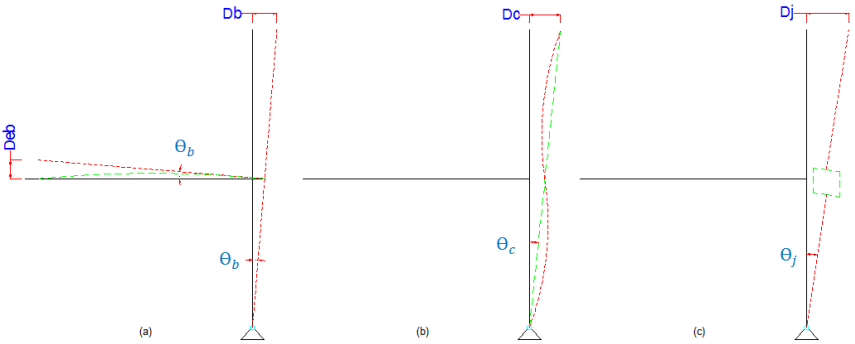

Fig. D.3: Contribution of beam, column and joint to the total lateral displacement

D.4 Rotation of beam at the flexural plastic hinge

Referred to Fig. D.4, the rotation of beam at the plastic hinge located at the end of HMFC can be estimated as follows.

$$\theta_{bh} = \frac{(D_{bt} - D_{bb})}{h_v} \qquad (D.10)$$

where:

D_i is measured change in gage length of LVDT and

h_v is vertical distance of horizontal LVDTs at the end of HMFC.

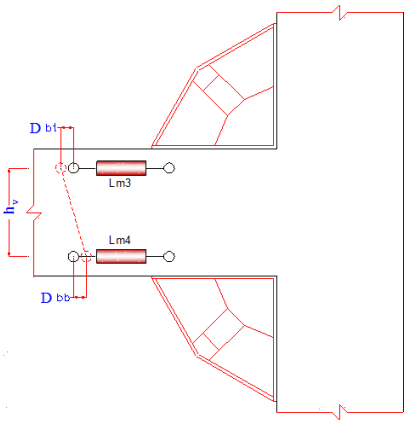

Fig. D.4: Measurement of beam rotation at the end of HMFC

In retrofitted specimens, the deformation of the beam is composed of displacements caused by the beam flexural deformation, beam fix-end rotation and plastic hinge rotation (Fig. D.5).

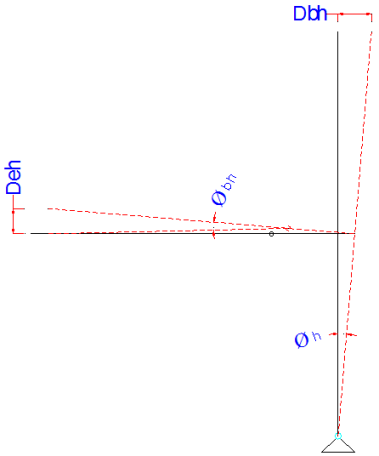

Fig. D.5: Contribution of beam at the end of HMFC to the total lateral displacement

Appendix E: Concept of Relative Energy Dissipation Ratio

According to the report of ACI Committee 374, [ACI 374.1-05], the relative energy dissipation ratio concept is illustrated for the third cycle to the drift ratio of 3.5%. If the hysteresis loop of Fig.E.1 is related to the third cycle of the 3.5% drift ratio and it is assumed that the test specimen has demonstrated different initial stiffness of $K(+)$ for positive, and $K(-)$ for negative force directions and that the peak lateral resistance for the positive and negative lateral loading directions, E1 and E2, also differ, the relative energy dissipation ratio will be defined by subtraction of the hatched area of the hysteresis loop for the third cycle, A_h, to the circumscribing polygon consists of two parallelograms, $ABCD$ and $DFGA$ so that the lines of AB and DC are parallel with $K(+)$ and AG and DF are parallel with $K(-)$. Therefore, the relative energy dissipation ratio can be calculated as:

$$\beta = \frac{A_h}{(E_1 + |E_2|)(\Theta'_1 + |\Theta'_2|)} \qquad (E.1)$$

where:

β is relative energy dissipation ratio

A_h is the area of the third cycle to the drift ratio of 3.5%

E_1 and E_2 are the peak lateral resistance for the positive and negative lateral loading directions, respectively

Θ'_1 and Θ'_2 are drift ratios in positive and negative directions, respectively

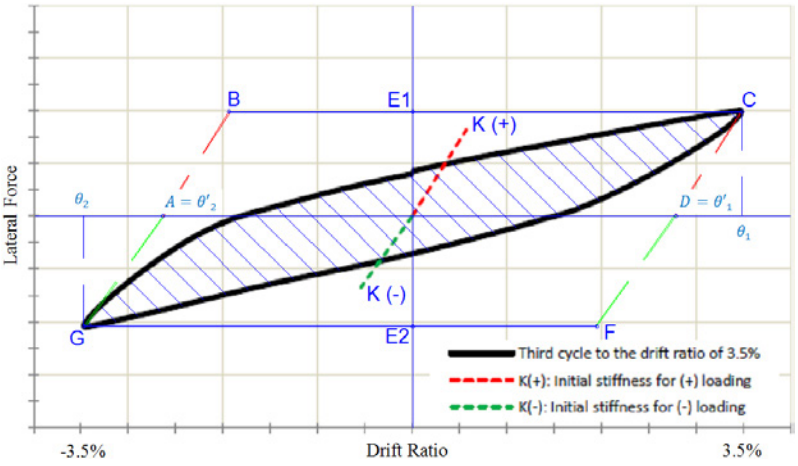

Fig. E.1: Concept of relative energy dissipation ratio

Mahdi Hayatrouhi

Strengthening of reinforced concrete beam-column joints to increase seismic resistance

The categorized literature review of retrofitting and strengthening methods of reinforced concrete (RC) beam-column joints clarified that non-disruptiveness; practical implementation, ductility and perseverance of lateral resistance as well as economical issues still remain the most challenging aspects of seismically retrofitting the vulnerable existing RC beam-column joints. Current research attempted to observe the seismic design principals of RC frame structures in seismic retrofitting of the vulnerable frames as a strategy of retrofitting based on the capacity design concept. Accordingly, the beam sidesway mechanism was redefined for seismic retrofitting by relocating the beam plastic hinges far enough away from the joints. Consequently, with introducing innovative energy dissipation devices such as Multi Functional Corbels (HMFC) and Harmonica Damper Plates (HHDP), the innovative Retrofitting Techniques 1 and 2 (RT1 and RT2) were proposed. The introduced devices of HMFC and HHDP as a passive energy dissipation system absorb energy through inelastic deformations. The proposed RT1 and RT2 were experimentally evaluated through a series of 3/4-scale beam-column joint specimens under an extremely severe loading history. The excellent performance of retrofitted specimens through the experimental study confirmed that the proposed retrofitting techniques (RT1 and RT2) are able to retain structural integrity with the minimum strength and stiffness degradation. As intended, the energy dissipation capacity was dramatically increased and beam sidesway mechanism was actually formed. Furthermore, a series of non-linear finite element analysis using ATENA was carried out on all reference and retrofitted specimens. The FEM models were validated with experimental outcomes. Subsequently, the validated models were utilized to develop a new simplified method for upgrading based on the advantages of RT1 and RT2. In the new proposed innovative Retrofitting Technique 3 (RT3), HHDP was replaced by Frictional-Bending Damper Plate (HFBDP) which dissipates energy based on friction and bending. The effectiveness and reliability of the proposed RT3 was investigated through a numerical analysis. As confirmed through experimental and numerical investigation, all acceptance criteria of ACI Committee 374 [ACI 374.1-05] were effectively satisfied by the proposed retrofitting techniques.

ISBN 978-3-8167-9177-5